DEVELOPING A LOAD ACQUISITION SYSTEM FOR A MULTIAXIAL TEST FRAME

by

Aaron James Carpenter

A thesis submitted in partial fulfillment
of the requirements for the degree

of

Master of Science

in

Mechanical Engineering

MONTANA STATE UNIVERSITY
Bozeman, Montana

November 2019

©COPYRIGHT

by

Aaron James Carpenter

2019

All Rights Reserved

ACKNOWLEDGEMENTS

The pursuit of my graduate degree has been a challenging endeavor, and I owe a great deal of thanks and appreciation to the many people who helped me along the way. First, I would like to thank my advisor Dr. David Miller for his guidance, advice, and patience throughout the entire project. I would also like to thank the other members of my committee, Dr. Douglas Cairns and Dr. Michael Edens for their knowledge and assistance. Dan Samborsky has also been a tremendous help providing me with his knowledge of materials testing, creativity, and sense of humor. The assistance of Glenn Foster in the machine shop was crucial to the completion of the manufacturing process. I would also like to thank Los Alamos National Laboratory for their support of my work.

Fellow graduate and undergraduate students have also aided me through the completion of this process. I would like to particularly thank Gavyn Pendleton for all his help as an undergraduate assistant this fall and past summer. I would also like to recognize everyone in Roberts 421 who have provided assistance, encouragement, and distraction along the way. I want to also acknowledge Kathy Campbell and Dagny Mest in the MIE office, they are an incredible resource for sorting out any logistical issues associated with being a graduate student in the department. Lastly, I never would have reached this point without the love and support of my family and friends.

TABLE OF CONTENTS

1. INTRODUCTION 1

Introduction to Material Testing 1
A Need for Multi-Axial Testing 1
Applications of the IPL 2
Motivation 3

2. THE MONTANA STATE IN-PLANE LOADER 4

The Original Naval Research Laboratory IPL 4
The IPL at Montana State University 5
Original Design 5
First Revisions 7
Second Revisions 9
Third Revisions 10
Recent Revisions 10
IPL Shortcomings 13

3. DIGITAL IMAGE CORRELATION 16

4. OBJECTIVES OF WORK 23

Problem Statement 23
Design Criteria and Requirements 25
Validation Objective 26

5. DESIGN AND MANUFACTURE 27

Description of Design 27
Components of Design 27
Mechanical Design 28
Resolving Load Components: 36
Load Cells 39
Software Component 40
Coupon Geometry 40
Changing Coupon Geometry: 42
Fulfillment of Design Criteria 42
Manufacture and Installation 43

6. SYSTEM CALIBRATION 45

7. VALIDATION AND RESULTS 50

TABLE OF CONTENTS – CONTINUED

Materials and Preparation 50
ASTM Standard Testing Procedures 50
IPL Testing Procedure 54
DIC Methods 58
Results and Discussion 62
Accuracy in Load Readouts 66
Y-Direction 67
X-Direction 73
Analytical Shear Modulus: 80
Analyzing Force vs Displacement: 81
IPL Shear Test Bending: 84
Analyzing the Multi-Axial Loading: 86

8. CONCLUSIONS 92

Conclusions 92
Future Work 95
High Strain Rate Testing 95
DIC recommendations 95
IPL/Multi-axial testing recommendations 96

9. REFERENCES CITED 99

10. APPENDICES 102

APPENDIX A: TEST DATA 103
APPENDIX B: DRAWING PACKAGE 138
APPENDIX C: ADDITIONAL DESIGN INFORMATION 160
APPENDIX D: IPL USER GUIDE 170

LIST OF TABLES

Table Page

1. Accuracy intervals for the IPL load components 67
2. Modulus data comparison between ASTM E8 and IPL tensile data. 72
3. Yield strength data comparison between ASTM E8 and IPL tensile data. 73
4. Modulus (G) data comparison between ASTM Iosipescu and IPL shear tests. 79
5. Shear strength (τ_y) data comparison between ASTM Iosipescu and IPL shear tests. 80

LIST OF FIGURES

Figure Page

1. Schematic representation of NRL load frame [3]. 5

2. The original design of the IPL at MSU detailed in the work of Ritter [4]. 6

3. Detailed view of load cell orientation [4]. 7

4. IPL including first revisions with coordinate system defined [6]. 9

5. Rendering of the most recent grips. A: Hydraulic Piston, B: Carbide-Textured Grip Plates, C: Transverse Support Plates, D: Coupon Gripping Area [2]. 11

6. IPL including fourth design revisions. A: Out-of-plane constraints, B: Next generation grip assembly [2]. 12

7. IPL stage report from ARAMIS V6. NOTE: 'Moment vs. Time' value and path [1]. 15

8. Illustration of DIC camera angles describing how the software identifies points in 3D space [10]. 17

9. Example of an application of a point tracking study in GOM ARAMIS [10]. 18

10. Example of a surface correlation study [10]. 19

11. A DIC facet with a unique pattern of black and white (left), and its corresponding matrix stored in the software (right) [10]. 20

12. The same DIC facet and matrix after motion [10]. 21

13. Report Image from ARAMIS V6 detailing inaccurate load data from the IPL. 24

14. Schematic describing typical load cell orientation in uniaxial load frames [14]. 29

15. Omega LC202 single axis tension/compression load cell [15]. 30

LIST OF FIGURES – CONTINUED

Figure Page

16. Free body diagram illustrating concept of double pinned joints. 30

17. Cut-away model view of the updated IPL load acquisition system with three load cells (red) oriented to read in-plane loading. 32

18. Dimetric model view of proposed design (without grips). NOTE: Load cells are housed between two mounting plates. 33

19. Isometric view of proposed design. NOTE: Mounting plate omitted for clarity. (A) Grip mounting plate. (B) Pinned joints. (C) Load Cells. (D) Housing. 34

20. Dimetric view of full proposed design. 36

21. Free body diagram describing the loads applied to the system. NOTE: The reaction forces are oriented around the center of the coupon and all loads are drawn in their respective positive orientation. 37

22. Detailed coupon geometry. NOTE: Notch geometry can change based on material and test parameters. 41

23. Circuit diagram detailing a shunt calibration [20]. 46

24. Load cell calibration using various known loads. 47

25. Load cell calibration curves for three new load cells generated using three known loads. 48

26. Schematic detailing Wyoming Test Fixtures' V-Notched Shear (Iosipescu) fixture [23]. 52

27. Idealized shear-moment diagrams for ASTM D5379 test and fixture. NOTE: bending is zero at the center of the specimen [23]. 53

28. IPL tensile test coupon used to validate the IPL load system in the Y-direction. 55

LIST OF FIGURES – CONTINUED

Figure Page

29. IPL double notched shear coupon used to validate the load system in the X-direction. 57

30. Detailed view of stochastic pattern showing facet size and facet distance used to create a surface component in GOM-ARAMIS. 59

31. Left camera view of Iosipescu test coupon with a DIC surface component overlaid. 60

32. Deformed surface of Iosipescu test showing tensor shear strain (ε_{xy}), the selected area is used to calculate a mean value of ε_{xy} throughout the test. 61

33. Axial loads vs. time: collected with the original load acquisition system. 63

34. Rotational load vs. time: collected with the original load acquisition system. 64

35. Axial Loads vs. time: collected using the updated load system. 65

36. Rotation Load vs. time: collected with the updated load system. 66

37. Left camera view of using DIC to calculate axial strain (ε_{yy}) during an IPL quasi-tensile test. 68

38. Failed Copper 110 tensile specimens. Left: ASTM E8 coupon. Right: IPL quasi-tensile coupon. Coupon width is 1” for reference. 69

39. Stress vs. strain data for five Instron ASTM E8 tensile tests. 70

40. Stress vs. strain data from seven IPL quasi-tensile tests. Strain data was collected using GOM-ARAMIS 2018 digital image correlation software. 71

41. Stress vs. strain data outlining the 0.2% strain offset method to estimate yield strength (σ_y). 72

LIST OF FIGURES – CONTINUED

Figure Page

42. Left camera view showing the use of DIC to calculate shear strain (ε_{xy}) during an ASTM Iosipescu test. 74

43. Left camera view showing the use of DIC to calculate shear strain (ε_{xy}) during an IPL shear test. 75

44. Shear stress vs. shear strain data collected during twelve Instron ASTM Iosipescu shear tests. 76

45. Shear stress vs. shear strain collected during six IPL shear tests. 77

46. Stress-strain curve for an IPL shear test (test 4) outlining the 0.002 radian offset line to estimate shear strength (τ_y). 78

47. Stress-strain comparison between an ASTM Iosipescu test (test 8) and an IPL shear test (test 4). 79

48. Image showing the two points used to observe the X force versus X displacement relationship in an IPL shear test. 82

49. X force vs X displacement curves for points directly above (top) and below (bottom) the notched cross-section of IPL shear test 4. 83

50. X force vs relative X displacement curve for IPL shear test 4. The displacement is corrected to eliminate the effects of bending and grip slippage. 84

51. Shear diagram over the length of the IPL shear coupon 85

52. Moment diagram over the length of the IPL shear coupon. 85

53. Moment diagram magnified to detail the non-zero value at the center of the IPL shear coupon. 86

54. Four-color view schematic from GOM-ARAMIS detailing the bending present during an IPL shear test at observed yield point (test 2) 87

LIST OF FIGURES – CONTINUED

Figure Page

55. Axial strain vs notch-to-notch length (non-dimensional) detailing the bending present during an IPL shear test at observed yield point (Test 4). The axial strain at the clamped condition at the beginning of the test is also shown for reference. 88

56. Maximum shear effective stress on cross section at observed yield point for IPL shear test (test 4). 90

57. Von Mises effective stress on cross section at observed yield point for IPL shear test (test 4). 90

58. Stress vs strain curves from both the old and new load systems. 93

59. Shear stress vs shear strain curves using both the old and new load systems. 94

60. Stress-strain curve for Instron tensile test 1. 104

61. Stress-strain curve for Instron tensile test 2. 105

62. Stress-strain curve for Instron tensile test 3. 105

63. Stress-strain curve for Instron tensile test 4. 106

64. Stress-strain curve for Instron tensile test 5. 106

65. Stress-strain curve for IPL Quasi-Tensile test 1. 107

66. Stress-strain curve for IPL Quasi-Tensile test 2. 107

67. Stress-strain curve for IPL Quasi-Tensile test 3. 108

68. Stress-strain curve for IPL Quasi-Tensile test 4. 108

69. Stress-strain curve for IPL Quasi-Tensile test 5. 109

70. Stress-strain curve for IPL Quasi-Tensile test 6. 109

71. Stress-strain curve for IPL Quasi-Tensile test 7. 110

72. Shear stress-shear strain curve for Iosipescu test 1. 111

LIST OF FIGURES – CONTINUED

Figure Page

73. Shear stress-shear strain curve for Iosipescu test 2. 111

74. Shear stress-shear strain curve for Iosipescu test 3. 112

75. Shear stress-shear strain curve for Iosipescu test 4. 112

76. Shear stress-shear strain curve for Iosipescu test 5. 113

77. Shear stress-shear strain curve for Iosipescu test 6. 113

78. Shear stress-shear strain curve for Iosipescu test 7. 114

79. Shear stress-shear strain curve for Iosipescu test 8. 114

80. Shear stress-shear strain curve for Iosipescu test 9. 115

81. Shear stress-shear strain curve for Iosipescu test 10. 115

82. Shear stress-shear strain curve for Iosipescu test 11. 116

83. Shear stress-shear strain curve for Iosipescu test 12. 116

84. Force-displacement curve for Iosipescu test 1. (NOTE: Force-displacement data is not presented for tests 2-8) 117

85. Force-displacement curve for Iosipescu test 9. 117

86. Force-displacement curve for Iosipescu test 10. 118

87. Force-displacement curve for Iosipescu test 11. 118

88. Force-displacement curve for Iosipescu test 12. 119

89. Shear stress-shear strain curve for IPL shear test 1. 120

90. Shear stress-shear strain curve for IPL shear test 2. 120

91. Shear stress-shear strain curve for IPL shear test 3. 121

92. Shear stress-shear strain curve for IPL shear test 4. 121

93. Shear stress-shear strain curve for IPL shear test 5. 122

LIST OF FIGURES – CONTINUED

Figure Page

94. Shear stress-shear strain curve for IPL shear test 6. 122

95. Force-displacement curves for IPL shear test 1. Data sets for displacements directly above (top) and below (bottom) the notched cross-section. 123

96. Force-relative displacement curve for IPL shear test 1. Displacement is corrected to eliminate effects of bending and grip slippage. 123

97. Force-displacement curves for IPL shear test 2. Data sets for displacements directly above (top) and below (bottom) the notched cross-section. 124

98. Force-relative displacement curve for IPL shear test 2. Displacement is corrected to eliminate effects of bending and grip slippage. 124

99. Force-displacement curves for IPL shear test 3. Data sets for displacements directly above (top) and below (bottom) the notched cross-section. 125

100. Force-relative displacement curve for IPL shear test 3. Displacement is corrected to eliminate effects of bending and grip slippage. 125

101. Force-displacement curves for IPL shear test 4. Data sets for displacements directly above (top) and below (bottom) the notched cross-section. 126

102. Force-relative displacement curve for IPL shear test 4. Displacement is corrected to eliminate effects of bending and grip slippage. 126

103. Force-displacement curves for IPL shear test 5. Data sets for displacements directly above (top) and below (bottom) the notched cross-section. 127

104. Force-relative displacement curve for IPL shear test 5. Displacement is corrected to eliminate effects of bending and grip slippage. 127

LIST OF FIGURES – CONTINUED

Figure Page

105. Force-displacement curves for IPL shear test 6. Data sets for displacements directly above (top) and below (bottom) the notched cross-section. 128

106. Force-relative displacement curve for IPL shear test 6. Displacement is corrected to eliminate effects of bending and grip slippage. 128

107. Axial strain (ε_{yy}) between notches for IPL shear test 1; reported at the yield point. Length is reported as a fraction of the length. The increasing trend from 0 to 1 describes considerable bending in the sample..... 129

108. Axial strain (ε_{yy}) between notches for IPL shear test 2; reported at the yield point. Length is reported as a fraction of the length. The increasing trend from 0 to 1 describes considerable bending in the sample..... 129

109. Axial strain (ε_{yy}) between notches for IPL shear test 3; reported at the yield point. Length is reported as a fraction of the length. The increasing trend from 0 to 1 describes considerable bending in the sample..... 130

110. Axial strain (ε_{yy}) between notches for IPL shear test 4; reported at the yield point. Length is reported as a fraction of the length. The increasing trend from 0 to 1 describes considerable bending in the sample..... 130

111. Axial strain (ε_{yy}) between notches for IPL shear test 5; reported at the yield point. Length is reported as a fraction of the length. The increasing trend from 0 to 1 describes considerable bending in the sample..... 131

112. Axial strain (ε_{yy}) between notches for IPL shear test 5; reported at the yield point. Length is reported as a fraction of the length. The increasing trend from 0 to 1 describes considerable bending in the sample..... 131

113. Maximum-shear effective stress across notches; reported at the observed yield point for IPL shear test 1..... 132

LIST OF FIGURES – CONTINUED

Figure Page

114. Von-Mises effective stress across notches; reported at the observed yield point for IPL shear test 1. 132

115. Maximum-shear effective stress across notches; reported at the observed yield point for IPL shear test 2. 133

116. Von-Mises effective stress across notches; reported at the observed yield point for IPL shear test 2. 133

117. Maximum-shear effective stress across notches; reported at the observed yield point for IPL shear test 3. 134

118. Von-Mises effective stress across notches; reported at the observed yield point for IPL shear test 3. 134

119. Maximum-shear effective stress across notches; reported at the observed yield point for IPL shear test 4. 135

120. Von-Mises effective stress across notches; reported at the observed yield point for IPL shear test 4. 135

121. Maximum-shear effective stress across notches; reported at the observed yield point for IPL shear test 5. 136

122. Von-Mises effective stress across notches; reported at the observed yield point for IPL shear test 5. 136

123. Maximum-shear effective stress across notches; reported at the observed yield point for IPL shear test 6. 137

124. Von-Mises effective stress across notches; reported at the observed yield point for IPL shear test 5. 137

125. ANSYS FEA screenshot detailing deformation of large clevis (111-003-001) with 1000 lbf applied to the threaded hole. 161

126. ANSYS FEA screenshot detailing deformation of large X clevis (111-003-004) with 1000 lbf applied to the threaded hole. 162

LIST OF FIGURES – CONTINUED

Figure Page

127. ANSYS FEA screenshot detailing deformation of a portion of the housing assembly (333-014-001) with 1000 lbf applied in the X direction. 163

128. ANSYS FEA screenshot detailing deformation of a portion of the housing assembly with 2000 lbf applied in the Y direction. 164

129. ANSYS FEA screenshot detailing deformation of X side clevis (111-003-002) with 500 lbf applied axially to the hole. (NOTE: There are two of these hence 1000 lbf/2 = 500 lbf) 165

130. ANSYS FEA screenshot detailing deformation of the free X clevis (111-001-001) with 1000 lbf applied to the threaded hole. 166

131. ANSYS FEA screenshot detailing deformation of bushing (111-004-001) with 1000 lbf applied vertically to the pin hole. 167

132. Validation curve for the X direction of the IPL. The process was completed by attaching a calibrated load cell in line with a cable and pulling on a gripped coupon. The small error is considered friction and off-axis loading associated with the procedure. 168

133. LabVIEW screenshot of sub VI titled "ProcessAxisLoads.vi" which contains the MATLAB script that resolves load components. 169

134. IPL User Guide reference figure. 172

135. Snapshot of the 'LVDT_Calib' VI. 174

136. Snapshot of the 'IPL_V1' VI. 175

ABSTRACT

Material testing has traditionally been completed by using a uniaxial load frame which isolates a single stress component. Engineers however, design components for applications in a multi-axial world to withstand stress in multiple directions. The In-Plane Loader (IPL) at Montana State University expands the realm of material testing to three degrees of freedom within a two-dimensional plane. Applications of the IPL include composite material testing and experimental validation of constitutive models in multiple axes.

The multi-axial test frame has been in place at MSU for several years. One of the primary challenges associated with the IPL is its ability to accurately measure multi-axial load components. The purpose of this work was to develop and validate an updated multi-axial load acquisition system for the IPL. The procedure included design, manufacture, implementation, and validation of the system. Validating the system in multiple axes required isolating single stress components along each of the planar axes. Tension tests were completed to isolate the vertical component, and shear tests were completed to isolate the horizontal component. Each of the results were compared to results of standardized test procedures designed to isolate their respective stress components. Digital image correlation was implemented as a non-contact method of measuring displacement for the testing procedures.

The data collected in this study provides confidence in the ability to measure multi-axial loading in combination with digital image correlation to expand the capabilities of multi-axial testing. The system provides the ability to study load dependent failure of materials as well as displacement dependent failure. The information presented provides an understanding of challenges associated with multi-axial testing which hopes to assist in the development of future multi-axial test frames.

INTRODUCTION

Introduction to Material Testing

A crucial component of any mechanical design is material selection. To understand mechanical behavior of materials and to characterize them for design, testing of small material samples, or coupons, is completed. Properties analyzed during testing include, but are not limited to, strength, stiffness, and toughness. Data collected during material testing at the coupon level helps engineers design components to withstand conditions unique to each application.

Traditional testing methods attempt to isolate a single failure mode or apply a single stress component. This approach is used to understand how a material behaves purely in tension, compression, torsion, shear, or bending. Few traditional testing methods are capable of applying multi-axial loading conditions to a sample and are limited to bi-axial two degree of freedom loading. Often times, designs are required to withstand more complex loading. Therefore, this typical testing approach leads to substantial testing of designs on subcomponent and component levels to verify performance.

A Need for Multi-Axial Testing

Typical material testing methods limit stress states to a single component of stress. However, real world applications generally require materials to endure combined stress states. The purpose of the In-Plane Loader (IPL) at Montana State University is to expand the capabilities of material testing to three degrees of freedom. Methods to apply multi-axial stress states at the coupon level can be used to better understand material behavior in

realistic applications. The data collected can potentially decrease time spent testing designs on subcomponent and component levels.

Applications of the IPL

Although not perfected, the IPL at MSU has been used for several projects since its inception. Research using the IPL includes attempting to validate plasticity models and observing composite material behavior.

Constitutive models are mathematical models developed to describe relationships between stress and strain in materials. Some models, more complex than others, are used to model plastic behavior in addition to elastic behavior. Validation of these models is difficult, and generally completed under idealistic loading conditions. Stroili [1] used the IPL and digital image correlation (discussed later) to compare strain and displacement data to finite element models created using a plasticity model. The work focused on isotropic materials under multiaxial loading conditions and at elevated strain rates.

The IPL has also been used extensively to characterize strength and damage in composite materials. Due to the variables associated with laminate design, understanding damage in composites is often difficult and costly. The goal of much of the research completed on the IPL has been to better understand damage in composite materials and to use the data to predict damage response of designs [2]. Much of the work includes analyzing dissipated strain energy in the material during the damage process.

Motivation

After realizing the capabilities and limitations of the IPL, it is evident advancements in the technology are required to further advance multi-axial testing. Improvements to the load acquisition system can be used to better understand the multi-axial stress states provided by the frame's unique loading ability. A better understanding of the use of digital image correlation to collect strain data can also help to further develop multi-axial testing technology. The purpose of this work is to characterize, improve, and re-validate the In-Plane Loader in order to expand the capabilities of multi-axial testing. The work also hopes to provide a base understanding of system challenges to better develop the next generation of multi-axial test frames.

4

THE MONTANA STATE IN-PLANE LOADER

The IPL is a multi-axial load frame located in the MSU Composites laboratory. It was originally developed for composite material research. The concept of the machine is a three degree of freedom load frame capable of sliding (X motion), opening/closing (Y motion), and rotation (about Z axis) [3]. The IPL is capable of any combination of the three degrees of freedom. For consistency, the coordinate system for the IPL will be described as X being the horizontal axis, Y being the vertical axis, and Z being out of/into the page for the remainder of this work. The described coordinate system is shown later in Figure 4. Several previous theses have contributed to the development and improvement of the IPL. Each revision of the IPL discussed in this chapter consists of five major components: the frame, actuators, motion control, load acquisition, and displacement acquisition. This chapter will refrain from discussing specific material research conclusions found using the IPL. Instead, the original conception, design upgrades, and shortcomings of the IPL are discussed.

The Original Naval Research Laboratory IPL

The IPL was inspired by the work of the Naval Research Laboratory (NRL) as a method to characterize failure behavior and internal damage in composite materials. The NRL work focused on monitoring energy dissipation as a method to measure damage accumulation of composite coupons under multi-axial loading conditions. The IPL's ability to apply multiaxial loads on a single plane relies on constraining the actuators to the previously mentioned plane and the non-orthogonality of the three actuators. Unique

combinations of actuator lengths can be mapped into specific combinations of the three basic in-plane motions discussed above. A basic schematic of the NRL load frame is pictured in Figure 1 below [3].

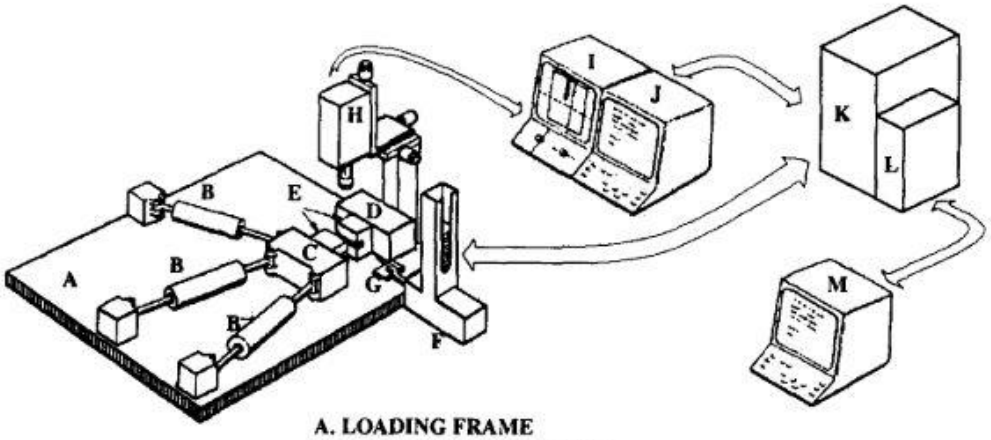


Figure 1: Schematic representation of NRL load frame [3].

The IPL at Montana State University

Original Design

The IPL at MSU began as a Senior Mechanical Engineering Design (ME404) project by Eric Booth, Marc Schaff, and Kim Higgins in 2001. It was later completed by several graduate and undergraduate students as part of Will Ritter's [4] graduate work.

Much of the machining was completed by students in the machine shop, and purchased parts were implemented where ever possible. The load system was designed with pancake load cells located at the ends of each actuator, and the load components were to be resolved based on the frame geometry and cross-head position throughout a test. The IPL was originally oriented on its side, similar to the design outlined by NRL. The instrumentation and controls used to acquire data and control the motion of the machine were written using LabVIEW, Mathematica, and MATLAB software packages [4]. Photographs detailing the original design of the IPL are seen in Figures 2 and 3.

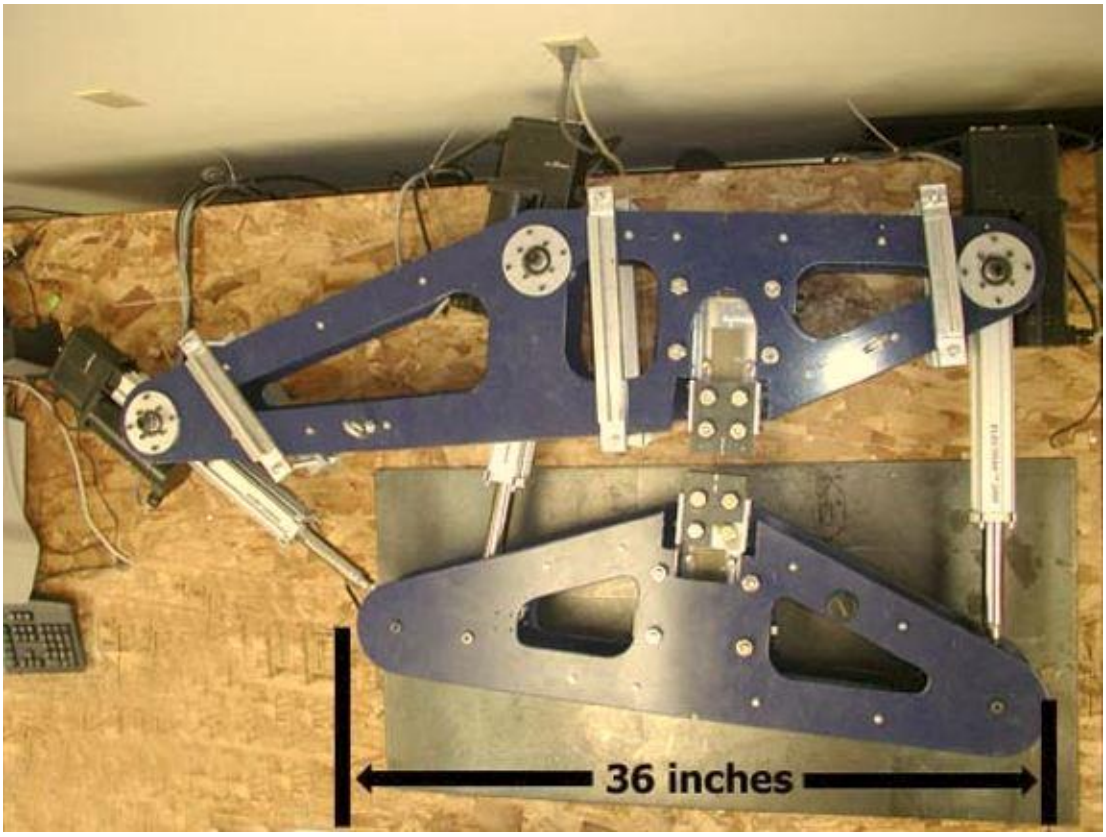


Figure 2: The original design of the IPL at MSU detailed in the work of Ritter [4].



Figure 3: Detailed view of load cell orientation [4].

The main drawback outlined with this design of the IPL was the tendency of the machine to experience bearing backlash. Ritter describes the bearing backlash as "the amount that the bearing will displace perpendicular to the load" [4]. A small amount of backlash is manageable in mechanical testing. However, with the crosshead displacement data being recorded based on the three actuator controllers, the load vs. displacement curves showed a significant period of zero load with recordable displacement near the beginning of each test cycle. It was concluded the cylindrical roller bearings attaching the actuators to the load frame caused the backlash, and the work suggested they be replaced for future IPL research [4].

First Revisions

The first set of revisions on the IPL design is outlined in the work of Aaron Collet [5]. This iteration included several design upgrades to the IPL. First, to mitigate the previously mentioned bearing backlash, the cylindrical roller bearings were replaced with tapered roller bearings. Also, to further improve the displacement control, LVDTs were

mounted near the grips, and the position-read virtual instrument (VI) was updated in LabVIEW [5].

Next, the original grip assembly was unable to incorporate differing coupon thicknesses. This was due to the rigid back plate of the grips which caused the center plane of the coupon (Z coordinate) to be dependent on the coupon thickness. The effect of the varying center plane was induced out-of-plane bending in the sample. This iteration incorporated a self-centering grip system which eliminated the issue. Other grip improvements included increased gripping area and more efficient gripping action [5].

Lastly, these revisions oriented the IPL vertically to save space. To restrict out-of-plane motion in the new orientation, tongue and groove connectors were connected to each of the IPL frames. Shortcomings observed with this iteration included out-of-plane deflection, grip deflection, grip slippage, and inaccuracies in the load readings [5]. An image of the IPL incorporating the first set of revisions is seen in Figure 4.

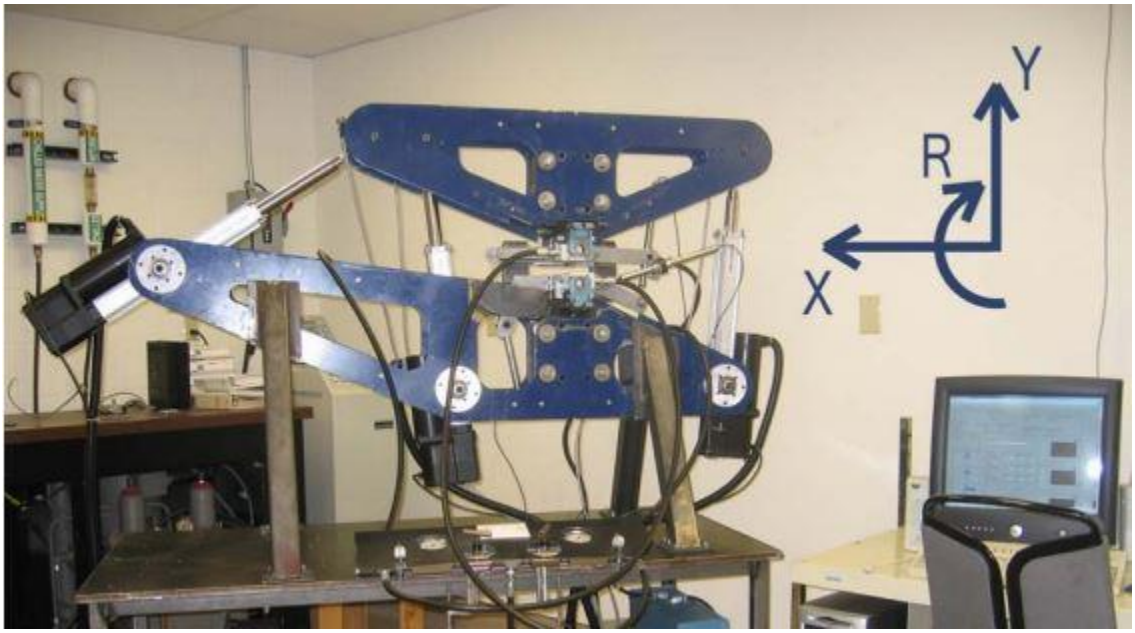


Figure 4: IPL including first revisions with coordinate system defined [6].

Second Revisions

Three design features were incorporated into the next iteration of IPL. First, between the work of Collet [5] and Smith [6], three Omega DMD-465 load cell amplifiers were integrated into the data acquisition system. These amplifiers significantly decreased the standard deviation of the raw load data [5]. The amplifiers are still integrated in the current configuration of the IPL.

Two updates were incorporated to improve the grips. A new hydraulic pump was added for increased gripping pressure. Additionally, the hydraulic pump had the option to be operated with a foot pedal. The purpose of the upgrade was to decrease the cycle time between tests. The last update to this iteration of the IPL was the addition of textured grip

faces. The grip texturing was applied by Carbinite Metal Coatings. The purpose of the coating was to minimize the grip slippage during a test [6].

Third Revisions

Schmitt's thesis [7] outlines the updates included in the third set of revisions to the IPL. Few mechanical or software components were incorporated to the IPL during this time. The primary upgrade for this revision was the addition of a digital camera to monitor the distortion of the test coupon. The camera was rigidly mounted to the lower frame, and a fine speckle pattern was sprayed on the coupon. The algorithm was limited to resolving displacements to single pixel accuracy. This addition was the first attempt at using Digital Image Correlation (DIC) to monitor displacement rather than using the position control incorporated into the IPL software [7]. The low-cost two-dimensional DIC software was developed by Parker [8] in 2009. Since then, the Mechanical Engineering department has purchased a commercial DIC system, GOM-ARAMIS. Details about this system and how it applies to this work is discussed later. For further details about the history of DIC, how it can be used in engineering applications, and the development of this system, refer to Parker [8].

Recent Revisions

At the start of this work, the IPL had undergone a fourth set of design revisions. Details of these revisions of the IPL are outlined in Jette's thesis [2]. Up to this point, components from the original design including the ball screw actuators, pancake load cells, and the frame had not undergone significant changes. This iteration considered many of

the suggestions from previous works to improve the performance and reliability of the load frame.

First, a completely new grip assembly was designed and incorporated into the machine. The new grips were integrated to further mitigate the continued issue of grip slippage in the IPL. Similar to the old grips, the new system relied on hydraulic pistons to apply gripping pressure to the test specimen, and incorporated carbide textured grip plates. The new grip assembly eliminated the self-centering feature. Instead, the fixed grip plates were designed with interchangeable shims to incorporate varying coupon thickness. The grip feature which significantly improved machine performance was the addition of transverse support plates. The plates were designed to mechanically constrain the coupon from slipping, rather than relying only on the gripping pressure and grip texture. A rendering of the updated grip assembly is seen in Figure 5.

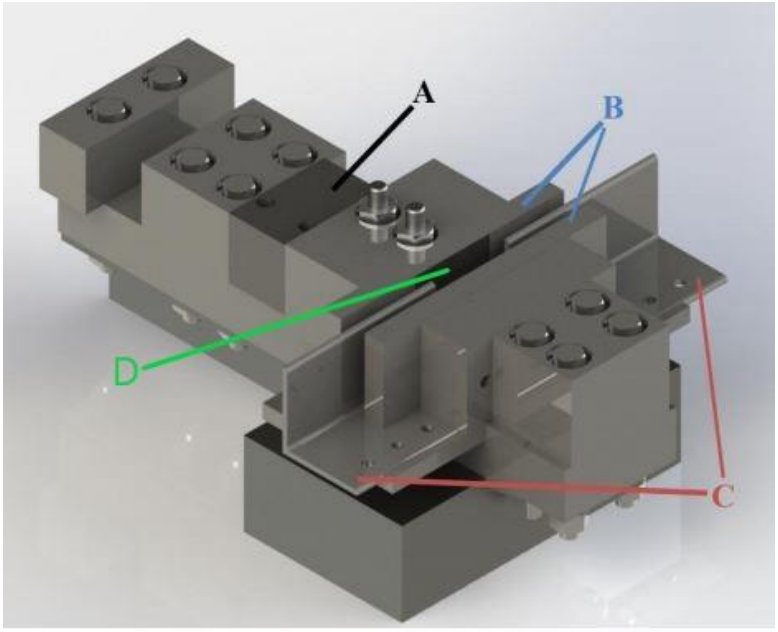


Figure 5: Rendering of the most recent grips. A: Hydraulic Piston, B: Carbide-Textured Grip Plates, C: Transverse Support Plates, D: Coupon Gripping Area [2].

The next improvement addressed the continued concern of out-of-plane motion. New out-of-plane constraints were added by mounting slewing bearings to the frame, then mounting a linear carriage and bearing rail to each pair of slewing bearings. This design allowed for unrestricted in-plane motion but restricted any out-of-plane displacement of the cross-head. The described IPL with out-of-plane constraints is seen in Figure 6 below.

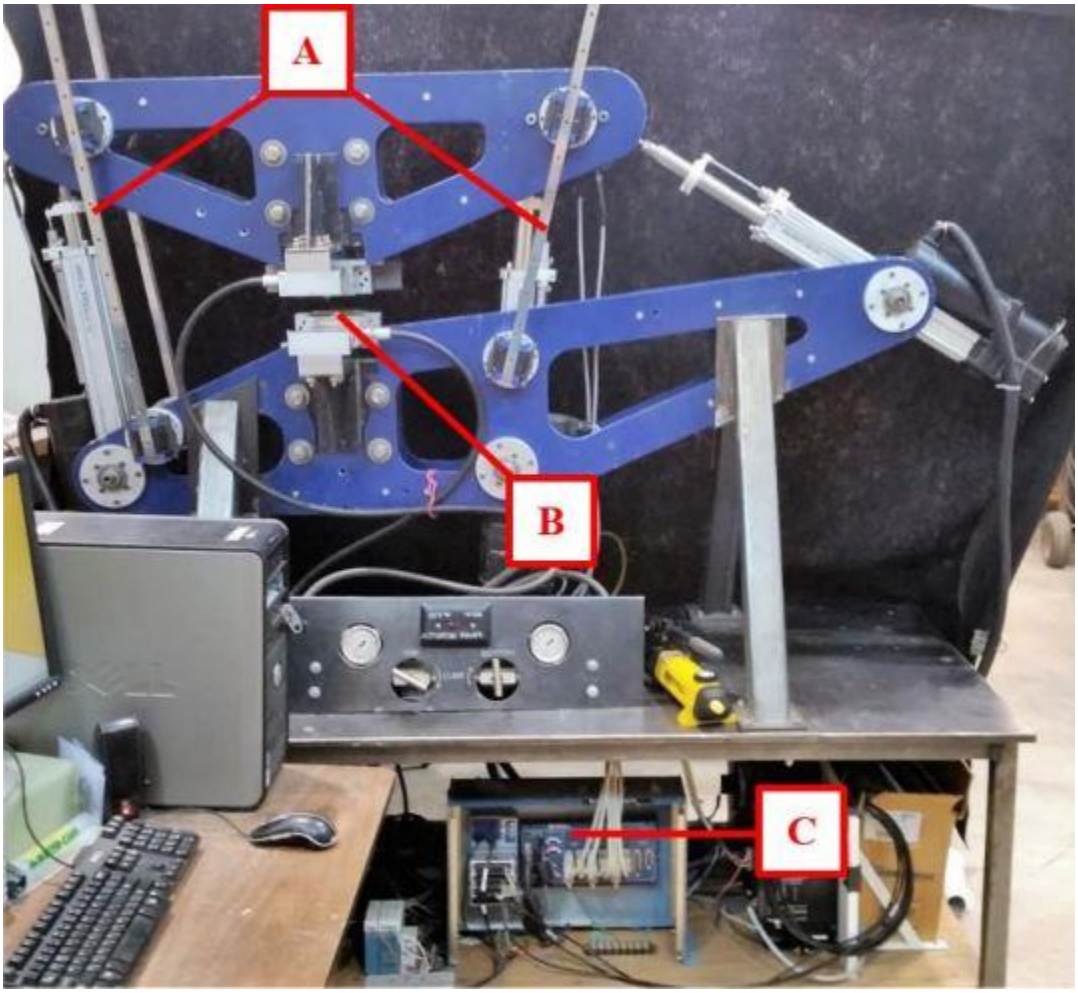


Figure 6: IPL including fourth design revisions. A: Out-of-plane constraints, B: Next generation grip assembly [2].

Further improvements included in this iteration included an updated data acquisition module (DAQ) and actuator control module. The LVDTs previously used to track the position of the IPL were repurposed to help calibrate the actuator lengths. The control software was updated to use the new actuator control module to track the cross-head position. Further details about these updates are found in Jette's thesis [2].

IPL Shortcomings

Each of the projects incorporating the IPL outline several drawbacks and suggestions for improvement, many of which were remedied throughout the development process. However, some issues proved difficult to solve. The most common issue mentioned was out-of-plane displacement. After the integration of Jette's [2] constraints, the issue was minimized but not eliminated, especially when performing compression tests. Common suggestions to solve the issue include re-orienting the IPL on its side and incorporating a bearing plate on both sides of the cross-head. At this point, this would require a major design project, and likely a complete re-design of the frame.

Next, originally outlined in Smith's [6] work, and re-iterated in Jette's [2] work, frame compliance continues to be a problem. In an ideal material testing situation, the load frame should be considered infinitely rigid compared to the test specimen. The IPL frame is plenty sufficient to withstand the stress of a testing situation. However, under high loads the frame flexes and stores energy. The IPL and its components are acting as a spring which causes a variety of issues. First, since the machine is position controlled by the actuator encoders, the prescribed displacement input is not equal to the actual displacement observed in the test specimen. Next, when using the IPL to analyze damage in a composite

material, the stored energy in the frame is released into the specimen upon reaching the critical damage level which causes further specimen damage [2]. It was suggested that orienting the position control closer to the grips could mitigate the displacement discrepancy. This method was employed with the first design revisions, but the system was removed due to signal noise in the LVDT's. Regardless of the location of the position control, the issue of stored energy in the frame would be still be present. Without a complete redesign of a significantly more rigid frame, frame compliance will continue to be an issue associated with the IPL at MSU.

Other drawbacks recognized in this work and past work [7] are related to the IPL controls. The actuators are operated using stepper motors, so many times the IPL motion is not smooth. The load path is divided into discrete steps which causes jumps in displacement instead of smooth displacement paths. IPL tests generally take 20 to 30 minutes, so several features to automate the testing process such as a home position have also been suggested [2], [6], [7].

Stroili's thesis [1], the most recent work on the IPL, discovered maybe the most concerning short-coming of the IPL. The IPL's software mathematically resolves loads in the X and Y directions, and a moment about the Z axis. When attempting to analyze the stress state of the test coupon it was discovered the IPL reported unrealistically high moment values given the displacements, material, and geometry. The moment load path also did not seem to realistically fit the nature of the tests. A report page from Stroili's thesis showing the described load issue is shown in Figure 7. The moment value reported shows a magnitude exceeding 11,000 in-lbf. To put into perspective, the moment reported

is enough to yield a 3.25” x 0.188” cross section of the same material (304L stainless steel, σ_y=30.5 ksi) [9]. As the loads were further analyzed, it was also discovered the X and Y loads had not incorporated appropriate zero-load offset values. Luckily, much of the previous research on the IPL had been strain dependent rather than load dependent. Several other short-comings were noticed during this work, all of which are outlined later in the future work section.

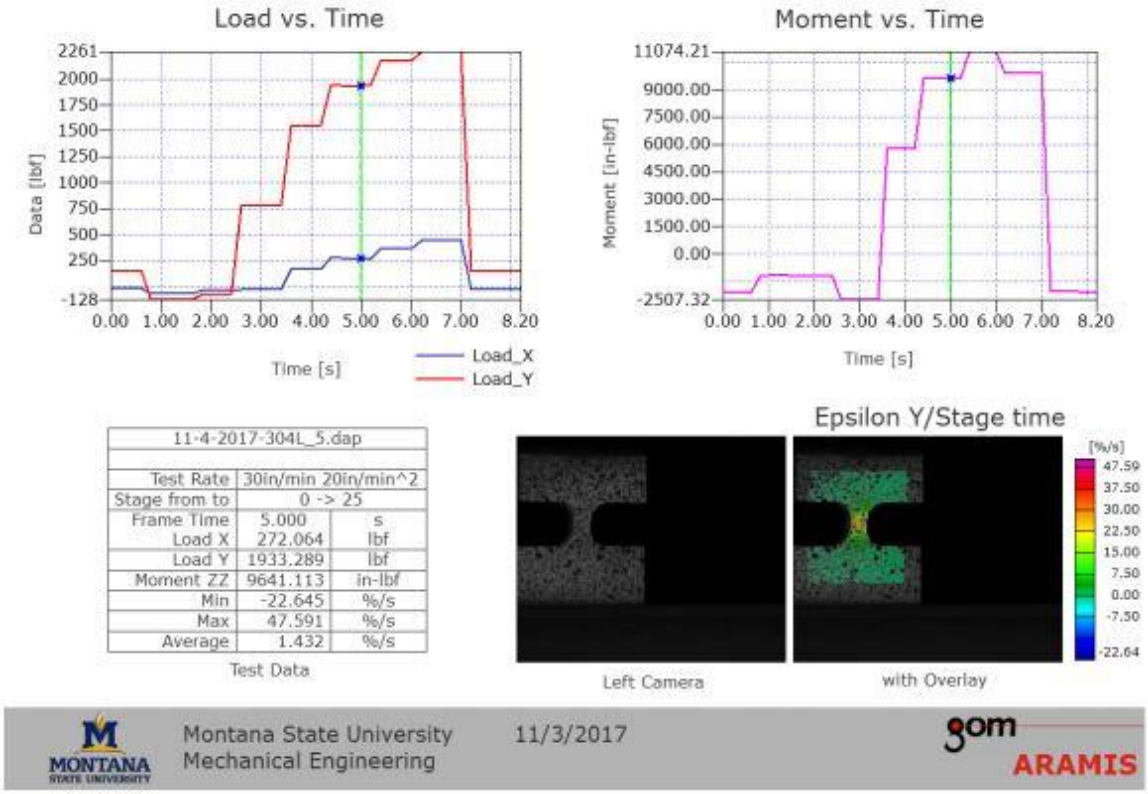


Figure 7: IPL stage report from ARAMIS V6. NOTE: 'Moment vs. Time' value and path [1].

DIGITAL IMAGE CORRELATION

The DIC system has been discussed in previous works, but recent training from Trilion Quality Systems has increased understanding of the software [10]. The Mechanical Engineering department at MSU has recently upgraded from GOM ARAMIS V6 to GOM ARAMIS 2018 [11].

DIC is a full-field non-contact measuring system which can measure displacements in 3D space. It is useful for testing over all time scales, and for tests on the material, component, and assembly scales. The software uses two cameras angled inward about 25 degrees towards a target. The software is capable of understanding where points are in 3D space because of the mounting angle. The second camera at an angle gives the software depth perception similar to human vision. The concept is illustrated in Figure 8.

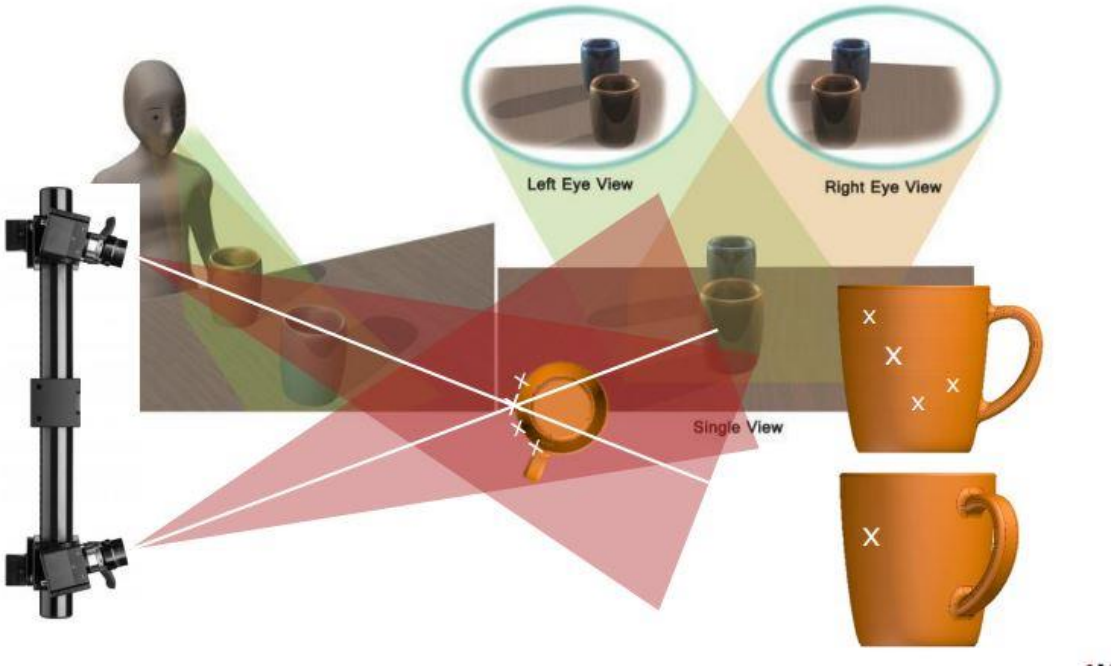


Figure 8: Illustration of DIC camera angles describing how the software identifies points in 3D space [10].

GOM ARAMIS can be used to complete two different types of displacement studies. The first type of study it is used for is point tracking. Point tracking is useful for studying the displacement and velocities of individual points in space where entire surface displacement fields are not needed. This type of study is useful to validate motion in CAD models, and for large scale displacements. Applications for point tracking with GOM ARAMIS include analyzing wind blade deflection, prosthetic design, and automotive collisions (see Figure 9).

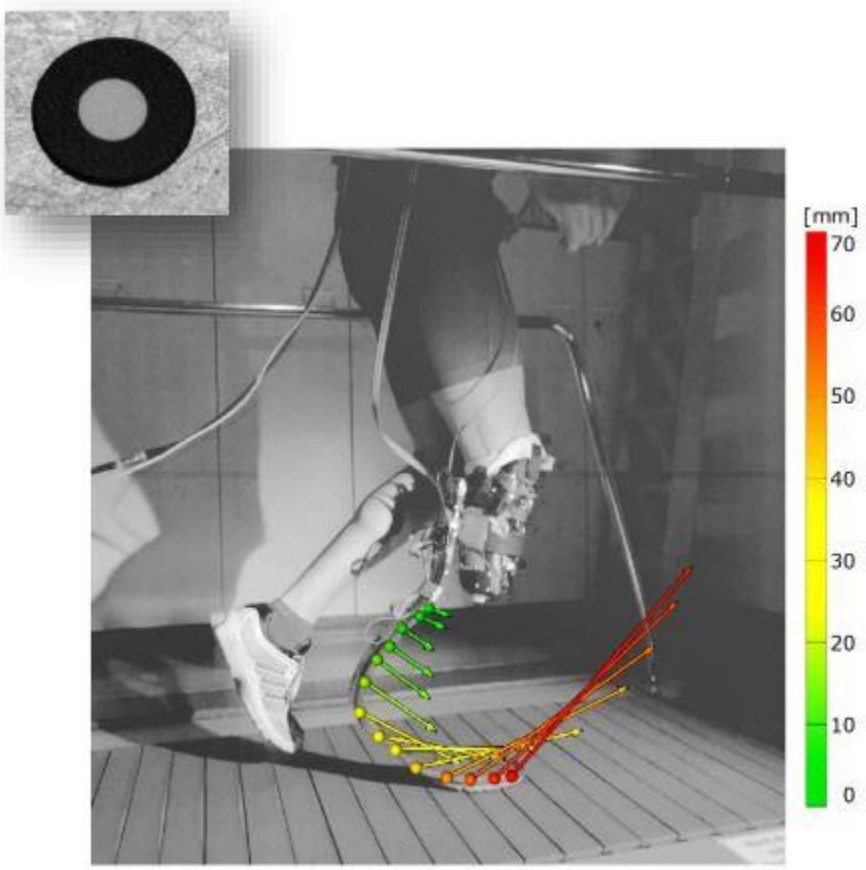


Figure 9: Example of an application of a point tracking study in GOM ARAMIS [10].

The second type of study GOM ARAMIS is capable of completing is surface correlation. Surface correlation reads displacements across an entire surface by tracking a stochastic pattern. A stochastic pattern is generally a white background sprayed with a random and unique black speckle pattern. An example can be seen in Figure 10. This type of study is suitable for material testing applications, such as the testing described later in this work. A surface correlation study can produce full field strain and displacement data

across an entire surface rather than just individual points. The DIC software eliminates the need for strain gauges and extensometers in material testing.

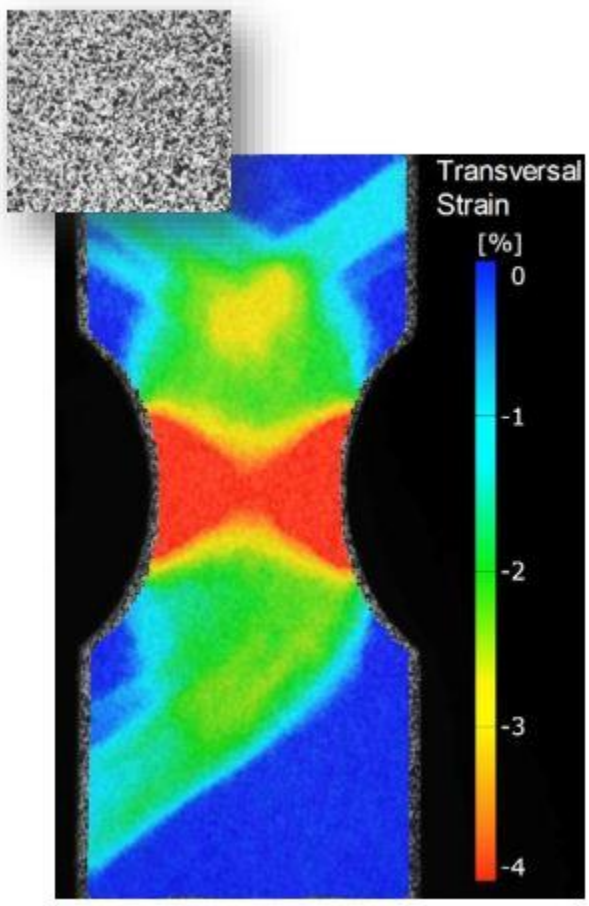


Figure 10: Example of a surface correlation study [10].

The basic principle behind GOM ARAMIS's ability to track points across a surface is facet tracking. A facet is a square group of pixels generally 10 to 30 pixels in size. Each facet contains its own unique pattern of white and black pixels. The software creates a matrix for each facet containing a value of brightness for each pixel (0 being pure black, and 100 being pure white). The software is then capable of finding each facet in both

cameras and can track its motion throughout a test. If the facet deforms in the XY plane, the facet will translate along the X or Y axes. If the facet deforms along the Z axis (closer or further from the cameras), the facet will change in size. The concept is illustrated in figures 11 and 12.

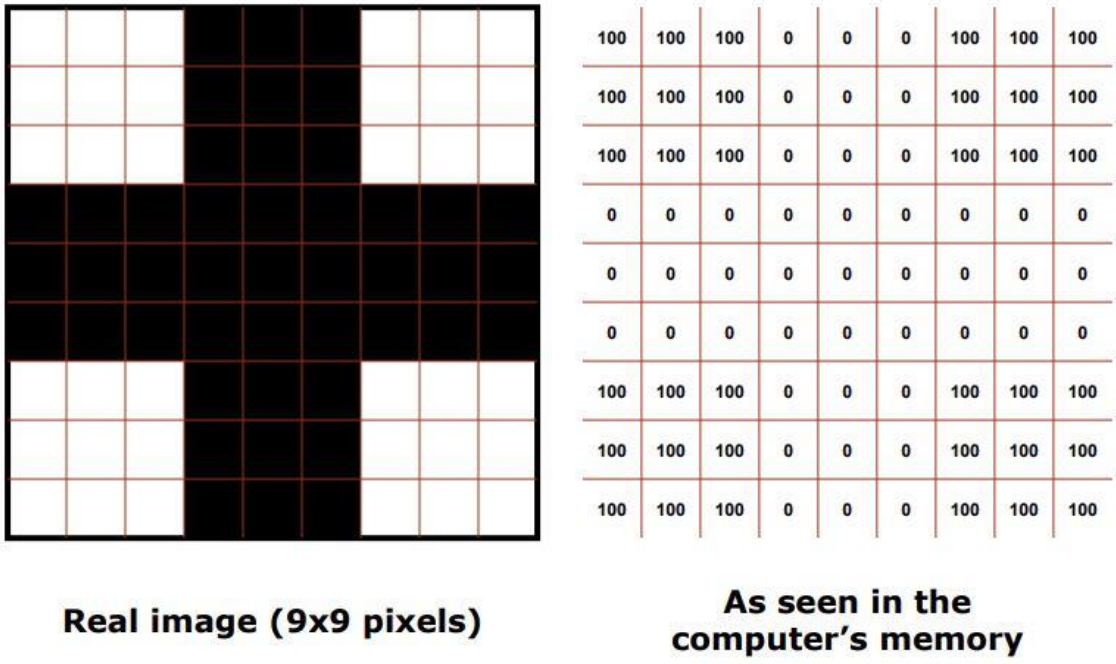


Figure 11: A DIC facet with a unique pattern of black and white (left), and its corresponding matrix stored in the software (right) [10].

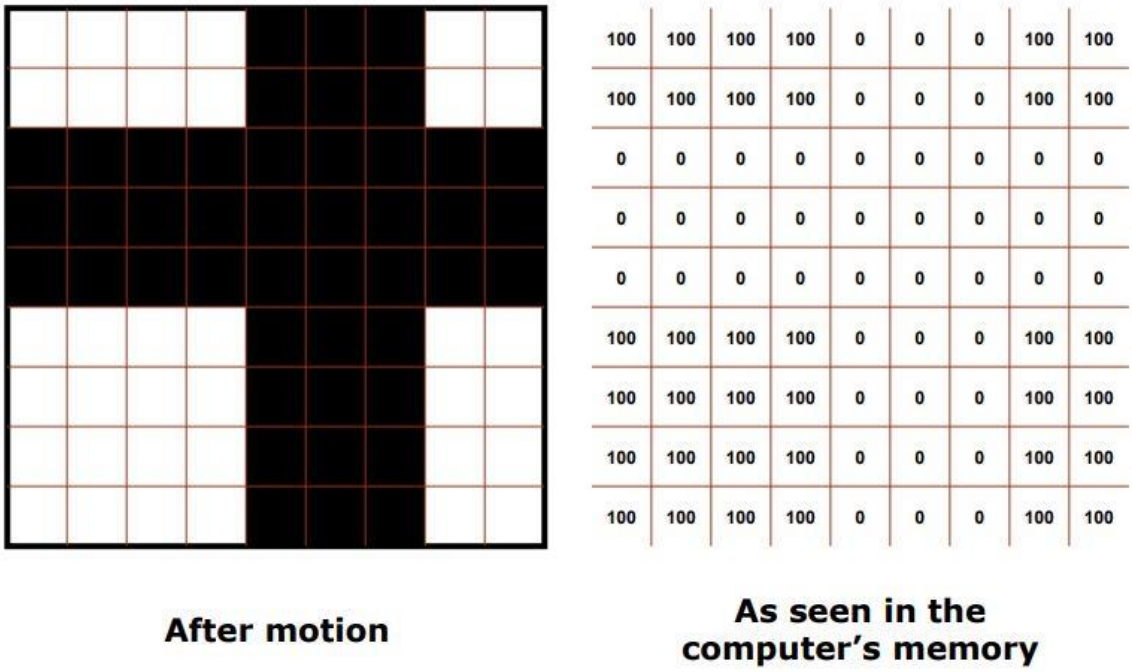


Figure 12: The same DIC facet and matrix after motion [10].

GOM ARAMIS is also capable of what is called subpixel interpolation. Subpixel interpolation is the software's ability to track the facet matrix at an accuracy much smaller than just one pixel. The software is capable of tracking the facet motion as small as $1/100^{th}$ of a pixel in the X-Y plane, and $1/30^{th}$ of a pixel in the Z direction. Some accuracy is sacrificed when moving closer or further from the cameras. Although satisfactory for most applications, it should be considered when choosing the orientation of the cameras.

GOM offers an entire DIC software suite, which is available as a resource in the department. First, GOM offers photo acquisition software in both 2D and 3D, which is used only to acquire photos to be post processed later. This software is called GOM Snap. GOM Correlate and GOM Correlate Professional are the second software packages available.

The Correlate software is used to inspect and post process the camera images acquired from a separate software. The standard version is a free software available for download, but limits inspection features. The last software, which is discussed above is GOM ARAMIS which is a complete do-all software used to acquire images, analyze, and post process data. For specific instructions for use and more information on DIC and GOM software, refer to the GOM manual [12] or the various resources provided by Trilion Quality Systems [10].

OBJECTIVES OF WORK

Problem Statement

Obvious drawbacks of the IPL exist, many of which are outlined previously. This work focuses on repairing the issue involving the IPL load data which was originally outlined in Stroili's thesis [1]. At the beginning of this work, it was discovered the load outputs during a test were inconsistent with understood knowledge of engineering mechanics and material properties. First, the Y direction loads neglected to incorporate the cross-head weight in their respective offset values. The issue was likely overlooked when the IPL was re-configured vertically. This issue could be easily solved by editing the software which transformed the loads into the X and Y components. Next, the moment output, or rotational load, was unrealistic, as previously described. The output magnitudes were significantly large, and the DIC system did not produce strain or displacement data consistent with a sample under such loading. This issue is detailed in Figure 13 below. The test reported in Figure 13 is a Y-displacement test of Delrin on the IPL. The moment loading path reports a 4000 in-lbf magnitude change throughout the tensile test. The recorded rotational load is not only geometrically infeasible, but also would result in coupon failure well before it is observed in the test. The algorithm used to calculate the loads was re-evaulated for accuracy, and the issue was determined to be mechanical.

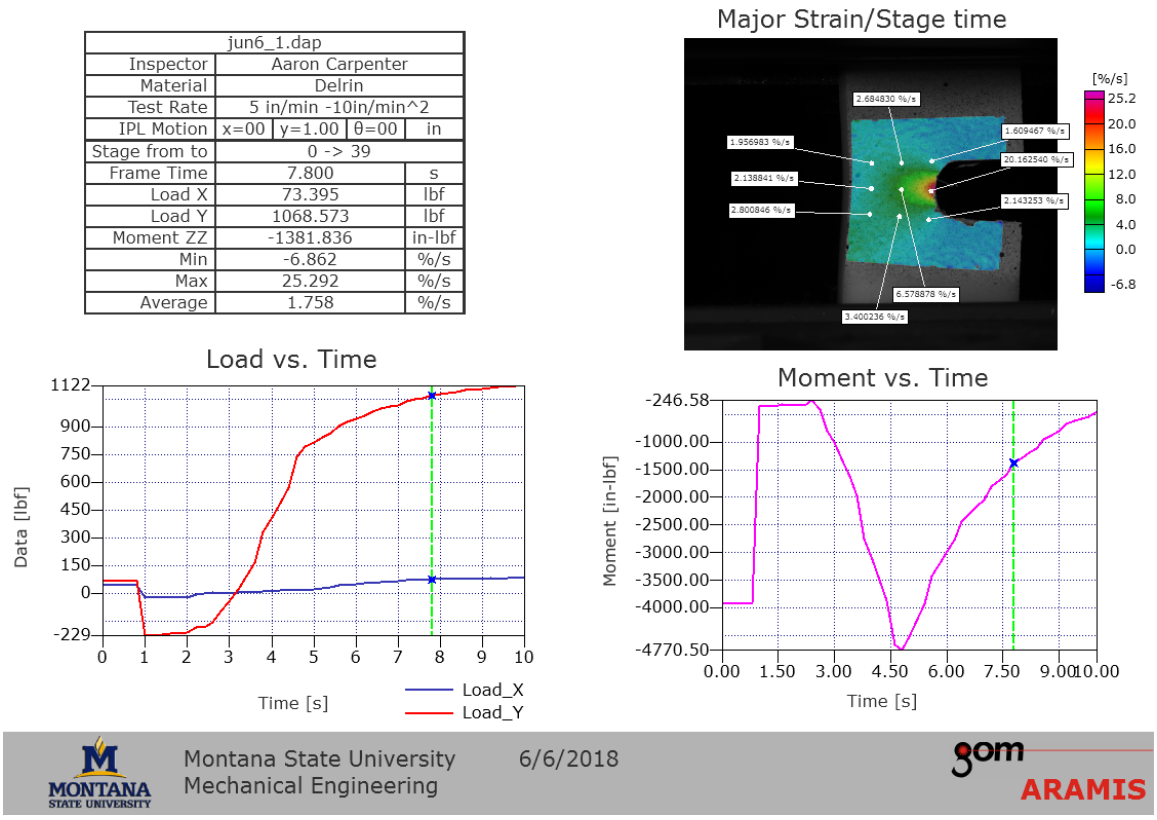


Figure 13: Report Image from ARAMIS V6 detailing inaccurate load data from the IPL.

The IPL load system is designed with pancake load cells (Omegadyne LCHD-2k) mounted on the ends of each actuator [5]. The frame geometry is such that the load lines of the actuators are far away from the grips. Because of this, a small amount of binding between the actuators, can result in a significant error in the moment readout. Also, because the load cells are mounted on the moving cross head of the IPL, the load components (X, Y, and Mzz) are dependent on both the IPL's current position, and the angles of each actuator. The IPL control software does track cross-head position and actuator angle in real time during a test. However, the frame compliance issue outlined previously, along with other errors associated in the actuator control system carry directly into the calculation of

the load components. When multiplied, by a moment arm (also dependent on IPL controls), even more error is present in the rotational load data.

The objective of the work discussed in the next chapters was to design, manufacture, and validate a solution to the load output issue. The system was to be retrofittable into the current IPL configuration, and was to be designed to read all three in-plane load components more directly.

Design Criteria and Requirements

This section provides a detailed description of each of the design requirements for the next generation IPL load system. Each requirement was to be achieved for the design project to be considered successful.

- The system was to be designed to solve the three in-plane load components applied by the IPL (X-load, Y-load, and Moment about Z-axis). It must withstand at least 2000 lbf in the Y-direction, and 1000 lbf in the X direction. The load capacity was chosen to be near the capacity of the load frame.
- The new load system was to be ‘retro-fittable’ into the current IPL and incorporate the current grips. Any solution should not require significant modifications or disassembly to install into the IPL.
- The system was to solve the loading condition independent of actuator length and cross-head position. As stated above, the current load system depends on the accuracy of the IPL position control, which potentially introduces unwanted error in the load values. Any new system must eliminate this problem.

- To save cost, the majority of the design was to be manufacturable in the student machine shop at MSU. Outsourcing parts increases costs significantly, and the project should be cost effective.
- A new load measurement system would not alter the load acquisition system currently in place on the fifth-generation IPL. By leaving the current system in place, a comparison study describing system improvements is straightforward. Also, in the event of a failed design, the current IPL functionality remains.

Validation Objective

In order to prove the accuracy of the updated load system, a validation plan must be in place. This section outlines a brief overview of the initial validation plan for the design. A detailed description of the system validation is discussed later in the validation chapter.

The moduli (stiffnesses) of a material are consistent regardless of heat treating, tempering, or annealing. Therefore, using a load frame to find these known material properties is an efficient and useful tool to validate the machine. Validating the updated IPL will involve designing and performing tests to find modulus values in both the X (shear modulus) and Y (elastic modulus) directions. The data will then be used to compare calculated moduli to values found performing ASTM standard tests using a uni-axial machine (Instron 8562). The two ASTM standard tests to be performed will be ASTM E8 (tensile) and ASTM D5379 (Iosipescu shear). Further details about these tests are discussed later in the validation chapter.

DESIGN AND MANUFACTURE

Description of Design

Components of Design

The purpose of the design was to record and calculate loads in the X-Y plane. To successfully plan a design, the required components were outlined. The design would need to convert loads applied to a specimen into voltage signals capable of being output from a data acquisition system. To complete this task the design would need to consist of three major components:

- Software component – integrated into the IPL's National Instruments LabVIEW virtual instrument, raw voltage data would be collected, filtered, transformed into components, recorded, and output via analog channels into the DIC system.
- Load Cells – the electro-mechanical interface converts applied force into voltage signals using a bridge circuit which are collected and analyzed by the IPL software.
- Mechanical component – a mechanical frame and connecting components are used to transfer loads from the specimen to the load cells. The mechanical component must also serve as the mechanical interface between the current IPL frame, and the new load system.

Mechanical Design

All figures presented in this section (Figures 17-20) detail the final revision of the design which was designed using SolidWorks [13]. The first purpose of the mechanical component is to act as an interface between the load cells and the current IPL frame. The second purpose of this component is to successfully transfer loads from the test specimen to the load cells in a manner which is simple and provides readable loads easily transformed into cartesian components.

To achieve the goal of reading loads directly and eliminating the transformation algorithm's dependency on actuator angle and cross-head position, the new load system would be incorporated into the fixed (lower) frame of the IPL. Typically, commercially available uniaxial load frames used for material testing incorporate the load cell between the grips and the actuating device. The load cell location requires load to be transferred from the specimen, through the grips, and into the load cell. Therefore, the load cell directly reads the load applied to the test specimen. The simple concept was the inspiration behind the updated IPL load system. A schematic showing the basic load cell orientation in a uniaxial machine is seen in Figure 14 below.

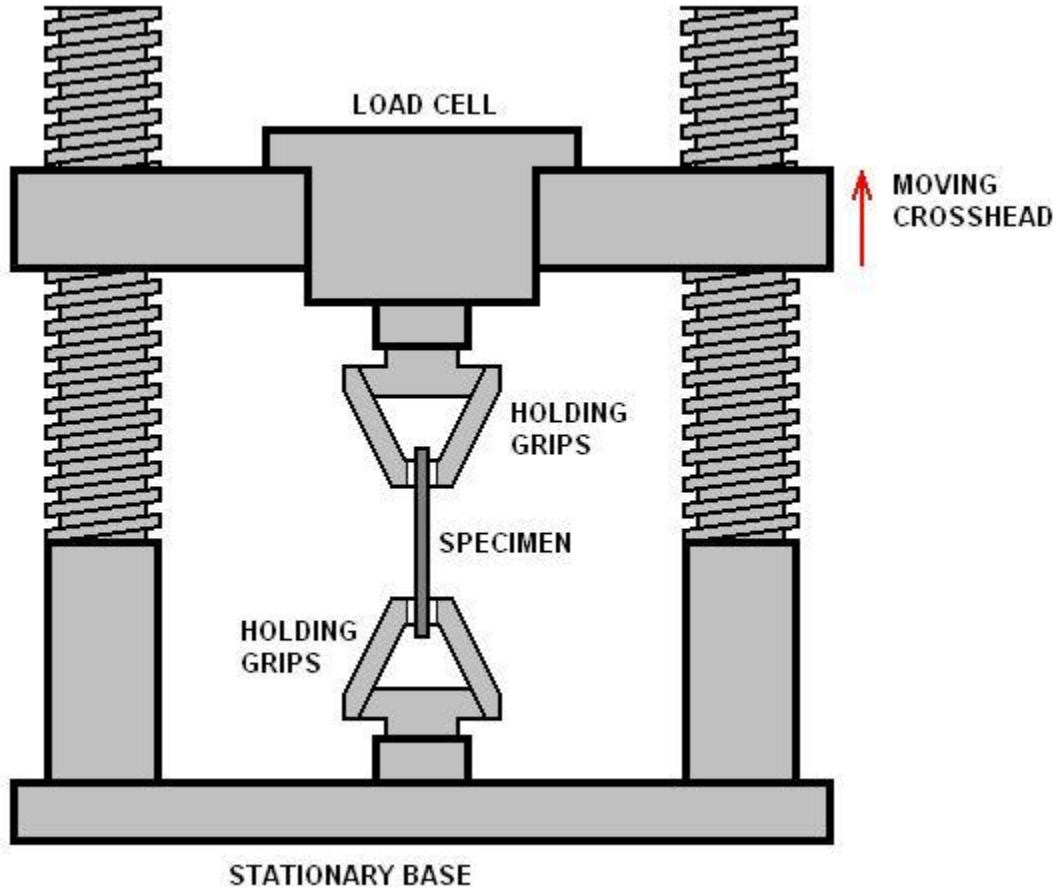


Figure 14: Schematic describing typical load cell orientation in uniaxial load frames [14].

Uni-axial test frames however, are only required to read loads in a single direction. The multi-axial nature of the IPL presents challenges when incorporating load cells in-line with the gripping fixture. Load cells generally are single degree of freedom devices. Which means a tensile/compression load cell (pictured below: Figure 15) is designed to read loads only along the loading axis. In Figure 15, the load axis is oriented horizontally through the threaded mounting studs. Any off-axis loads applied to the load cell can result in inaccuracies in data or device failure.



Figure 15: Omega LC202 single axis tension/compression load cell [15].

Restricting off-axis loading through the load cells was a major consideration in the design of the new load acquisition system. To ensure the load transferred through each load cell was only through the its respective load axis the load cells were mounted using a method of pinned joints (see Figure 16).

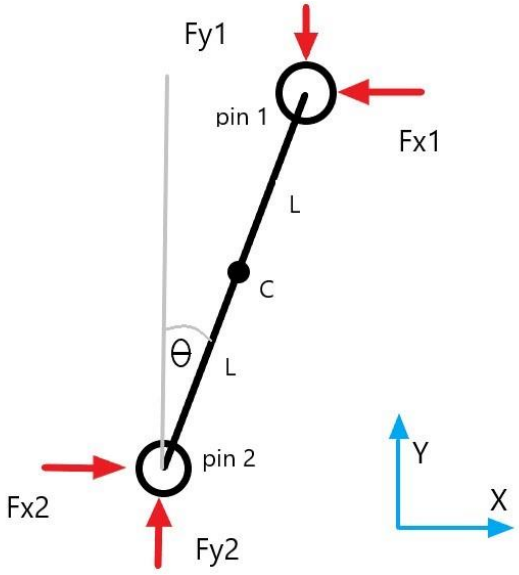


Figure 16: Free body diagram illustrating concept of double pinned joints.

Theoretically, a pinned joint cannot support a moment, or rotational load, through the joint, therefore a pinned joint on both ends of load bearing member ensures the loading is oriented along the axis of the member. This concept is illustrated in the free-body-diagram above (Figure 16). Equations 1-3 are used to complete a 2D static analysis of the in-plane forces applied to a massless member attached with pin joints at each end. Using equations 1 and 2 to solve equation 3 proves the resultant force must be oriented at the angle θ for the member to remain static. The solution is then shown in Equation 4.

$$\sum F_x = 0 = -F_{x1} + F_{x2} \tag{1}$$

$$\sum F_y = 0 = -F_{y1} + F_{y2} \tag{2}$$

$$\sum Mzz_C = 0 = L(F_{x1}\cos\theta + F_{x2}\cos\theta - F_{y1}\sin\theta - F_{y2}\sin\theta) \tag{3}$$

$$F_{y1}\sin\theta = F_{x1}\cos\theta \tag{4}$$

Often referred to as frame compliance, the grips were required to remain rigid in order to function properly. Maintaining frame compliance requires mechanical constraints for all six degrees of freedom, translation and rotation along each of the three axes. The load acquisition system needs to read the in-plane loading condition. Therefore, the mechanical constraints for X and Y translation, and rotation about the Z axis must be equipped with instrumentation to read loads. This required the implementation of at least three load cells into the design. A cut away of the load system design is shown in Figure 17 below.

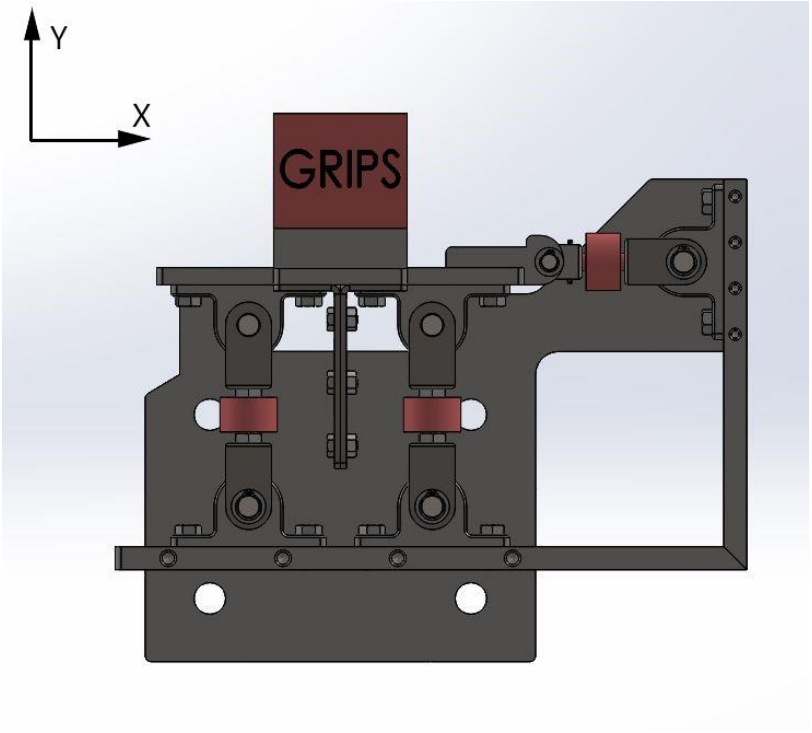


Figure 17: Cut-away model view of the updated IPL load acquisition system with three load cells (red) oriented to read in-plane loading.

Previously, the IPL grips had been secured to the IPL using a steel structure bolted in using four 5/8”-11 bolts through the frame. The structure can be seen below the grips in the current configuration IPL in the IPL chapter (Figure 6). For reasons discussed above, the new load system was to be mounted below the grips. Other than spatial constraints, integrating the design into the IPL was straightforward. The grip support structure would be removed, and the new system would be mounted inside the frame using the eight existing mounting holes.

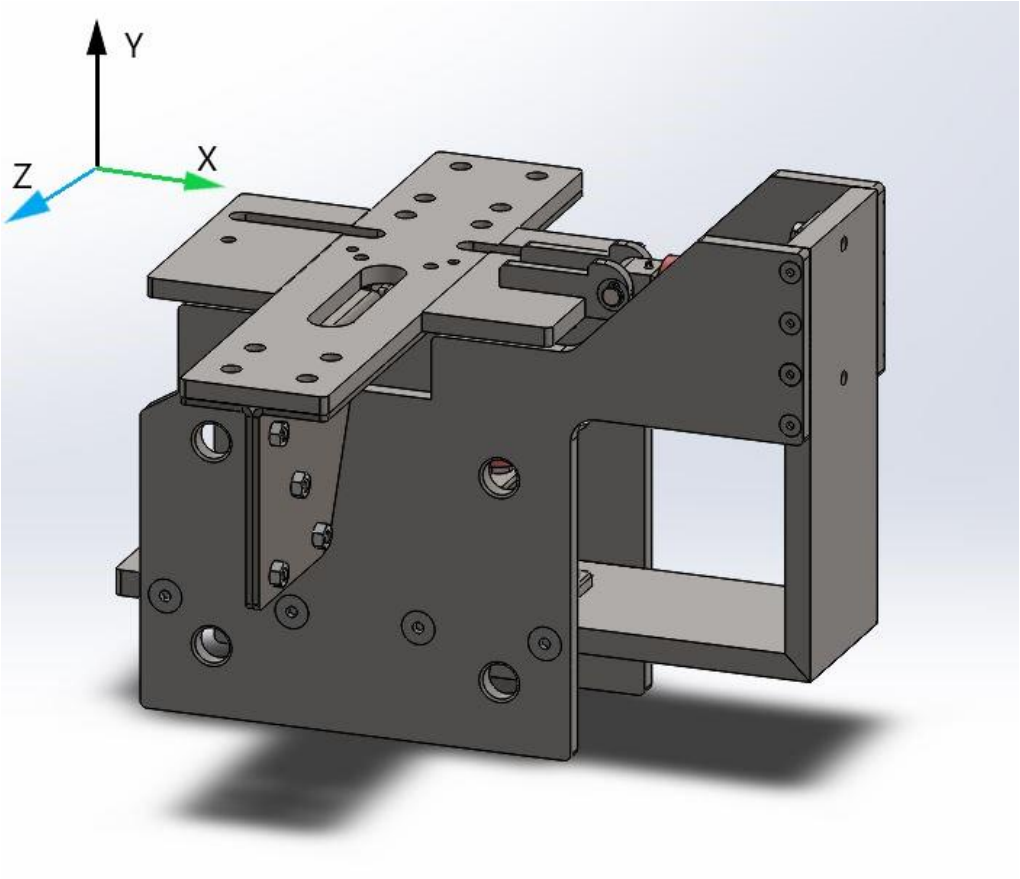


Figure 18: Dimetric model view of proposed design (without grips). NOTE: Load cells are housed between two mounting plates.

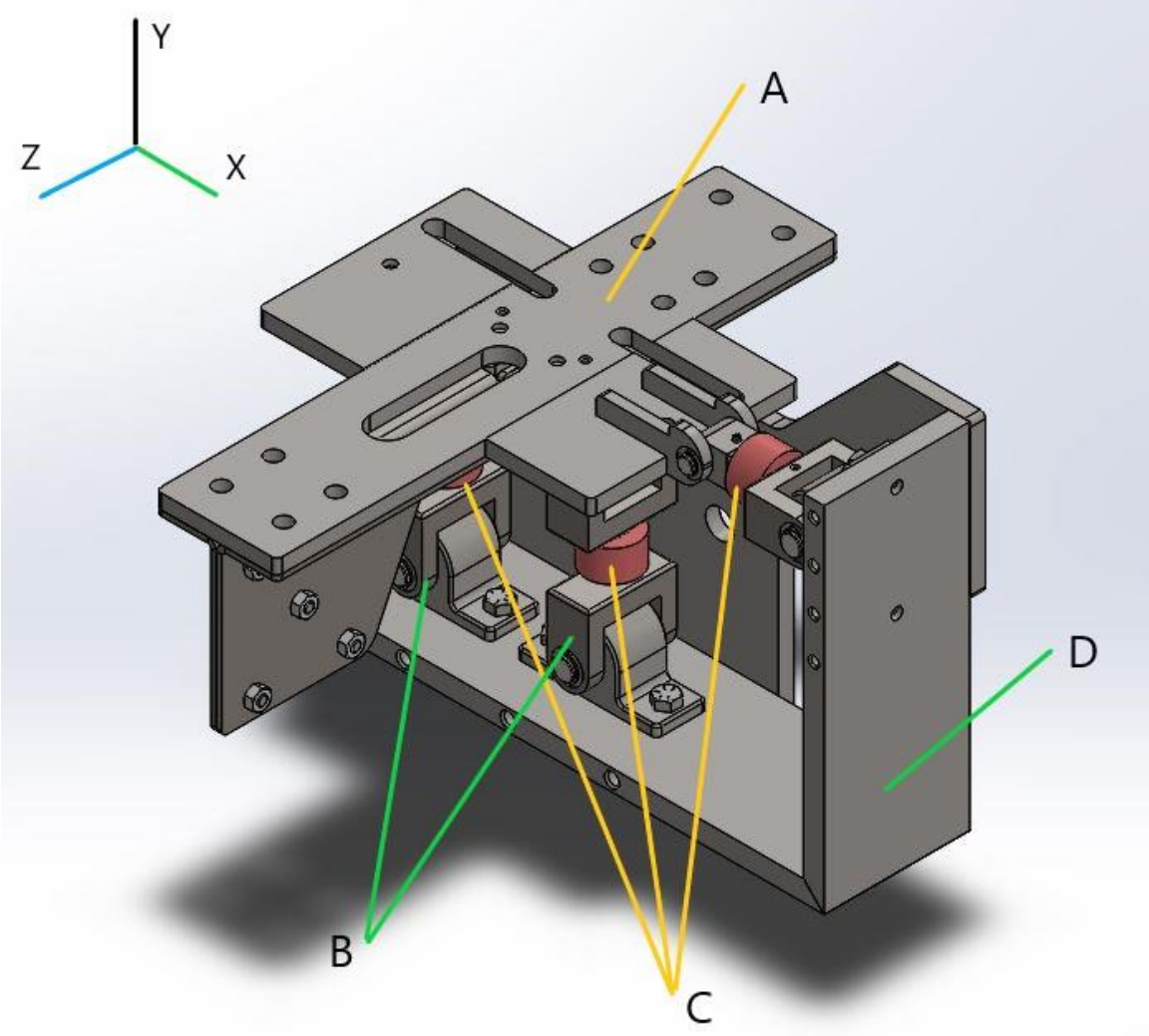


Figure 19: Isometric view of proposed design. NOTE: Mounting plate omitted for clarity. (A) Grip mounting plate. (B) Pinned joints. (C) Load Cells. (D) Housing.

Figures 18 and 19 above show model views of the proposed design for the mechanical components of the new load acquisition system. The grip plate (A) is supported above the housing (D) and IPL frame by three pinned members. Each member has a pinned joint at each end (B) and a load cell in the center (C). The design ensures the entirety of the grip loading is transferred and recorded through the load cells. The pinned joints, as

discussed above, ensure each member transfers and records loads only in the direction of its orientation. The design proposes two load cells oriented in the Y direction, and one oriented in the X direction. The rotational load can be determined by completing an elementary static analysis.

Each pinned joint is comprised of a clevis, pin, and bushing. Shims are used to compensate for machining tolerances between the bushing and clevis. The joint is designed to minimize out-of-plane bending and translation. An out-of-plane load, if present, would be transmitted through a load cell member. However, the load frame design restricts out-of-plane motion which alleviates this concern.

Another design feature worth noting is the grip stiffening bracket mounted to the bottom side of the grip mounting plate. It was found that the grip assembly and grip plate were not stiff enough to support significant gripping pressure. The gripping process applied a bending moment about the X-axis, causing significant displacement in the grip plate. The stiffener made from two pieces 10 gauge (0.130”) mild steel was incorporated to mitigate the grip bending.

Frame compliance has been a concern during previous works on the IPL. Stiffness of the new load system was taken into consideration. Static analysis using ANSYS Finite Element Analysis [16] software was completed on all relevant manufactured parts to ensure a controllable total displacement of less than 0.005” during maximum IPL loading conditions. Most IPL testing applications do not exceed displacements of 0.5”. The controllable displacement was chosen to be less than 1% of the largest displacements observed during testing. Snapshots of the FEA simulations are seen in Appendix C. A

complete drawing package and parts list for manufacturing the system is also included in Appendix B. A model view of the entire assembly including the grip assembly is seen in Figure 20.

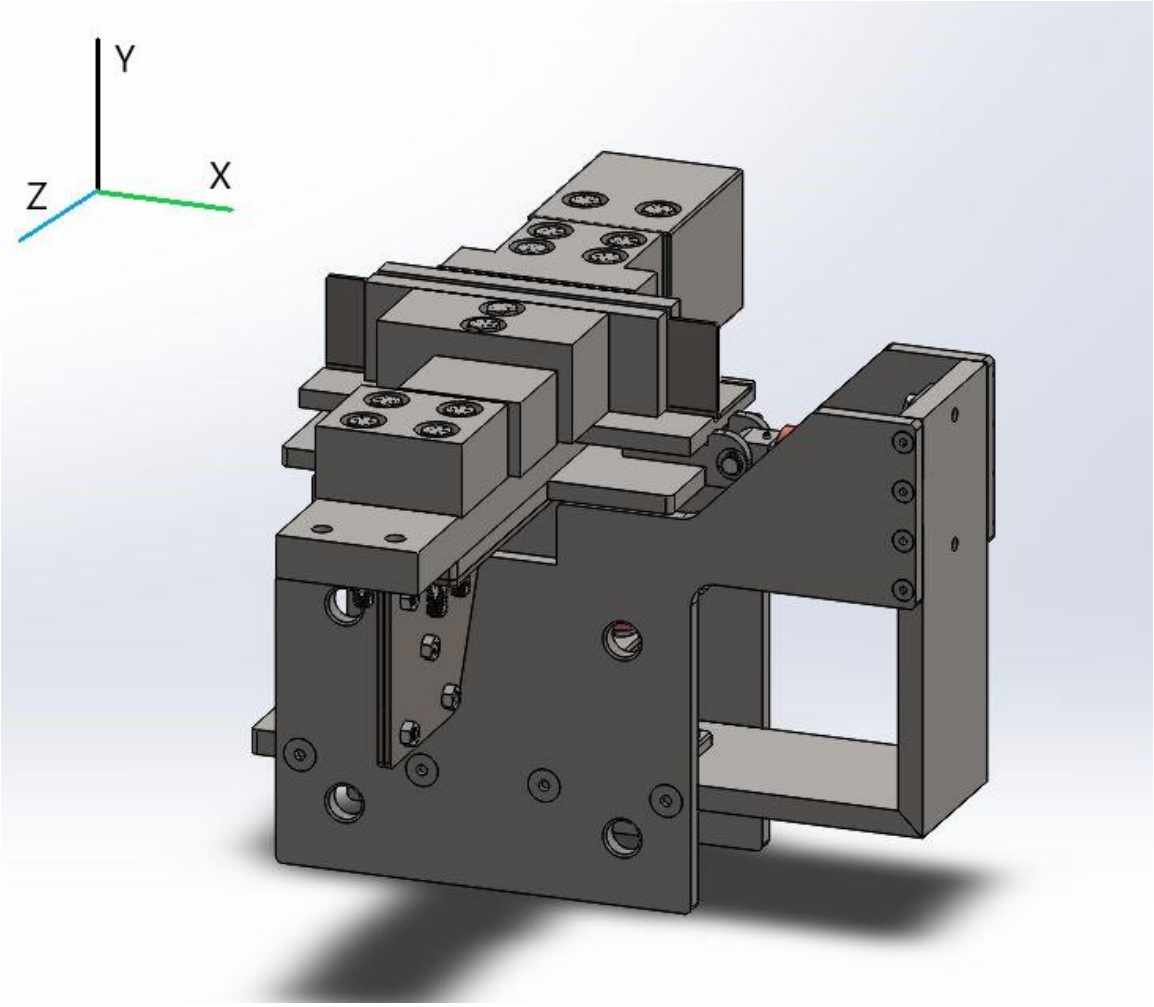


Figure 20: Dimetric view of full proposed design.

Resolving Load Components: Resolving the three load components in the coupon requires a static analysis of the grip system. The static analysis was based upon an imaginary cut through center of the coupon. For the system to remain in static

equilibrium, all three equilibrium equations must be satisfied. The three equilibrium equations are below in Equation 5, 6, and 7. The free body diagram used to resolve the loads in the system is seen in Figure 21.

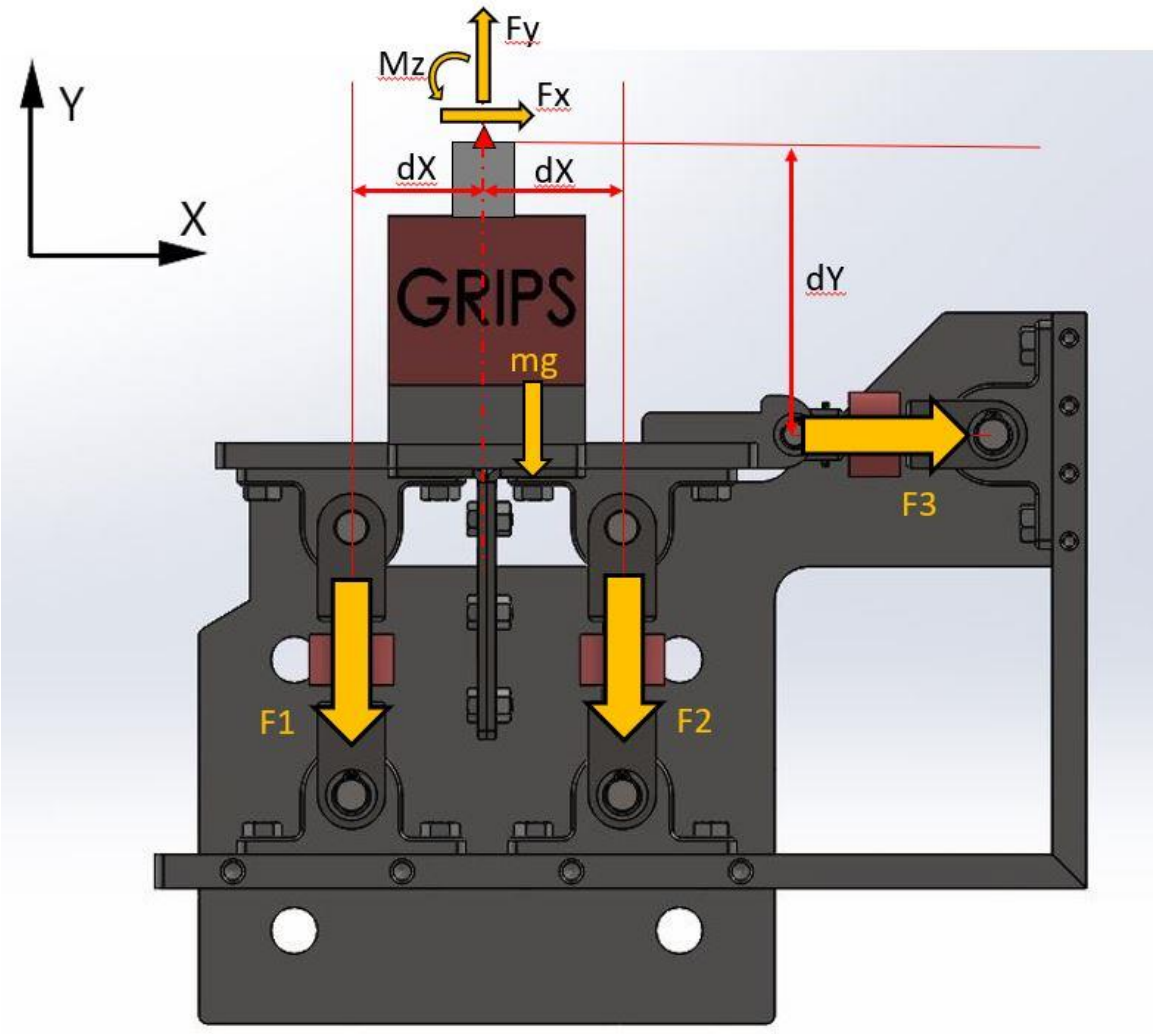


Figure 21: Free body diagram describing the loads applied to the system. NOTE: The reaction forces are oriented around the center of the coupon and all loads are drawn in their respective positive orientation.

$$\Sigma F_x = 0 \tag{5}$$

$$\Sigma F_y = 0 \tag{6}$$

$$\Sigma M_z = 0 \tag{7}$$

To resolve the reaction forces at the center of the coupon, the forces and dimensions described in the free body diagram (Figure 21) are input to the three equilibrium equations. In this case, ‘dX’ and ‘dY’ are 2 inches and 3.48 inches, respectively. These values are coded into the MATLAB script which resolves the loads in the IPL software. The resolved reaction forces (Fx and Fy) and moment (Mz) are shown in Equations 8, 9, and 10. It is important to note the constant ‘C’ in Equation 10 is the moment applied by the weight of the system.

$$F_x = -F_3 \tag{8}$$

$$F_y = F_1 + F_2 + mg \tag{9}$$

$$M_z = (-dX * F_1) + (dX * F_2) - (dY * F_3) + C \tag{10}$$

The solution above is based off the assumption that the center of the coupon is rigid throughout the test. This is not entirely accurate and presents some amount of error in the moment solution (Equation 10). However, the ability to continuously read the position of the center of the coupon and communicate that position change to the IPL software would be an incredibly complex system.

Load Cells

Load cells are an electro-mechanical device capable of converting mechanical loading into voltage signals. Load cells use a Wheatstone bridge circuit generally with four strain gauges [17]. A strain gauge type load cell requires an input voltage to power the bridge circuit. As force is applied to the cell, the resistances of the strain gauges change which results in an output voltage change across the bridge. The voltage signal is then amplified and conditioned using a load cell conditioner.

For load cell selection, the main considerations were load direction, size, and capacity. First, the design requires the ability to read loads in both compression and tension, so cells capable of reading loads in both directions along the load axis were necessary. The next consideration was size as it was important to find a load cell which fit into the limited design volume under the IPL grips. Miniature load cells with two male threaded studs to thread into the clevises were selected. Lastly, the system needed to be capable of reading at least 2000 lbf in the Y-direction and 1000 lbf in the X-direction. Omega LC202-3K miniature load cells were chosen (pictured above in Figure 15). The 3000 lbf capacity exceeded the necessary capacity of the system, but satisfied the requirement nonetheless. More information on the load cells can be found in the Omega Engineering data sheet [15].

To compliment the load cells, load cell conditioners were employed to amplify and filter the output signals from the load cells. Load cell output signals are generally in the range of ±30mV, which is difficult to read using a data acquisition system. A load cell conditioner amplifies the signal to a range of ±10V and filters out signal noise. Omega Engineering DMD-465 load cell conditioners were chosen for consistency with the load

system already in place. More information on load cell conditioners and DMD-465 specifications is found in the Omega data sheets [18].

Software Component

The IPL position control and load acquisition software are written using a combination of National Instruments LabVIEW and MATLAB. The load acquisition software was already in place for the three existing load cells. Integrating the new load system included finding the signals in LabVIEW, tracking them through several sub-VI's, and creating three new load cell channels. The LabVIEW software incorporates MATLAB scripts into the VI. A static analysis of the mechanical design was completed to write the MATLAB script which was used to transform the loads from respective cells into cartesian components.

Coupon Geometry

A coupon 5.5" in length, 1" in width with 0.188" material thickness was used for all of this work. The MATLAB script resolves load components assuming all tests performed on the IPL would be completed using a 5.5" long coupon, and the grips are configured for 1" coupon width and 0.188" material thickness. Notch geometry was not a primary concern for standardizing a coupon, notch geometry should be selected based on material strength, IPL motion, and desired failure mode. An example of an IPL test coupon is seen in Figure 22.

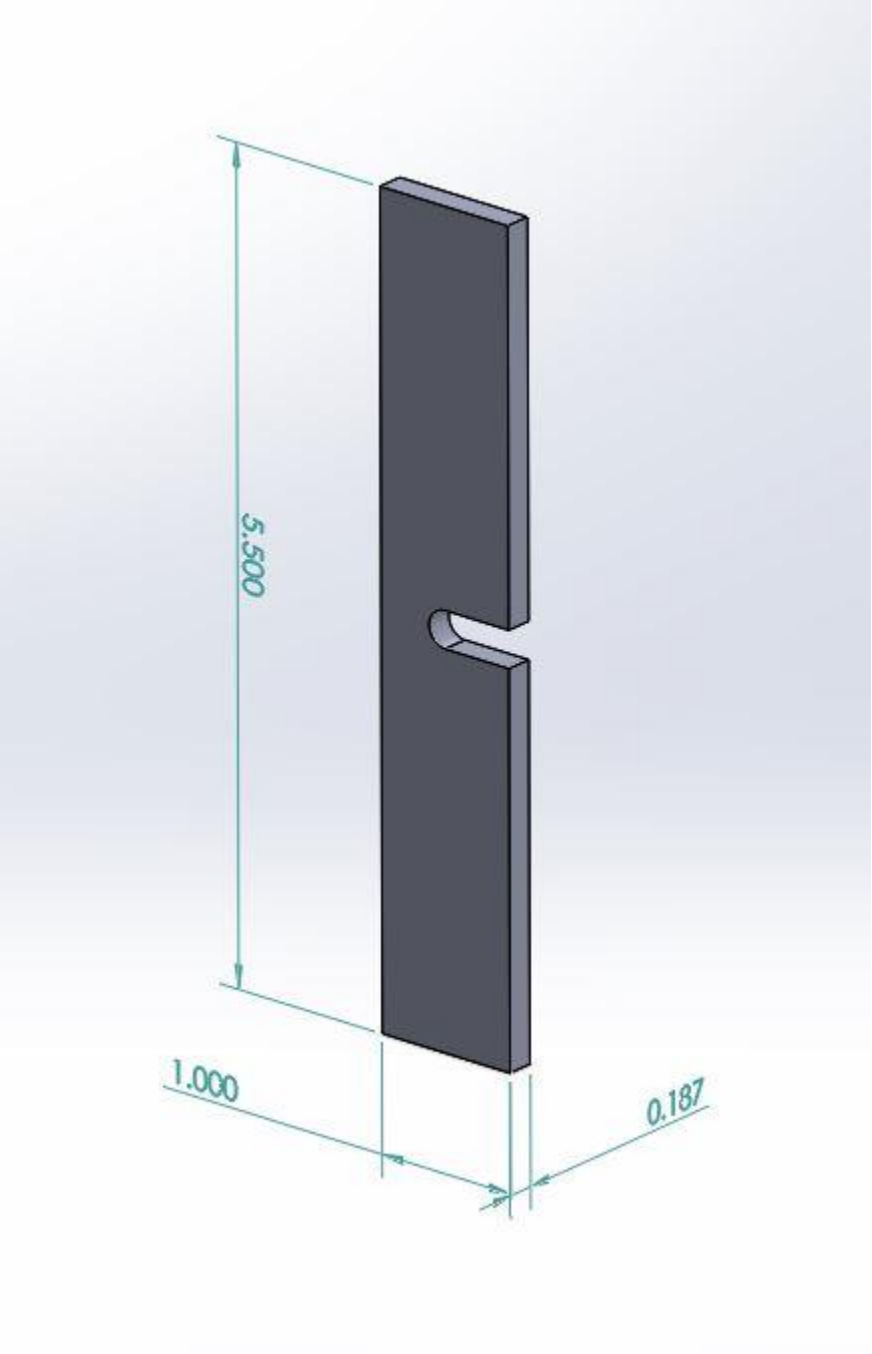


Figure 22: Detailed coupon geometry. NOTE: Notch geometry can change based on material and test parameters.

Changing Coupon Geometry: If changing coupon geometry is necessary, it is important both the software is changed, and the grips are reconfigured. The rotational load component is dependent on coupon length and the grip spacers are oriented to keep a 0.188” coupon centered on the load plane. To adjust the coupon length, the MATLAB script calculating the load components is modified. The moment is dependent on the distance (Y) between the X load cell and the center of the coupon. The distance is currently set to 3.48” which incorporates half the coupon length and assembly geometry. The MATLAB script is found in the VI titled ‘ProcessAxesLoads.vi’. It is also shown in Figure 133 in Appendix C.

To adjust the coupon width, the fixed side supports on the grips (left side from IPL controls) must be adjusted to where the coupon is centered in the grips. To significantly adjust the material thickness, the grip spacers located behind the fixed grip faces must be changed to a thickness where the center plane of the coupon is centered inside the IPL frame.

Fulfillment of Design Criteria

This section briefly describes how the proposed design satisfies the design requirements which are all outlined above.

- The system is designed to solve all three in-plane load components (X, Y, and M_{zz}) using three load cells and elementary static analysis techniques. The components were designed to limit controllable deformation to 0.005” under 2000 lbf in the Y-direction and 1000 lbf in the X-direction.

Controllable deformation includes all manufactured parts. (i.e. housing, bushings, and clevises)

- The system is easily installed into the IPL lower frame by removing the current grip support block. The new load acquisition system is mounted into the frame via the same eight mounting holes. (NOTE: see manufacture and installation chapter)
- Having been designed to fit under the fixed grips, the updated load system eliminates the load measurements' dependency on the actuator angle and cross-head position.
- Each of the mechanical components are simple and manufacturable using resources available to students in the Montana State University machine shop. (NOTE: see Manufacture and Installation section.)
- The proposed design incorporates three new voltage channels into the IPL control software leaving the original three in place. The mechanical modifications to the frame also do not alter the current load acquisition system.

Manufacture and Installation

Manufacturing began in February 2019 and was completed in April 2019. Later however, several minor modifications were manufactured after initial assembly and testing. As previously mentioned, much of the manufacturing was completed in the MSU student machine shop using manual milling machines, lathes, and a three-axis CNC machine. Parts not manufactured in the student machine shop were manufactured by J.E. Soares, a sheet

metal manufacturer in Belgrade, MT. Necessary welding was completed in the MSU welding shop. Initially, pillow block ball bearings were purchased to be used as supports for (5) pinned joints. However, a self-aligning feature allowed for significant out-of-plane bending. The bearings were replaced by machined bushings described in the previous chapter. The modification was completed during the assembly process. All parts and assemblies were manufactured to specifications outlined in the drawing package located in Appendix B.

Prior to final installation, each load cell was individually calibrated, and the system functionality was confirmed. Details regarding the calibration are outlined in the following chapter. Installation did require material removal from the IPL frame. The grip mounting location has been modified several times over years of projects and modifications on the load frame. A small amount of material was removed using a reciprocating saw to eliminate interference between the grip plate and the frame. The mounting holes in the frame were also required to be bored out due to a machining mistake when tapping the threaded mounting holes in the housing side plate (see Appendix B). After these minor modifications, installation was a drop-in procedure. The load cells and signal conditioners were installed per instructions [18], [19].

SYSTEM CALIBRATION

The software reads voltage signals from the load cell system. Each individual voltage corresponds to a unique load. However, a calibration was required in order to know how to convert each voltage into a load value.

Load cells are linear devices which makes calibration straightforward. If a voltage is recorded at two known load values, the sensitivity (slope) and intercept of the load cell/signal conditioner combination can be found. The first step to calibrate the system was to set up the load cell conditioners by adjusting the zero offset and voltage adjustment per the DMD-465 user guide [18]. Once the zero offset and the voltage adjustment has been set, the settings are not to be changed unless a new calibration is completed. Load cell calibration can be completed one of two ways. The first method is called shunt calibration. To perform a shunt calibration, a large precision resistor (59 kΩ) is bridged across an input and output lead of the load cell. The resistor simulates a load by changing the resistance of a leg of the Wheatstone bridge circuit [20]. A simulated shunt calibration load value for each individual load cell is supplied from the manufacturer. A circuit diagram showing a shunt calibration on a Wheatstone bridge is shown below (Figure 23).

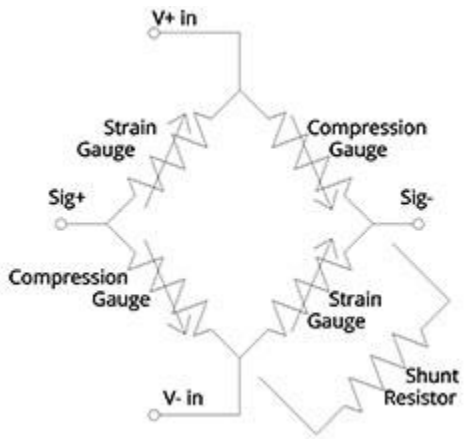


Figure 23: Circuit diagram detailing a shunt calibration [20].

The second method for calibrating load cells is to apply at least two different known weights and find the equation of the line. This method is most accurate when a load nearing the capacity of the load cell is applied. However, because of the instrument's linear nature, it is still simple and still very accurate when using smaller loads. The benefit of using this method is being able to calibrate a load cell the way it is configured in a system. In this case, jam nuts were used to lock the clevises in place on the load cell studs. Calibrating the load cells with the clevises secured meant the loads were calibrated for the system configuration. A photo of the calibration using a set of precision weights (100 lbf) is shown in Figure 24. The calibration curves for each of the three loads cells are also shown in Figure 25.



Figure 24: Load cell calibration using various known loads.

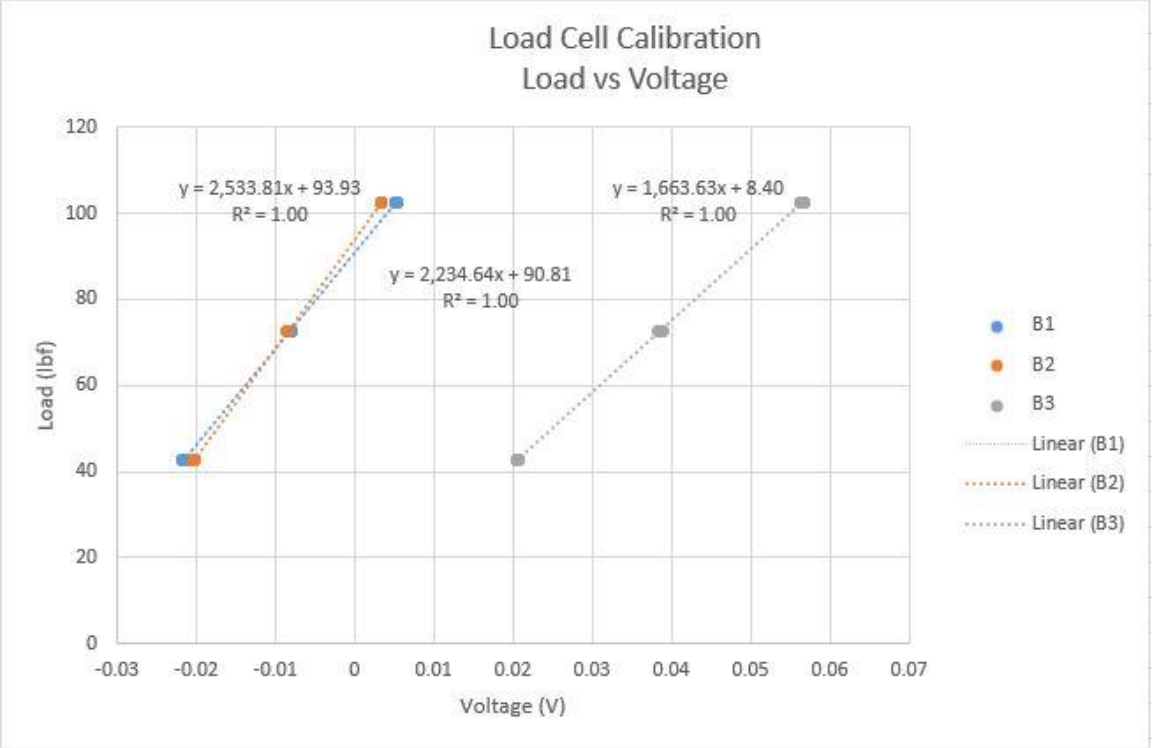


Figure 25: Load cell calibration curves for three new load cells generated using three known loads.

The linear fit equations for each load cell contained a sensitivity (slope) and a zero-load intercept. The LabVIEW software was written to accept both the sensitivity and the offset as input parameters.

The calibration discussed up to this point was completed prior to final assembly and installation. The final calibration step was required after the load acquisition system was installed. The weight of the grip assembly and the nature of bolted joints in the assembly preloaded the load cells. These values (zero-load offset values) needed to be subtracted off in the MATLAB script which converts the three load cell values into cartesian components. The offset values were found by collecting load data for an empty

test and finding the corresponding Y-offset and X-offset. The respective loads were subtracted directly from the cartesian load components rather than individual load cells.

VALIDATION AND RESULTS

The final step in the process was to validate the system. As previously discussed, the moduli of a material are consistent regardless of heat treating, tempering, or annealing. The goal of the validation process was to validate the updated IPL load acquisition system in both the X and Y directions. To validate the system in the Y direction, quasi-tensile tests were performed using the IPL and the DIC system. The elastic modulus was extracted from the data. To validate the system in the X direction, Iosipescu-inspired tests were performed on the IPL and shear modulus was extracted. The data were then compared to data collected during ASTM standard tests.

Materials and Preparation

The material selected to complete each validation test was Copper 110 (ASTM B187) [21]. The reported tensile strength is 37.5 ksi, and elastic modulus is 17.0 Msi. The material was chosen because of its machinability, and because the material properties are well understood.

ASTM Standard Testing Procedures

Data was collected from two different ASTM standard tests for the purpose of validating the IPL load system. The first test completed was ASTM E8, the standard method for tension testing of metallic materials [22]. The coupon is a standard dog bone profile. The coupon was tested on an Instron 8562 uniaxial load frame at a rate of 0.001 in/s. Elongation data for each of the tests was collected using an extensometer incorporated

into the load frame data acquisition system. For more information regarding the testing procedure, refer to the ASTM standard [22].

The second standard test completed was a double V notch shear test, also referred to as an Iosipescu shear test. The procedure was completed per the ASTM D5379 procedure [23]. DIC was used to collect strain data rather than using two orthogonal strain gauges. Testing was also completed using the Instron 8562 uniaxial load frame. The Iosipescu test also requires the use of Wyoming Test Fixtures' V-notch shear fixture. Figure 26 details the fixture and the testing procedure [24].

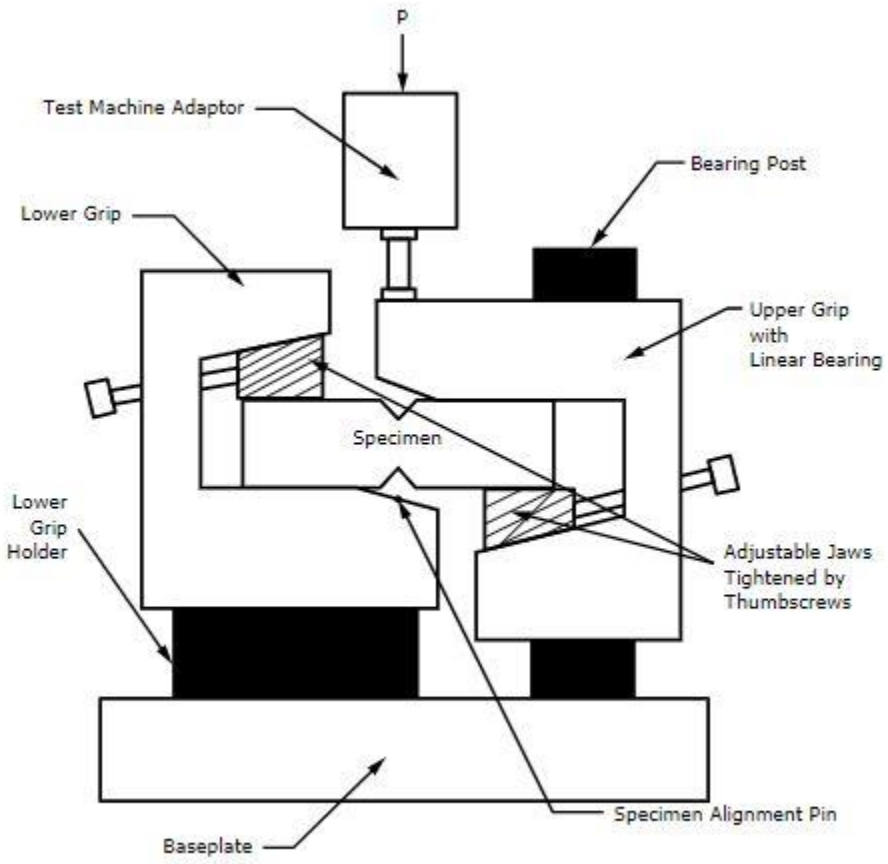


Figure 26: Schematic detailing Wyoming Test Fixtures' V-Notched Shear (Iosipescu) fixture [23].

The fixture is designed such that the bending in the test specimen is theoretically reduced to zero through the notched section. To minimize bending effects, it is important to pay attention to the specimen position in the fixture. The idealized shear-moment diagrams which detail the assumption of zero bending at the center of the specimen are seen below in Figure 27.

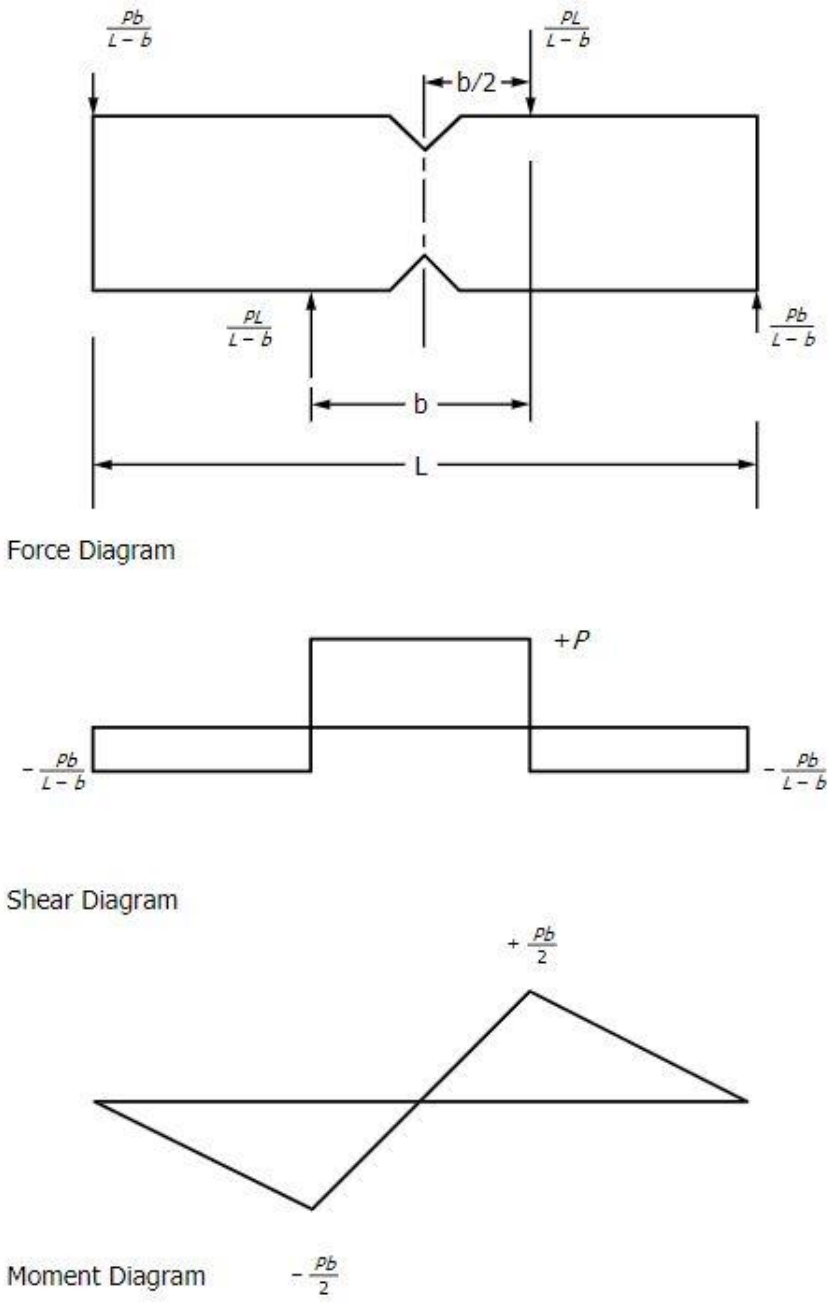


Figure 27: Idealized shear-moment diagrams for ASTM D5379 test and fixture. NOTE: bending is zero at the center of the specimen [23].

IPL Testing Procedure

In the past, the IPL used a single notched coupon similar to the coupon seen above in Figure 22. This coupon induces a multi-axial loading condition due to its lack of symmetry. The coupon works well for completing multi-axial material research, however, it does not lend itself to verifying the accuracy of the load system. To validate the updated load system, two tests were designed, one for each planar direction. The two tests were inspired by the ASTM standard testing procedures discussed previously, and the data were later compared to data collected using the ASTM testing procedures.

To validate the system in the Y (vertical) direction, a tensile test coupon was designed. The desired load capacity for the IPL is about 2000 lbf in tension, so the cross-sectional area needed to be small enough to yield before reaching that threshold. The coupon's dog bone section needed to be sufficiently long to align the stress uniformly across it. The ASTM tensile test performed was completed at a rate of 0.001 in/s. For consistency, the IPL rate input was equivalent. DIC was used to produce an arithmetic mean strain value through the gauge section. The Y displacement was input as 0.4 in. A solid model of the tensile coupon is seen in Figure 28.

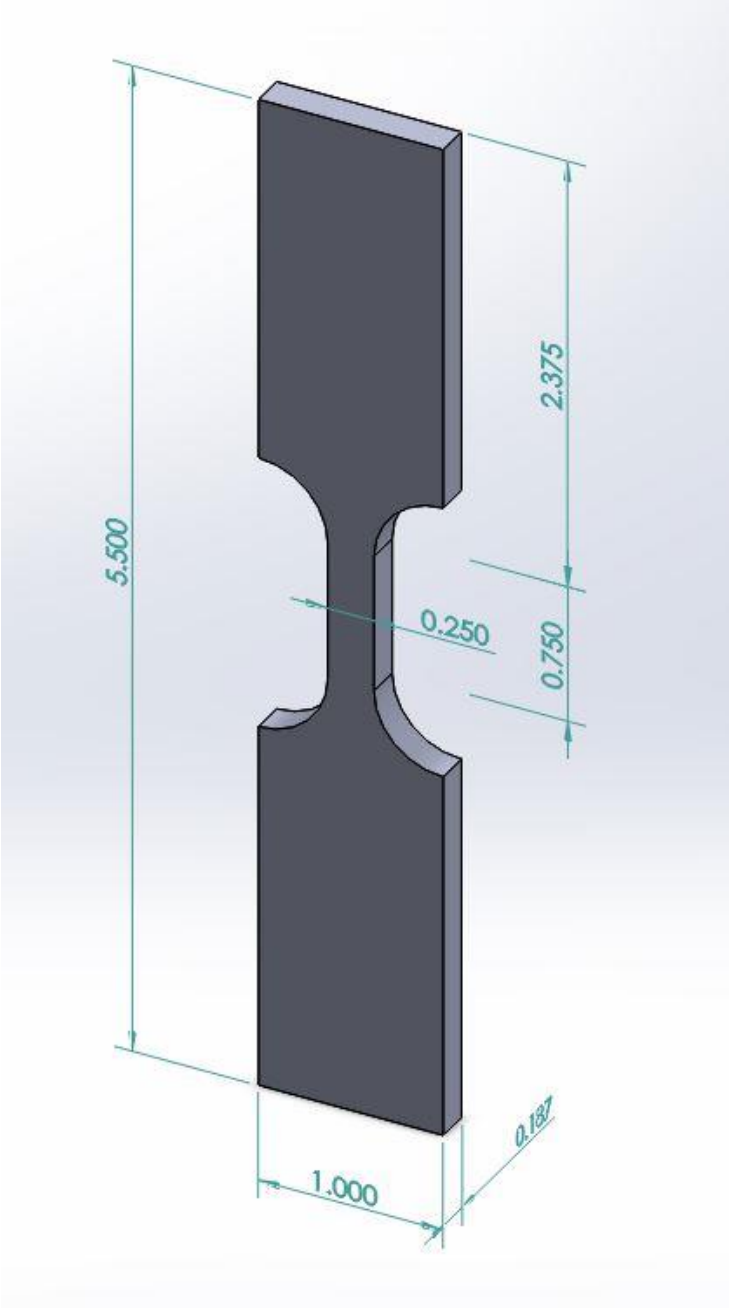


Figure 28: IPL tensile test coupon used to validate the IPL load system in the Y-direction.

Designing a test to validate the X direction presented more challenges. Grip slippage is still an issue when test motion is purely in the X direction, this needed to be

minimized. The standard Iosipescu test is generally used for composite materials instead of isotropic materials. However, the geometry of the coupon and prescribed motion lent itself to the IPL. Pure shear would be nearly impossible to create given the nature of the load frame, therefore, some bending was inevitable while using the IPL. Processing the data would require analyzing a multiaxial loading condition. Although bending is theoretically mitigated in the Iosipescu test, the idea was to generate similar values for shear modulus (G). The standard test was completed a rate of 0.001 in/s, so the IPL speed was set to the equivalent rate. The IPL X-displacement was set to 0.3 in. The IPL V-notched shear coupon used for validation is seen in Figure 29.

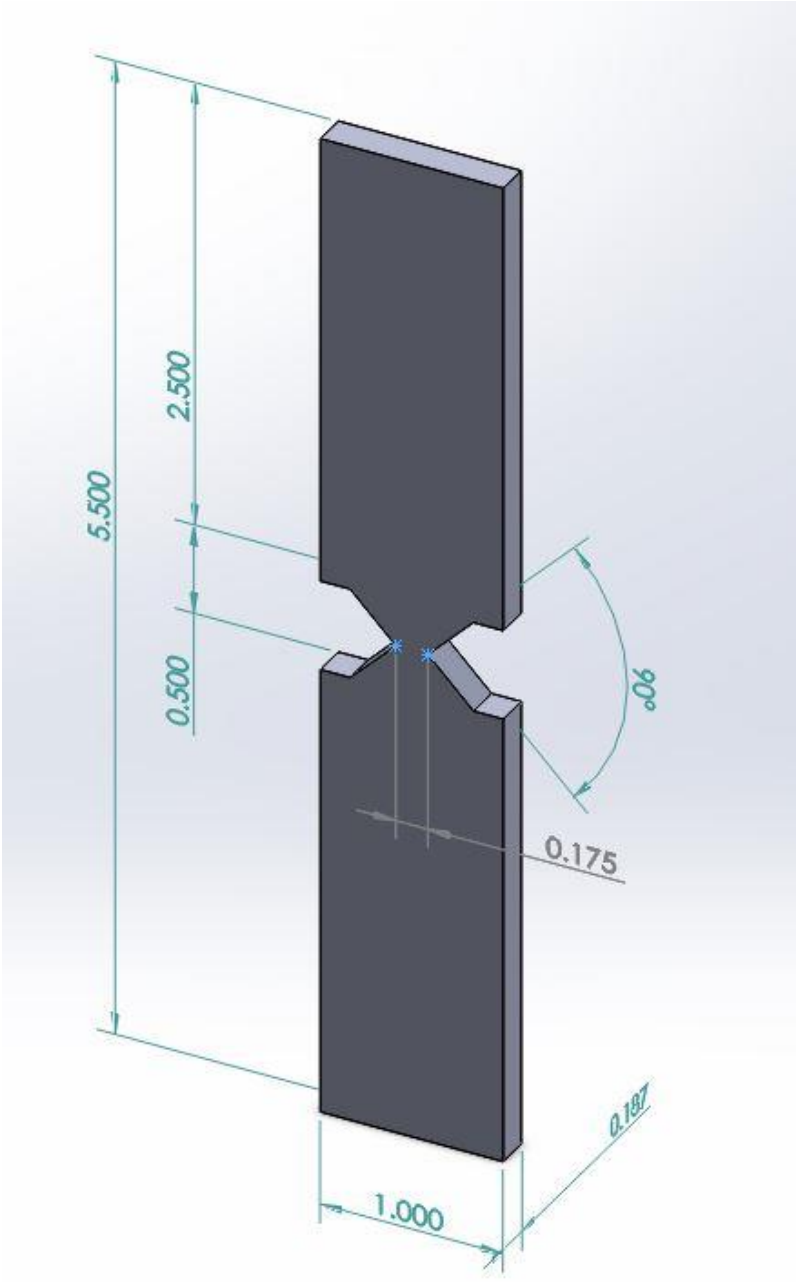


Figure 29: IPL double notched shear coupon used to validate the load system in the X-direction.

DIC Methods

ARAMIS is capable of reading voltage inputs though three analog channels. Load channels were connected to the DIC computer from either the Instron, or the IPL. The cameras were calibrated and an image series was acquired per the instructions provided by GOM [12]. Post processing included calculating, exporting, and plotting the data.

Calculating strain with ARAMIS requires creating a surface component. The surface is created based on two parameters, facet size and facet distance. Facet size is to be determined based on the size of the stochastic pattern and the camera distance. Generally, it is good practice to keep the facet size between 10 and 30 pixels [10]. The software performs best when each black speckle in the pattern is roughly 3 to 7 pixels, and the facet size is to be chosen to contain 3 to 7 speckles. Facet distance defines the overlap of facets on the surface. Facet distance should always be between half the facet size and the facet size. This prevents excessive overlap or gaps on the surface [10]. Figure 30 details facet size and facet distance for a stochastic pattern, and Figure 31 shows a DIC surface component on the surface of an Iosipescu test coupon. For most of this work, facet size was set to 17 pixels and facet distance was set to 10 pixels. However, for some later tests (Iosipescu B series), facet size was set to 25 pixels with a 17-pixel facet distance.

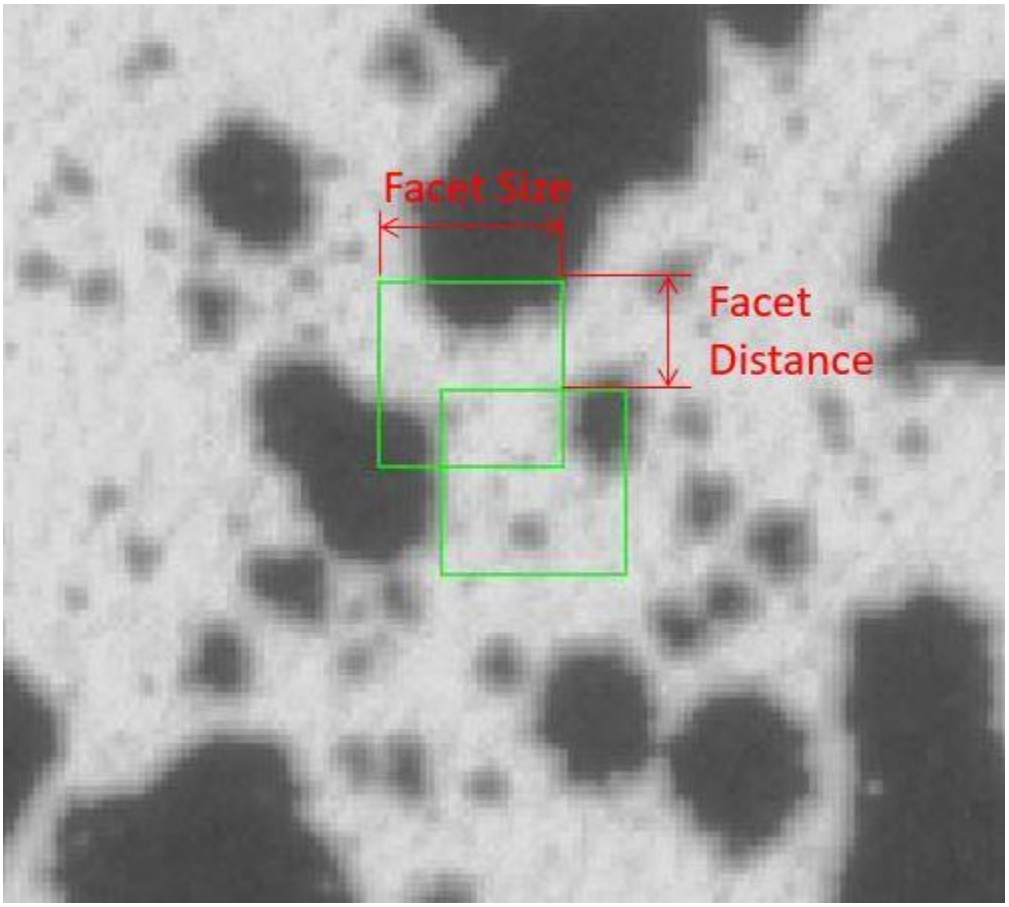


Figure 30: Detailed view of stochastic pattern showing facet size and facet distance used to create a surface component in GOM-ARAMIS.

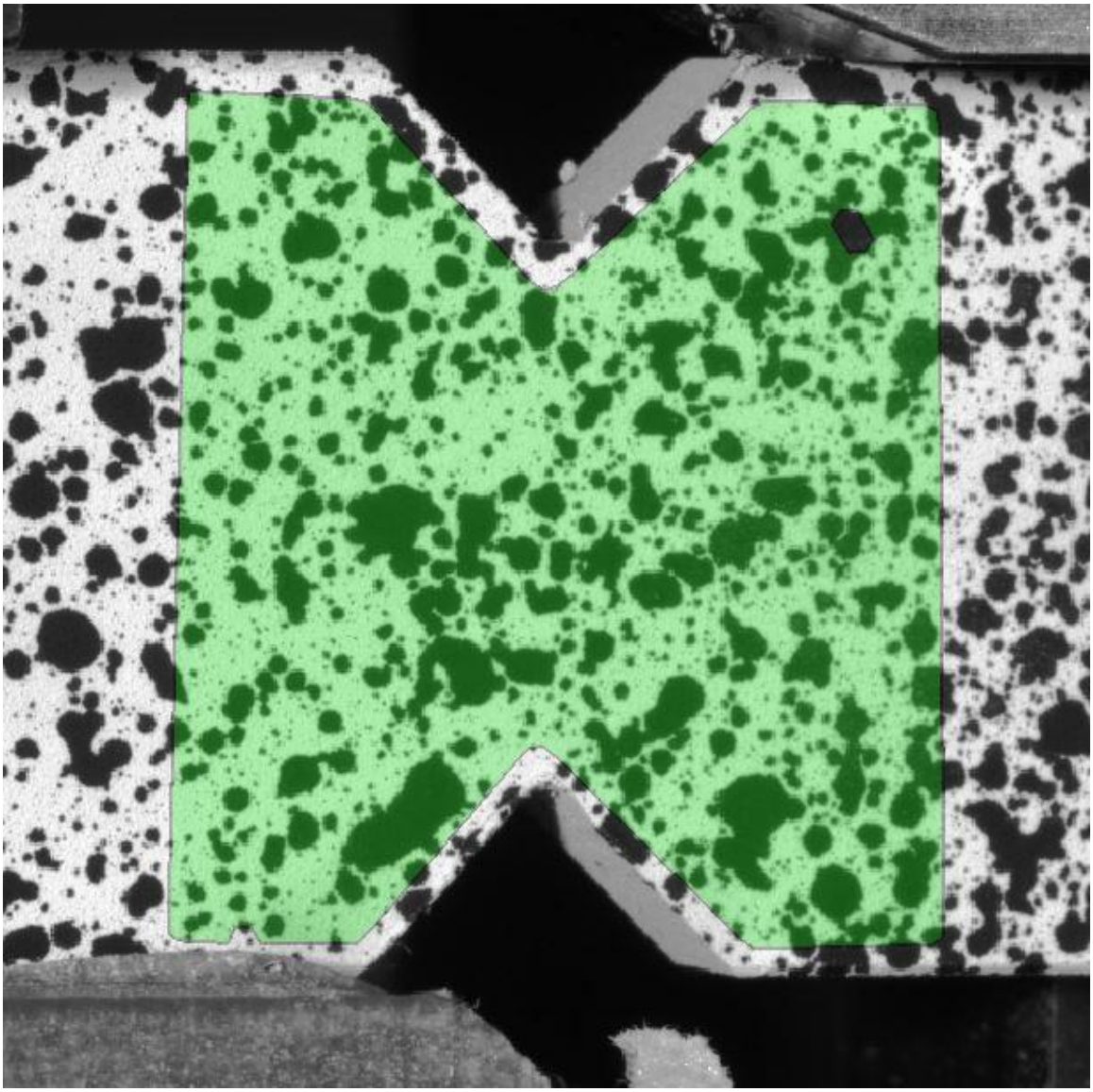


Figure 31: Left camera view of Iosipescu test coupon with a DIC surface component overlaid.

Once the surface is created, the desired strain dimension was selected to project a color view chart on the surface. Then an area of interest was selected to create a mean value inside the selected area. Many methods to evaluate shear strain for the Iosipescu style tests were used. Choosing a small area of interest between the notches where shear strain appears

to be constant around the yield point proved to be the most consistent method. This method is outlined in Figure 32 below.

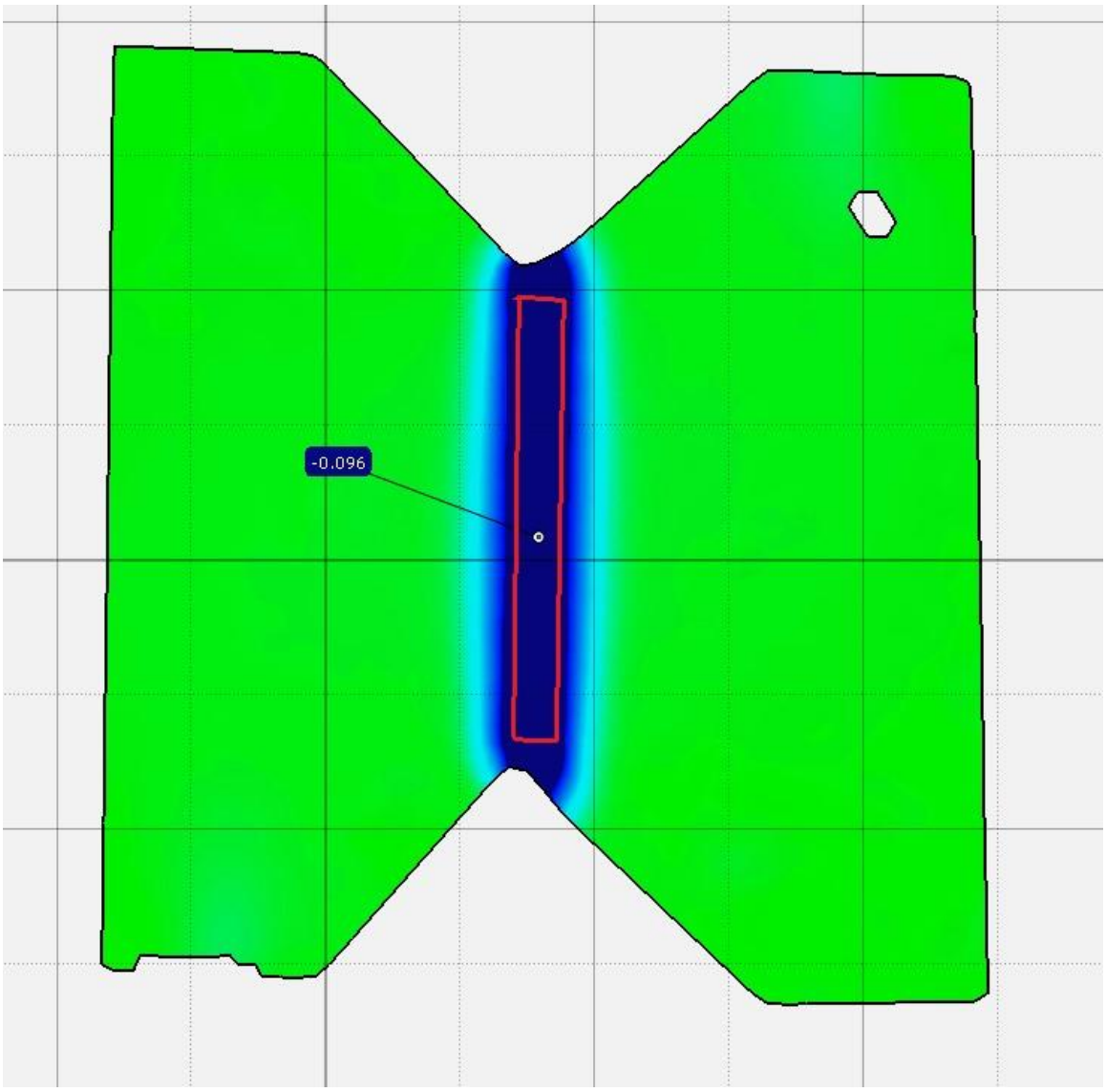


Figure 32: Deformed surface of Iosipescu test showing tensor shear strain (ε_{xy}), the selected area is used to calculate a mean value of ε_{xy} throughout the test.

The average value of the selected area's strain for each time step was then output from ARAMIS to a .csv file. The load data in the analog channels was exported to a .csv

file for post processing. The data was compiled in MATLAB and stress-strain curves were calculated. Further data sets which included displacements of individual points, or shear data across a section were evaluated and output using similar methods where a point, or section was evaluated rather than the surface component. It is important to note ARAMIS measures tensor shear strain (ε_{xy}), which is half the value of engineering shear strain γ_{xy} [25]. Shear modulus is calculated using engineering shear strain, so strain values were multiplied by two after being exported from ARAMIS.

Results and Discussion

A comparison of results from the testing procedures was completed. Analytical techniques to analyze multiaxial stress states and were also explored. Both quantitative and qualitative results are presented where appropriate. Excluding the extensometer data from the ASTM tensile tests, GOM-ARAMIS DIC software was used to collect all the strain data presented in this chapter.

The results from the initial comparison between the previous IPL load acquisition system and the updated system are seen in Figures 33 through 36. This test was completed using a single-notched nylon coupon. The purpose was to verify the performance and function of the new system. The three in-plane load components for both the original system, and the updated system are detailed. The new system recorded drastically smoother load paths and a significant difference in magnitudes. Differences are seen especially in the moment data (Figures 34 and 36). It is noted, both data sets were collected simultaneously during a test.

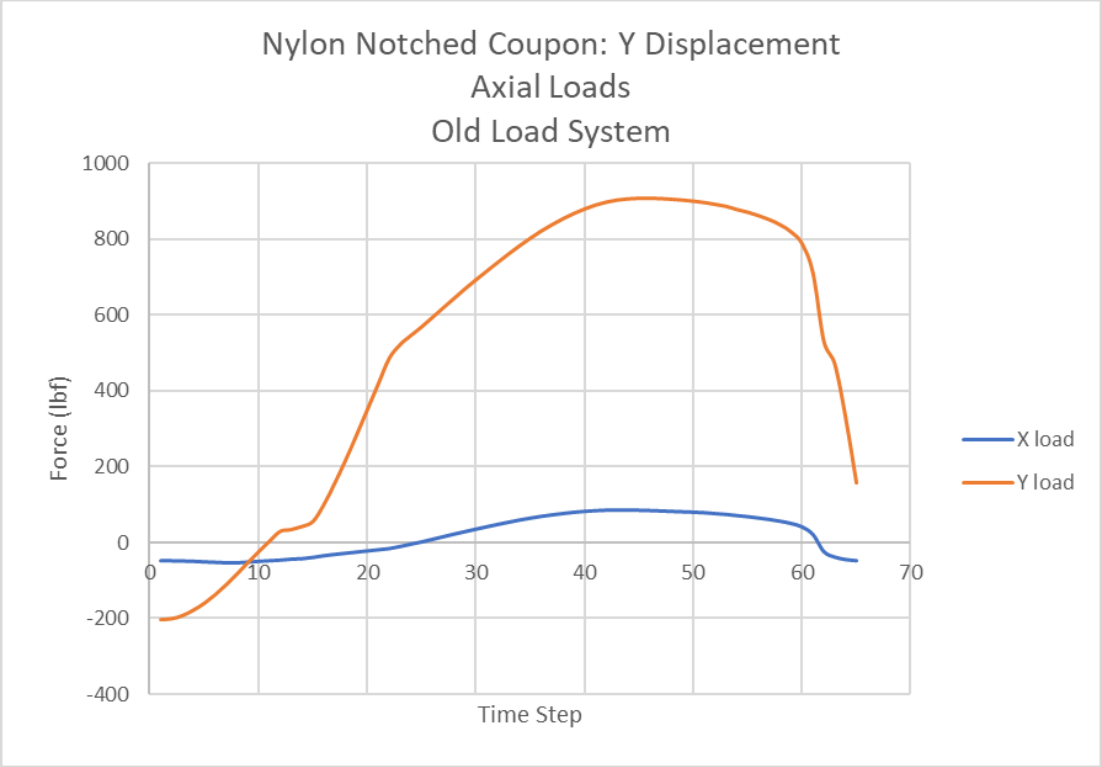


Figure 33: Axial loads vs. time: collected with the original load acquisition system.

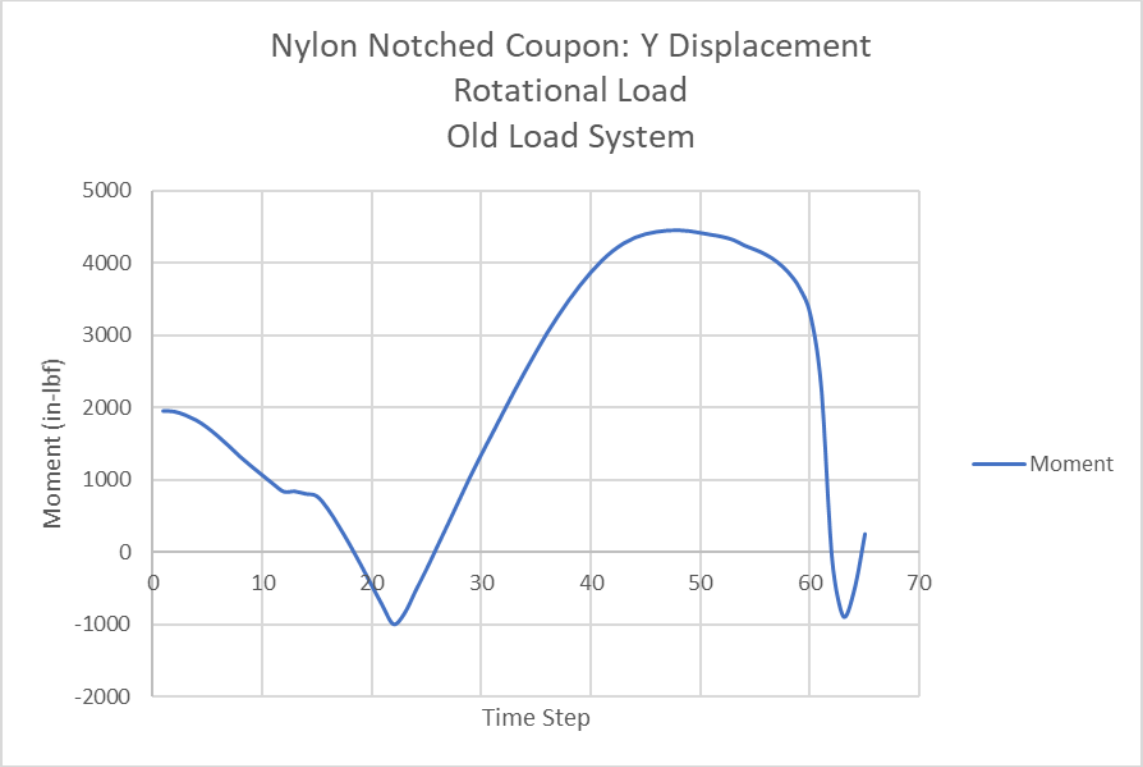


Figure 34: Rotational load vs. time: collected with the original load acquisition system.

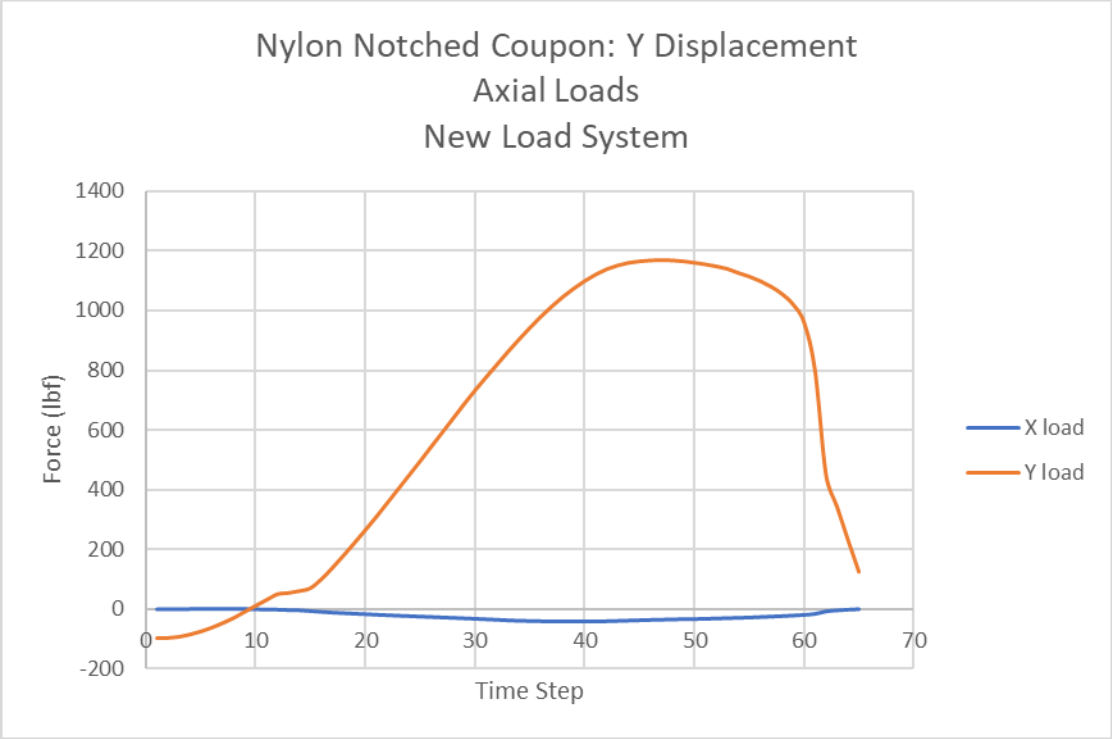


Figure 35: Axial Loads vs. time: collected using the updated load system.

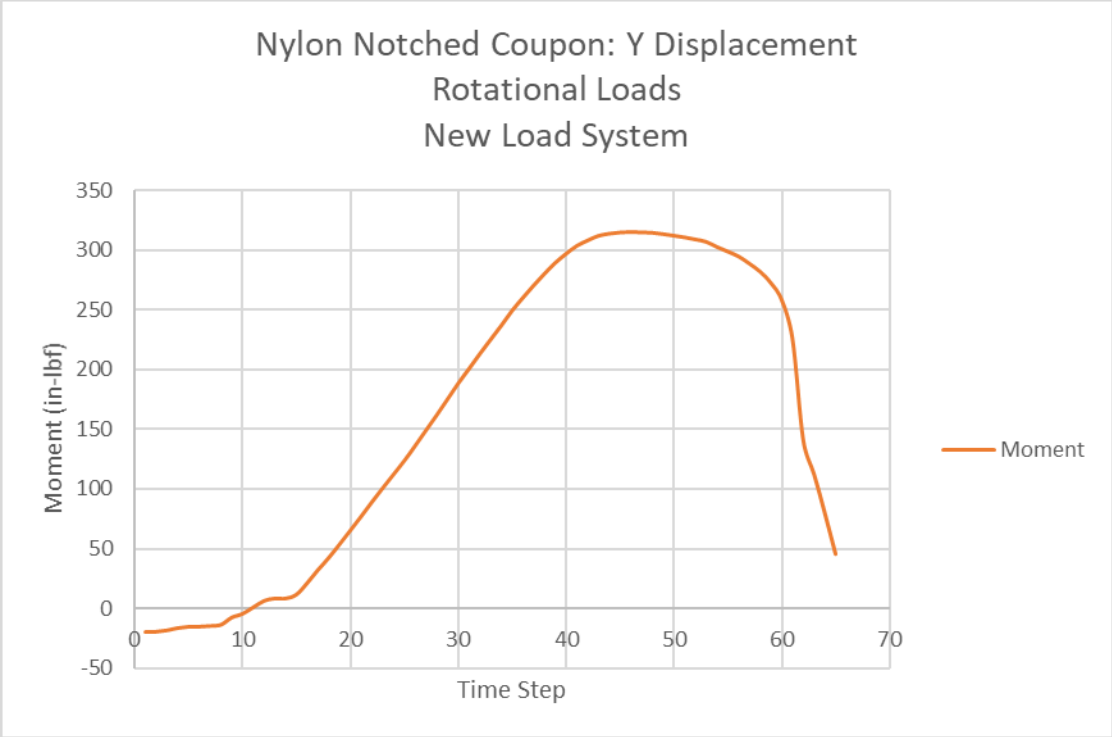


Figure 36: Rotation Load vs. time: collected with the updated load system.

Accuracy in Load Readouts

With any measurement, the accuracy of the load system should be reported. Load cell output voltage is heavily affected by system noise, which causes the readouts to fluctuate plus or minus two pounds in any direction. The accuracy of each reading was incorporated into the static analysis and is presented in Table 1. It should also be noted that these measurements assume the center of the coupon is fixed and does not experience effects of bending or grip slippage during the test, each of which will increase the error in the moment measurement.

Table 1: Accuracy intervals for the IPL load components

Accuracy of Load Readings	
Load Component	**Accuracy**
X-Direction	±2 lbf
Y-Direction	±4 lbf
Moment-Z	±16 in-lbf

Y-Direction

Validating the new IPL load system in the Y direction required the determination of material properties such as Elastic Modulus (E) and Yield Strength (σ_y). The properties were found using an ASTM E8 standard tensile testing procedure and an IPL testing procedure designed specifically for tension. Figure 37 shows the use of DIC to find axial strain, and examples of the failed coupons are seen in Figure 38. Stress-strain curves containing all the data from each test are also seen below (Figures 39 and 40).

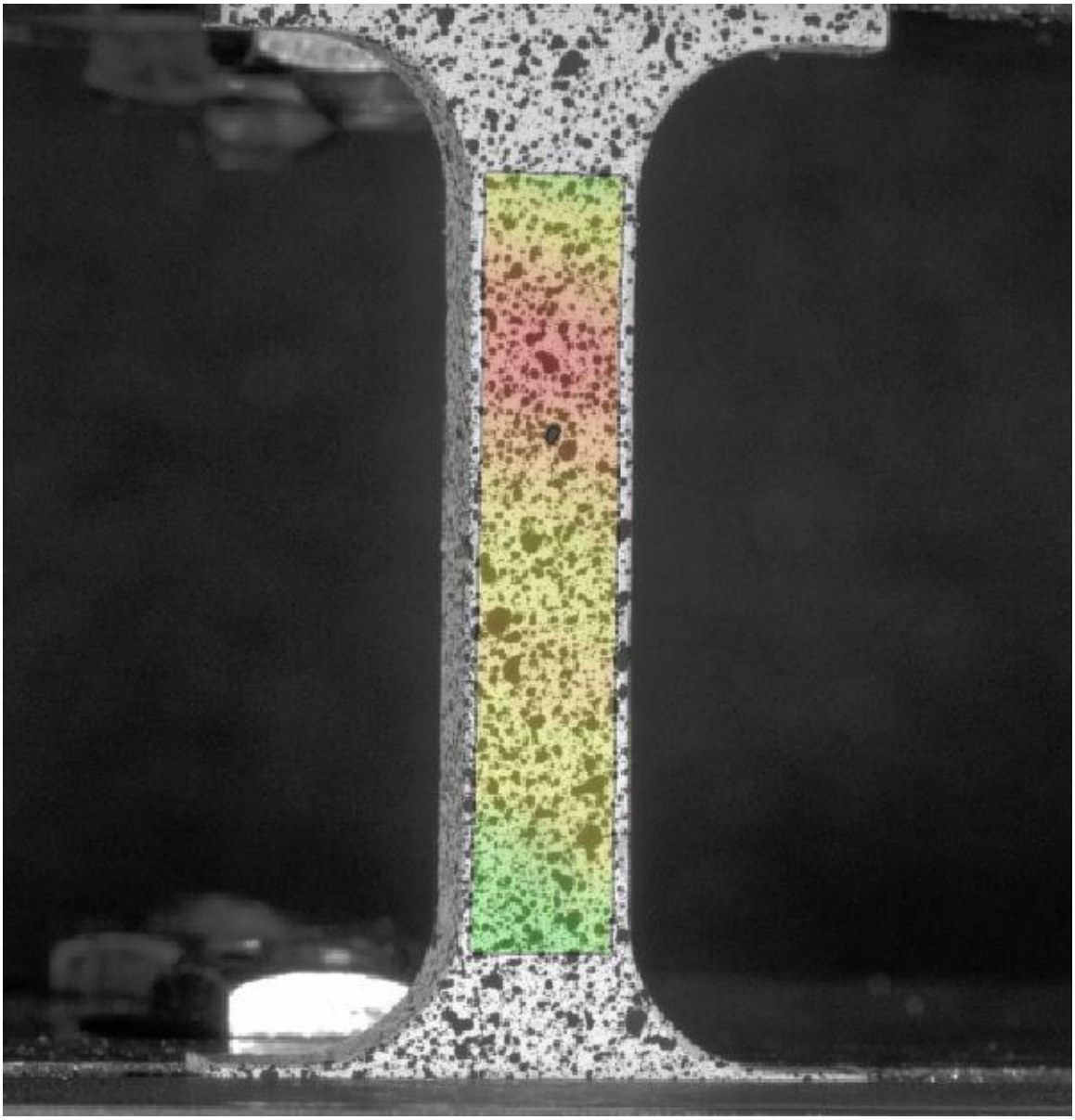


Figure 37: Left camera view of using DIC to calculate axial strain (ε_{yy}) during an IPL quasi-tensile test.



Figure 38: Failed Copper 110 tensile specimens. Left: ASTM E8 coupon. Right: IPL quasi-tensile coupon. Coupon width is 1” for reference.

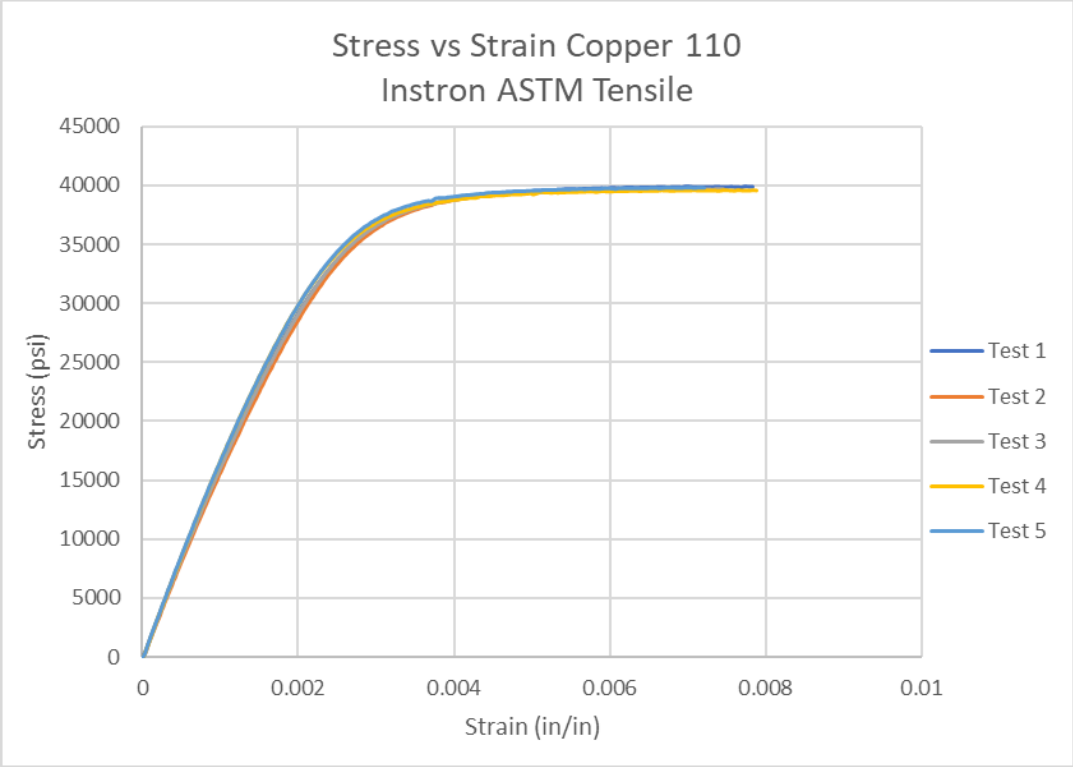


Figure 39: Stress vs. strain data for five Instron ASTM E8 tensile tests.

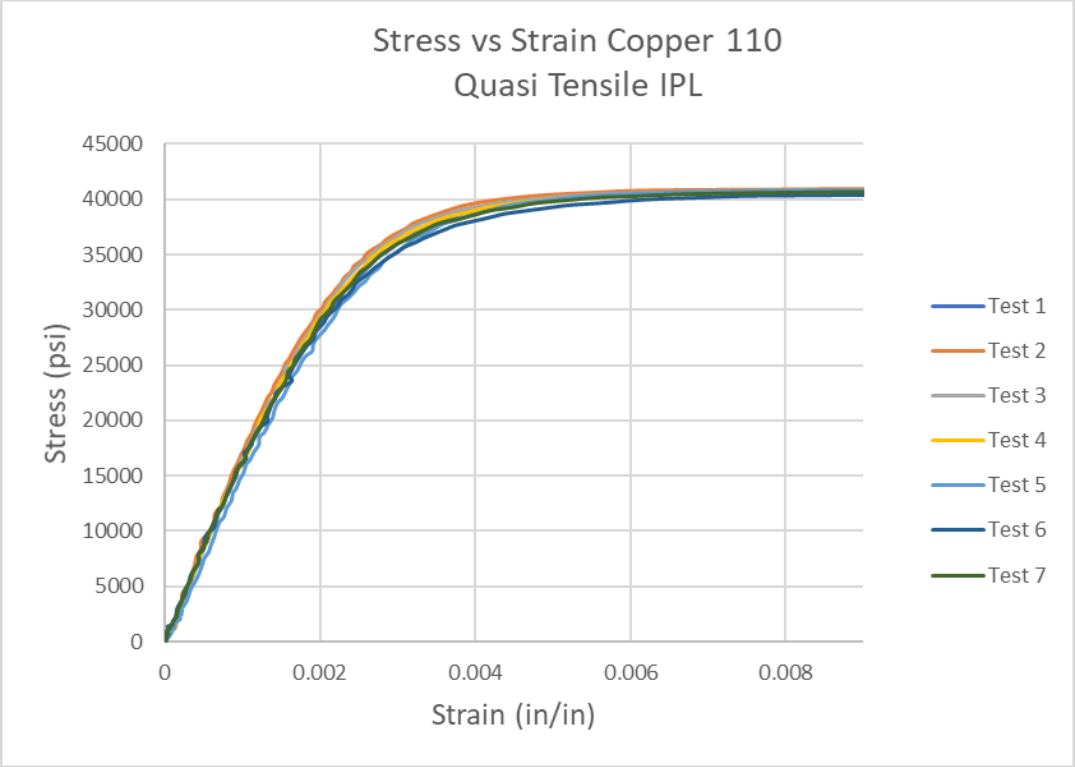


Figure 40: Stress vs. strain data from seven IPL quasi-tensile tests. Strain data was collected using GOM-ARAMIS 2018 digital image correlation software.

The data sets for each test were analyzed by producing a linear fit in the elastic region (5 ksi to 20 ksi) to determine the elastic modulus (E). The yield strength (σ_y) was estimated using the 0.2% strain offset method which is shown in Figure 41 for a single data set. Tables 2 and 3 present comparisons of results between the ASTM E8 tests and the IPL quasi-tensile tests.

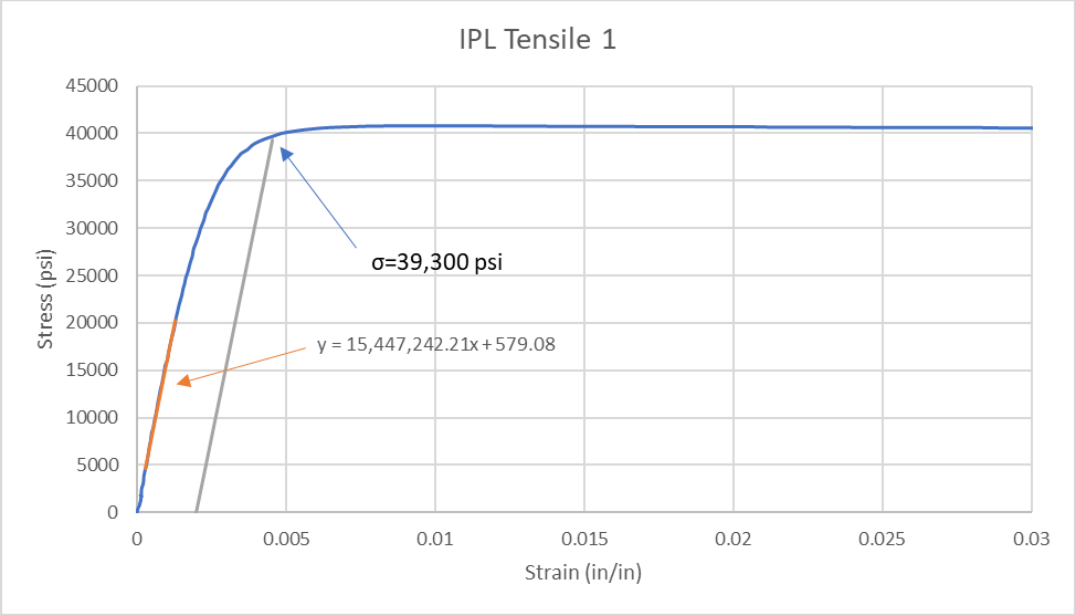


Figure 41: Stress vs. strain data outlining the 0.2% strain offset method to estimate yield strength (σ_y).

Table 2: Modulus data comparison between ASTM E8 and IPL tensile data.

	Elastic Modulus (E)			
	Minimum	Maximum	Standard Deviation	Mean
IPL	15,090,614 psi	16,549,288 psi	525,738 psi	15,720,351 psi
ASTM	15,023,349 psi	16,121,810 psi	399,961 psi	15,607,421 psi
Error (%)				0.72%

Table 3: Yield strength data comparison between ASTM E8 and IPL tensile data.

	Yield Strength (σ_y)			
	Minimum	Maximum	Standard Deviation	Mean
IPL	39,400 psi	39,600 psi	324 psi	39,229 psi
ASTM	39,000 psi	39,200 psi	80 psi	39,160 psi
Error (%)				0.18%

X-Direction

Validation of the updated IPL load system in the X direction included completing a series of IPL shear tests and a series of ASTM Iosipescu tests, both of which are outlined earlier in this work. Shear strain was collected over the area of interest between notches using DIC for both test procedures. Validation also included calculating an analytical shear modulus and analyzing the multi-axial stress state induced using the IPL. Below are detailed images from the DIC showing Iosipescu, and IPL shear tests (Figures 42 and 43). Figures 44 and 45 show shear stress vs. shear strain diagrams for both sets of tests.

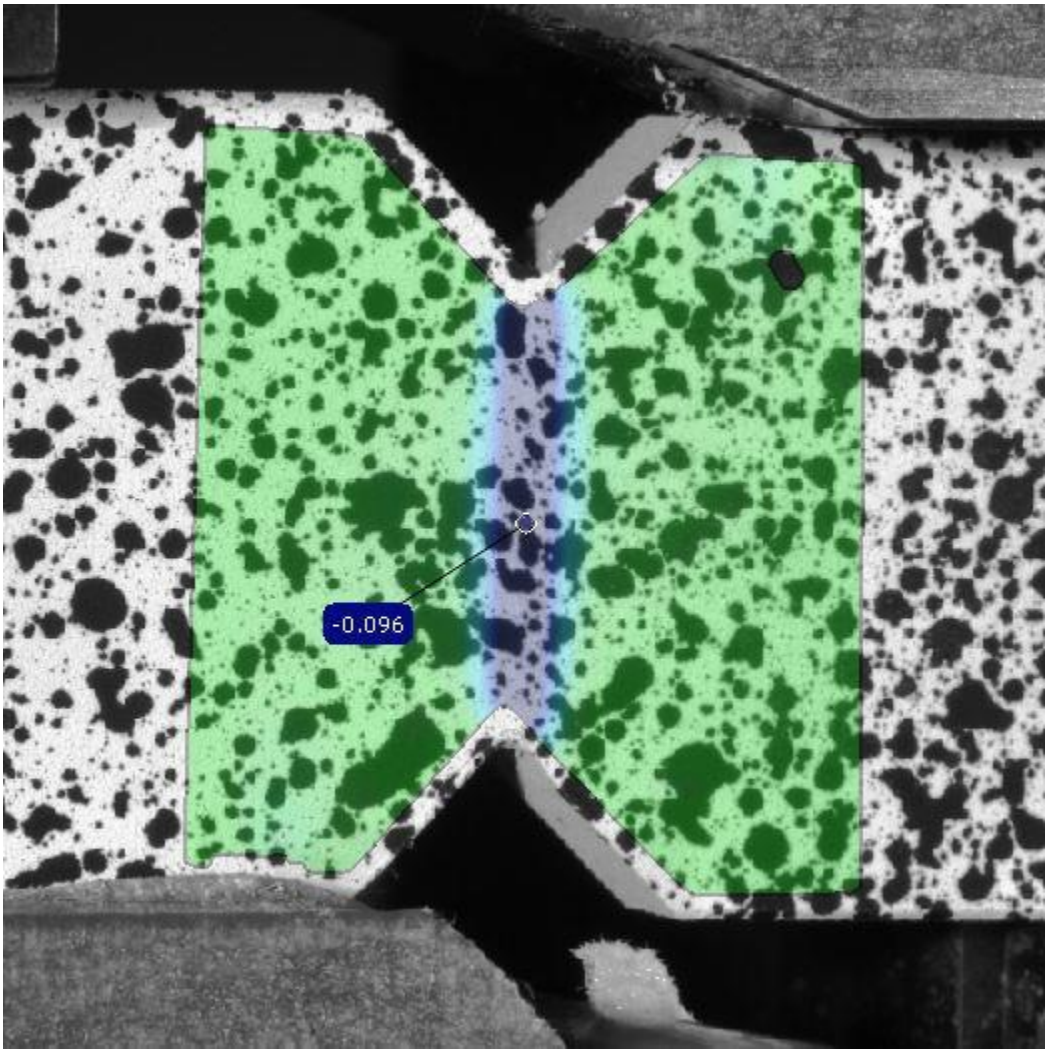


Figure 42: Left camera view showing the use of DIC to calculate shear strain (ε_{xy}) during an ASTM Iosipescu test.

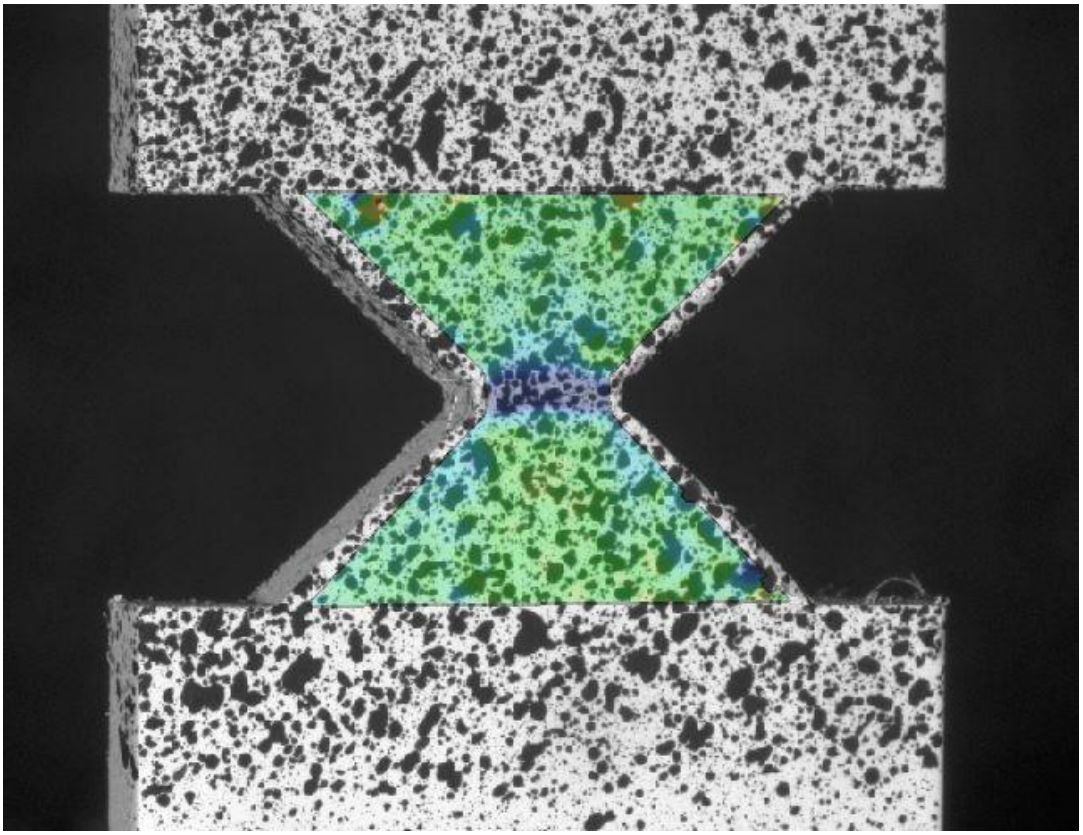


Figure 43: Left camera view showing the use of DIC to calculate shear strain (ε_{xy}) during an IPL shear test.

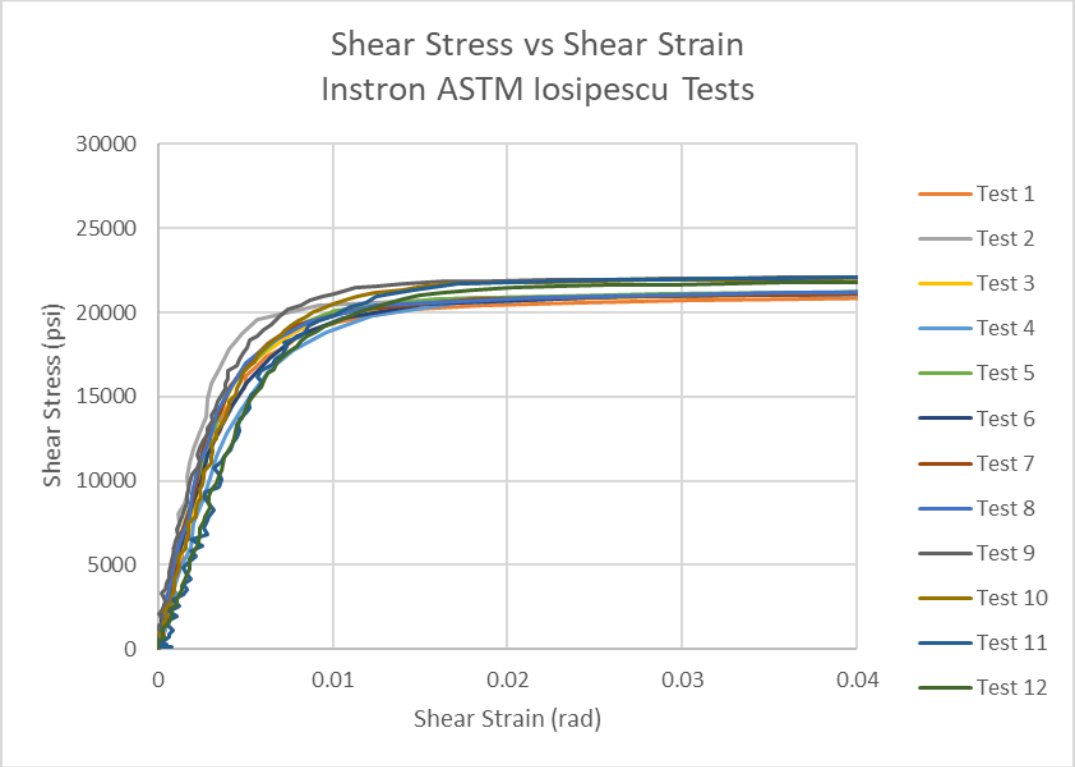


Figure 44: Shear stress vs. shear strain data collected during twelve Instron ASTM Iosipescu shear tests.

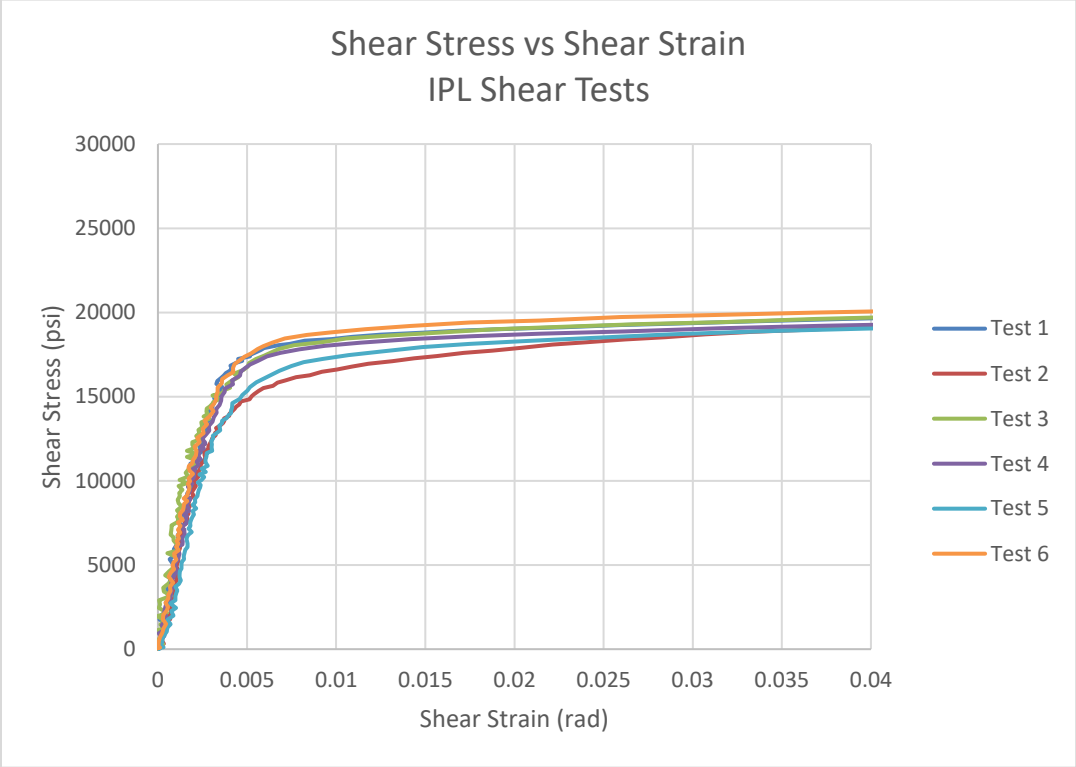


Figure 45: Shear stress vs. shear strain collected during six IPL shear tests.

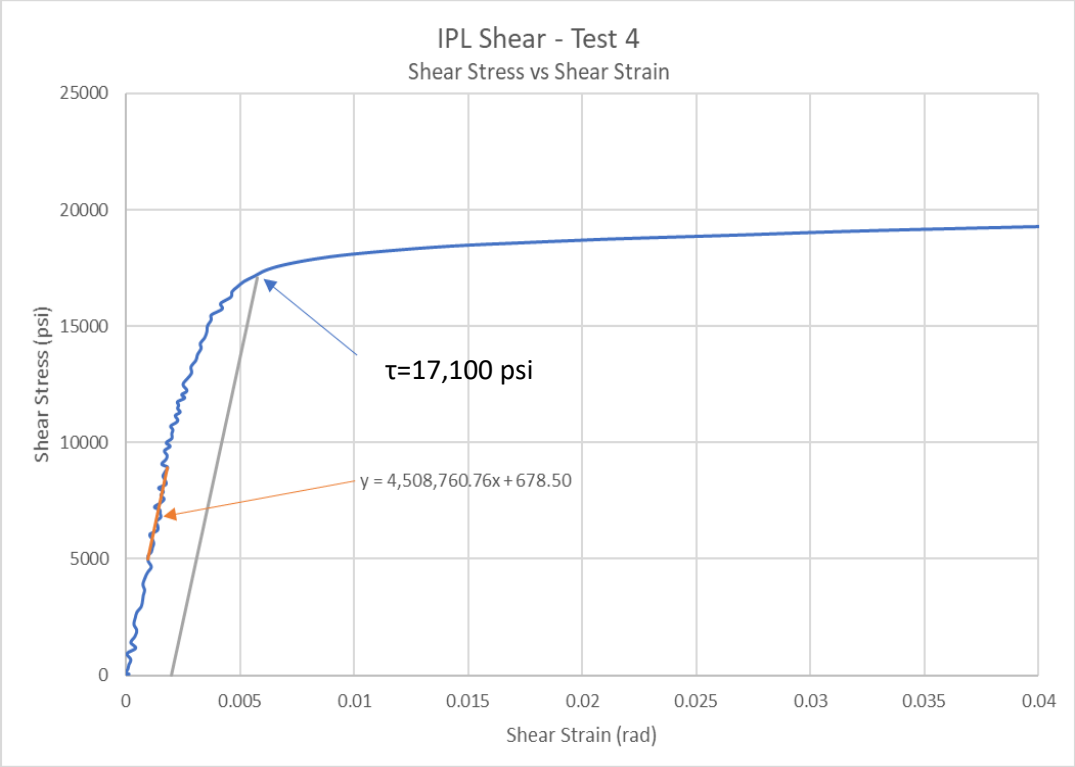


Figure 46: Stress-strain curve for an IPL shear test (test 4) outlining the 0.002 radian offset line to estimate shear strength (τ_y).

A linear fit for the elastic portion of each curve was produced, the slope of which is the respective shear modulus (G). A method using a 0.002 radian offset line was used to estimate the shear strength (τ_y). The method outlined for a single test is shown above in Figure 46.

Figure 47 below shows a comparison of stress-strain data between an Iosipescu test and an IPL test. The two data sets shown are both good representations of the mean values of modulus and strength for each set of tests. The figure details significantly larger shear strength in the Iosipescu test. Tables 4 and 5 present a comparison of results for both shear modulus (G) and shear strength (τ_y).

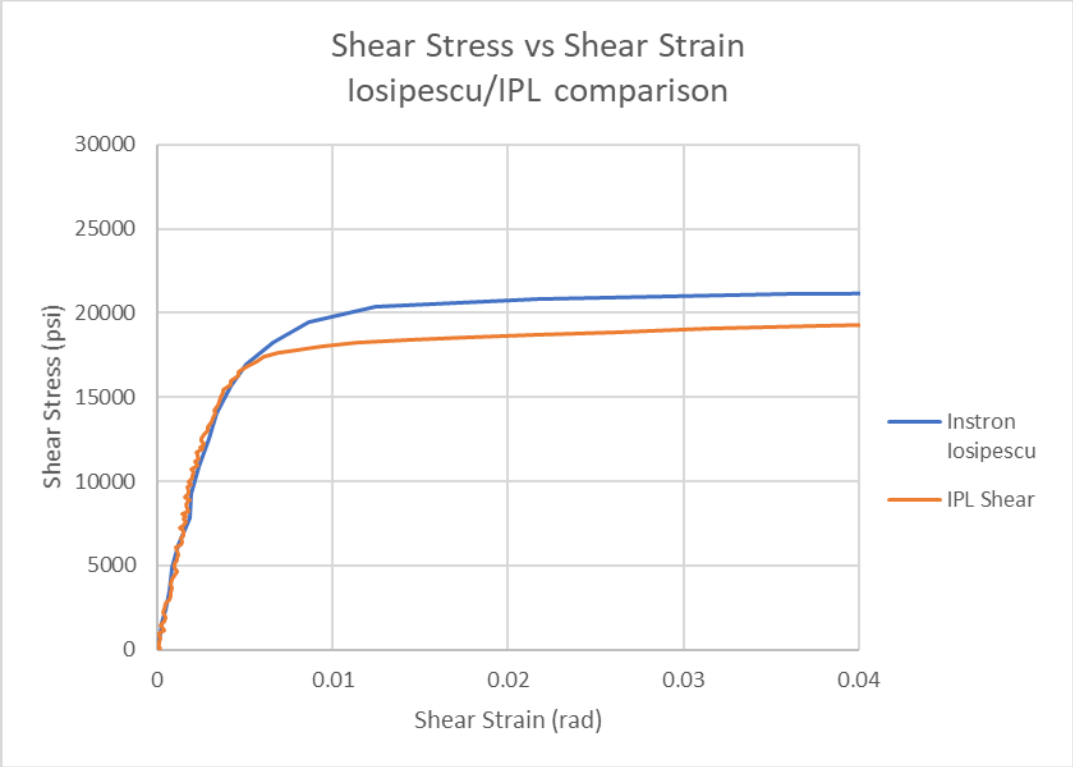


Figure 47: Stress-strain comparison between an ASTM Iosipescu test (test 8) and an IPL shear test (test 4).

Table 4: Modulus (G) data comparison between ASTM Iosipescu and IPL shear tests.

	Shear Modulus (G)			
	Minimum	Maximum	Standard Deviation	Mean
IPL	4,195,261 psi	5,310,733 psi	346,808 psi	4,705,798 psi
ASTM	2,717,986 psi	4,891,817 psi	574,355 psi	3,770,401 psi
Error (%)				24.8%

Table 5: Shear strength (τ_y) data comparison between ASTM Iosipescu and IPL shear tests.

	Shear Strength (τ_y)			
	Minimum	Maximum	Standard Deviation	Mean
IPL	14,800 psi	17,900 psi	1,125 psi	16,717 psi
ASTM	17,500 psi	19,700 psi	862 psi	18,350 psi
Error (%)				8.9%

The experimental shear modulus (G) from the IPL is considerably higher than the corresponding value from the Iosipescu tests. Both strain data sets were collected using the same DIC methods, so it was determined the error is a result of the IPL or the testing procedure. The error can be attributed to ongoing factors present in the IPL tests. Grip slippage and coupon bending in the sample significantly affect the machines ability to effectively measure pure shear. As previously mentioned, the Iosipescu test is designed to reduce bending to zero across the notches which makes it suitable to assume pure shear throughout the test.

Analytical Shear Modulus: An analytical solution for the shear modulus of isotropic materials is well documented and is calculated using an elastic modulus (E) and Poisson's ratio (ν), which are found experimentally. The experimental elastic modulus is presented above. The Poisson's ratio, which is the ratio between lateral and axial strains, was found to be 0.332 using the DIC strain data from the IPL quasi-tensile data. The solution is seen in Equation 11 below [26].

$$G = \frac{E}{2(1+\nu)} \tag{11}$$

The analytical shear modulus (G) was found to be 5.98 msi, which, when compared to the shear modulus (G) found using the IPL, presents a 21.3% error. The standardized Iosipescu shear modulus values should be considered more accurate for the material set tested. The analytical solution assumes a perfectly isotropic material. Many materials are elastically anisotropic, meaning elastic behavior varies with grain orientation [26]. The material tested is constructed from a rolled flat stock of copper. The rolling method used to manufacture the stock would undoubtedly orient the grain structure in a preferred direction which could potentially justify some of the large error. Since the Iosipescu data is further from the analytical value, it is assumed the actual shear modulus of the tested material does not match the analytical value.

Analyzing Force vs Displacement: The force-displacement relationship for an IPL shear test was observed to attempt to quantify the unwanted displacements. Two points were used as reference points to observe X force versus X displacement. One point is located just above the notched shear plane, and the second point is located just below the notched shear plane. The first point experiences displacements due to bending, grip slippage, and shear displacement. The second point however, only experiences significant displacements due to bending and grip slippage. Figure 48 describes the two reference points used to evaluate the force-displacement relationship in the IPL shear test.

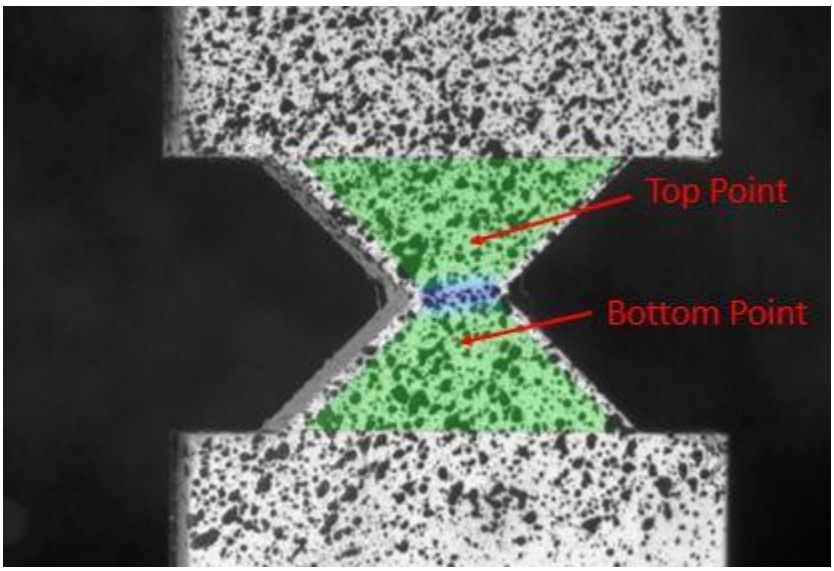


Figure 48: Image showing the two points used to observe the X force versus X displacement relationship in an IPL shear test.

Figure 49 shows the force-displacement curves for an IPL shear test using the two reference points described above. The displacements measured from the point below the notch (data set labeled 'Bottom': see Figure 49) are not affected by the shear displacement present in the reduced cross-section. An idealistic force-displacement curve will have a linear-elastic portion and a non-linear plastic portion. Figure 49 shows a change in slope in the elastic portion of the force-displacement curve. This change in slope suggests grip slippage during that loading period. The next figure (Figure 50) plots the force-displacement relationship using the relative displacement between the top and bottom of the notch. The elastic portion of the curve is now linear, as it would be in an ideal testing situation. Also, it is noted the displacement magnitude at failure is significantly smaller. This difference is attributed to both bending displacement and grip slippage during the test. The data presented explains the inability of the IPL to apply pure shear loading, and the

pure shear assumption should never be implemented when using the IPL. The effects of grip slippage and coupon bending are exaggerated in a purely X direction test and would be drastically reduced during regular use of the IPL.

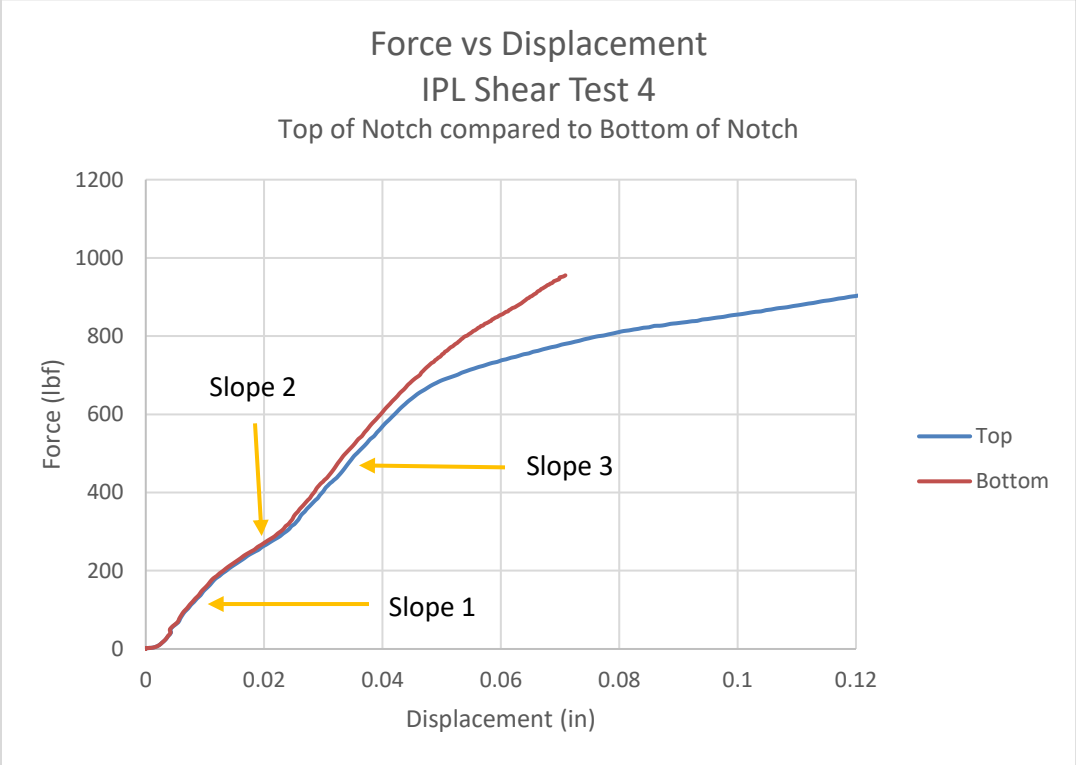


Figure 49: X force vs X displacement curves for points directly above (top) and below (bottom) the notched cross-section of IPL shear test 4.

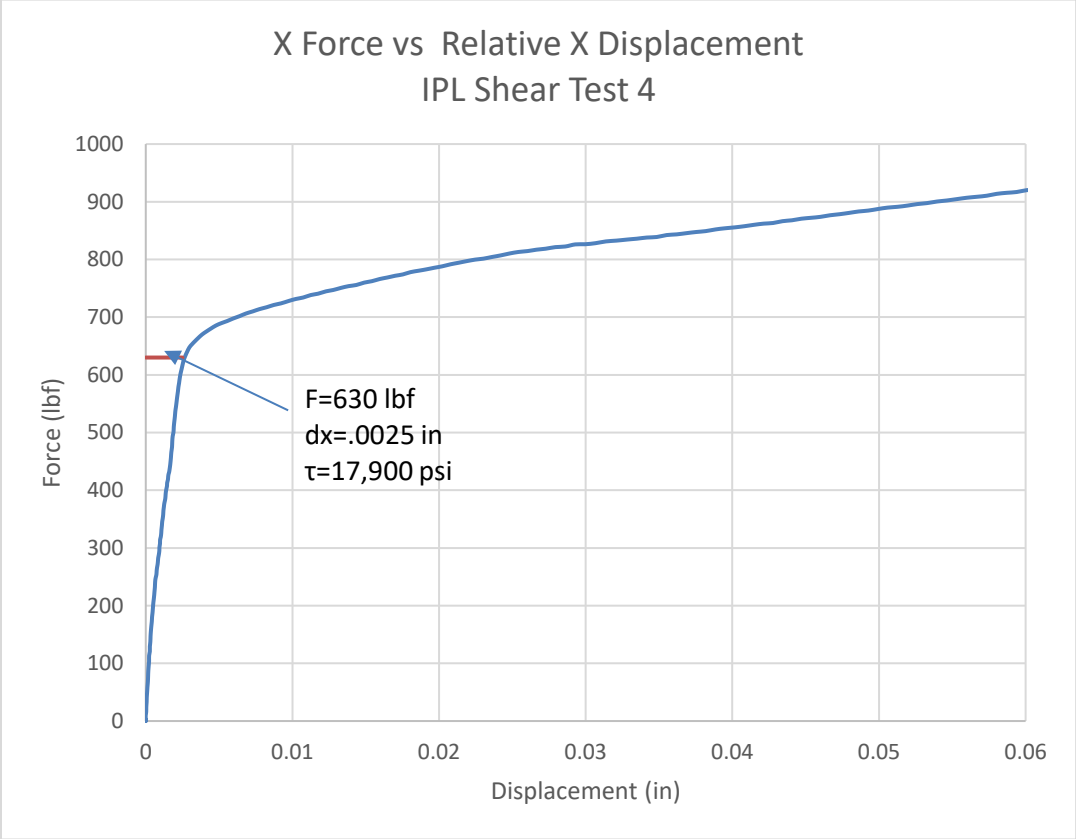


Figure 50: X force vs relative X displacement curve for IPL shear test 4. The displacement is corrected to eliminate the effects of bending and grip slippage.

IPL Shear Test Bending: Having understood the presence of the grip slippage and bending in the IPL shear test, the shear and moment diagrams were created to quantify the bending affects in the coupon. Unfortunately quantifying the grip slippage is an extremely complex task that was not completed. Using the loads collected with the new system, the shear and moment diagrams over the length of the coupon for an IPL shear test are shown in Figures 51 and 52. It appears bending is zero at the center of the

coupon. However, when magnified, it is evident that the bending moment has a non-zero value at the center. This is detailed in Figure 53.

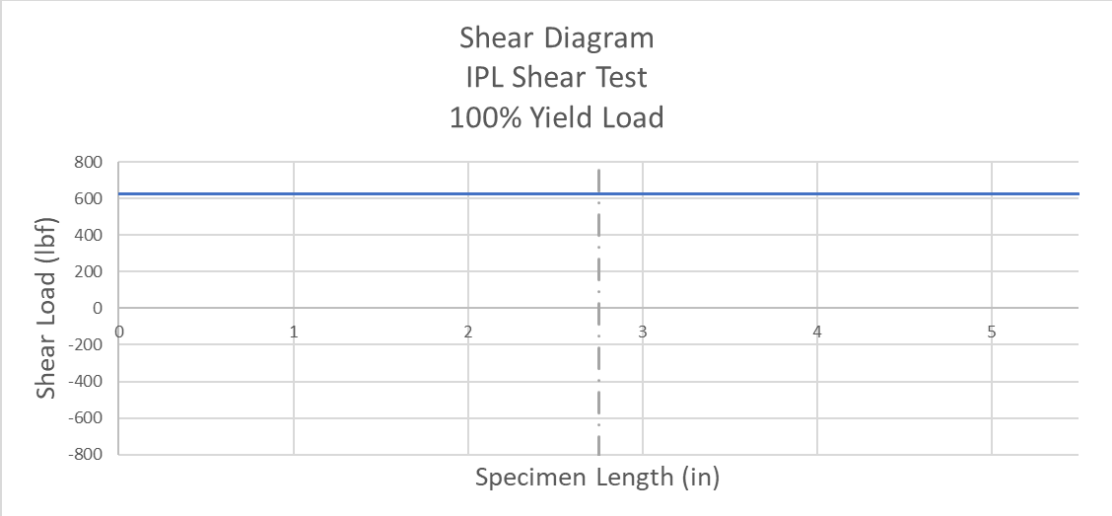


Figure 51: Shear diagram over the length of the IPL shear coupon

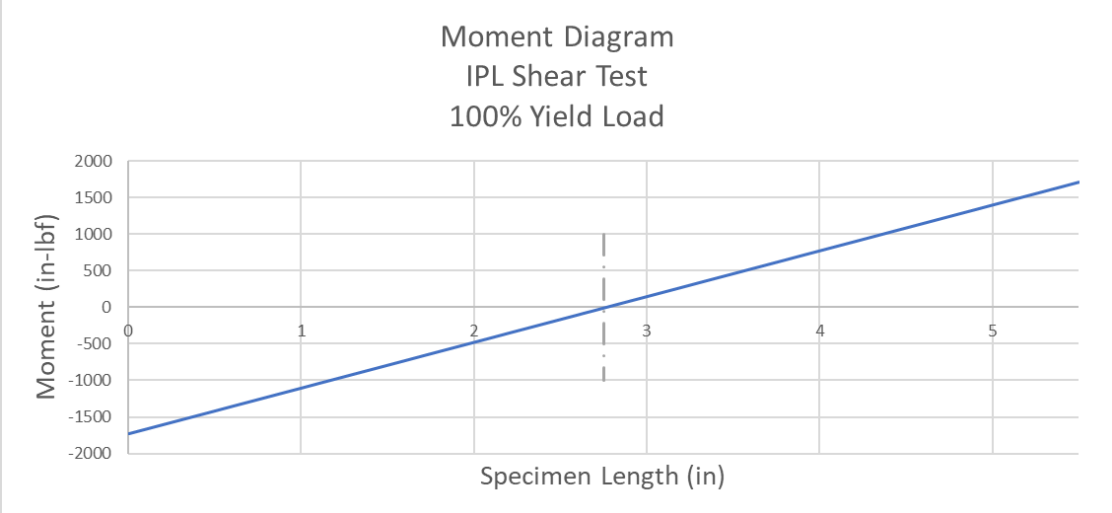


Figure 52: Moment diagram over the length of the IPL shear coupon.

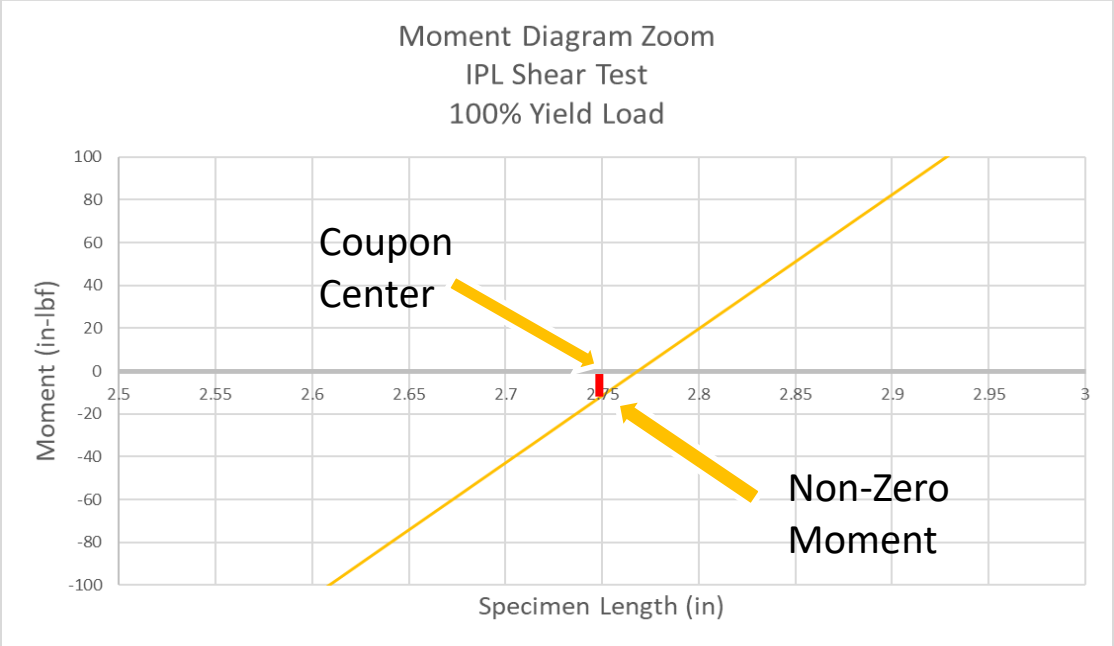


Figure 53: Moment diagram magnified to detail the non-zero value at the center of the IPL shear coupon.

Analyzing the Multi-Axial Loading: The data above present a significant reduction in shear strength in the IPL shear tests. The purpose of analyzing the multi-axial loading condition was to develop an understanding of the reduced shear strength in the IPL coupons. The length of the coupon and the sliding motion of the IPL introduce bending during the test similar to a cantilever beam. To visually understand the significance of the bending, axial strain (ε_{yy}) was analyzed using DIC. Figures 54 and 55 describe the bending at the observed yield point by plotting the axial strain across the notch of the sample. The difference in strain through the cross-section suggests significant bending in the sample.

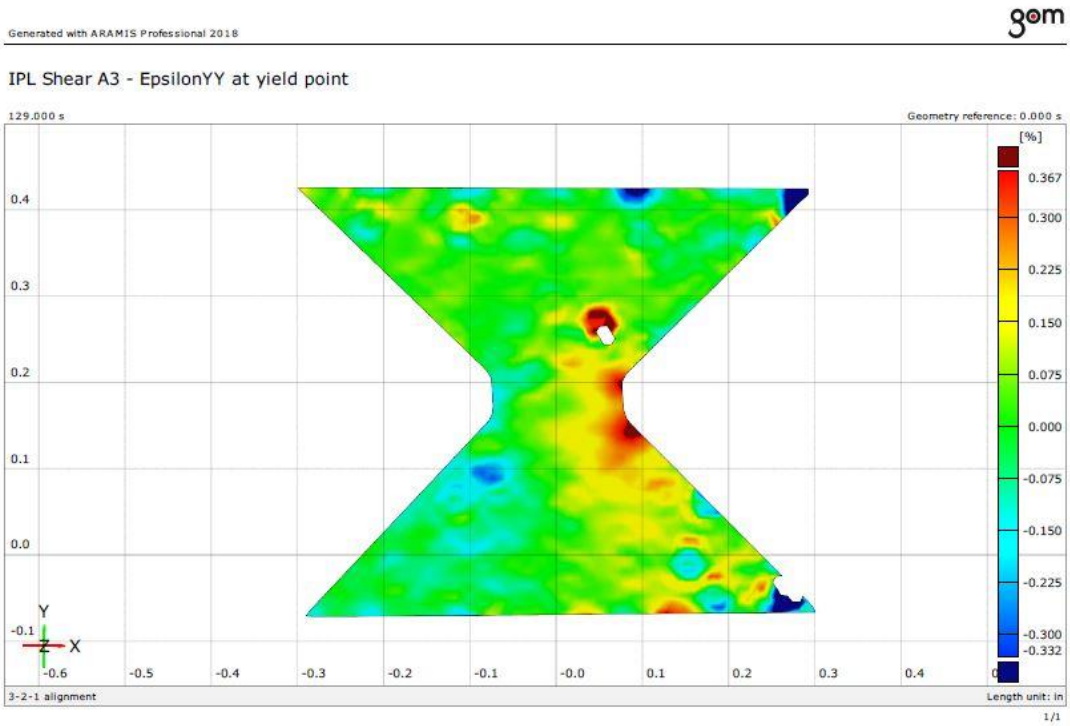


Figure 54: Four-color view schematic from GOM-ARAMIS detailing the bending present during an IPL shear test at observed yield point (test 2).

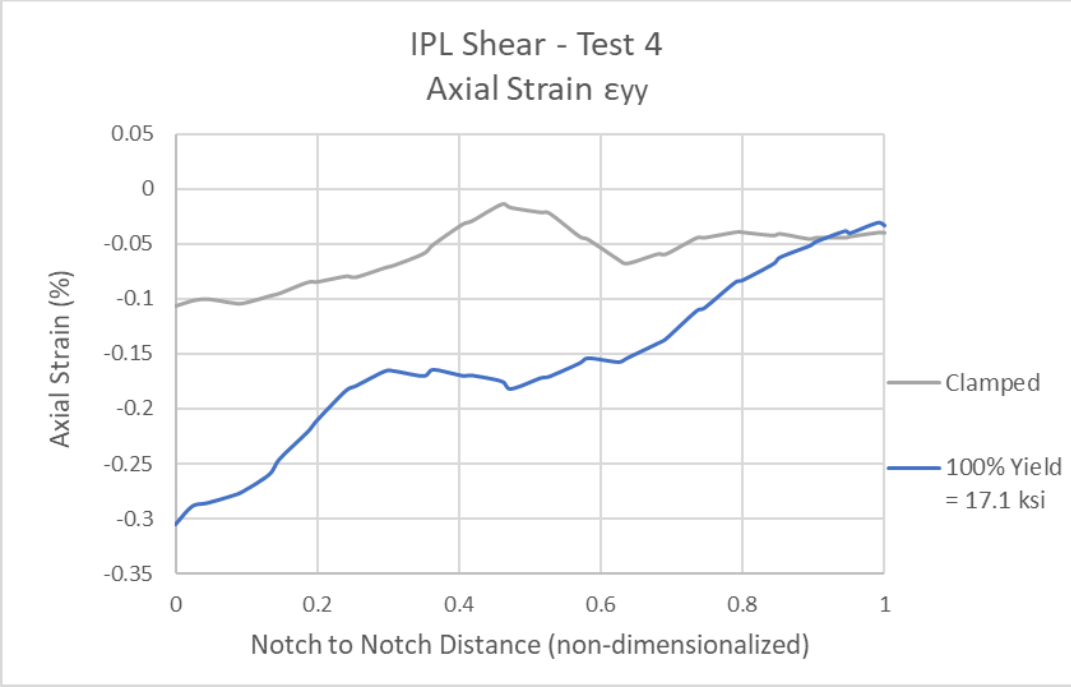


Figure 55: Axial strain vs notch-to-notch length (non-dimensional) detailing the bending present during an IPL shear test at observed yield point (Test 4). The axial strain at the clamped condition at the beginning of the test is also shown for reference.

The updated IPL load system was designed to record all three components of possible loading in a plane stress condition. To understand the effect of bending towards the yielding of the sample, a multi-axial loading analysis was completed. Two common failure criteria are commonly used to evaluate multi-axial loading, maximum shear criterion, and Von Mises failure criterion. Both methods return and effective stress value to compare the yield strength of the material. To begin the analysis, recorded loads at the observed yield point and sample geometry were used to find the cartesian components of stress in the sample. It is important to note the gripping force of the IPL also adds a compressive stress along the axis of the coupon (σ_{yy}). The stress analysis incorporates both

the compressive and bending components of axial force. First, the principal stresses were calculated (equation 12 and 13), then the effective maximum shear stress (equation 14) and the effective Von Mises stress (equation 15) were calculated through the cross section. The effective stresses were then compared to the yield strength found experimentally previously in the work. The multi-axial stress analysis for plane stress is outlined in the following equations [27].

$$\sigma_{1,2} = \frac{\sigma_{xx} + \sigma_{yy}}{2} \pm \left[\left(\frac{\sigma_{xx} - \sigma_{yy}}{2}\right)^2 + \sigma_{xy}^2\right]^{1/2} \tag{12}$$

$$\sigma_3 = 0 \tag{13}$$

$$\sigma_{\max shear} = \max(|\sigma_1 - \sigma_2|, |\sigma_1 - \sigma_3|, |\sigma_2 - \sigma_3|) \tag{14}$$

$$\sigma_{VM} = \left[\frac{1}{2}((\sigma_1 - \sigma_2)^2 + (\sigma_2 - \sigma_3)^2 + (\sigma_3 - \sigma_1)^2)\right]^{1/2} \tag{15}$$

Prior to completing the multi-axial analysis, each of the IPL shear tests failed at a much lower shear stress than the Iosipescu tests. After incorporating the bending induced during the test, a portion of each cross section reached an effective stress above the yield stress threshold. Figures 56 and 57 below show the maximum shear and Von Mises effective stress plotted across the notched cross section for IPL shear test 4, of which the bending strain is presented in Figure 55 above. The analysis was completed at the observed yield point for the shear tests. The bending stress component is a compressive load on the left side of the cross-section and a tensile load on the right side.

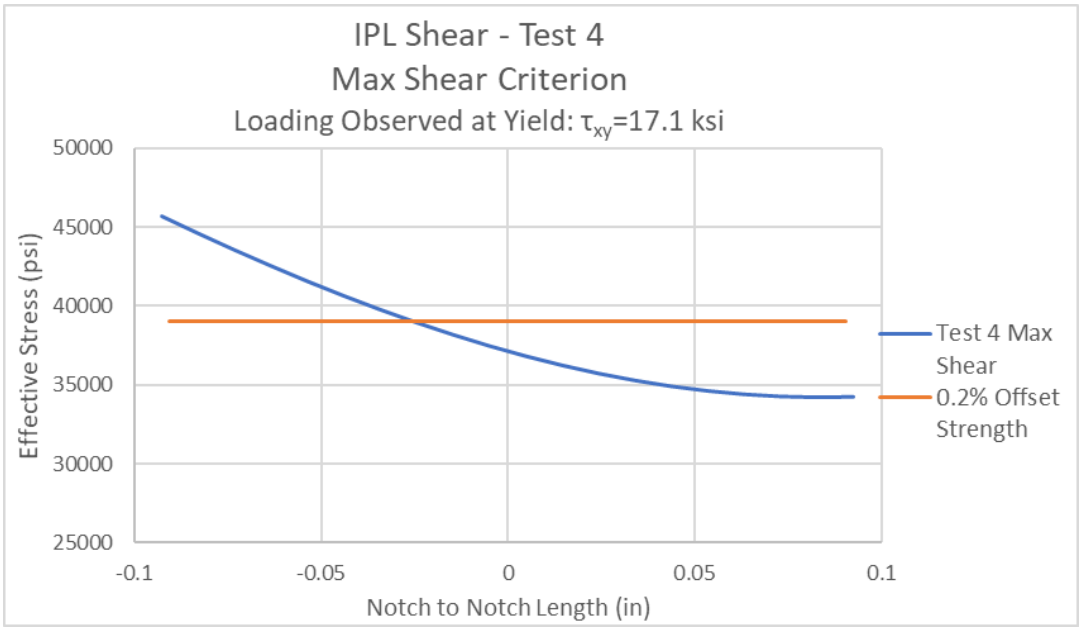


Figure 56: Maximum shear effective stress on cross section at observed yield point for IPL shear test (test 4).

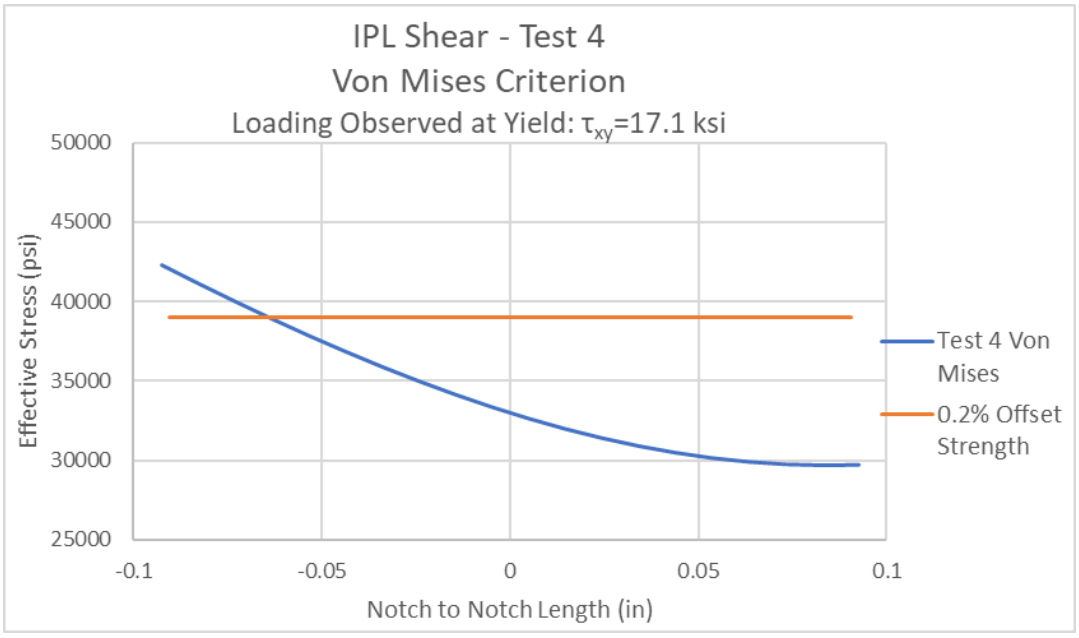


Figure 57: Von Mises effective stress on cross section at observed yield point for IPL shear test (test 4).

The figures above illustrate the reason behind a reduced experimental shear strength in the IPL shear tests. Although the shear stress in the sample is smaller than that of the Iosipescu tests, the effective stress from the combined loading has exceeded the yield stress causing failure initiation in the sample. The uncertainty in the moment measurement (±16 in-lbf) has a large effect on the bending stress of the small cross section, which, in this case, would change the maximum effective stress by roughly 20% in the cross-section. Grip slippage is also a concern during the test. Since the moment is calculated assuming the center of the coupon is fixed, when it moves in reference to the lower grips during a test error is presented into the moment measurement. The entire data set for the IPL shear tests is included in the Appendix A.

CONCLUSIONS

Conclusions

The motivation of this work was to understand, characterize, and improve the IPL multi-axial load frame at Montana State University. Multi-axial loading is a useful tool to expand the capabilities of material testing to three degrees of freedom. The IPL has been used to generate strength and damage models of composite materials, and to validate constitutive models of samples under multiaxial loading conditions. The work included the design, manufacture, and validation of an updated IPL load acquisition system which was incorporated under the IPL grips. The new system eliminated the load systems dependency on the position tracking algorithm and measured the plane-stress components more directly. The system contained three independent load cells to constrain motion of the grips, and provided values used to resolve the in-plane load components.

Validating the system included designing testing procedures to assess the capabilities of the machine in the two in-plane cartesian directions. The testing procedures were designed to imitate ASTM standard testing procedures which would allow for straightforward comparison of results. GOM-ARAMIS digital image correlation software was used to collect displacement data. Copper was chosen as the material to test because its properties are widely understood. Elastic properties and material strengths were collected from each of the tests and compared.

The first test validated the system in the Y-direction. A dog-bone style coupon was designed and tested in tension. The results were compared to data from ASTM E8 uniaxial tension tests. The updated load system and the IPL proved to be accurate in tension. When

results were compared, both the elastic modulus (E) and yield strength (σ_y) were within 1% of the values found with the standard testing procedure. To detail the improvements made from the addition of the new load system, a comparison of stress-strain curves for an IPL quasi tensile test using both the old and the new load systems is shown in Figure 58.

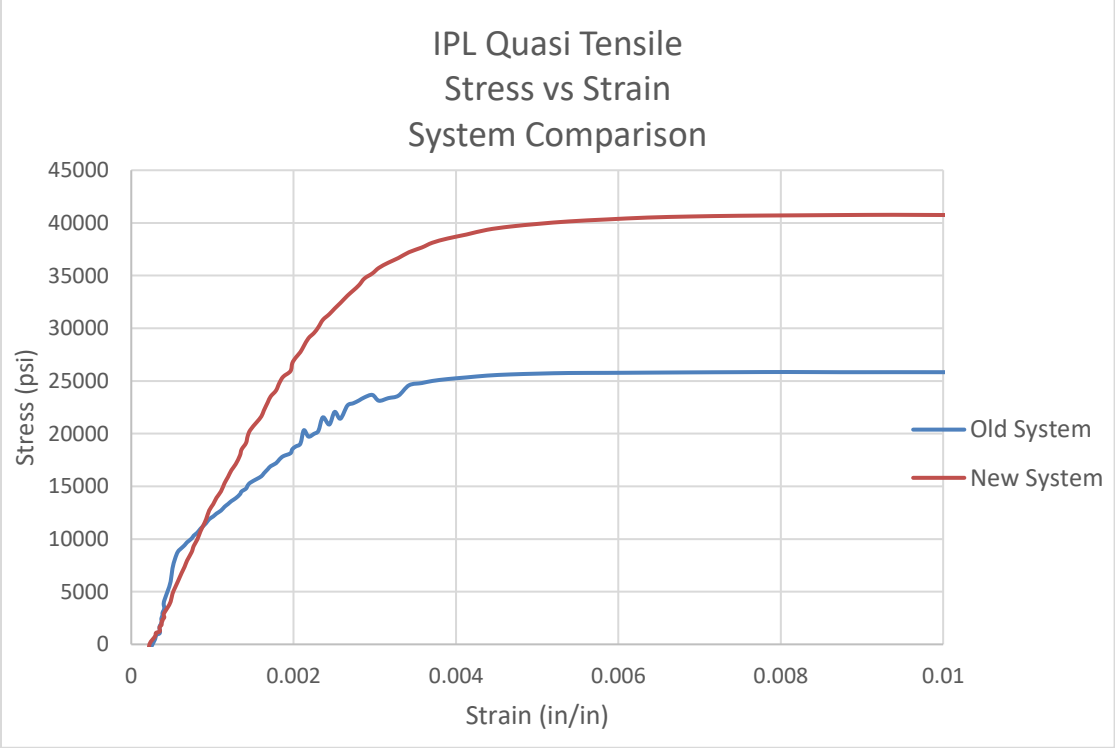


Figure 58: Stress vs strain curves from both the old and new load systems.

The second test hoped to validate the machine in the X-direction. The test was designed after the Iosipescu shear test (ASTM D5379). The objective of the test was to collect shear modulus (G) and shear strength (τ_y) data to match the respective uniaxial Iosipescu data. The IPL presented a significantly higher shear modulus value, and lower shear strength. The significant shear modulus error (25%) can be attributed to the effects of coupon bending and grip slippage which continue to plague the IPL. Because of these

issues, an assumption of pure shear should never be made using the IPL. The error in shear strength was determined to be a result of the induced bending during the test. Which, when the sample was analyzed using multi-axial failure criteria, the stress state had exceeded the yield strength of the material. Although significantly improved, testing in pure shear with the IPL still presents difficulties attributed to the geometry of the machine and the gripping mechanism. A shear stress vs shear strain curve using both the old and the new systems are shown Figure 59 to detail the system improvement.

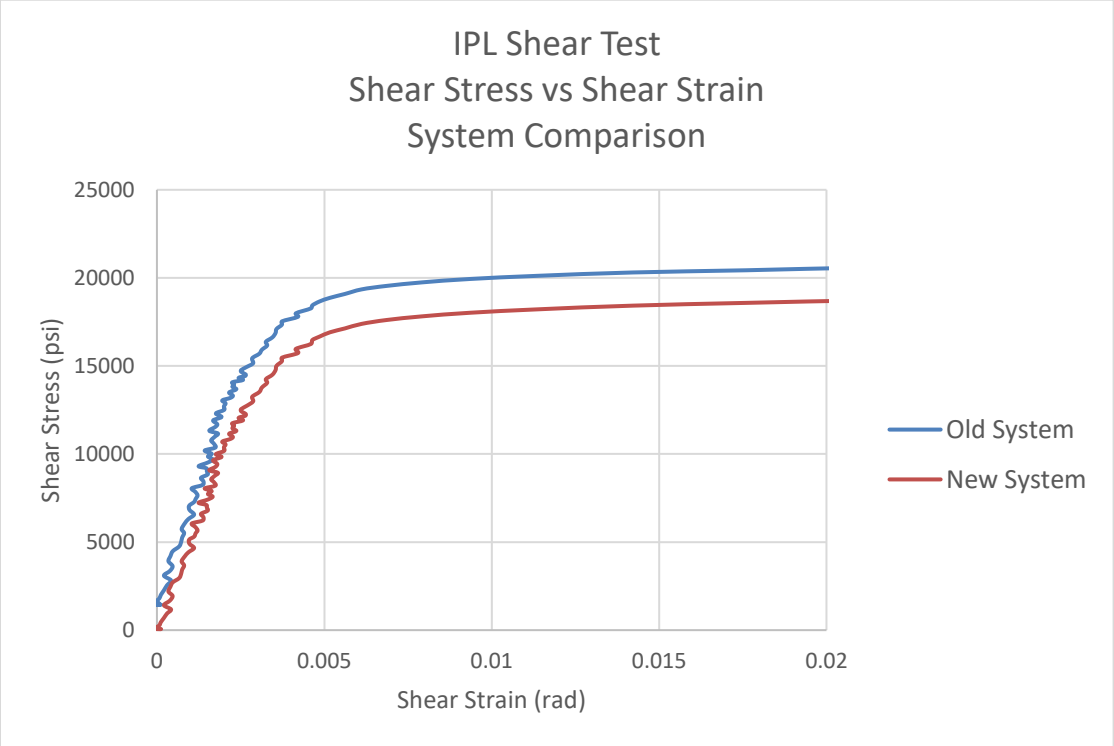


Figure 59: Shear stress vs shear strain curves using both the old and new load systems.

The updated load system developed in this work allows the IPL to be used to confidentially collect multiaxial load data. Previously, the research using the IPL was limited to displacement dependent failure. This work expands the capabilities of multi-

axial testing with the IPL by allowing load dependent failure to be analyzed. The work also hopes to provide an understanding of challenges and solutions to help develop the next generation multi-axial load frame at Montana State University.

Future Work

High Strain Rate Testing

Previously, the work of Stroili [1] used the IPL and DIC to test isotropic materials in multiple axes at high strain rates. The work focused on comparing experimental strain fields to Finite Element models computed using constitutive models. The recent improvements to the IPL, in combination with the capabilities of the newest DIC software from GOM broadens the system capacity to expand on the work of Stroili to validate constitutive models in multiple axes and at high strain rates.

DIC recommendations

This work used the newest version of GOM-ARAMIS to track surface deformation during tests. There is considerable interest in the composite materials research group at MSU to continue to use DIC to experimentally determine shear modulus in Iosipescu shear tests. This work presented substantial error between experimental and analytical values of shear modulus for copper. Future work using DIC and Iosipescu tests to determine shear moduli of known materials is recommended to develop methods to present accurate shear modulus values. This study will allow the group to easily determine shear modulus values of unknown composite laminates experimentally.

IPL/Multi-axial testing recommendations

This work solved one of the drawbacks of the IPL; however, the load frame is far from perfected. This sub-section discusses further recommendations to improve the IPL and to provide instruction when developing a new generation multi-axial load frame. The composites research group recently acquired a hexapod, a machine which can move freely in 3D space. It provides promise for the future of multi-axial testing. The ongoing development of the IPL has provided significant knowledge to be used moving forward developing a hexapod load frame.

To better understand the IPL shear test completed in this work, further experimentation should be completed. The IPL shear coupon was designed to yield under the loading capabilities of the IPL. However, the Iosipescu coupons were machined based on the geometry suggested in the ASTM D5379 standard [23]. Creating an Iosipescu coupon with the same cross section of the IPL shear coupon could potentially uncover conclusions about the IPL shear test not realized in this study.

Gripping continues to be a challenge involved with multi-axial testing. Several iterations of IPL grips have been developed, each of which presented their own issues. Originally the grips could not incorporate varying coupon thickness and employed threaded fasteners to apply gripping force. Next, a set of self-centering grips were employed, but failed to restrict lateral motion. Jette [2] added lateral constraints to the grips which significantly reduced lateral grip slippage, but did not entirely eliminate the issue when using the IPL for purely X loading. The newest grips also somewhat limit varying coupon thickness. Currently the grips are set up to accept coupons from 0.180” to 0.200” thick. To change the coupon thickness, the aluminum spacers behind the fixed grip face on both sets

of grips need to be changed to new thicknesses. This will ensure the coupon is centered on the IPL loading plane. This modification could potentially require changing the lateral constraints to remain between the grip faces as well. Designing grips for multi-axial testing might involve using wedge style self-centering grips. To prevent lateral slippage, redesigning the sample geometry to have a round or triangular cross section would allow the wedge grips to have three components to restrict motion in all directions. This would be particularly helpful for the design of a six degree-of-freedom system.

Load control and a home position would help to streamline the IPL testing procedure. The gripping action applies a compressive pre-load along the length of the coupon which is then recognized as the zero-strain reference by the DIC. Load control incorporated into the software of a new system would ensure samples are at a zero-stress state at the beginning of each test. Also, after each test the IPL must be finessed into the correct position to ensure the grips are aligned correctly. A home position incorporated into the software would significantly reduce testing time and user frustration. Several other shortcomings of the IPL could be improved in the future, many of which are outlined earlier in this work, and in the previous theses referenced in the IPL chapter.

Lastly, shortcomings of the updated load system exist and are present. For future testing, the new load system is designed to withstand 2000 lbf in the Y-direction and 1000 lbf in the X-direction. Both of these thresholds are near the limits of the machine itself. Although these limits could be slightly expanded, to ensure safe operation, coupons should be designed to fail under these loading conditions. The load system is designed to where the grips are supported by three pinned members, which causes some concern about the

rigidity of the lower grips. As a result of manufacturing capability, there is some slop in the pinned joints which allows the grip plate to rotate slightly about the X-axis. The restricted motion of the machined and the balance of the load system mitigate the potential out-of-lane effects, but the issue would require attention if another revision of the load system was designed. Also, the grips during a test appear to displace about 0.010”. The displacement increases with load, so it is not an issue associated with backlash in the pinned joints. Instead, it appears to be deflection in the system; potentially in the threads or deflection of the load cells. If a future project involved improving upon this work, enhancing the rigidity of the lower grips would require consideration. The load system improvements developed in this work expand the capabilities of multiaxial testing at MSU and will contribute to advancements towards a next-generation multiaxial test frame.

REFERENCES CITED

[1] C. Stroili, “Validation of High Strain Rate, Multiaxial Loads using an In-Plane Loader, Digital Image Correlation,” Montana State University: Bozeman, MT, 2018.

[2] J. T. Jette, “Damage Characterization of Fiber Reinforced Composite Materials by Means of Multiaxial Testing and Digital Image Correlation,” Montana State University: Bozeman, MT, 2017.

[3] P. W. Mast, G. E. Nash, J. G. Michopoulos, R. Thomas, R. Badaliance, and I. Wolock, “Characterization of strain-induced damage in composites based on the dissipated energy density part III. General material constitutive relation,” *Theor. Appl. Fract. Mech.*, vol. 22, no. 2, pp. 97–114, 1995.

[4] W. J. Ritter, “Application of Energy Methods to Modeling Failures in Composite Materials and Structures.,” Montana State Univeristy: Bozeman, MT, 2004.

[5] A. B. Collett, “A VALIDATION STUDY OF THE MONTANA STATE UNIVERSITY IN-PLANE LOADER,” Montana State University: Bozeman, MT, 2006.

[6] J. D. Smith, “Internal Damage Characterization for Composite Materials Under Biaxial Loading Configuration,” Montana State University: Bozeman, MT, 2007.

[7] J. T. Schmitt, “Damage Initiation and Post-Damage Response of Composite Laminates by Multiaxial Testing and Nonlinear Optimization,” Montana State University: Bozeman, MT, 2013.

[8] J. W. Parker, “Development and Implementation of a Low Cost Image Correlation System to Obtain Full-Field In-Plane Displacement and Strain Data,” Montana State University: Bozeman, MT, 2009.

[9] “Matweb Material Property Data,” 2019. [Online]. Available: http://matweb.com/search/DataSheet.aspx?MatGUID=e2147b8f727343b0b0d51efe02a6127e. [Accessed: 15-Sep-2019].

[10] T. Q. Systems, “TRILION QUALITY SYSTEMS Optical Measuring Techniques ARAMIS Training.”

[11] “GOM ARAMIS.” GOM mbH, Braunschweig, Germany, 2018.

[12] GOM, “GOM ARAMAS, PONTOS User Manual.” GOM mbH, Braunschweig, Germany, 2008.

[13] “SolidWorks.” Dassault Systems, 2018.

[14] “Tensile Test,” *Engineering Archives*. [Online]. Available: http://www.engineeringarchives.com/les_mom_tensiletest.html.

[15] “Miniature universal load cells,” *Omega Engineering*. [Online]. Available: https://assets.omega.com/pdf/test-and-measurement-equipment/load-and-force/load-cells/LC202.pdf.

[16] “ANSYS Workbench.” ANSYS inc., 2019.

[17] “Omega Engineering - Load Cells and Force Sensors,” 2018. [Online]. Available: https://www.omega.com/en-us/resources/load-cells. [Accessed: 17-Sep-2019].

[18] Omega Engineering, “Omega DMD-465 User Guide.” .

[19] “Omega Engineering-Miniature Universal Load Cells.” [Online]. Available: https://assets.omega.com/pdf/test-and-measurement-equipment/load-and-force/load-cells/LC202.pdf. [Accessed: 17-Sep-2019].

[20] “Automation Products Group - What is a Shunt Cal and How does it Work?,” 2019. [Online]. Available: https://www.apgsensors.com/about-us/blog/what-is-shunt-cal-and-how-does-it-work. [Accessed: 18-Sep-2019].

[21] ASTM Int., “ASTM B187/B187M-19 ‘Standard Specification for Copper, Bus Bar, Road, and Shapes and General Purpose Rod, Bar, and Shapes.’” pp. 1–9, 2019.

[22] ASTM Int., “Standard Test Methods for Tension Testing of Metallic Materials 1 - ASTM E8M-13a,” *ASTM Standards*, no. C. pp. 1–28, 2014.

[23] ASTM Int., “ASTM D5379/D5379M ‘Shear Properties of Composite Materials by the V-Notched Beam Method,’” *ASTM Standards*, no. February. pp. 1–13, 2005.

[24] “Wyoming Test Fixtures,” 2019. [Online]. Available: https://www.wyomingtestfixtures.com/. [Accessed: 01-Oct-2019].

[25] GOM, “Digital image correlation and computation basics,” *GOM GmbH*, vol. 004, no. 0. pp. 1–30, 2016.

[26] W. D. Callister, *Fundamentals of Materials Science and Engineering: An Integrated Approach*, 5th Editio. John Wiley & Sons, 2016.

[27] A. P. Boresi and R. J. Schmidt, *Advanced Mechanics of Materials*, Sixth Edit. John, 2003.

APPENDICES

APPENDIX A

APPENDIX A: TEST DATA

ASTM E8 TENSILE DATA

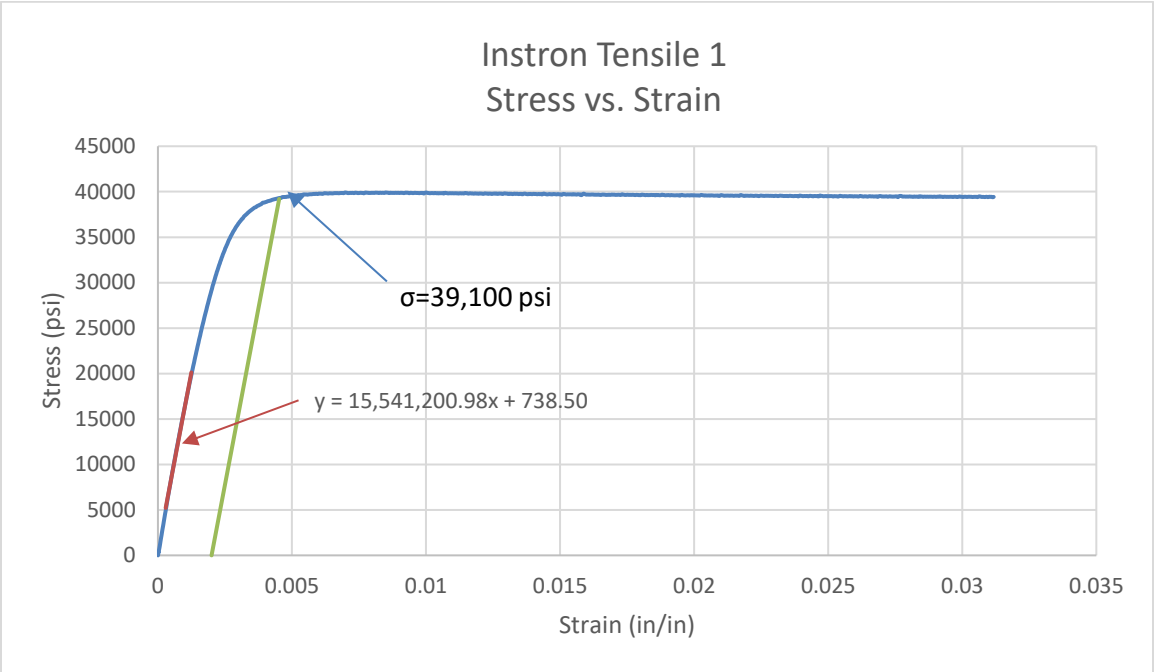


Figure 60: Stress-strain curve for Instron tensile test 1.

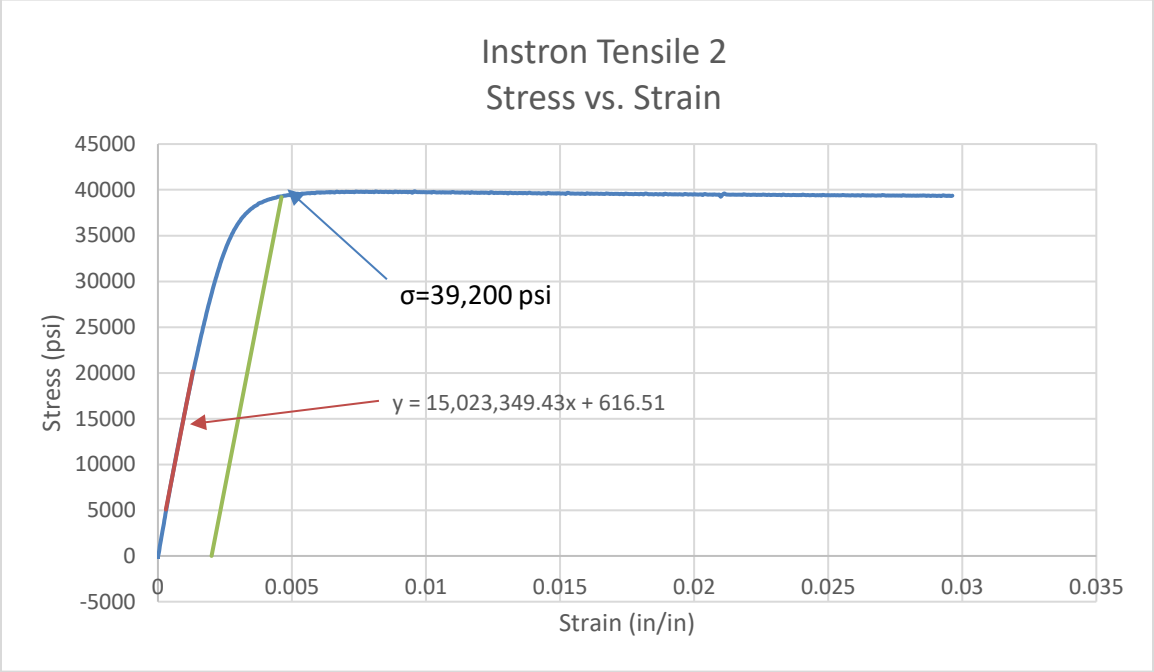


Figure 61: Stress-strain curve for Instron tensile test 2.

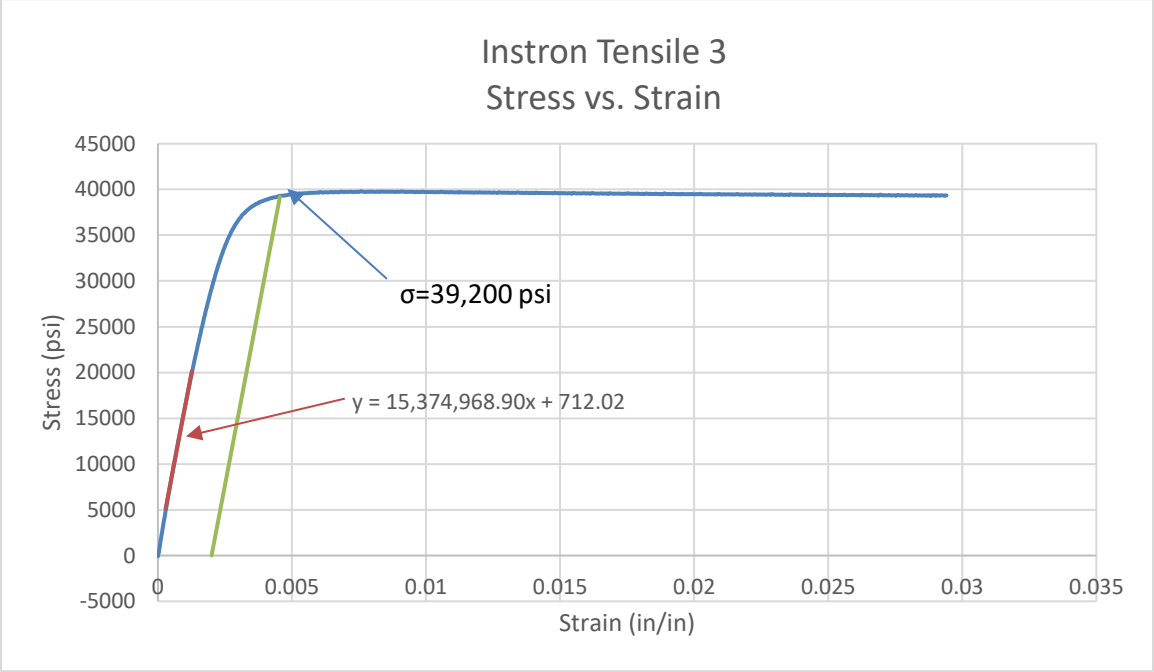


Figure 62: Stress-strain curve for Instron tensile test 3.

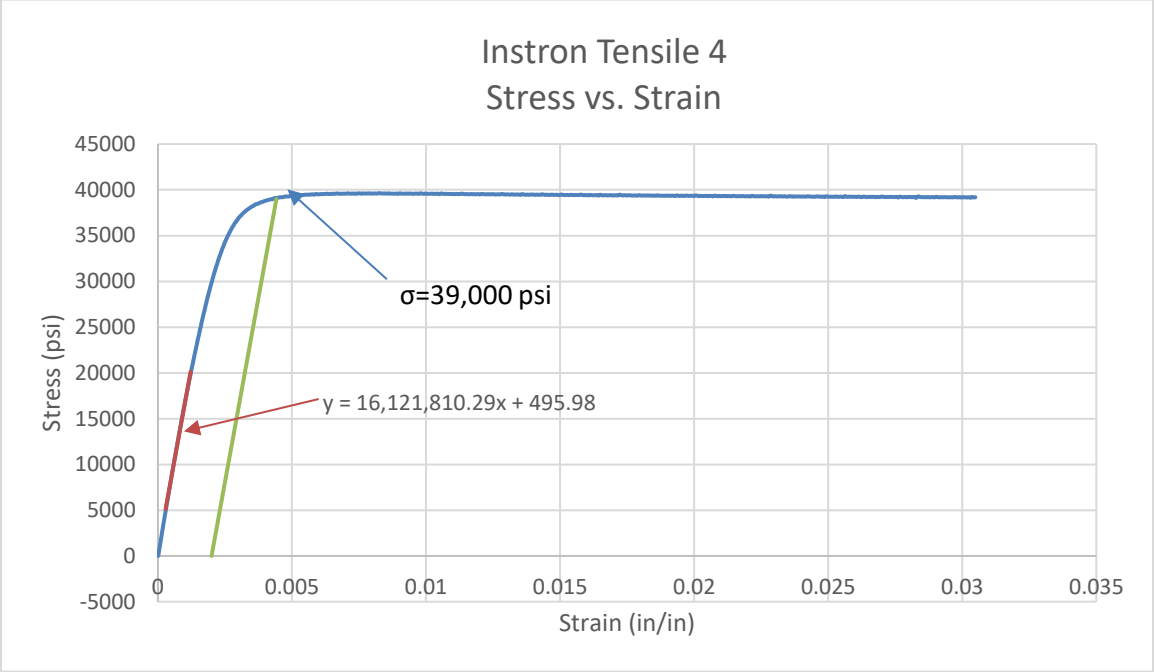


Figure 63: Stress-strain curve for Instron tensile test 4.

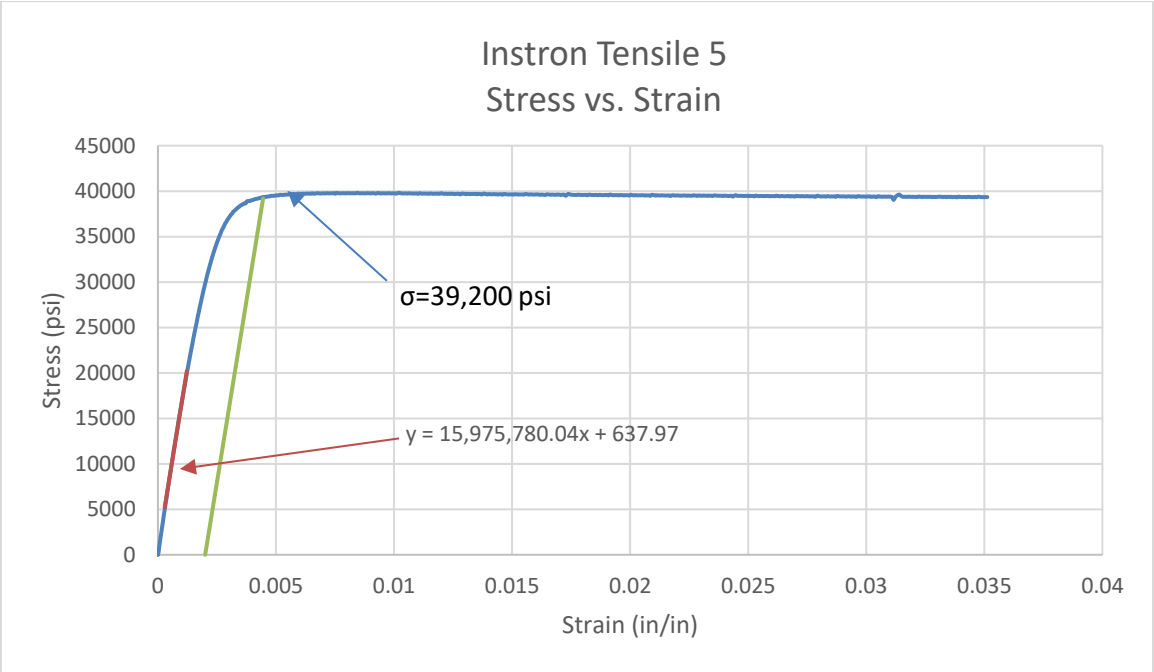


Figure 64: Stress-strain curve for Instron tensile test 5.

IPL TENSILE DATA

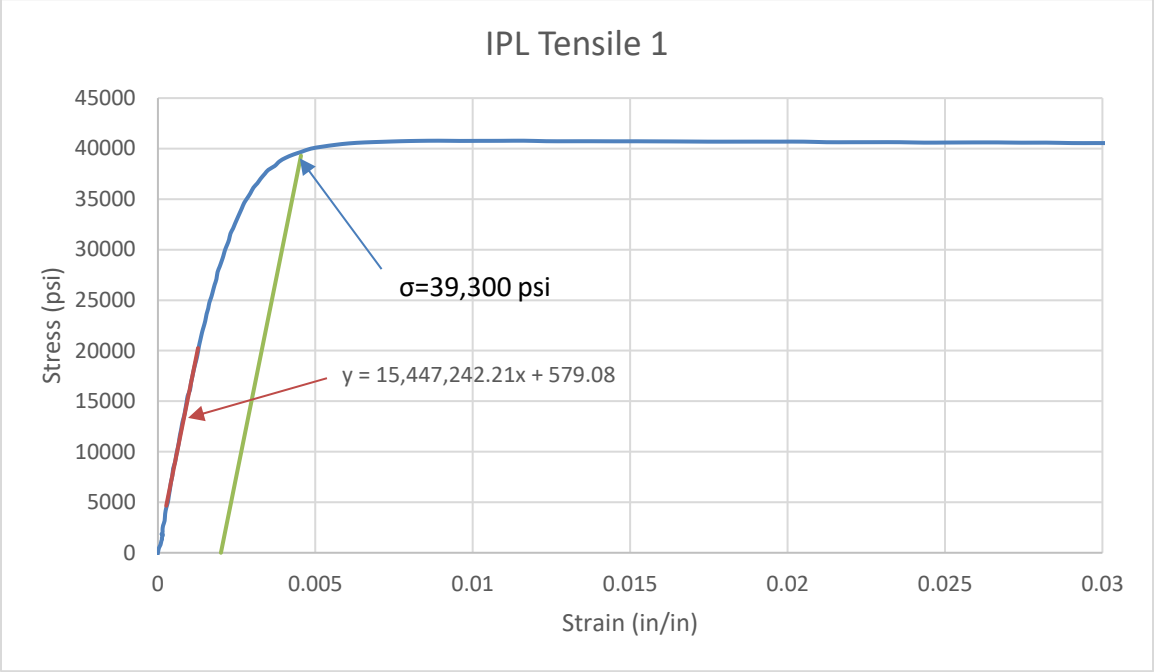


Figure 65: Stress-strain curve for IPL Quasi-Tensile test 1.

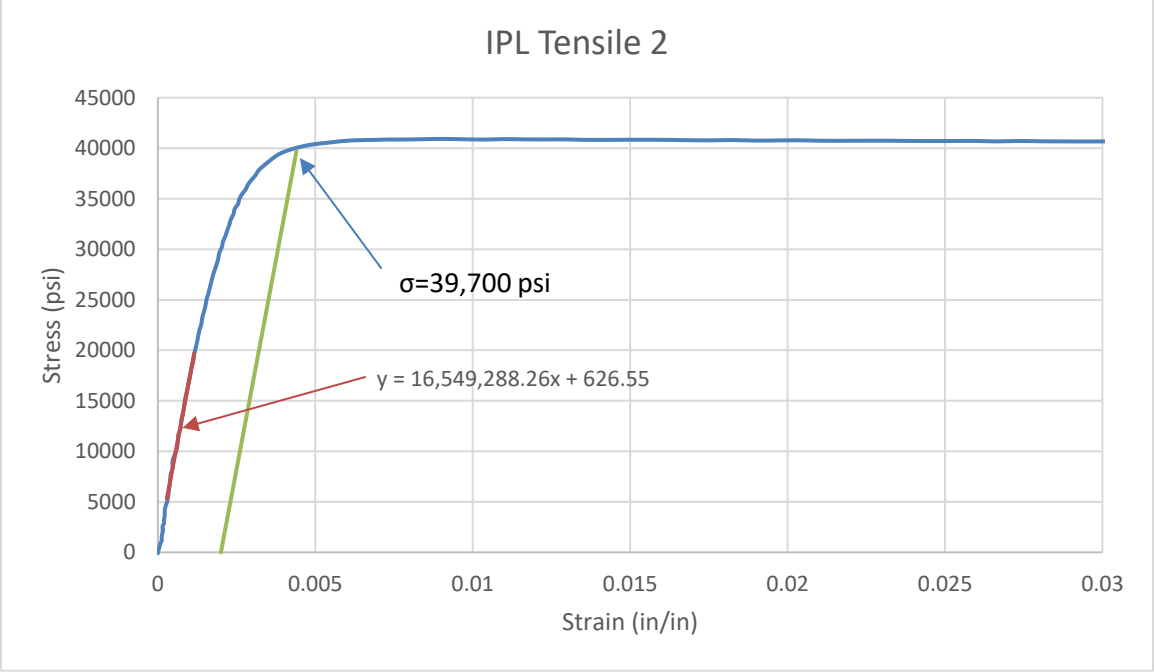


Figure 66: Stress-strain curve for IPL Quasi-Tensile test 2.

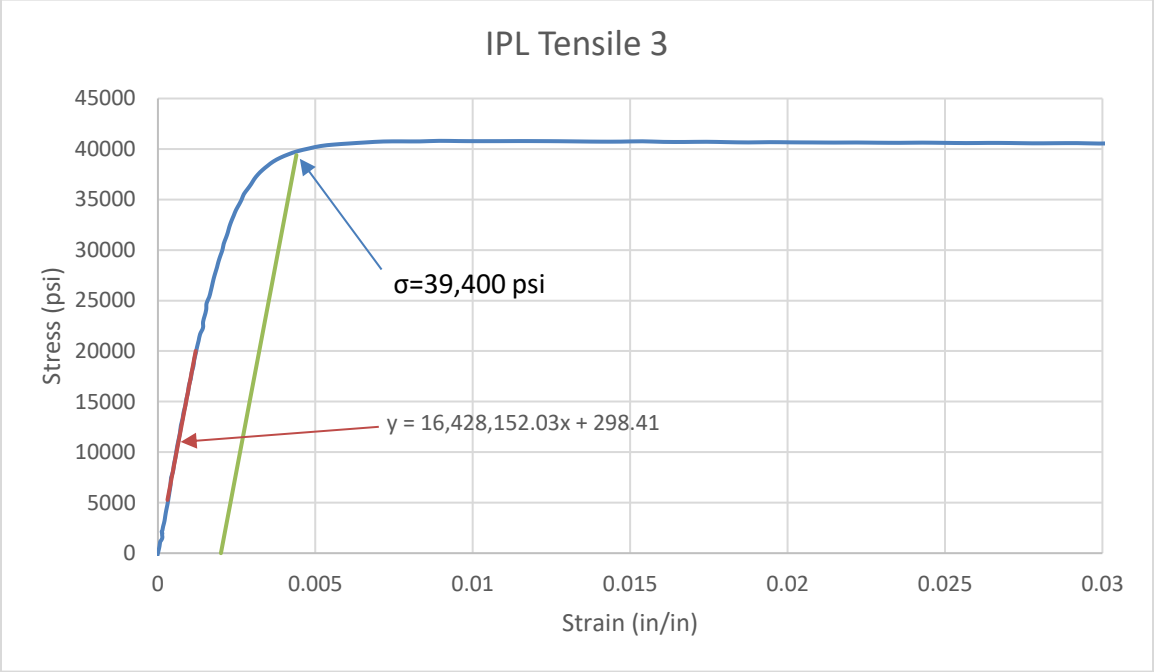


Figure 67: Stress-strain curve for IPL Quasi-Tensile test 3.

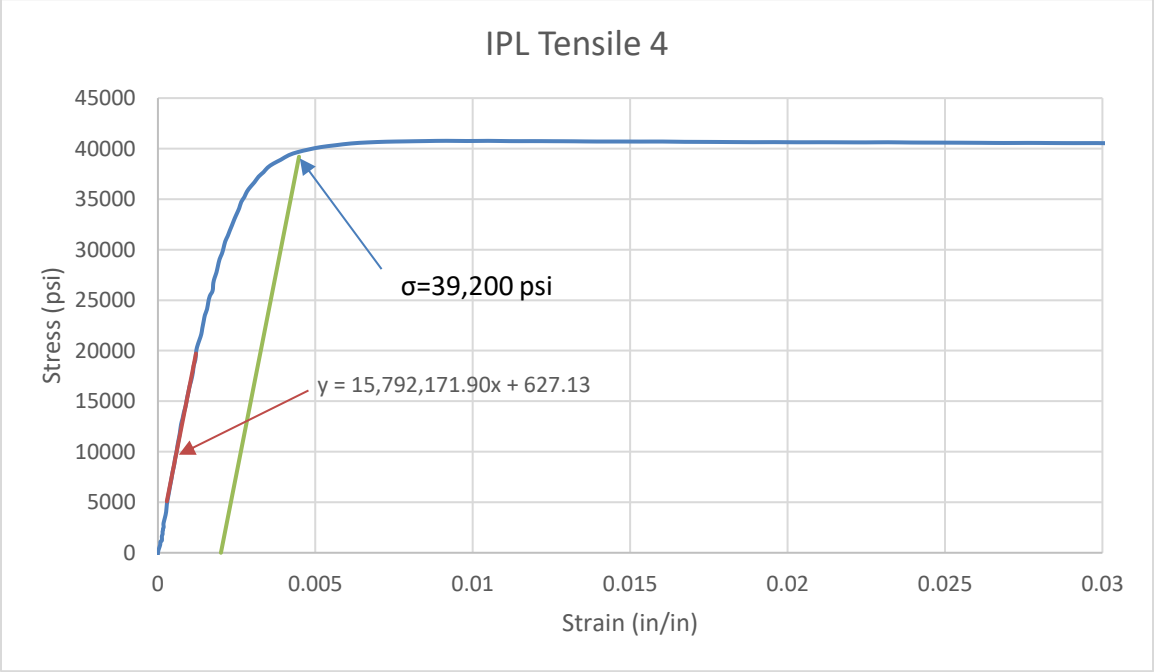


Figure 68: Stress-strain curve for IPL Quasi-Tensile test 4.

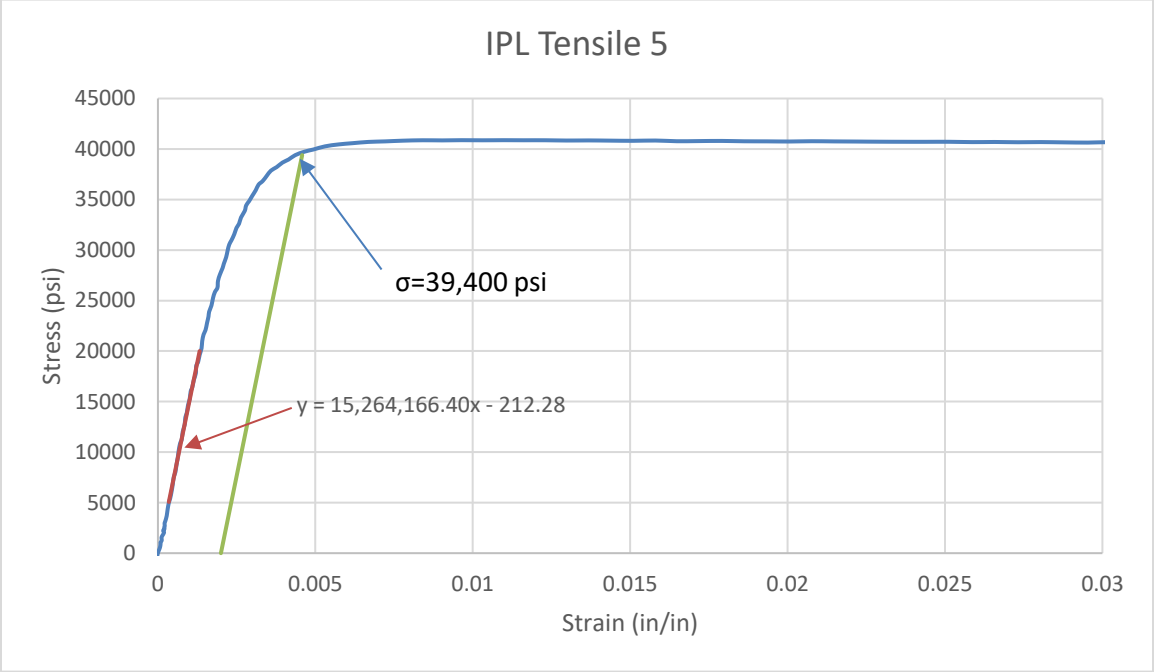


Figure 69: Stress-strain curve for IPL Quasi-Tensile test 5.

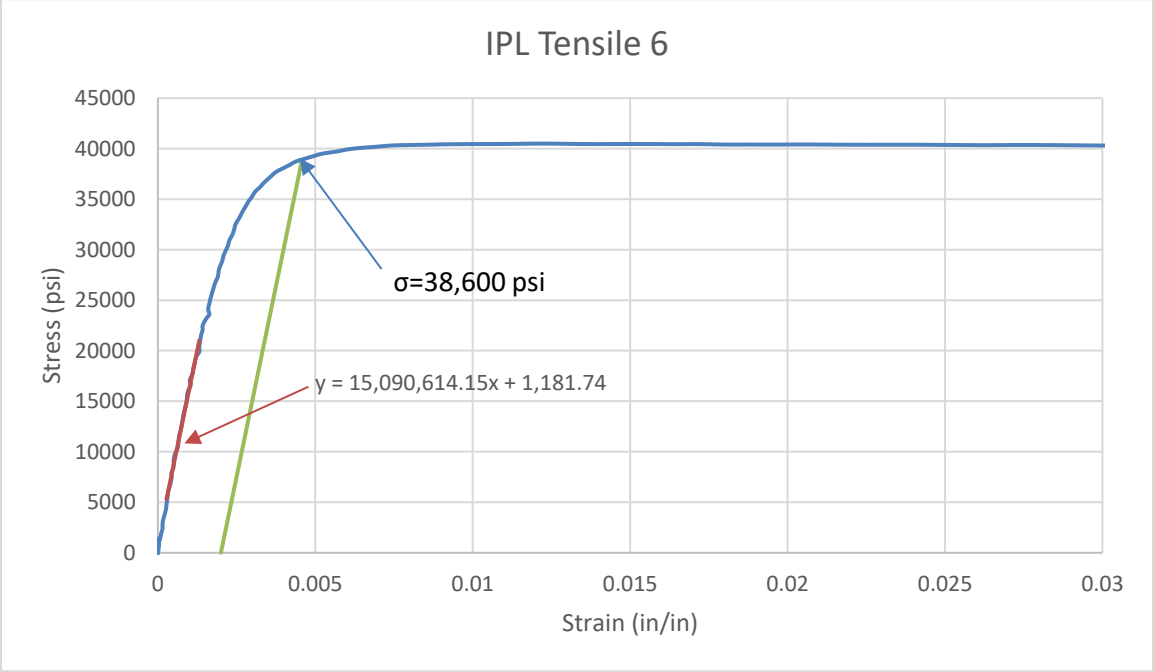


Figure 70: Stress-strain curve for IPL Quasi-Tensile test 6.

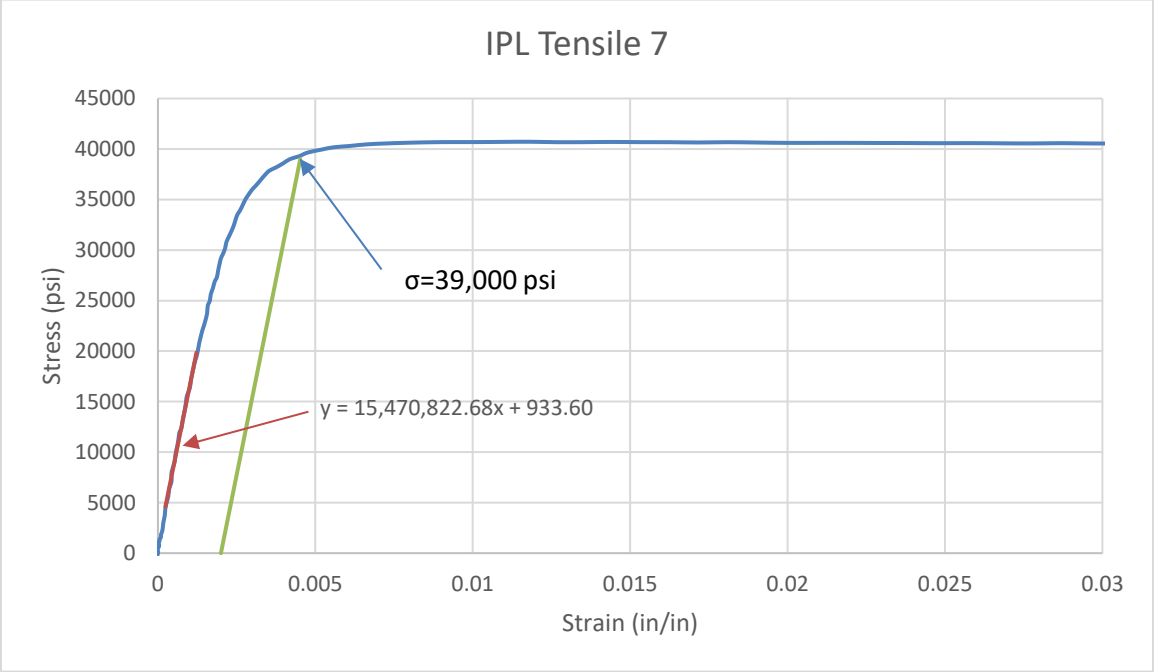


Figure 71: Stress-strain curve for IPL Quasi-Tensile test 7.

IOSIPESCU (ASTM D5379) SHEAR DATA

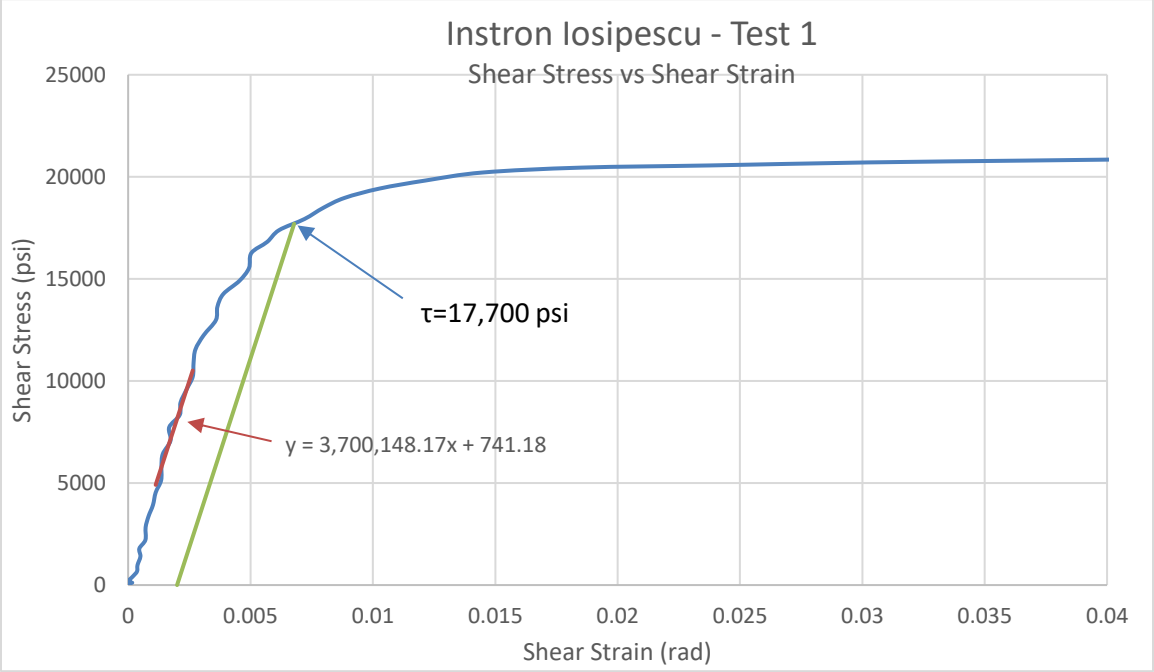


Figure 72: Shear stress-shear strain curve for Iosipescu test 1.

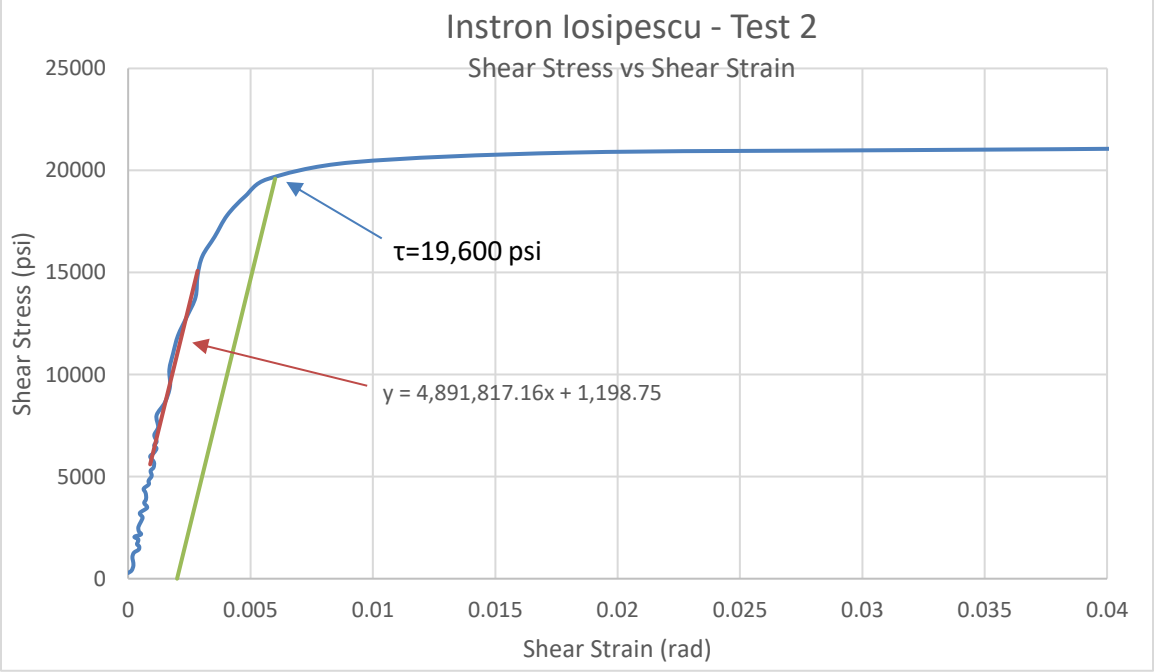


Figure 73: Shear stress-shear strain curve for Iosipescu test 2.

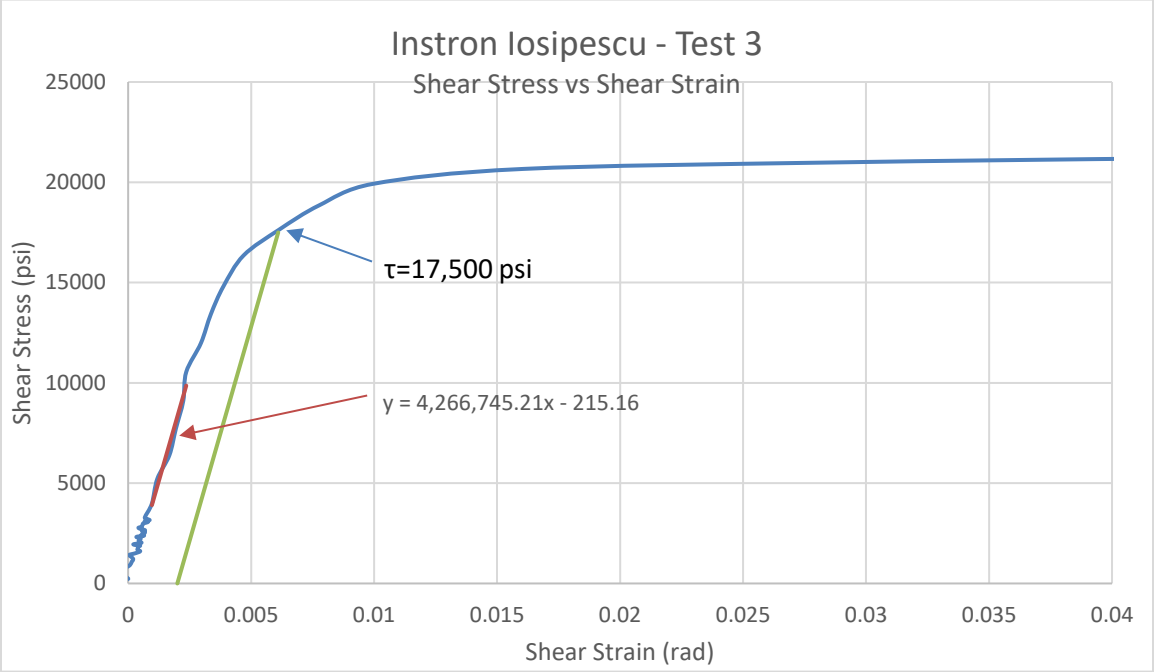


Figure 74: Shear stress-shear strain curve for Iosipescu test 3.

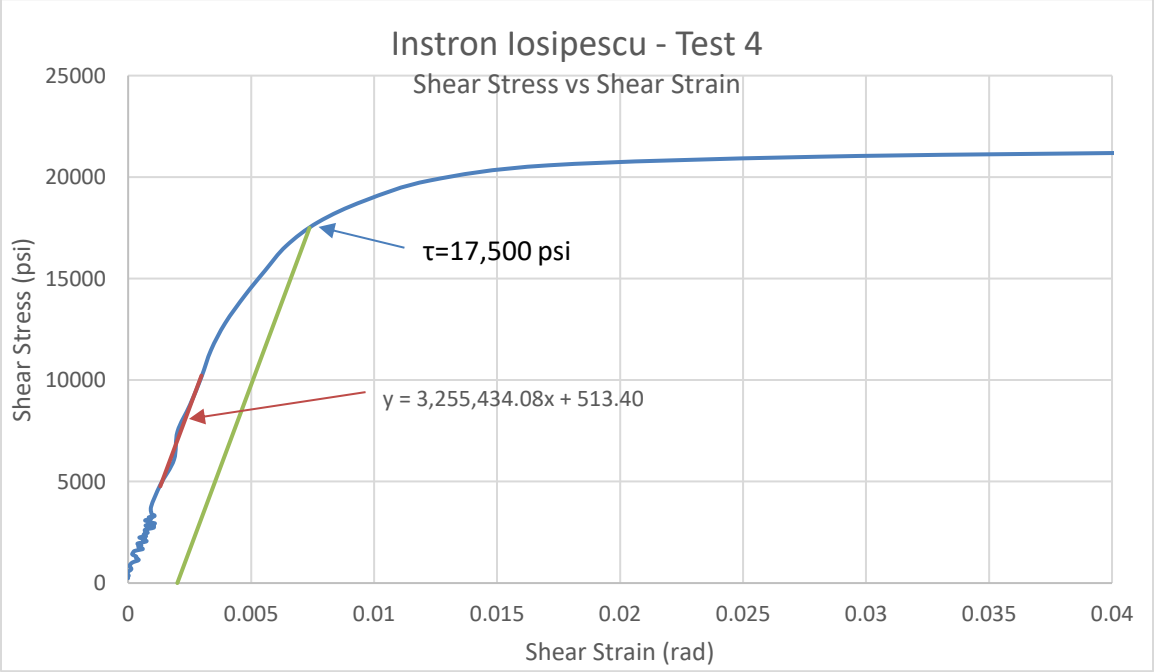


Figure 75: Shear stress-shear strain curve for Iosipescu test 4.

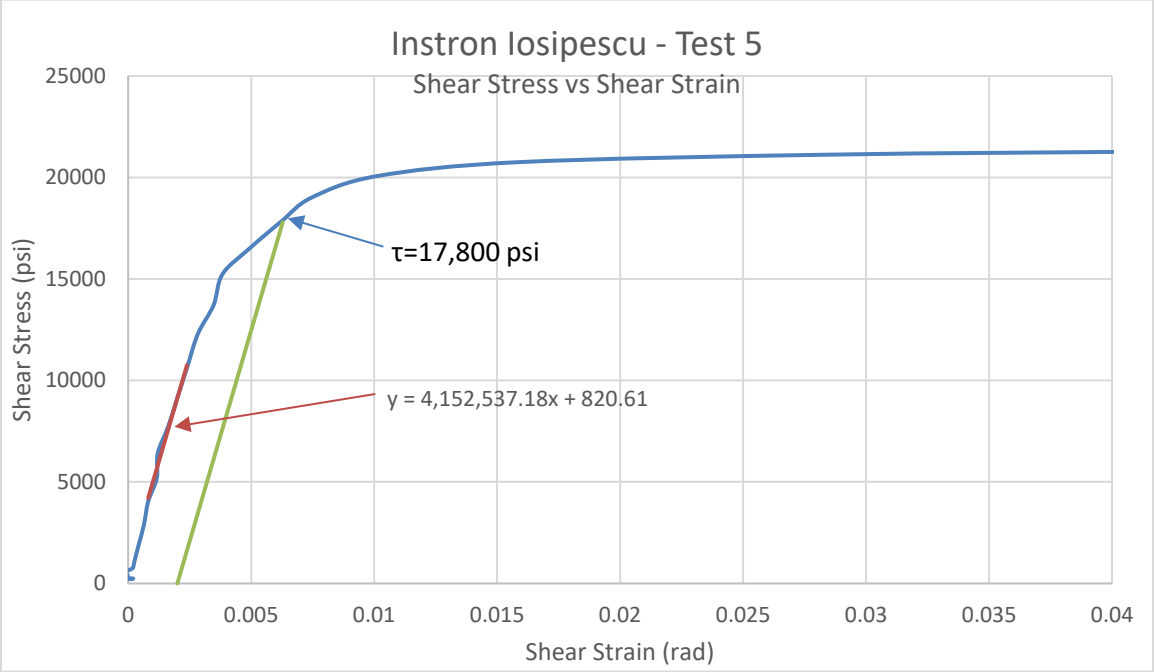


Figure 76: Shear stress-shear strain curve for Iosipescu test 5.

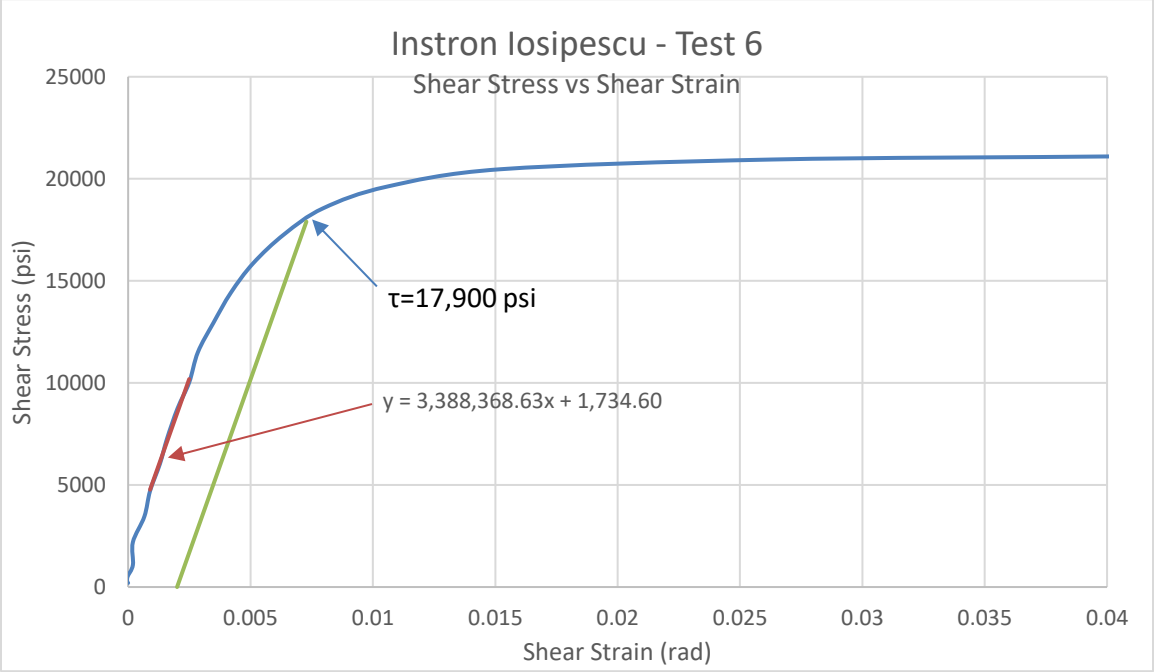


Figure 77: Shear stress-shear strain curve for Iosipescu test 6.

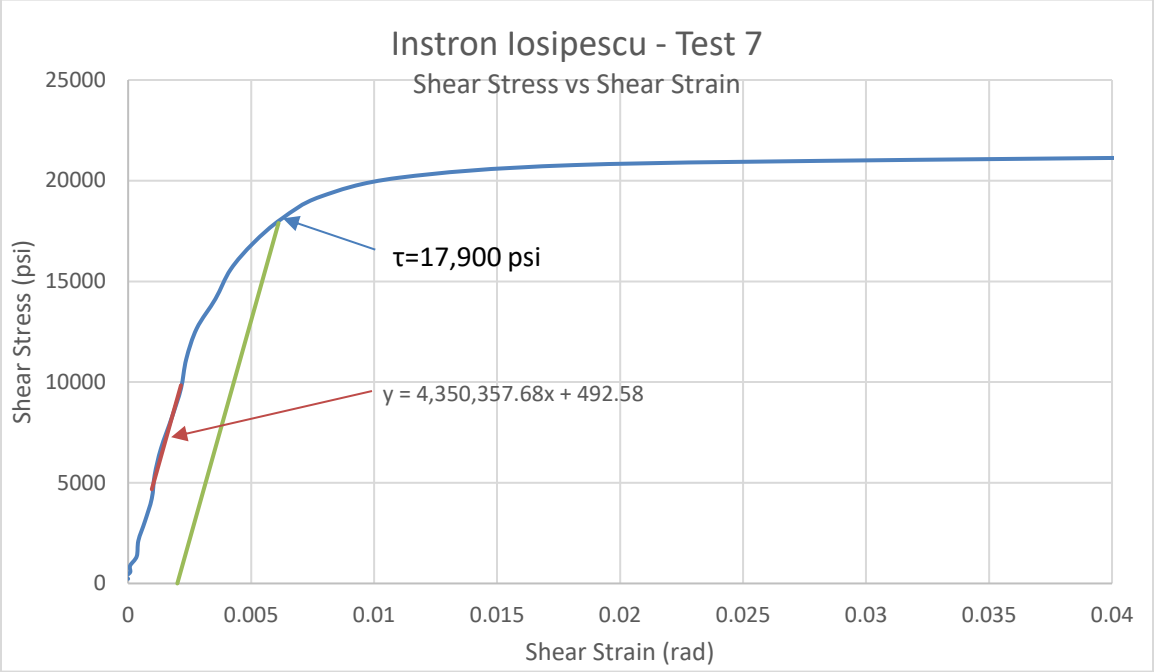


Figure 78: Shear stress-shear strain curve for Iosipescu test 7.

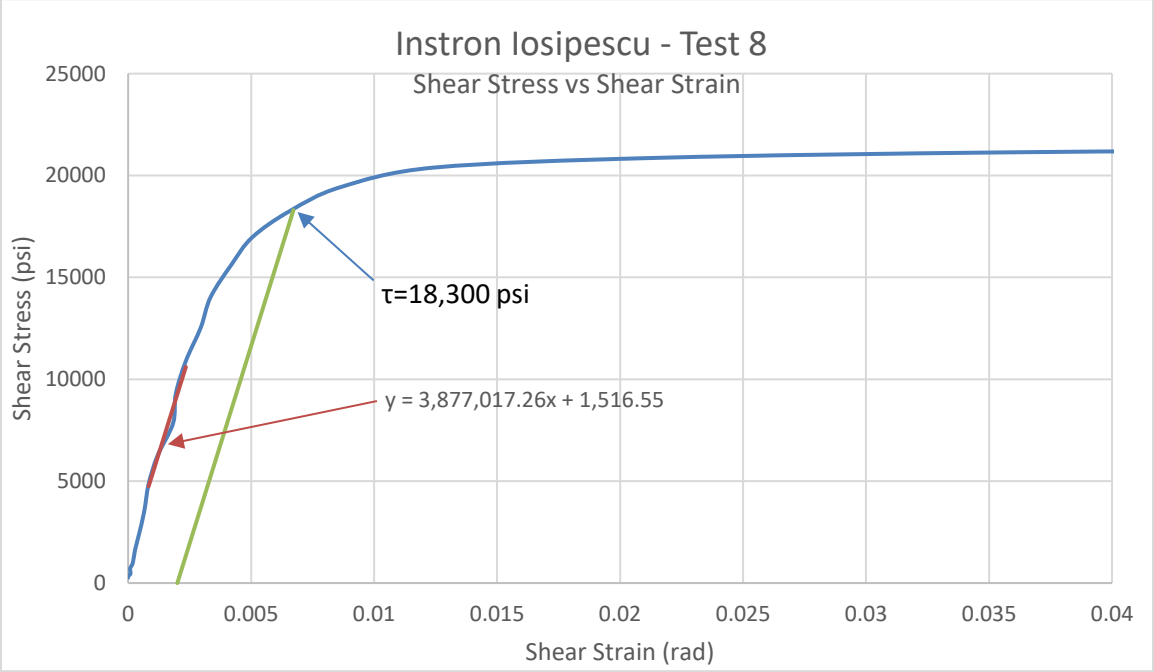


Figure 79: Shear stress-shear strain curve for Iosipescu test 8.

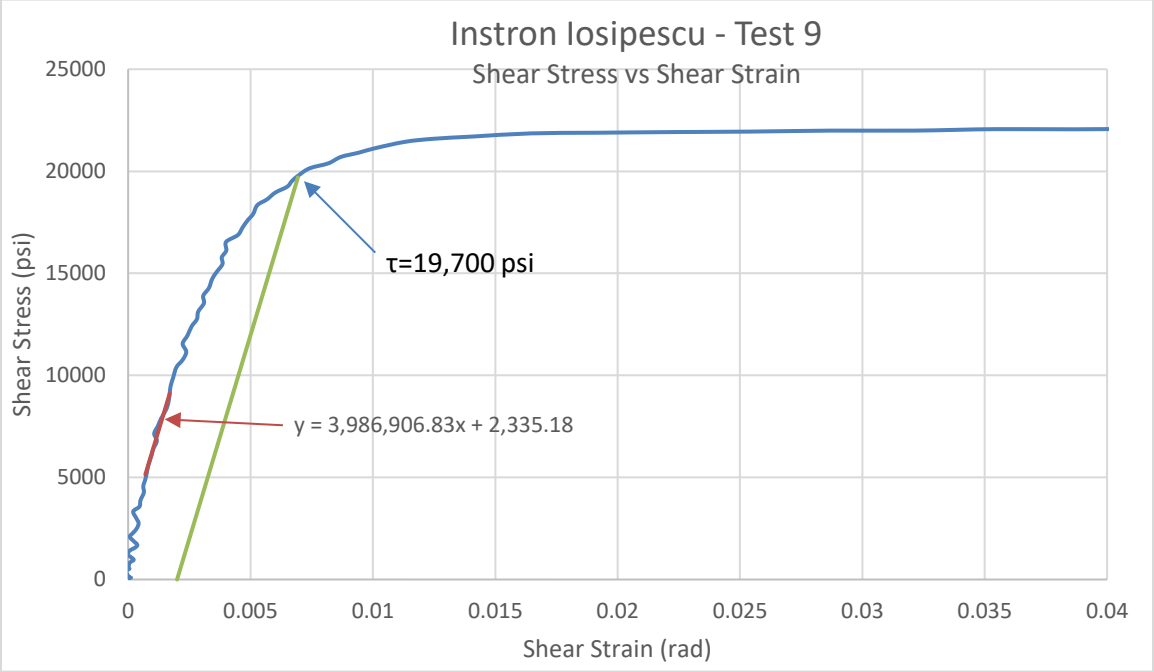


Figure 80: Shear stress-shear strain curve for Iosipescu test 9.

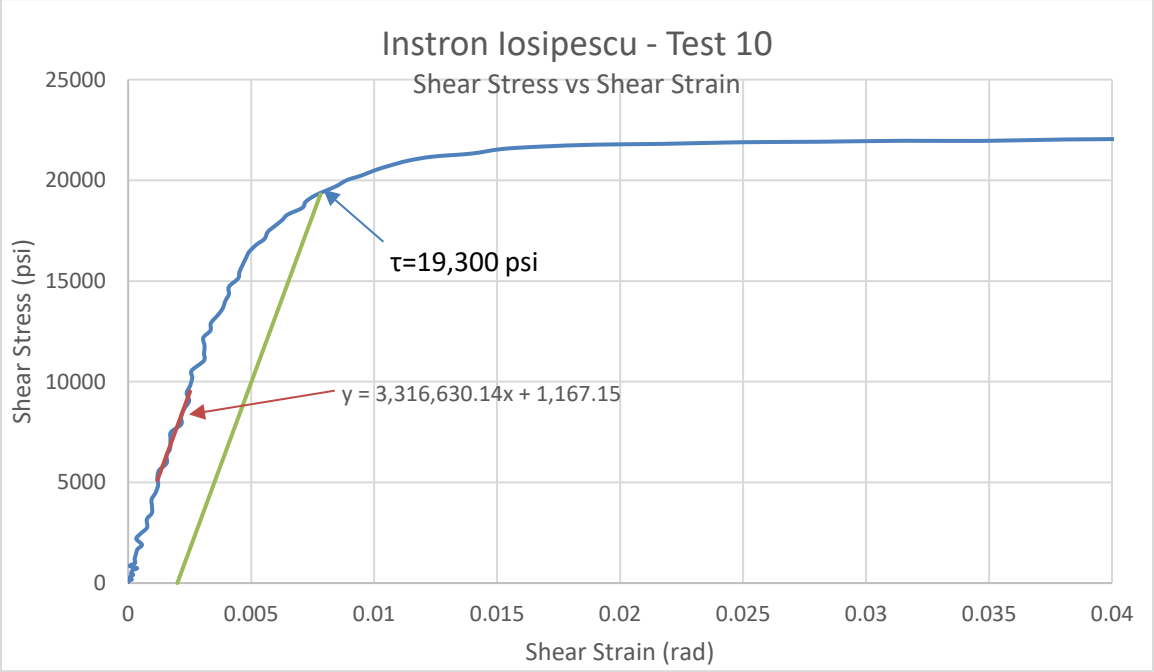


Figure 81: Shear stress-shear strain curve for Iosipescu test 10.

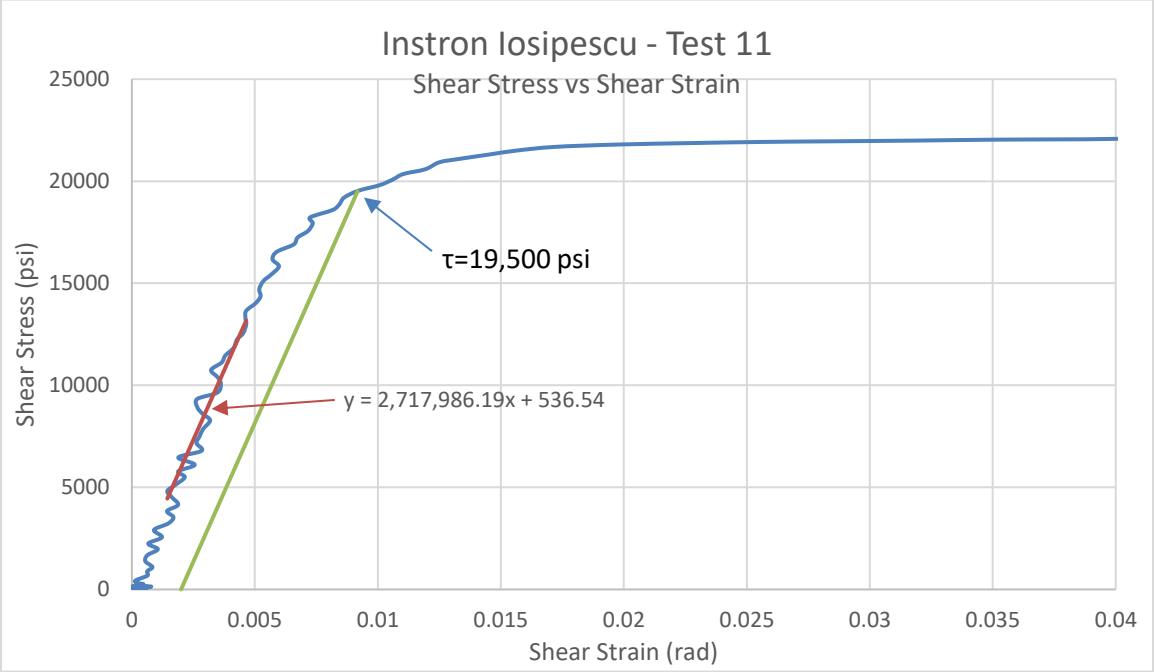


Figure 82: Shear stress-shear strain curve for Iosipescu test 11.

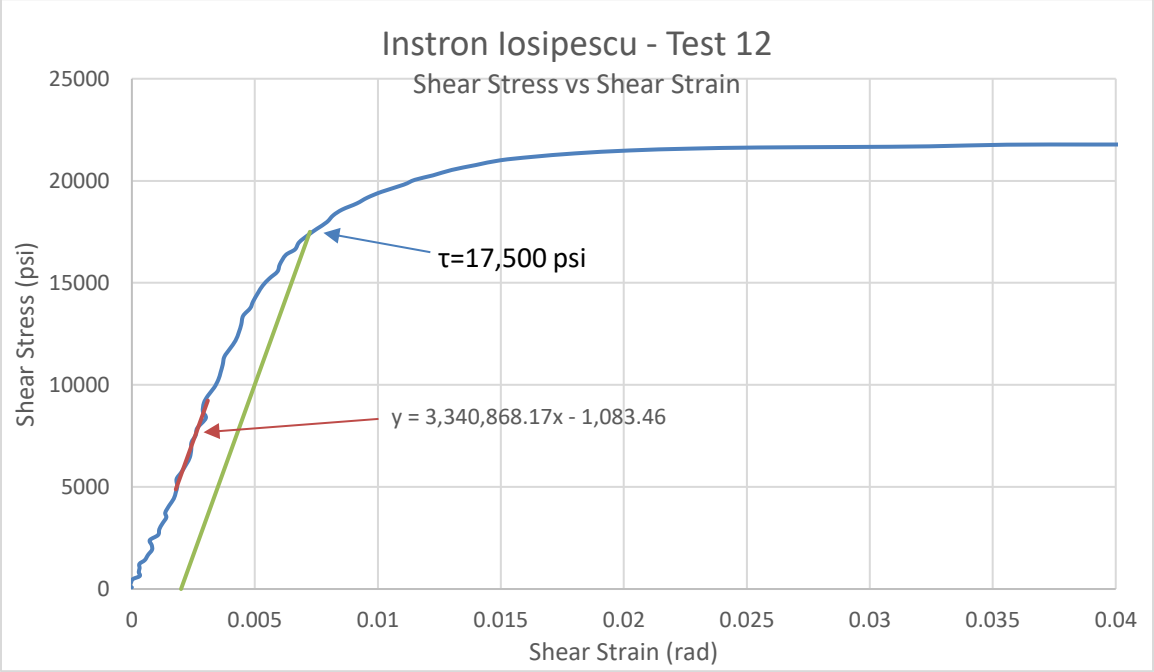


Figure 83: Shear stress-shear strain curve for Iosipescu test 12.

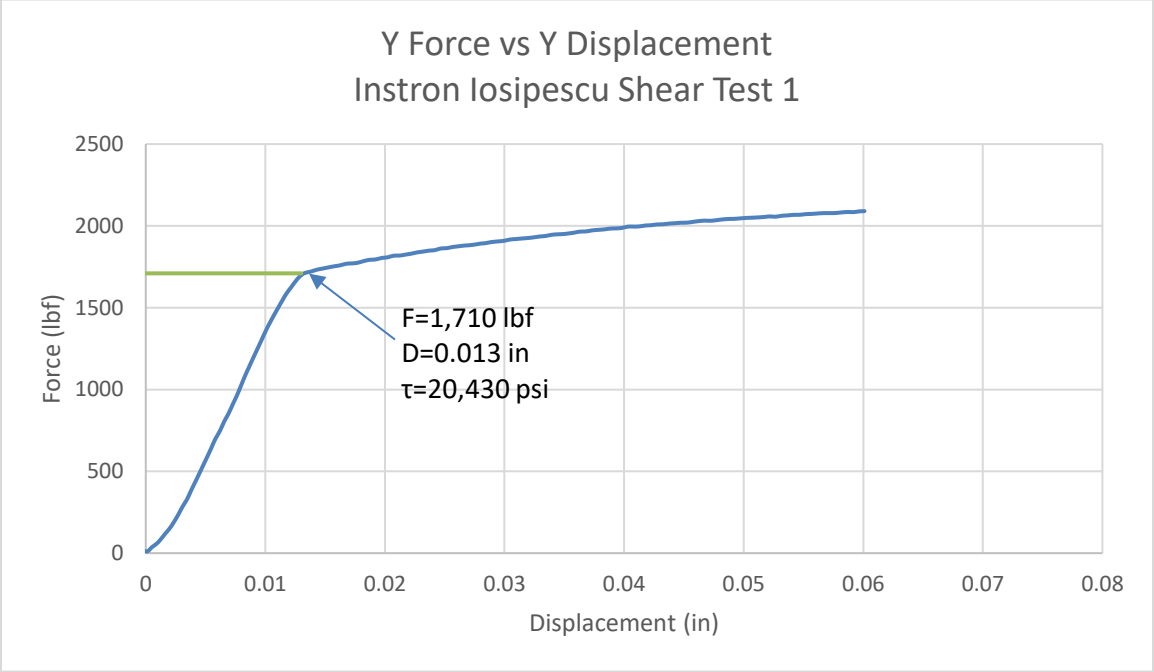


Figure 84: Force-displacement curve for Iosipescu test 1. (NOTE: Force-displacement data is not presented for tests 2-8)

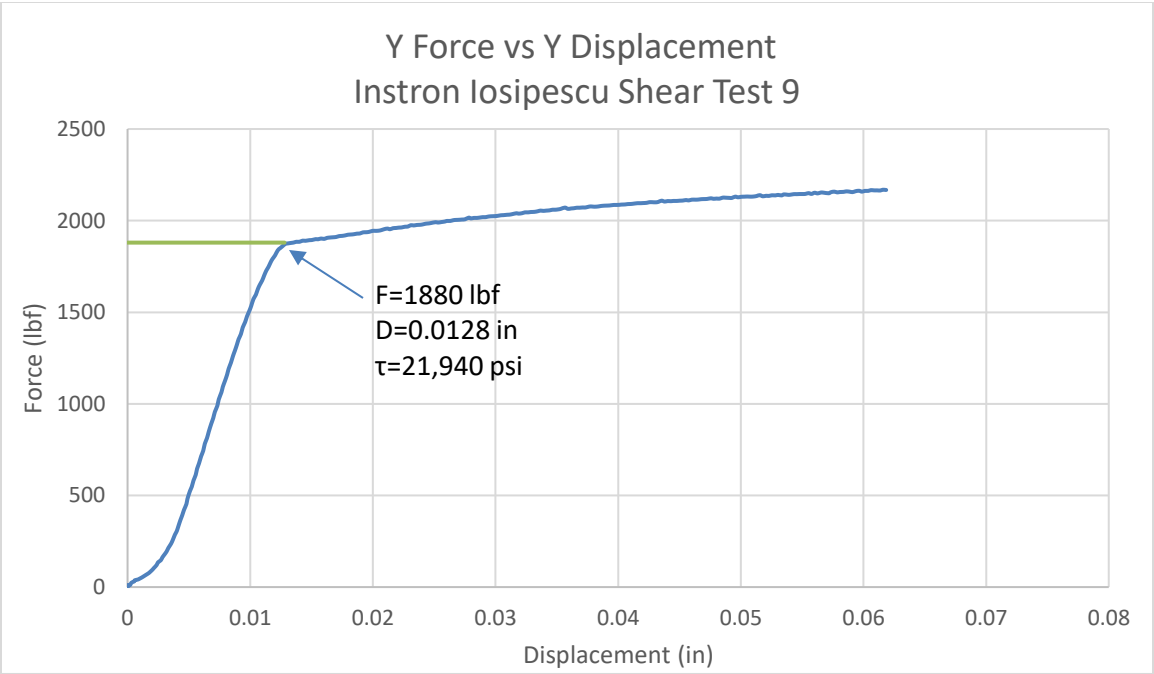


Figure 85: Force-displacement curve for Iosipescu test 9.

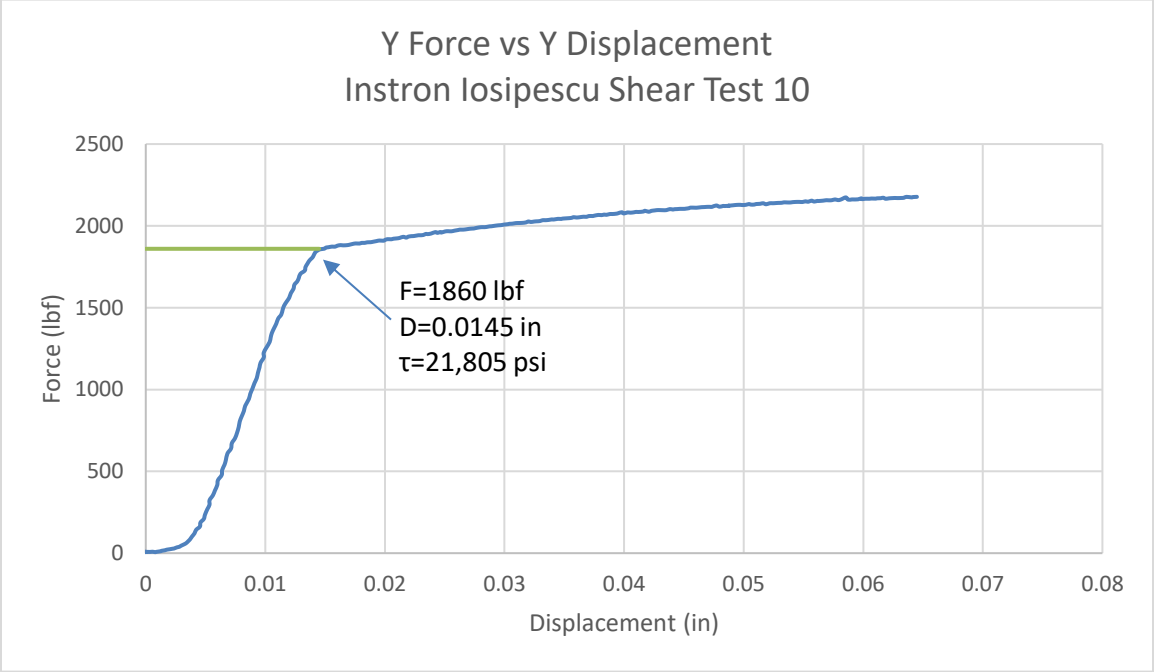


Figure 86: Force-displacement curve for Iosipescu test 10.

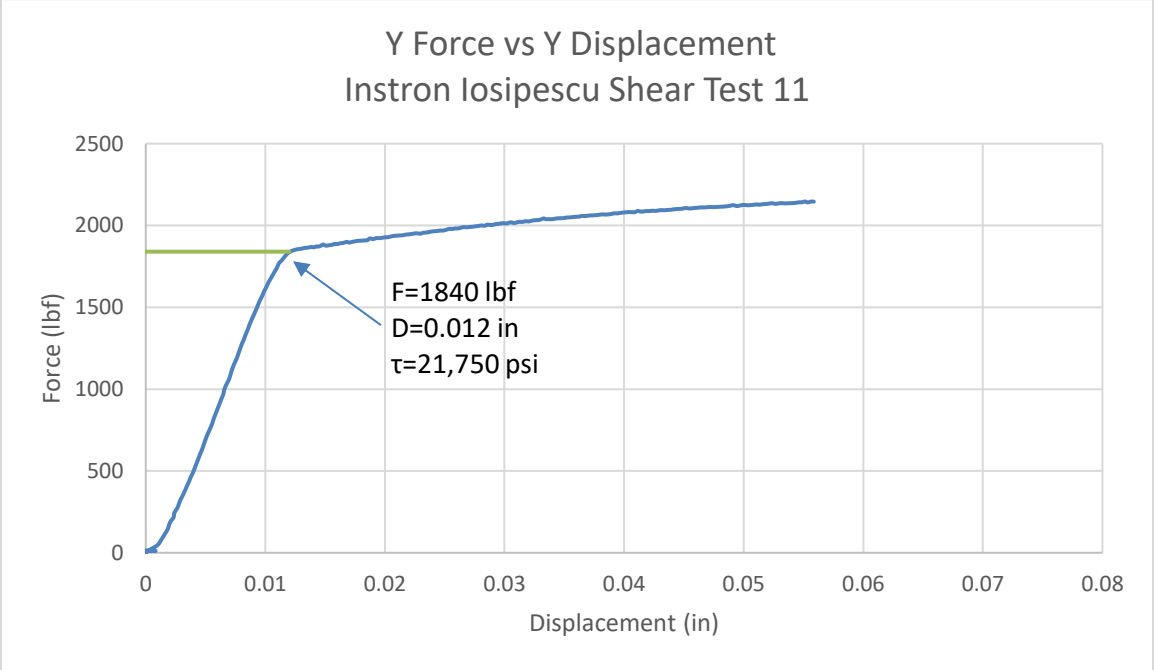


Figure 87: Force-displacement curve for Iosipescu test 11.

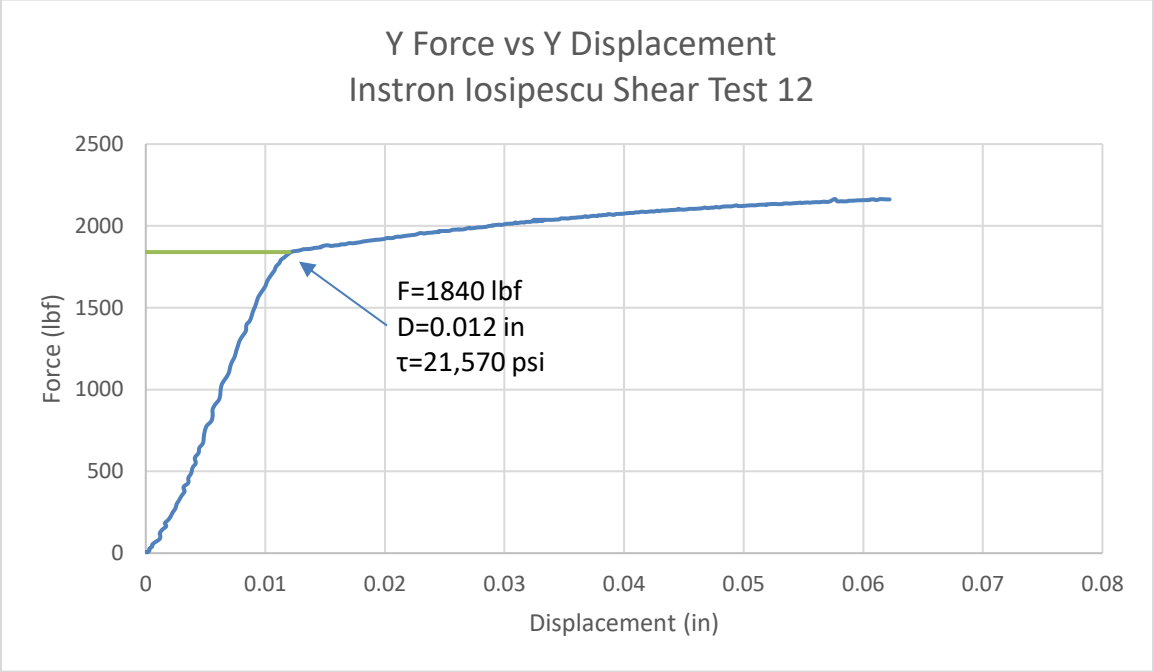


Figure 88: Force-displacement curve for Iosipescu test 12.

IPL SHEAR TEST DATA

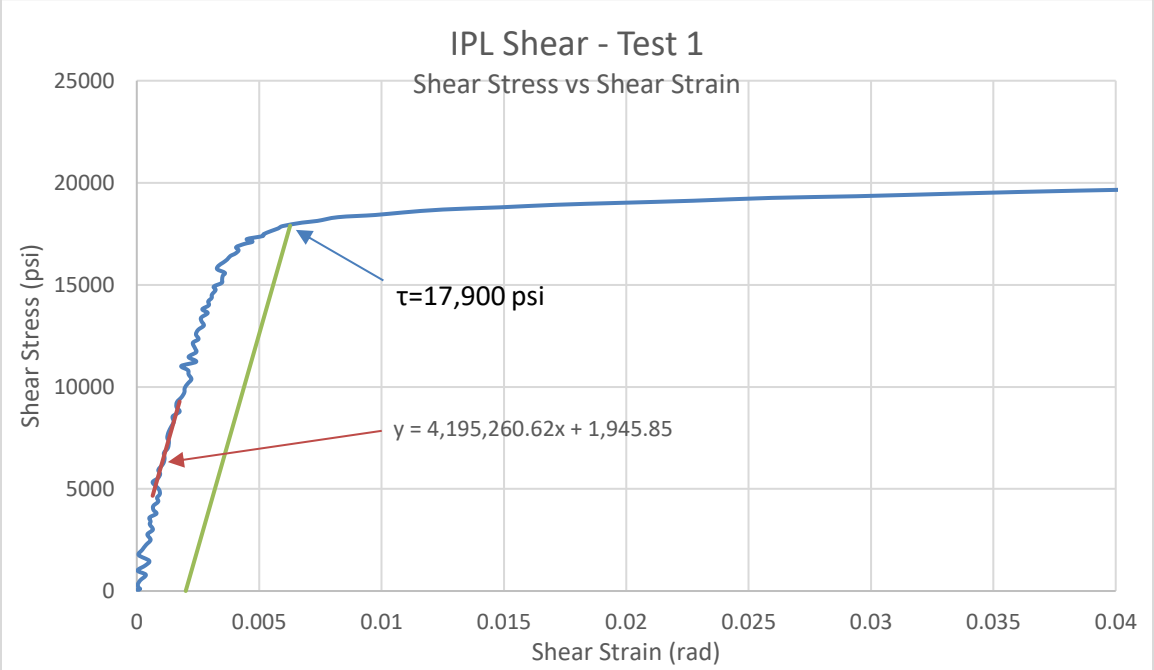


Figure 89: Shear stress-shear strain curve for IPL shear test 1.

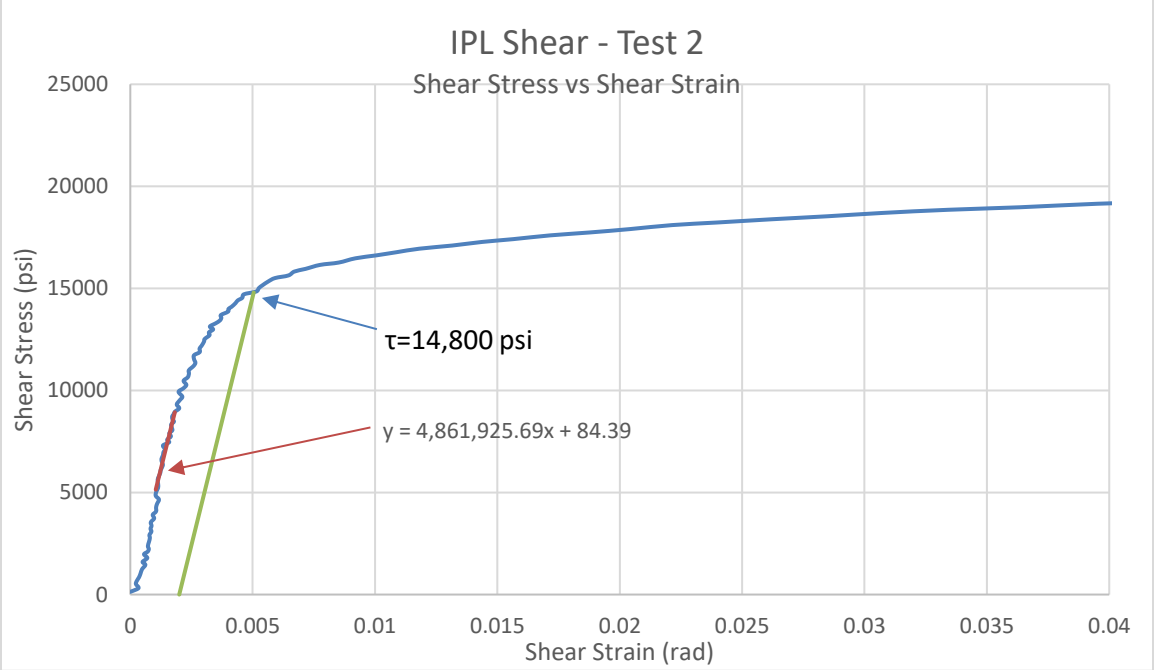


Figure 90: Shear stress-shear strain curve for IPL shear test 2.

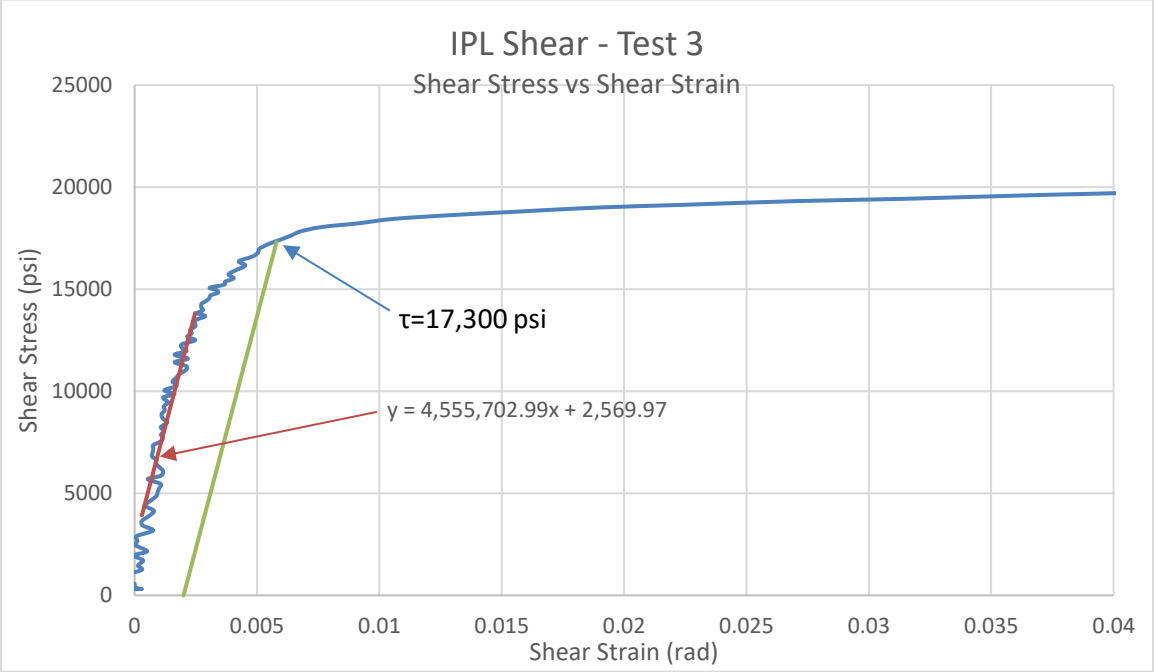


Figure 91: Shear stress-shear strain curve for IPL shear test 3.

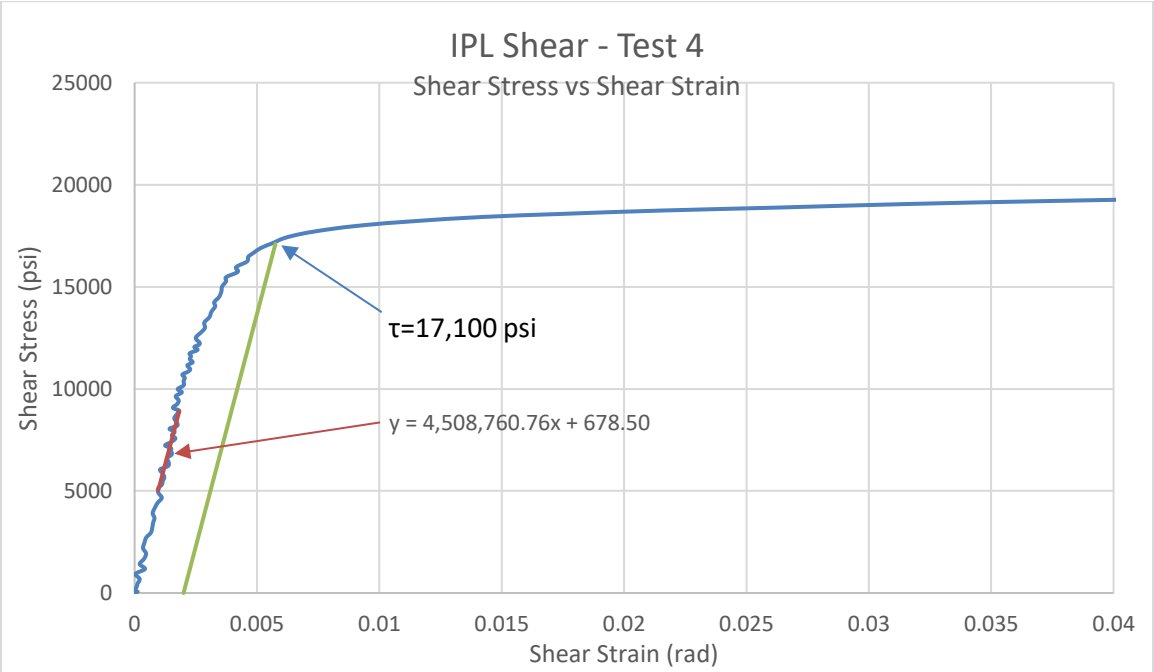


Figure 92: Shear stress-shear strain curve for IPL shear test 4.

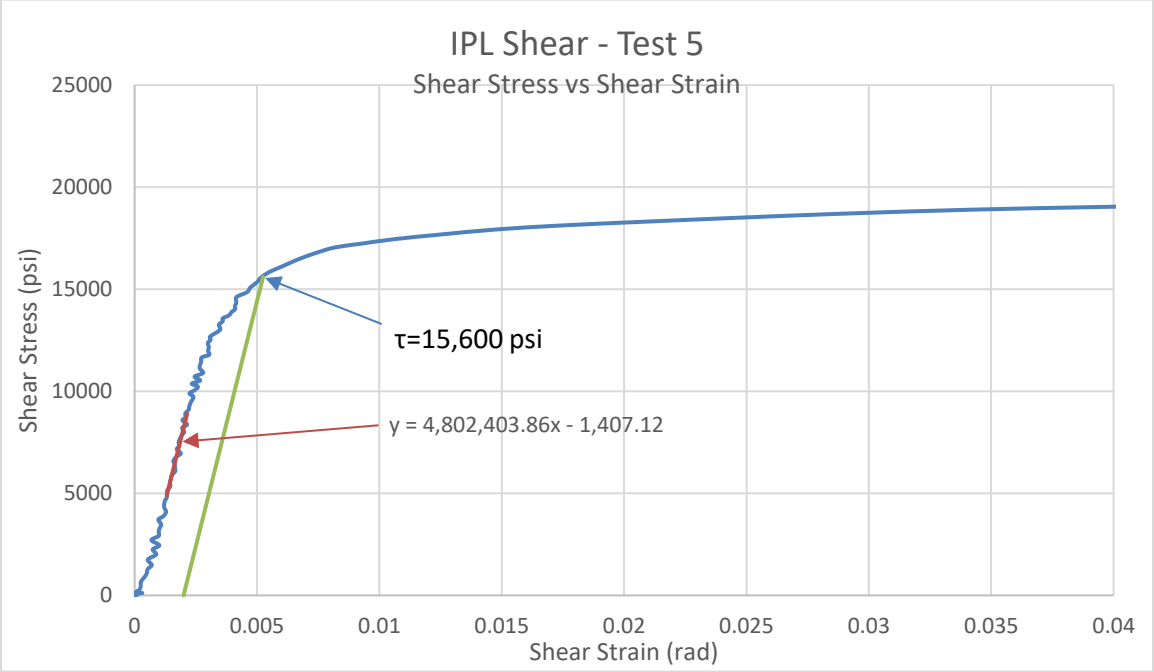


Figure 93: Shear stress-shear strain curve for IPL shear test 5.

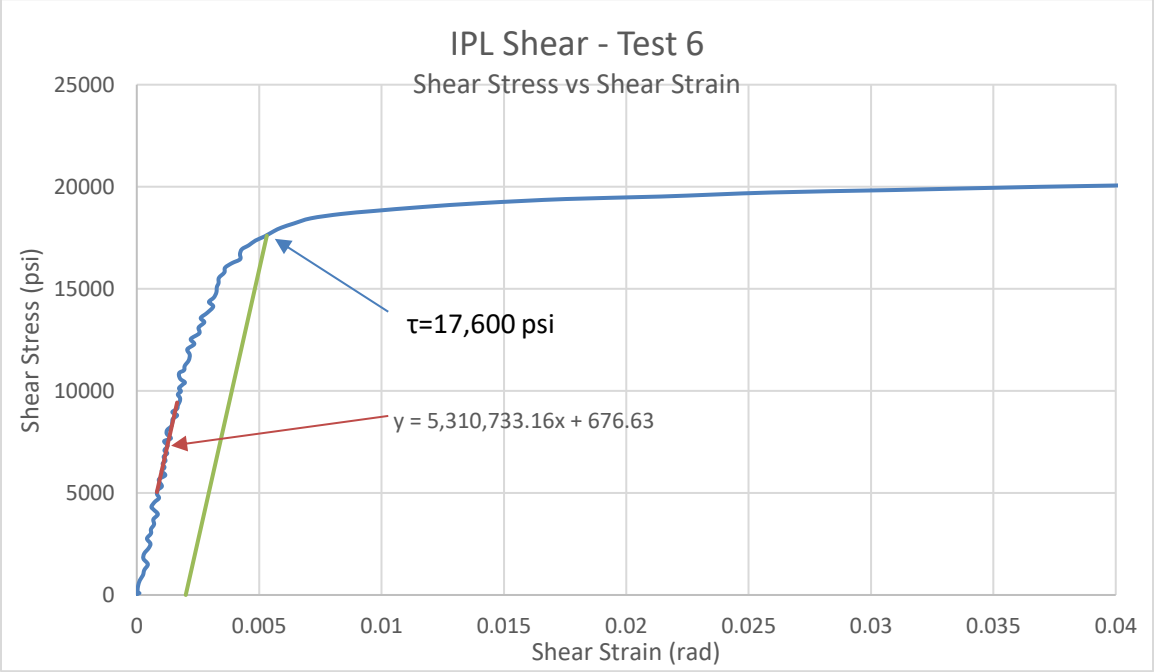


Figure 94: Shear stress-shear strain curve for IPL shear test 6.

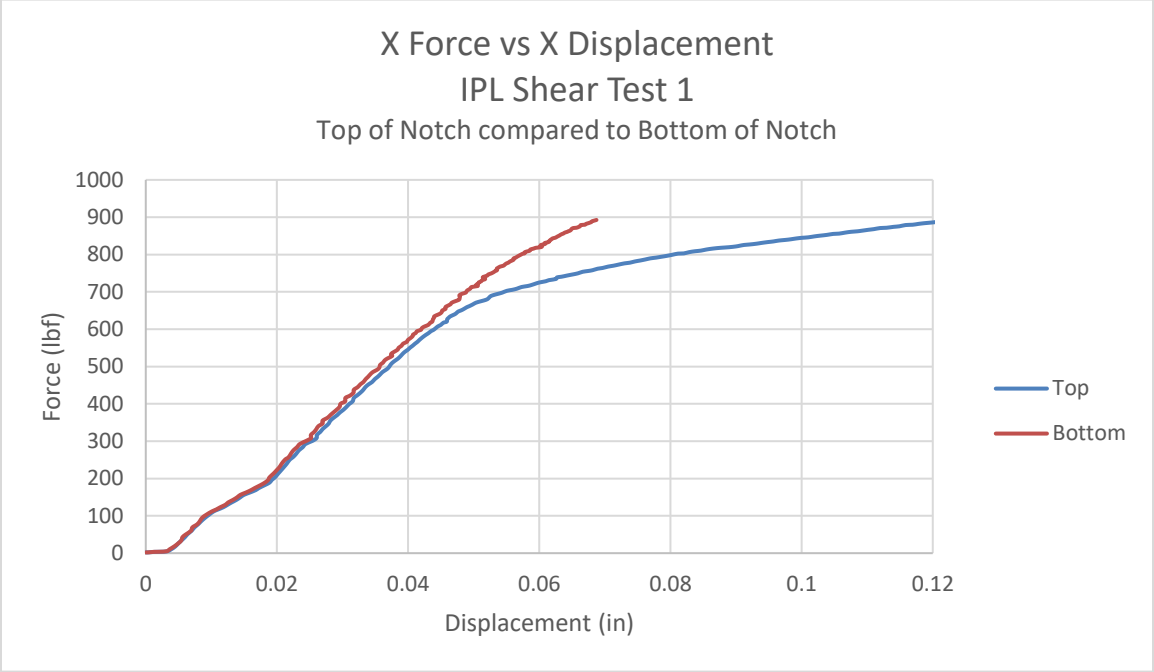


Figure 95: Force-displacement curves for IPL shear test 1. Data sets for displacements directly above (top) and below (bottom) the notched cross-section.

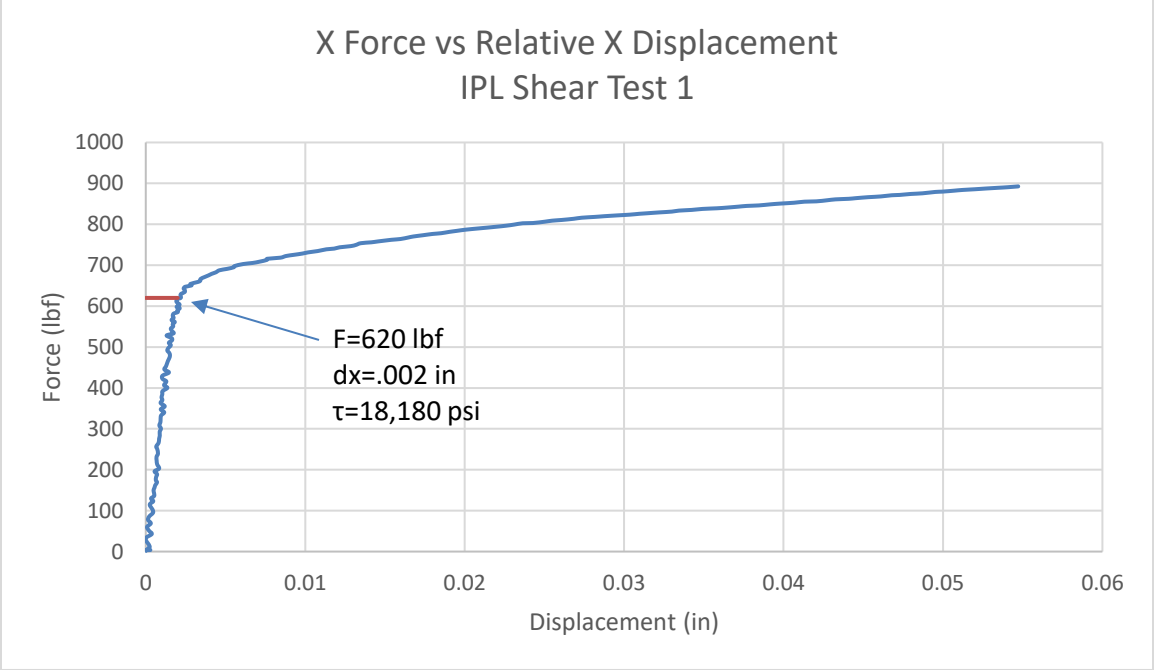


Figure 96: Force-relative displacement curve for IPL shear test 1. Displacement is corrected to eliminate effects of bending and grip slippage.

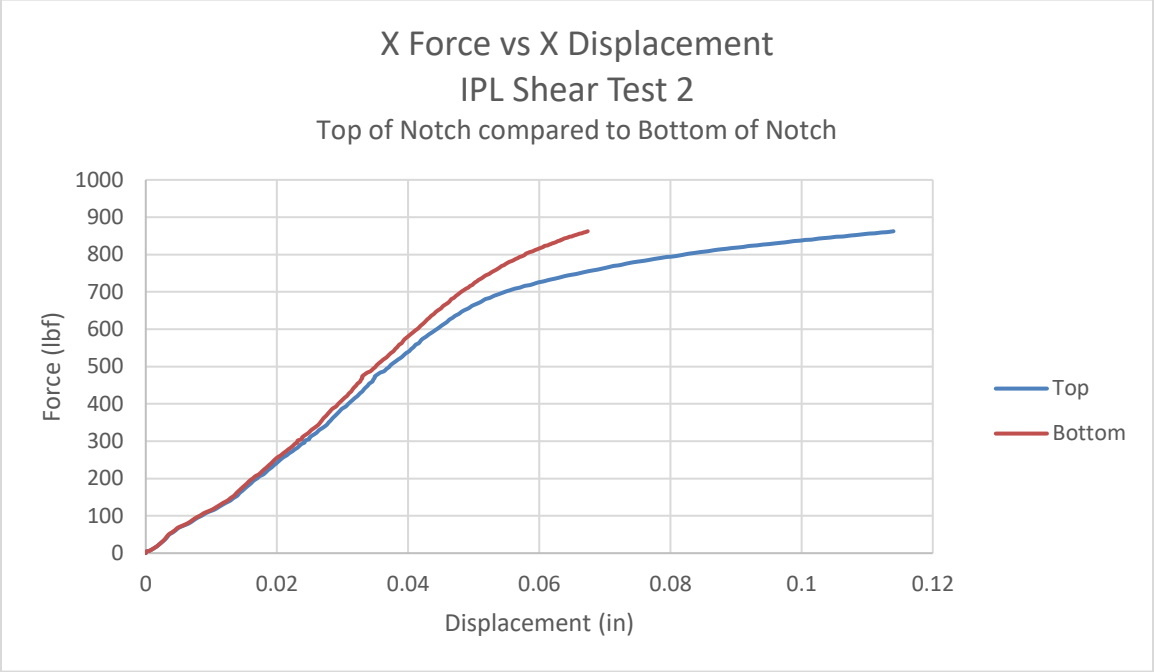


Figure 97: Force-displacement curves for IPL shear test 2. Data sets for displacements directly above (top) and below (bottom) the notched cross-section.

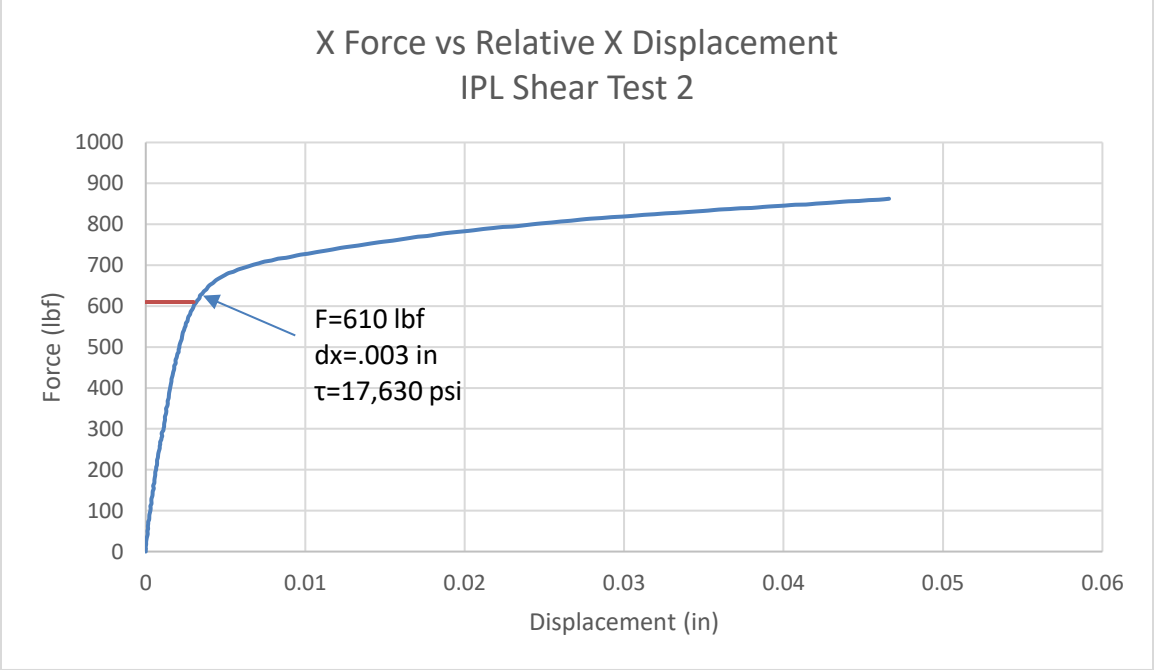


Figure 98: Force-relative displacement curve for IPL shear test 2. Displacement is corrected to eliminate effects of bending and grip slippage.

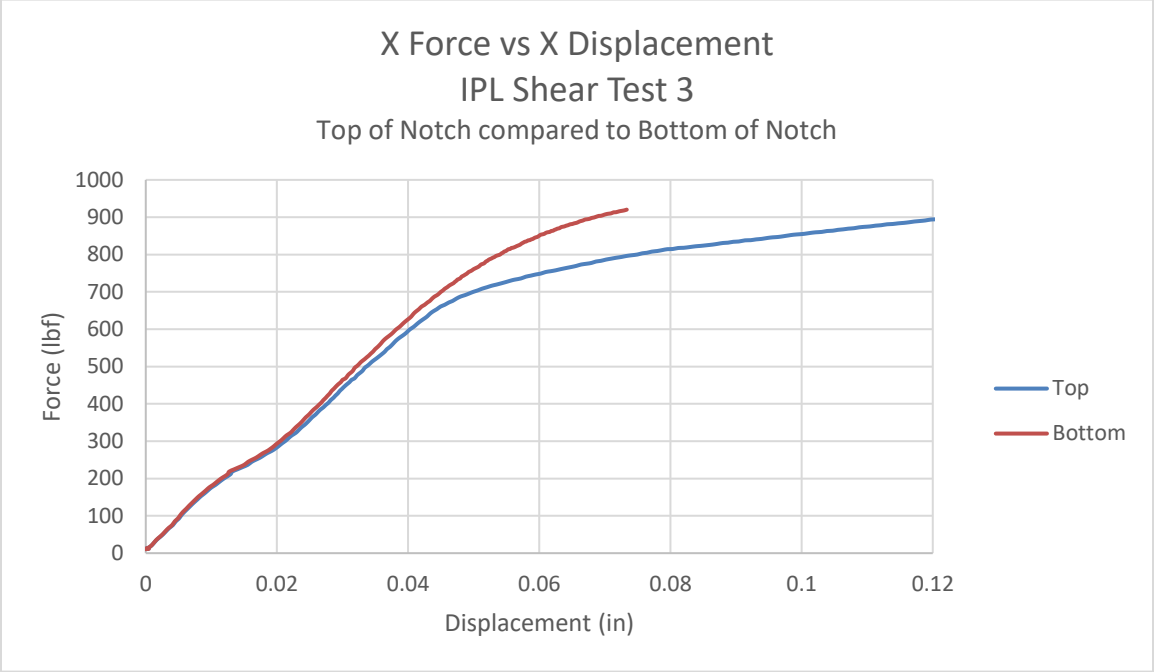


Figure 99: Force-displacement curves for IPL shear test 3. Data sets for displacements directly above (top) and below (bottom) the notched cross-section.

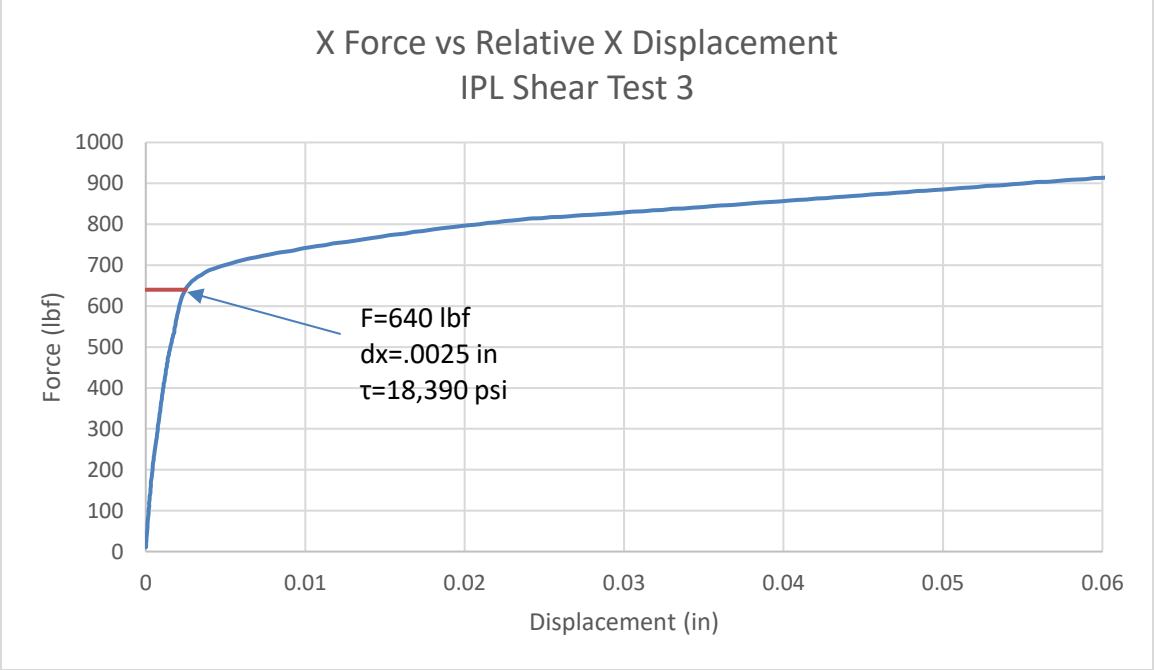


Figure 100: Force-relative displacement curve for IPL shear test 3. Displacement is corrected to eliminate effects of bending and grip slippage.

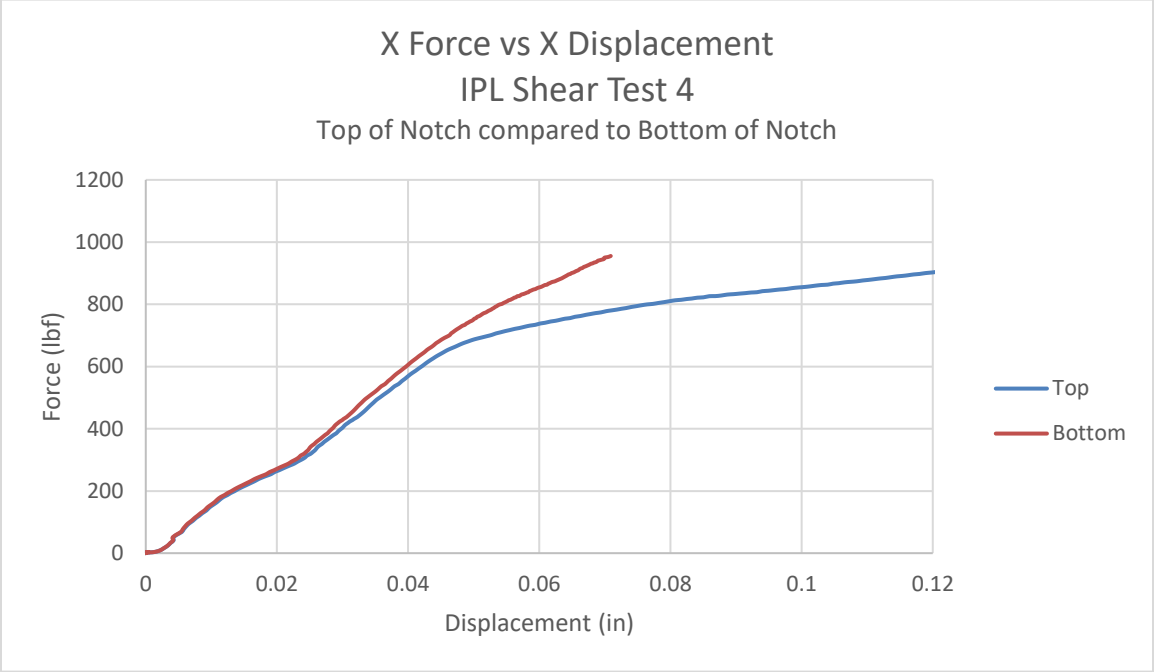


Figure 101: Force-displacement curves for IPL shear test 4. Data sets for displacements directly above (top) and below (bottom) the notched cross-section.

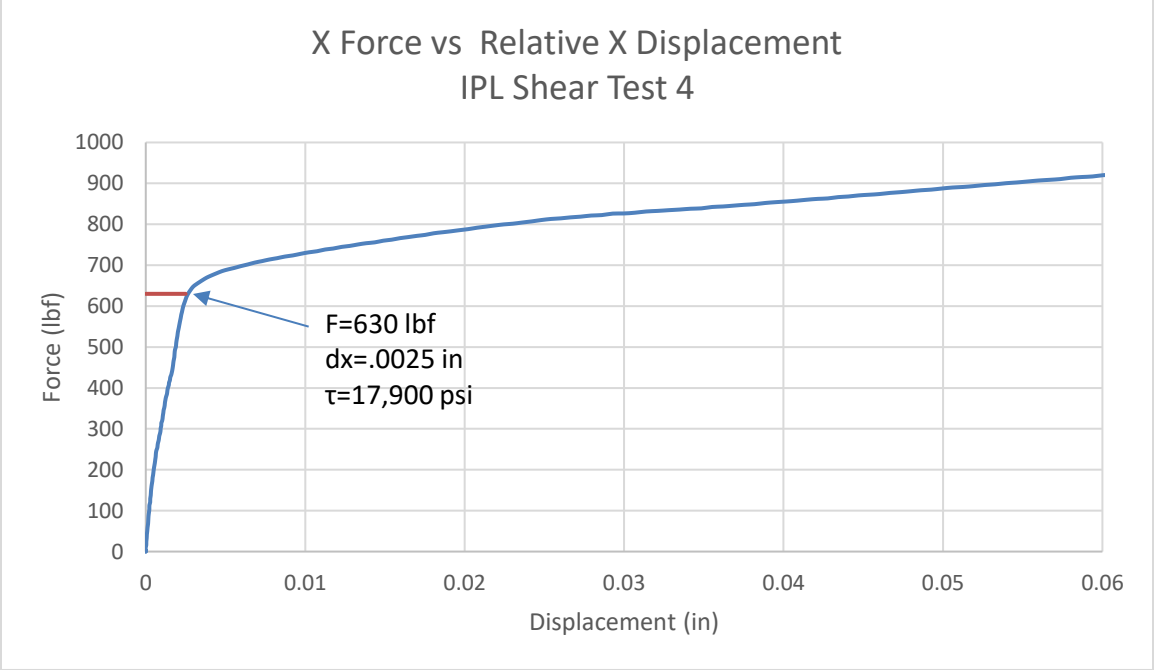


Figure 102: Force-relative displacement curve for IPL shear test 4. Displacement is corrected to eliminate effects of bending and grip slippage.

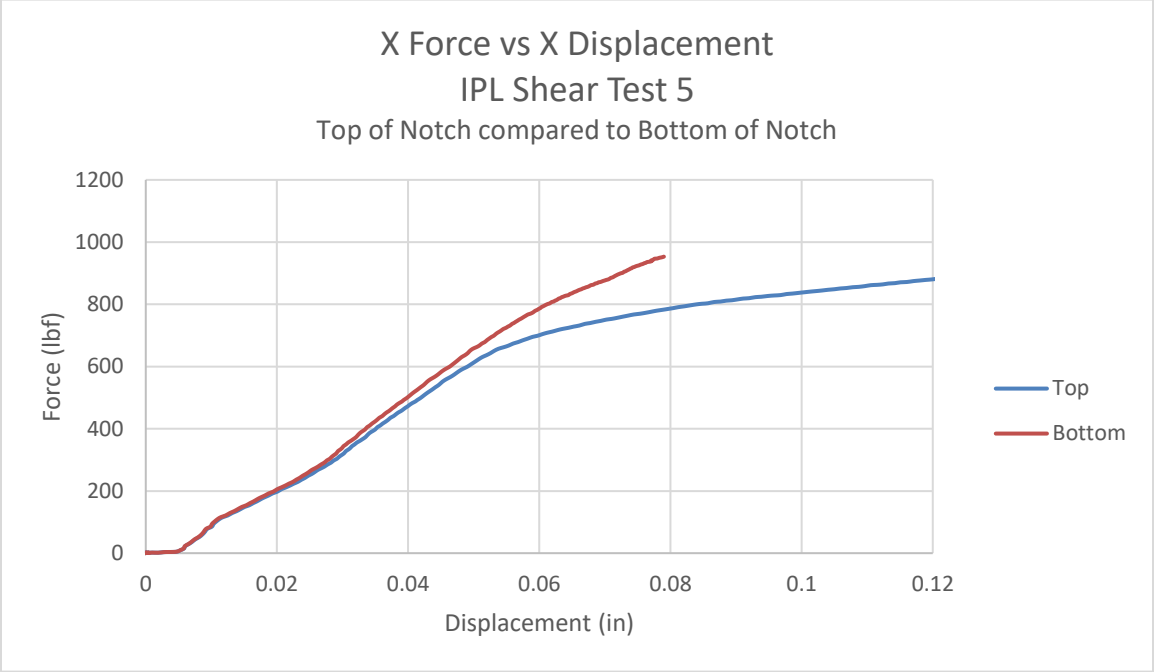


Figure 103: Force-displacement curves for IPL shear test 5. Data sets for displacements directly above (top) and below (bottom) the notched cross-section.

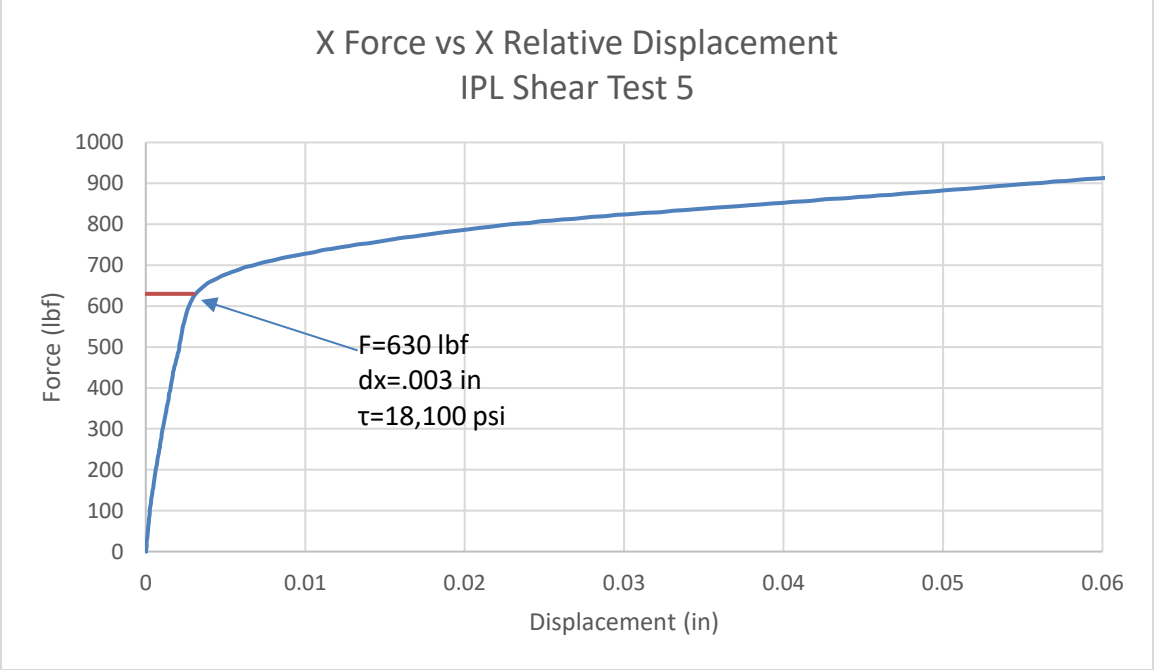


Figure 104: Force-relative displacement curve for IPL shear test 5. Displacement is corrected to eliminate effects of bending and grip slippage.

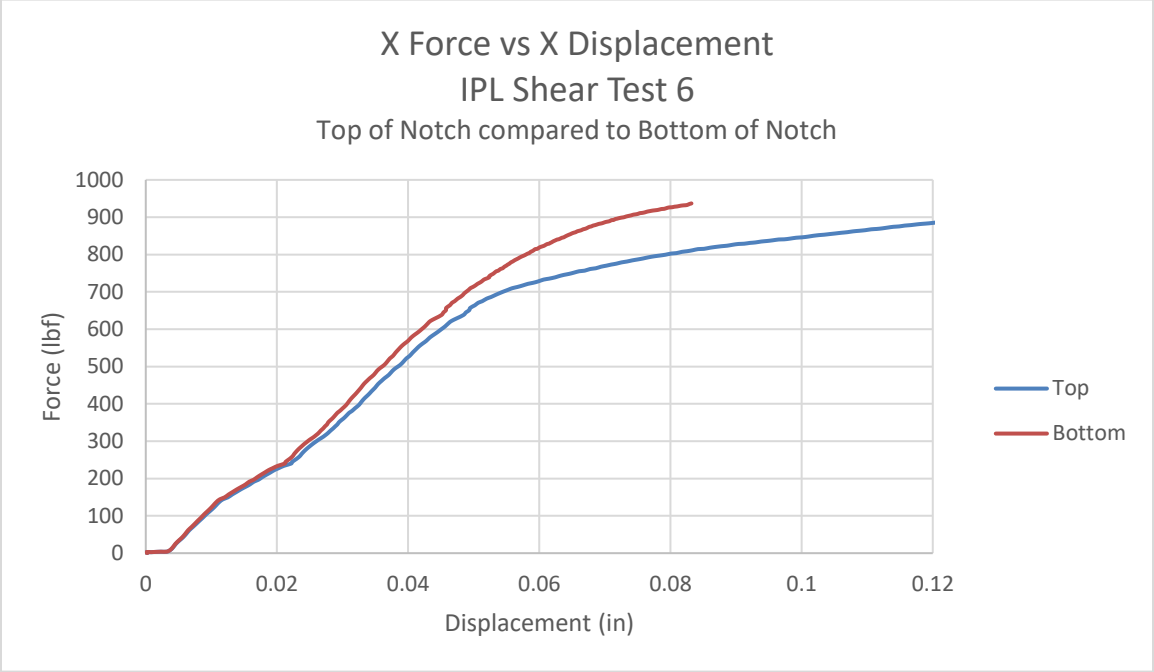


Figure 105: Force-displacement curves for IPL shear test 6. Data sets for displacements directly above (top) and below (bottom) the notched cross-section.

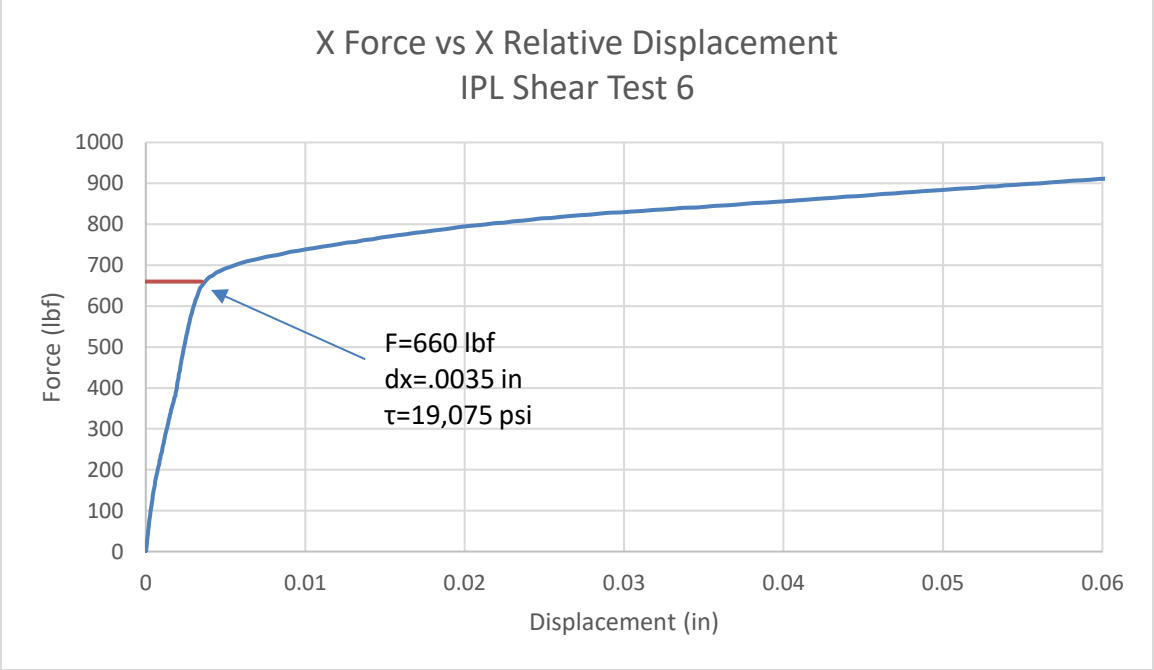


Figure 106: Force-relative displacement curve for IPL shear test 6. Displacement is corrected to eliminate effects of bending and grip slippage.

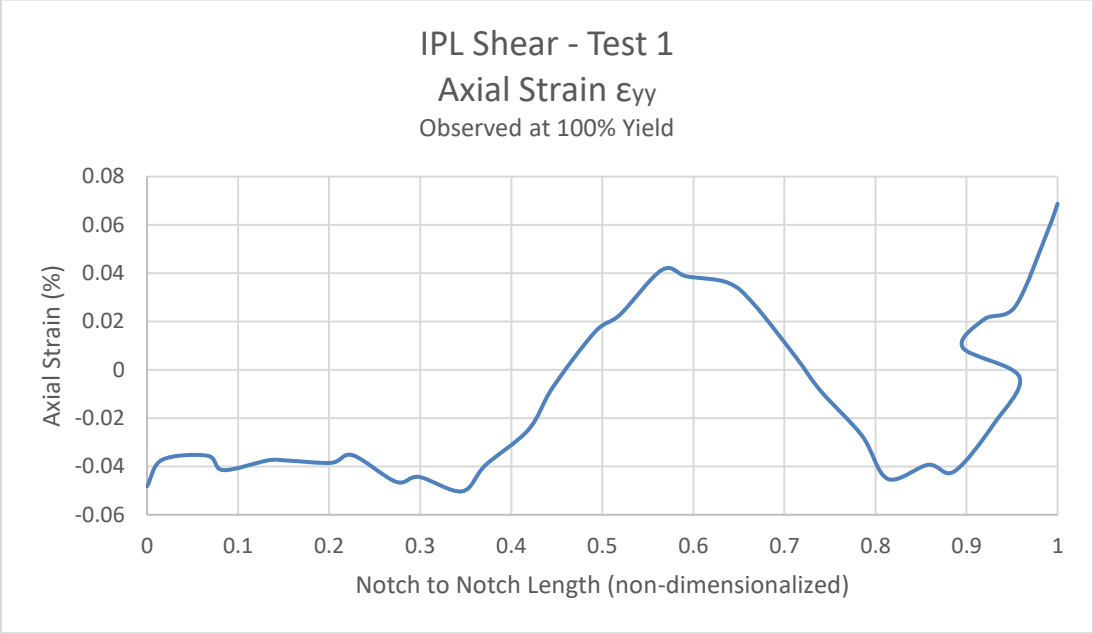


Figure 107: Axial strain (ε_{yy}) between notches for IPL shear test 1; reported at the yield point. Length is reported as a fraction of the length. The increasing trend from 0 to 1 describes considerable bending in the sample.

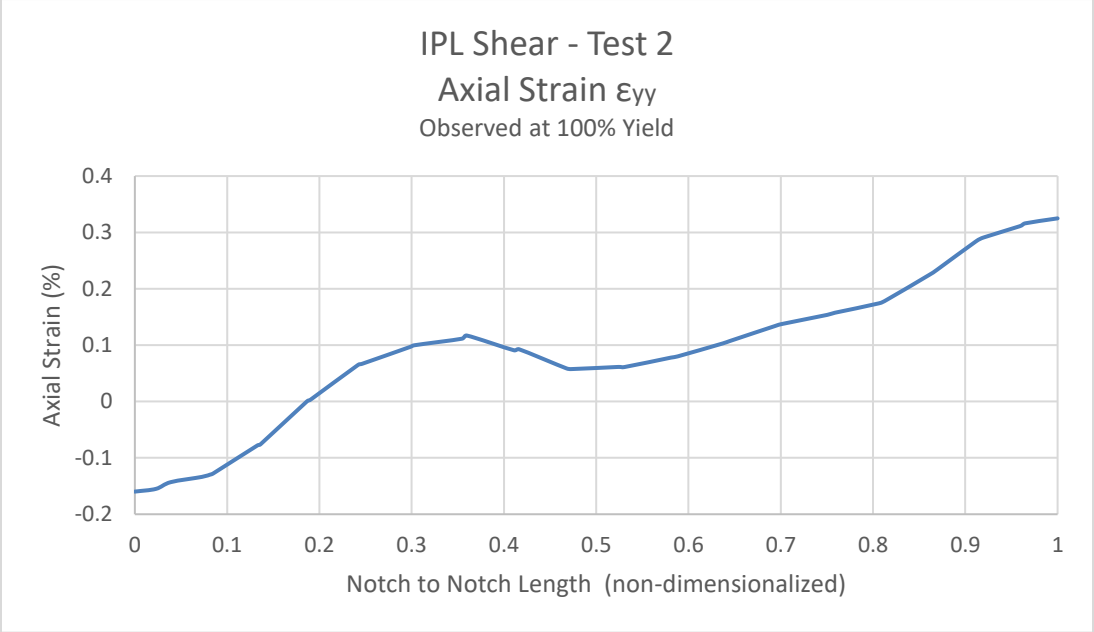


Figure 108: Axial strain (ε_{yy}) between notches for IPL shear test 2; reported at the yield point. Length is reported as a fraction of the length. The increasing trend from 0 to 1 describes considerable bending in the sample.

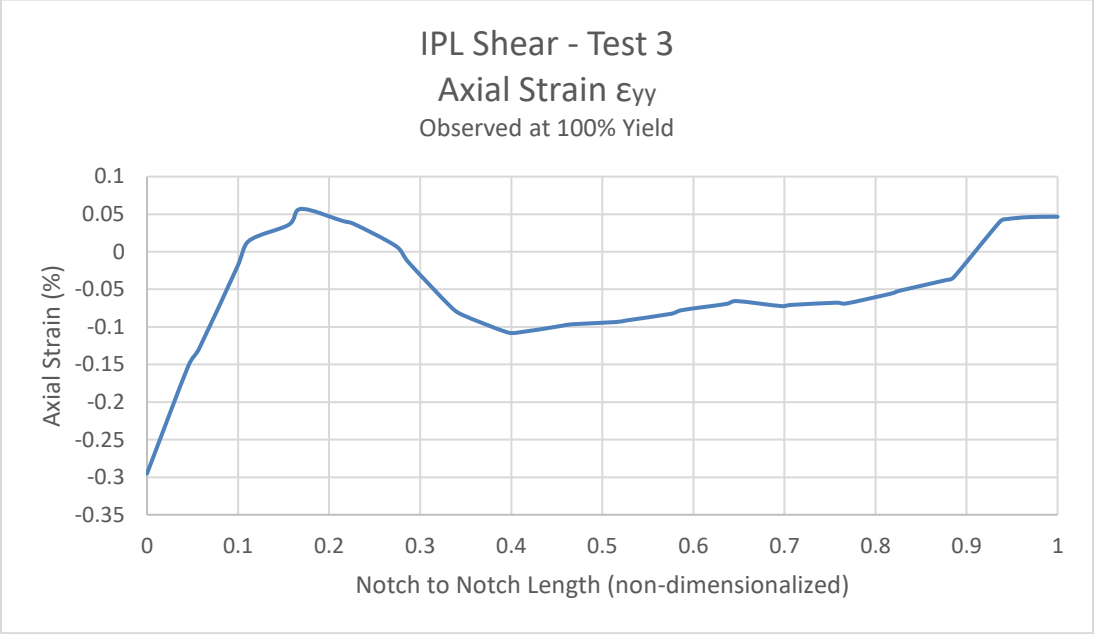


Figure 109: Axial strain (ε_{yy}) between notches for IPL shear test 3; reported at the yield point. Length is reported as a fraction of the length. The increasing trend from 0 to 1 describes considerable bending in the sample.

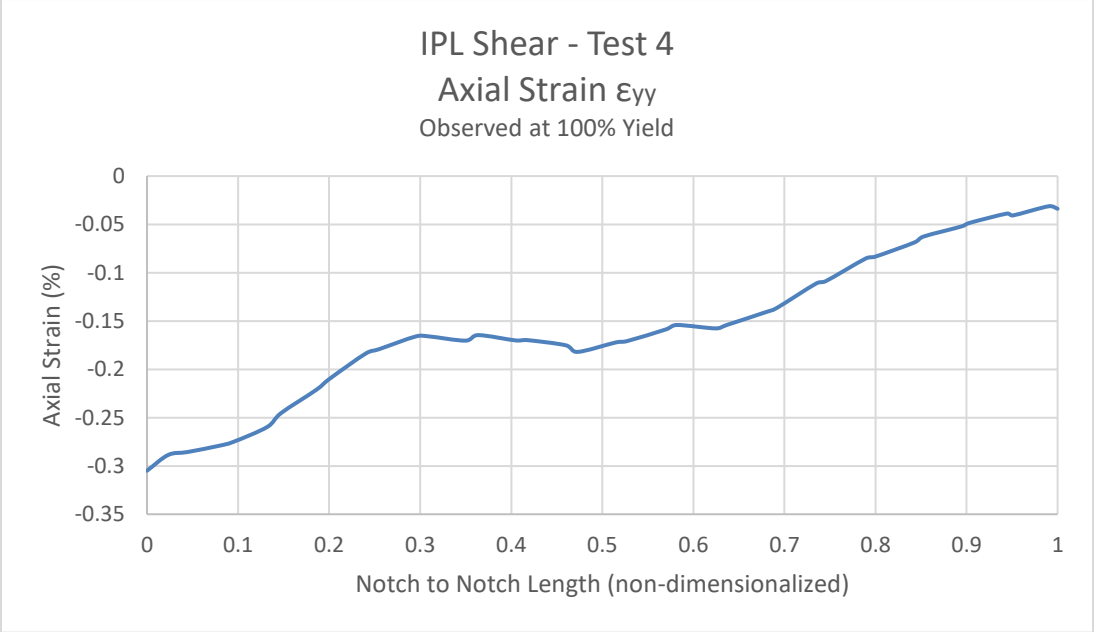


Figure 110: Axial strain (ε_{yy}) between notches for IPL shear test 4; reported at the yield point. Length is reported as a fraction of the length. The increasing trend from 0 to 1 describes considerable bending in the sample.

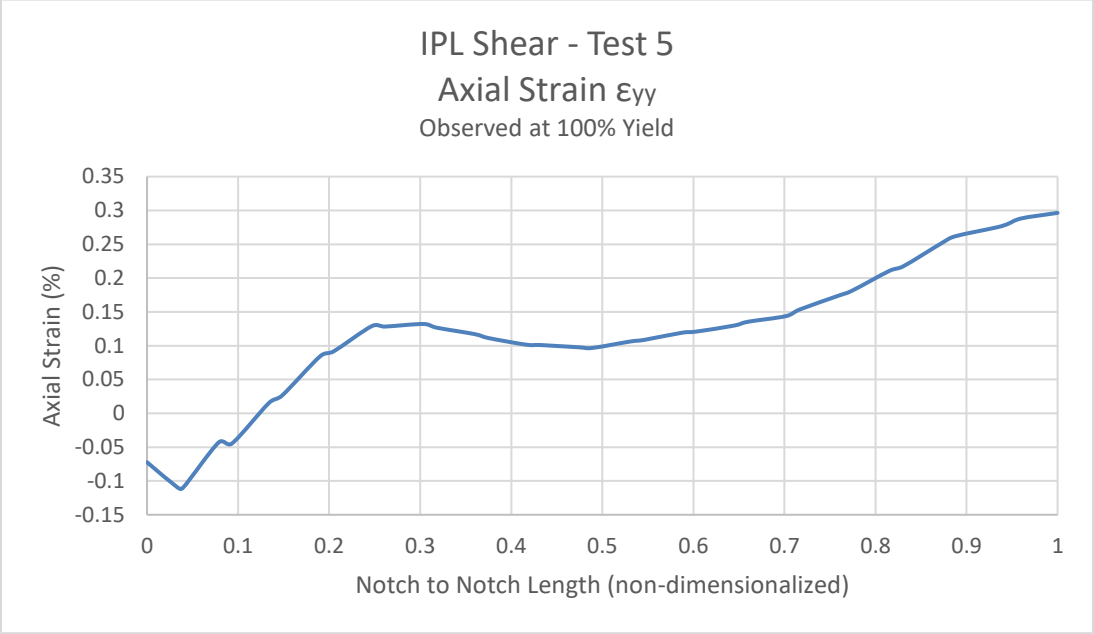


Figure 111: Axial strain (ε_{yy}) between notches for IPL shear test 5; reported at the yield point. Length is reported as a fraction of the length. The increasing trend from 0 to 1 describes considerable bending in the sample.

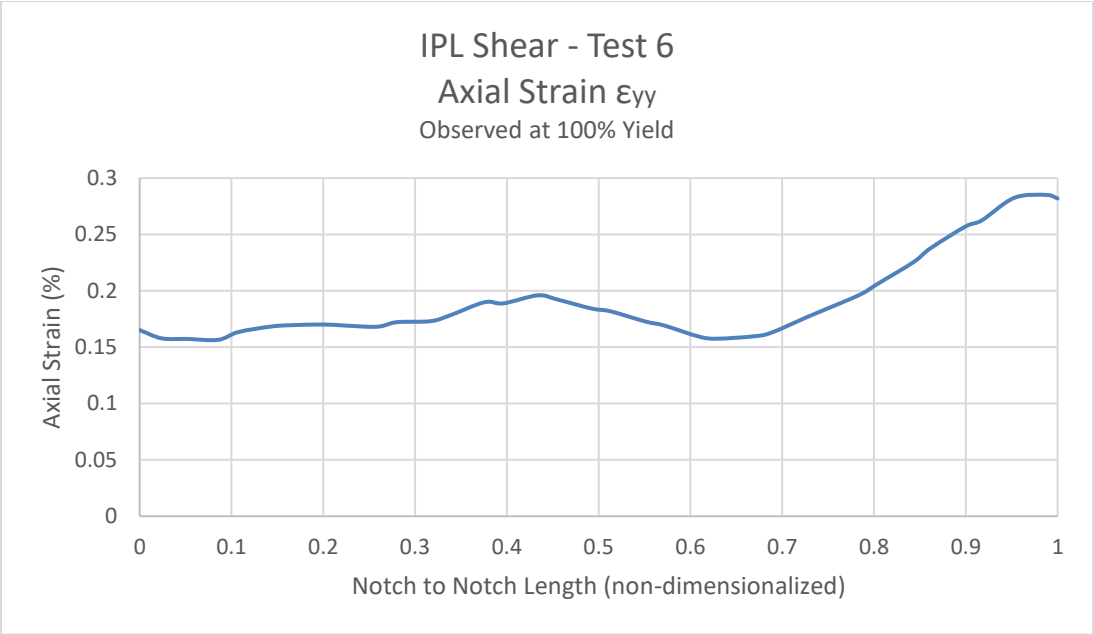


Figure 112: Axial strain (ε_{yy}) between notches for IPL shear test 5; reported at the yield point. Length is reported as a fraction of the length. The increasing trend from 0 to 1 describes considerable bending in the sample.

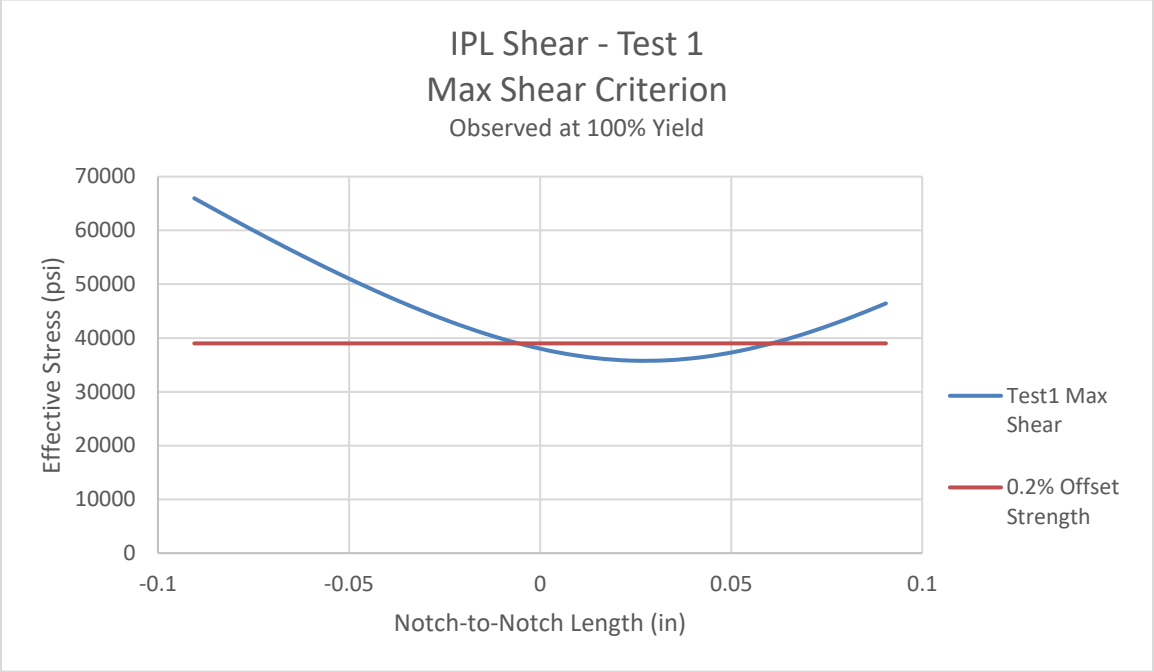


Figure 113: Maximum-shear effective stress across notches; reported at the observed yield point for IPL shear test 1.

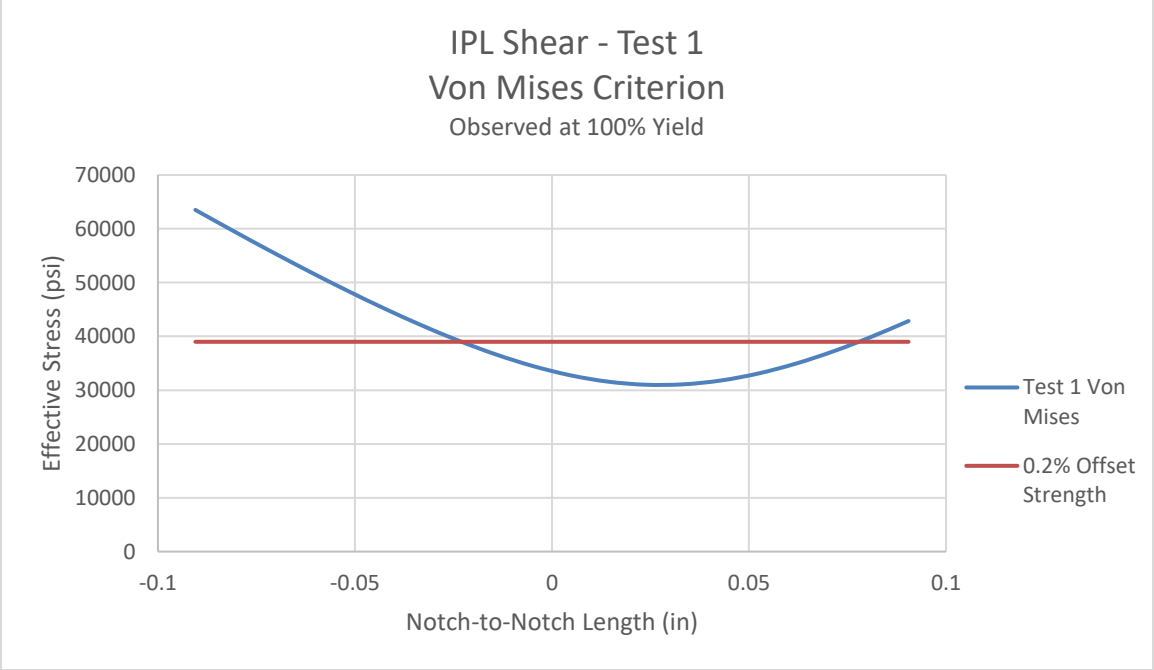


Figure 114: Von-Mises effective stress across notches; reported at the observed yield point for IPL shear test 1.

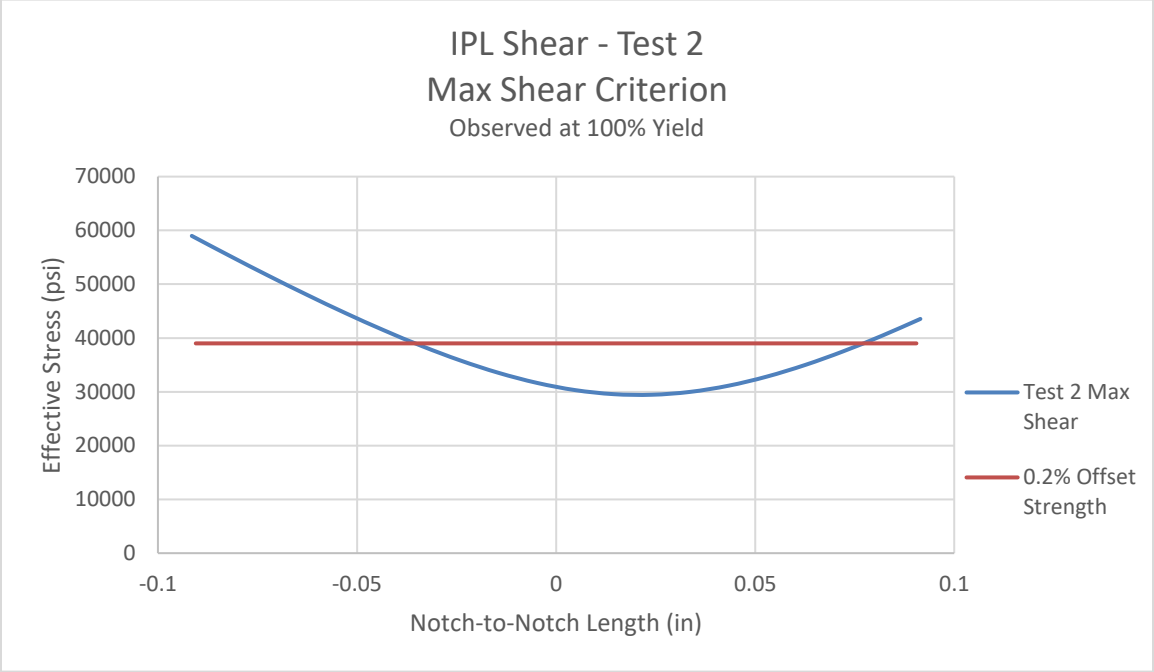


Figure 115: Maximum-shear effective stress across notches; reported at the observed yield point for IPL shear test 2.

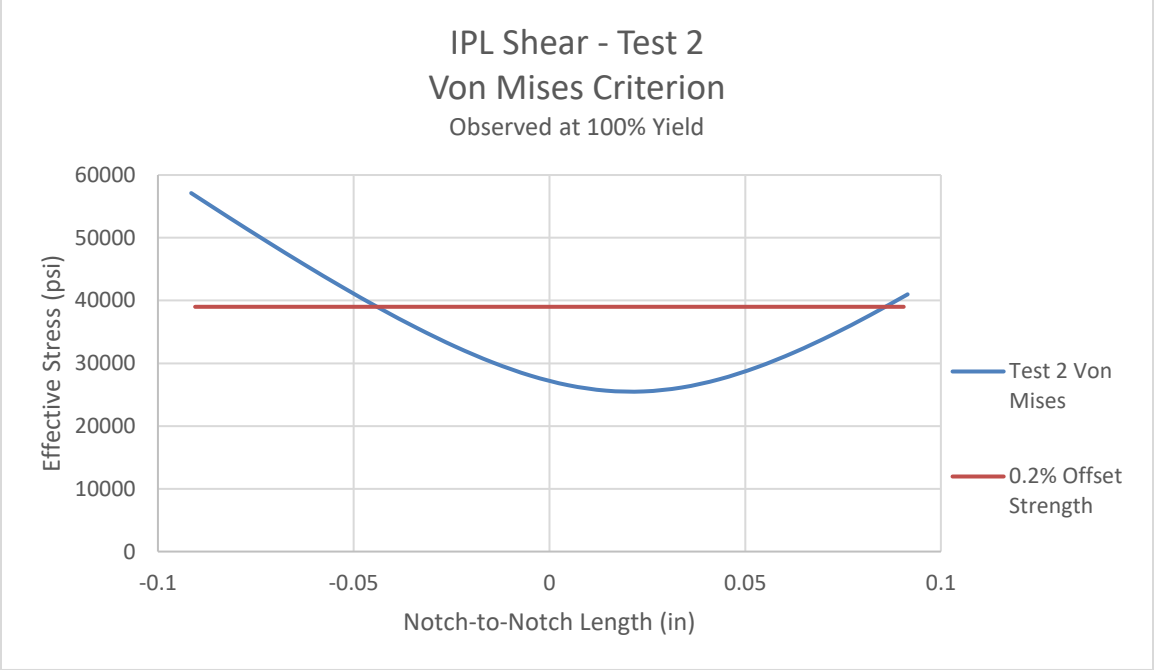


Figure 116: Von-Mises effective stress across notches; reported at the observed yield point for IPL shear test 2.

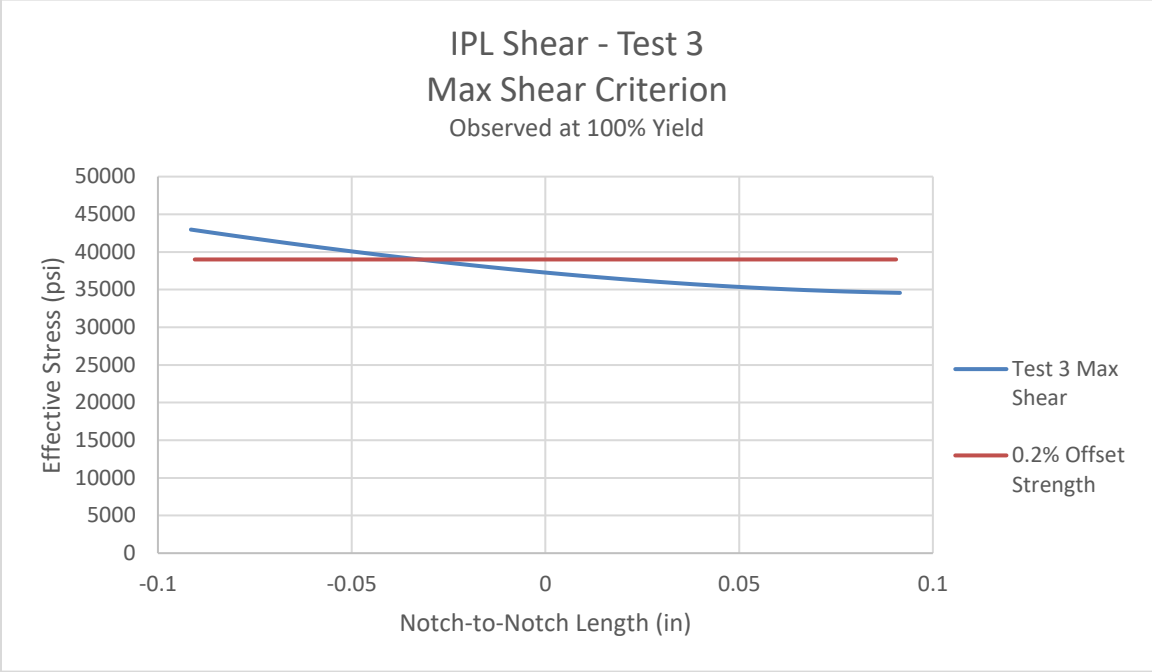


Figure 117: Maximum-shear effective stress across notches; reported at the observed yield point for IPL shear test 3.

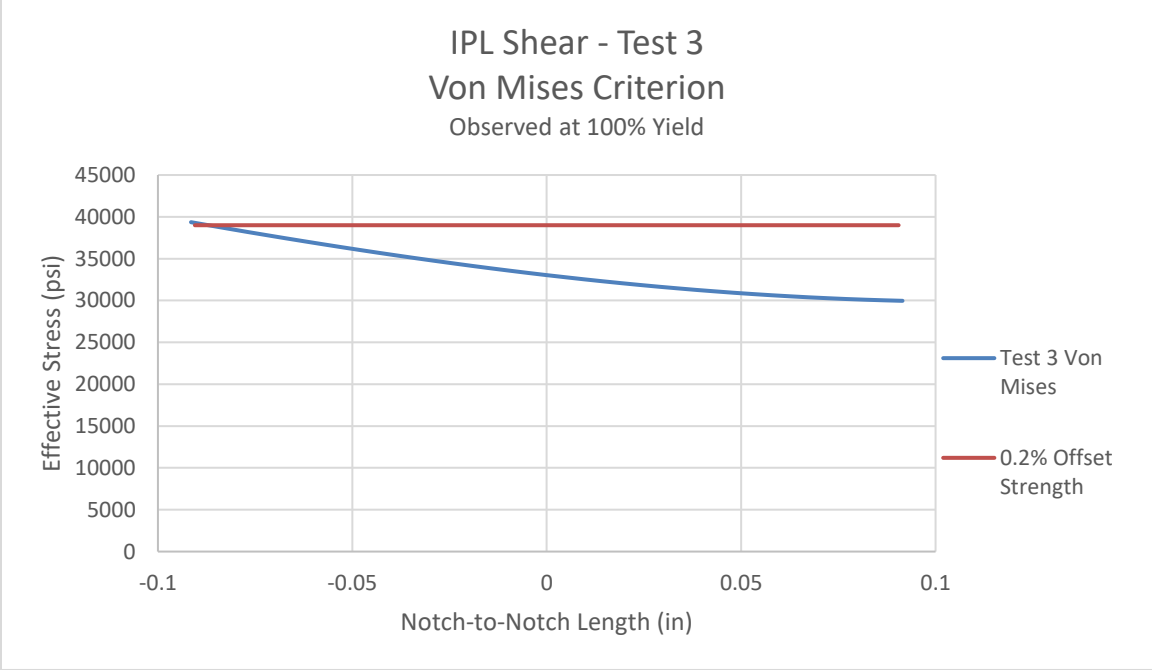


Figure 118: Von-Mises effective stress across notches; reported at the observed yield point for IPL shear test 3.

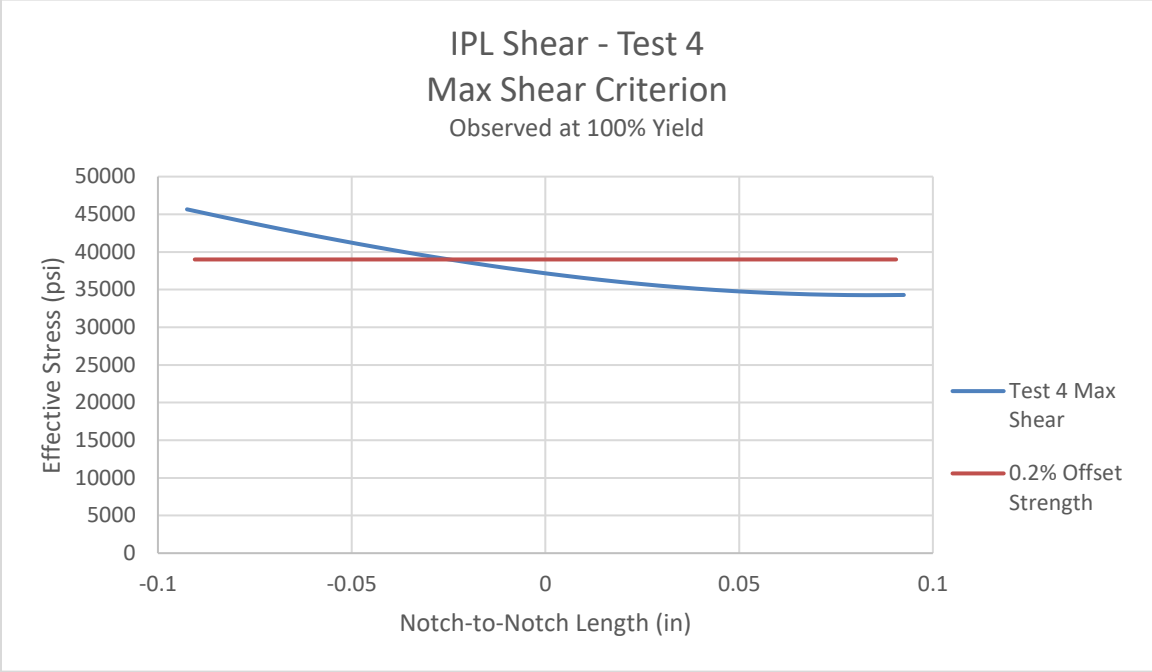


Figure 119: Maximum-shear effective stress across notches; reported at the observed yield point for IPL shear test 4.

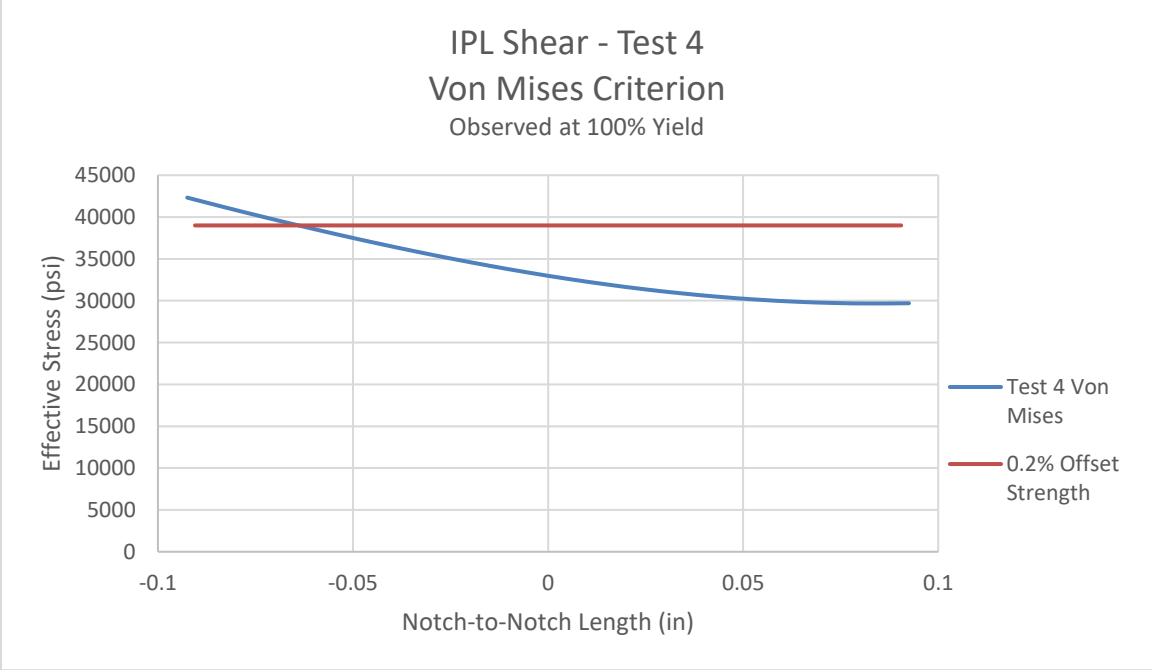


Figure 120: Von-Mises effective stress across notches; reported at the observed yield point for IPL shear test 4.

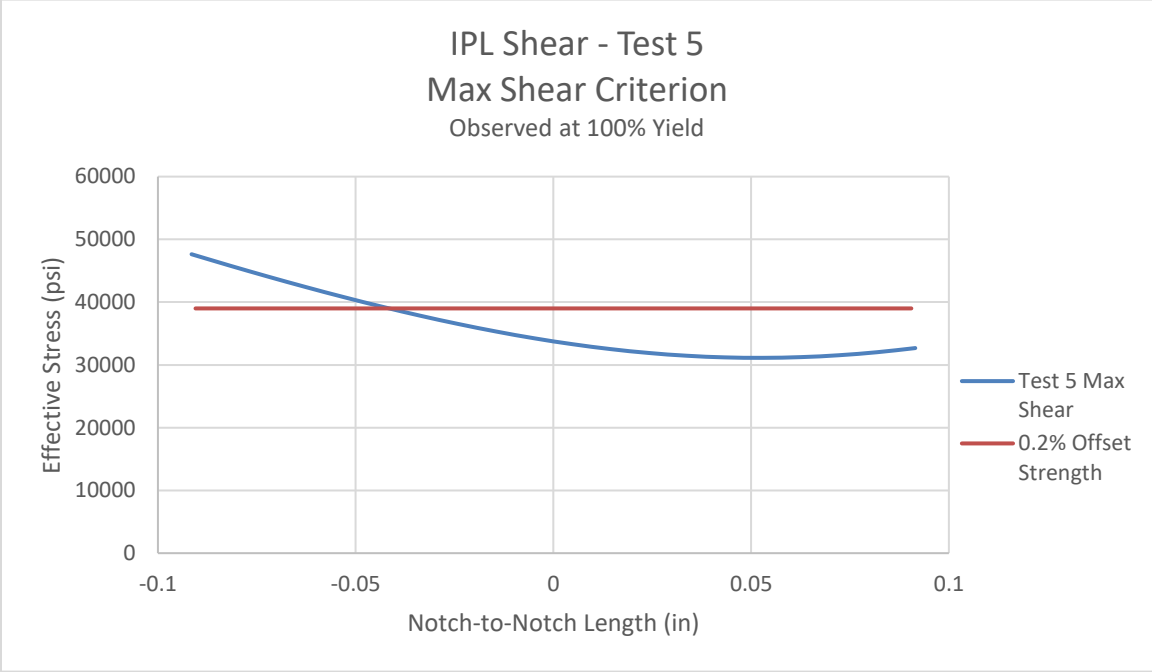


Figure 121: Maximum-shear effective stress across notches; reported at the observed yield point for IPL shear test 5.

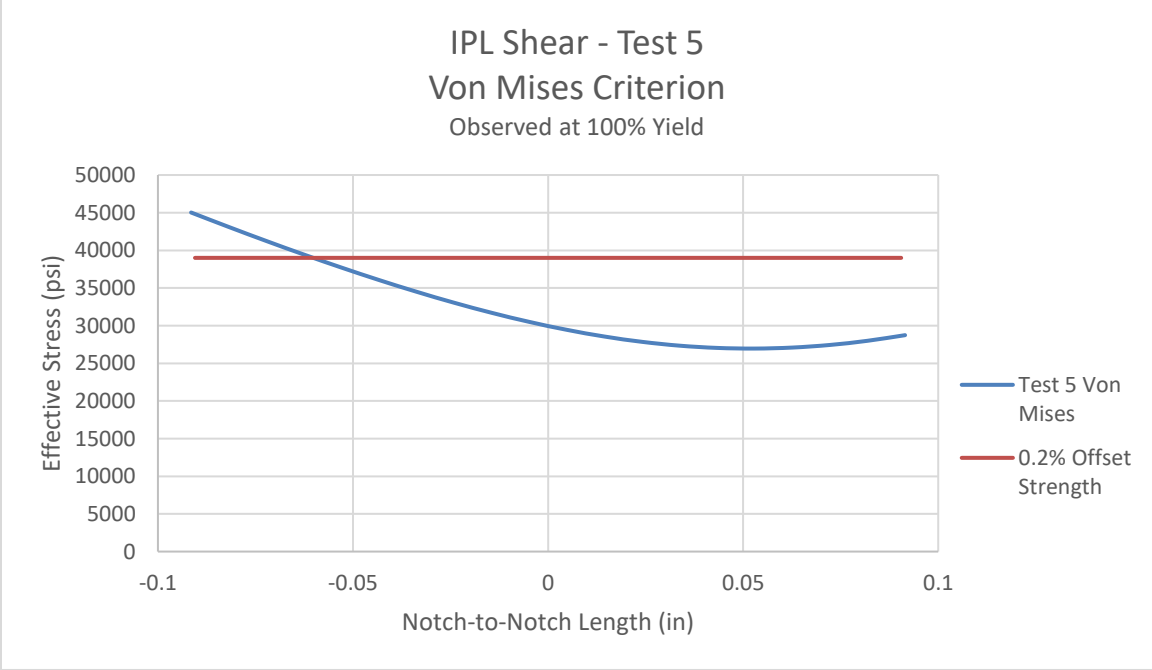


Figure 122: Von-Mises effective stress across notches; reported at the observed yield point for IPL shear test 5.

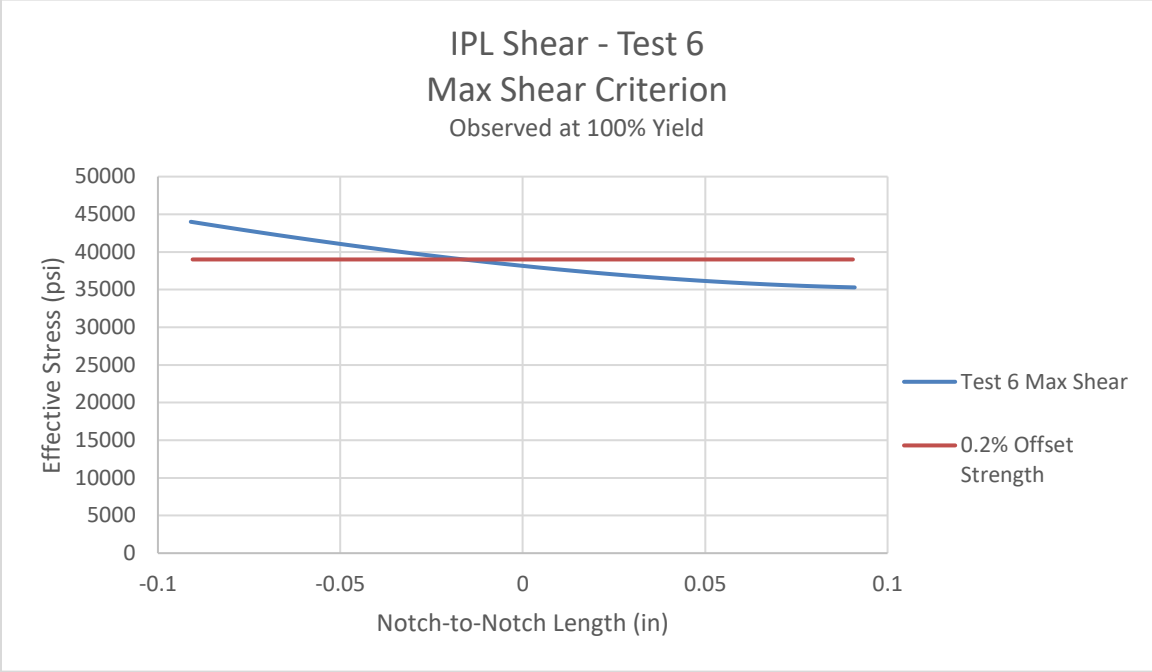


Figure 123: Maximum-shear effective stress across notches; reported at the observed yield point for IPL shear test 6.

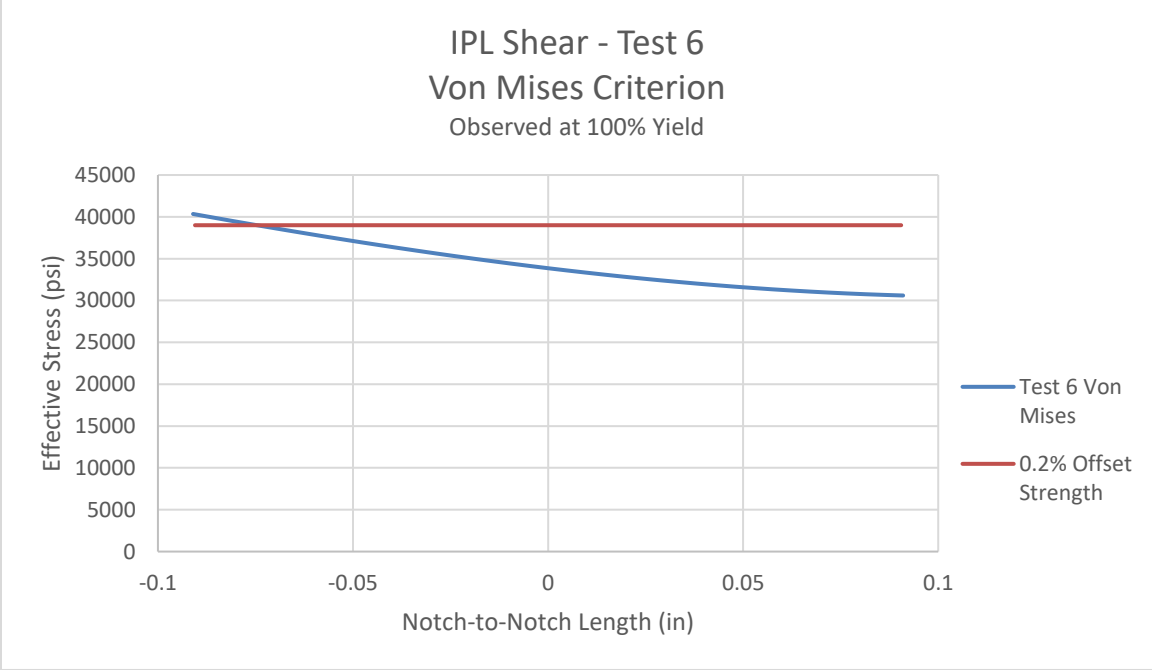
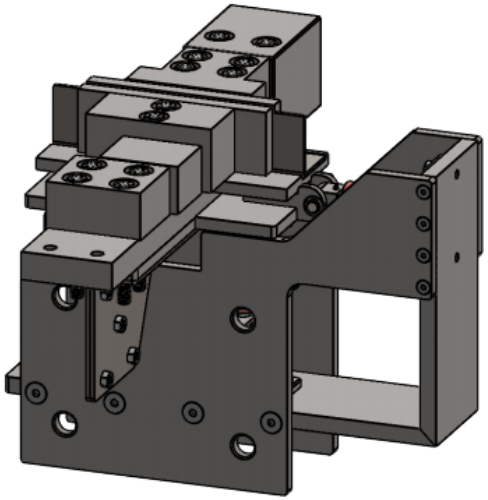


Figure 124: Von-Mises effective stress across notches; reported at the observed yield point for IPL shear test 5.

APPENDIX B

APPENDIX B: DRAWING PACKAGE

NOTES:
SEE EXPLODED VIEW (PAGE 3) AND BOM (NEXT PAGE) FOR QUANTITIES AND LOCATIONS



NOTICE OF PROPRIETARY RIGHTS THIS DOCUMENT CONTAINS PROPRIETARY INFORMATION IT MAY NOT BE REPRODUCED OR USED FOR ANY OTHER PURPOSE WITHOUT PRIOR WRITTEN PERMISSION.		UNLESS OTHERWISE SPECIFIED ALL DIMENSIONS ARE IN INCHES 1 PLACE DECIMALS ± 0.100" 2 PLACE DECIMALS ± 0.030" 3 PLACE DECIMALS ± 0.005" ANGLES ± 1° INTERPRET GEOMETRIC TOLERANCING PER ANSI Y14.5M-1994	MONTANA STATE UNIVERSITY	MECHANICAL & INDUSTRIAL ENGINEERING 220 ROBERTS HALL BOZEMAN, MT 59717	
DRAWN BY: AC	DATE: 1/29/19	MATERIAL:	TITLE: LOAD CELL MOD ASM		
CHECKED BY: AC	DATE: 1/29/19	MATERIAL SPEC:	DWG NO: 444014001_3		REV: 3
APPROVED BY:	DATE:	FINAL WEIGHT:	SIZE: A	SCALE: 1:4 DO NOT SCALE	SHEET: 1 OF 1

ITEM NO.	PART NUMBER	DESCRIPTION	QTY.
1	333014001_1	HOUSING ASM	1
2	122002001_1	OMEGA LC202 3K	3
3	111003001_1	CLEVIS LARGE	4
4	111003004_1	X CLEVIS LARGE	1
5	111001001_2	X CLEVIS, FREE	1
6	131003001_1	0.50 SHAFT	5
7	131002001_1	0.375 SHAFT	1
8	122001003_1	MMC 97022A33	6
9	122001001_1	MMC 97633A200	6
10	122001002_1	MMC 97633A170	2
11	122001004_1	MMC 97022A331	2
12	122001005_1	MMC92620A609	6
13	222014002_2	GRIP BASE WELDMENT	1
14	122001007_1	MMC 92620A605	4
15	111004001_1	BUSHING HOUSING	5
16	333014002_1	GRIP STIFFENER BOLTED ASM	1
17	122001010	MMC 94846A515	4
18	122001011	MMC 91381A671	4
19	GRIP ASSEMBLY	MODIFIED GRIP ASSEMBLY	1

NOTICE OF PROPRIETARY RIGHTS
THIS DOCUMENT CONTAINS PROPRIETARY INFORMATION.
IT MAY NOT BE REPRODUCED OR USED FOR ANY OTHER PURPOSE WITHOUT PRIOR WRITTEN PERMISSION.

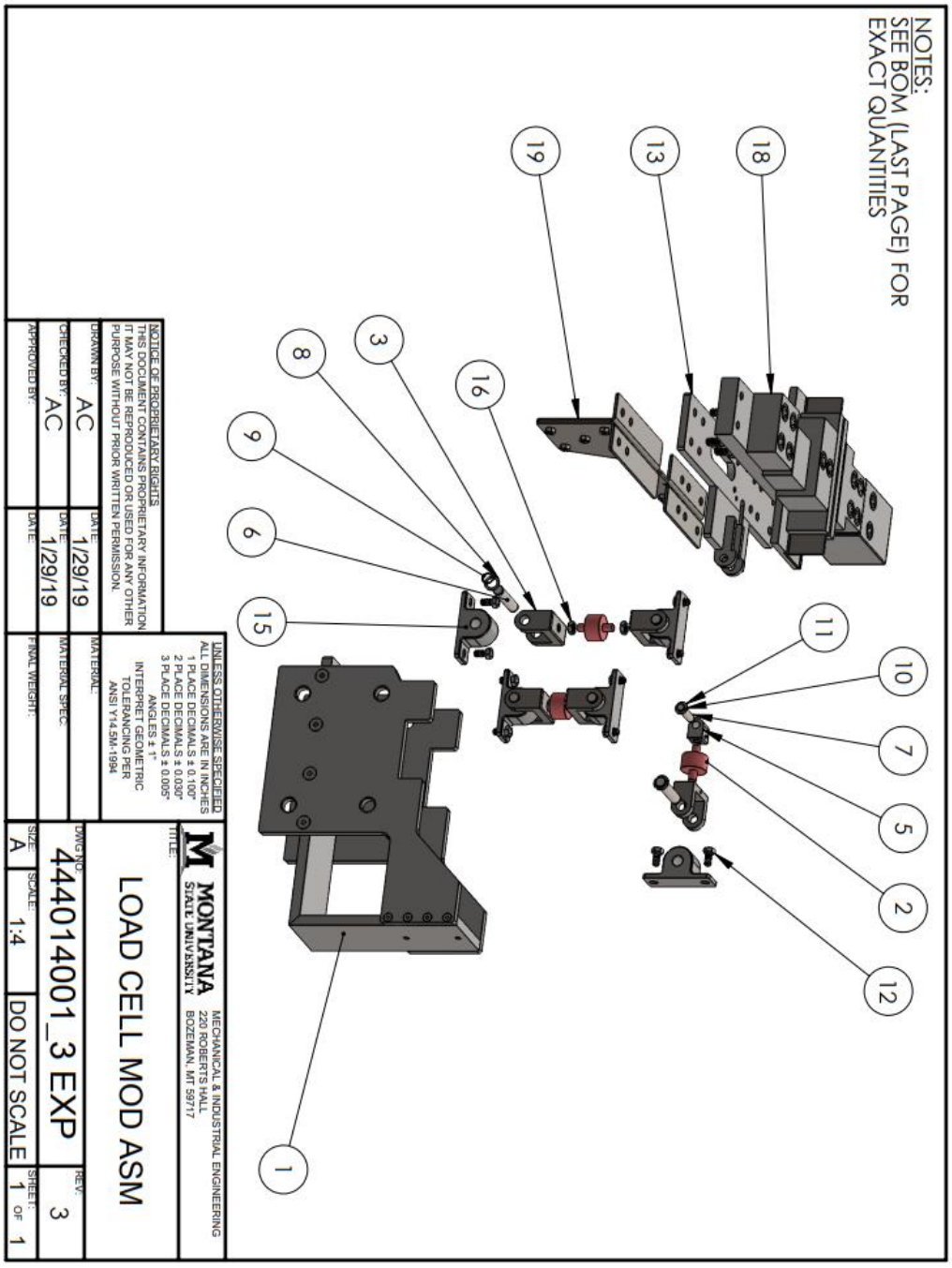
UNLESS OTHERWISE SPECIFIED
ALL DIMENSIONS ARE IN INCHES
1 PLACE DECIMALS ± 0.100"
2 PLACE DECIMALS ± 0.030"
3 PLACE DECIMALS ± 0.005"
ANGLES ± 1°
INTERPRET GEOMETRIC TOLERANCING PER ANSI Y14.5M-1994

DRAWN BY: AC	DATE: 1/29/19	MATERIAL:	
CHECKED BY: AC	DATE: 1/29/19	MATERIAL SPEC:	
APPROVED BY:	DATE:	FINAL WEIGHT:	

MONTANA STATE UNIVERSITY
MECHANICAL & INDUSTRIAL ENGINEERING
220 ROBERTS HALL
BOZEMAN, MT 59717

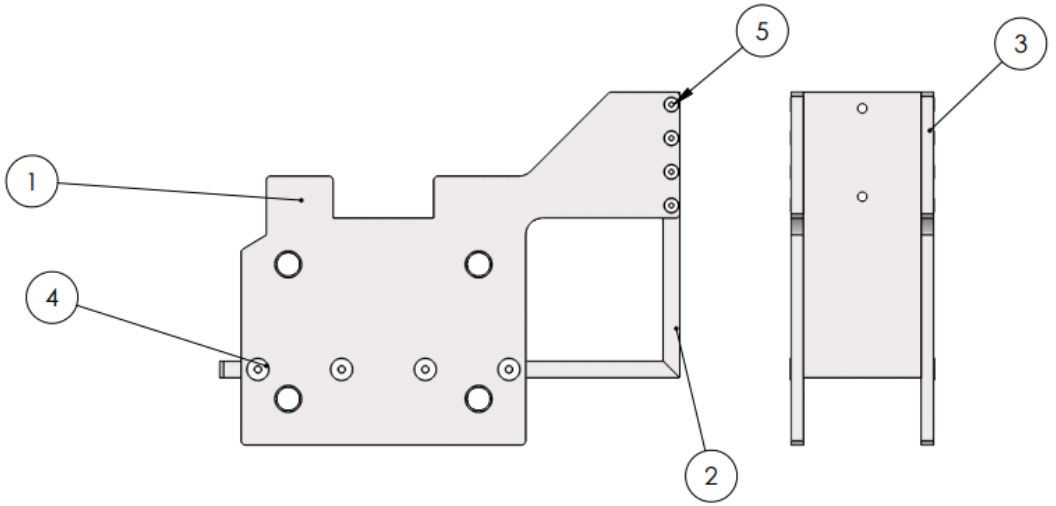
TITLE: LOAD CELL MOD ASM

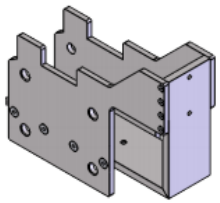
DWG NO: 444014001_3 BOM			REV: 3
SIZE: A	SCALE: NA	DO NOT SCALE	SHEET: 1 OF 1


NOTES:
SEE BOM (LAST PAGE) FOR
EXACT QUANTITIES
18
13
19
16
3
8
9
6
15
11
10
7
5
2
12
1
UNLESS OTHERWISE SPECIFIED
ALL DIMENSIONS ARE IN INCHES
1 PLACE DECIMALS ± 0.100"
2 PLACE DECIMALS ± 0.030"
3 PLACE DECIMALS ± 0.005"
ANGLES ± 1°
INTERPRET GEOMETRIC
TOLERANCING PER
ANSI Y14.5M-1994
MONTANA
STATE UNIVERSITY
MECHANICAL & INDUSTRIAL ENGINEERING
220 ROBERTS HALL
BOZEMAN, MT 59717
NOTICE OF PROPRIETARY RIGHTS
THIS DOCUMENT CONTAINS PROPRIETARY INFORMATION
IT MAY NOT BE REPRODUCED OR USED FOR ANY OTHER
PURPOSE WITHOUT PRIOR WRITTEN PERMISSION.
DRAWN BY: AC
DATE: 1/29/19
CHECKED BY: AC
DATE 1/29/19
APPROVED BY:
DATE
MATERIAL:
MATERIAL SPEC:
FINAL WEIGHT:
TITLE:
LOAD CELL MOD ASM
DWG NO.
44014001_3 EXP
REV:
3
SIZE
A
SCALE:
1:4
DO NOT SCALE
SHEET
1 OF 1

NOTES:
SEE BOM FOR QUANTITY, BALLOONS PLACED FOR CLARITY

ITEM NO.	PART NUMBER	DESCRIPTION	QTY.
1	111009001_2	HOUSING SIDE PLATE	1
2	222014001_2	HOUSING WELDMENT	1
3	111009003_2	HOUSING SIDE PLATE MIRROR	1
4	122001006_1	5/16-24 X .75 FH SCREW	8
5	122001008_1	12-24 X .75 FH SCREW	8





NOTICE OF PROPRIETARY RIGHTS
THIS DOCUMENT CONTAINS PROPRIETARY INFORMATION. IT MAY NOT BE REPRODUCED OR USED FOR ANY OTHER PURPOSE WITHOUT PRIOR WRITTEN PERMISSION.

UNLESS OTHERWISE SPECIFIED
ALL DIMENSIONS ARE IN INCHES
1 PLACE DECIMALS ± 0.100"
2 PLACE DECIMALS ± 0.030"
3 PLACE DECIMALS ± 0.005"
ANGLES ± 1°
INTERPRET GEOMETRIC TOLERANCING PER ANSI Y14.5M-1994

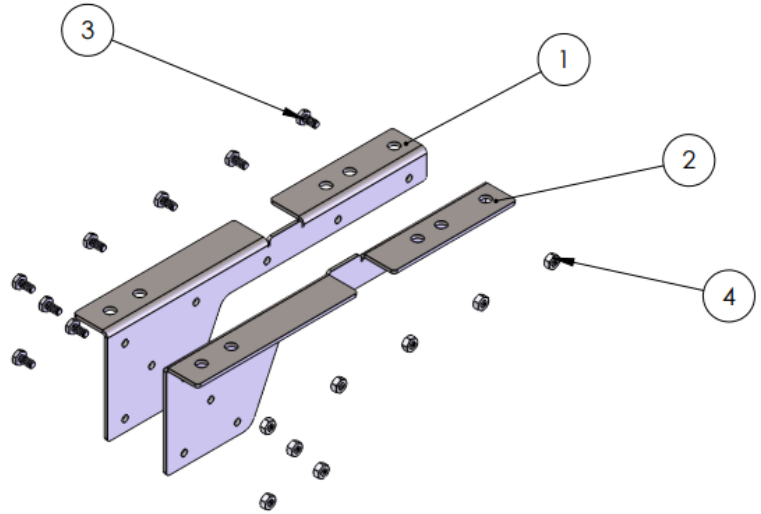
DRAWN BY: AC	DATE: 1/29/19	MATERIAL: NA	
CHECKED BY: AC	DATE: 1/29/19	MATERIAL SPEC:	
APPROVED BY:	DATE:	FINAL WEIGHT:	

MONTANA STATE UNIVERSITY
MECHANICAL & INDUSTRIAL ENGINEERING
220 ROBERTS HALL
BOZEMAN, MT 59717

TITLE: HOUSING ASM

DWG NO:	REV:	SIZE:	SCALE:		SHEET:
333014001_1	1	A	1:4	DO NOT SCALE	1 OF 1

ITEM NO.	PART NUMBER	DESCRIPTION	QTY.
1	111014004_1	GRIP PLATE STIFFNER	1
2	111014005_1	GRIP PLATE STIFFNER 2	1
3	122001012	MMC 92865A537	8
4	122001013	MMC 95462A029	8



NOTICE OF PROPRIETARY RIGHTS
THIS DOCUMENT CONTAINS PROPRIETARY INFORMATION. IT MAY NOT BE REPRODUCED OR USED FOR ANY OTHER PURPOSE WITHOUT PRIOR WRITTEN PERMISSION.

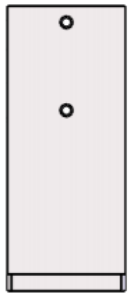
UNLESS OTHERWISE SPECIFIED
ALL DIMENSIONS ARE IN INCHES
1 PLACE DECIMALS ± 0.100"
2 PLACE DECIMALS ± 0.030"
3 PLACE DECIMALS ± 0.005"
ANGLES ± 1°
INTERPRET GEOMETRIC TOLERANCING PER ANSI Y14.5M-1994

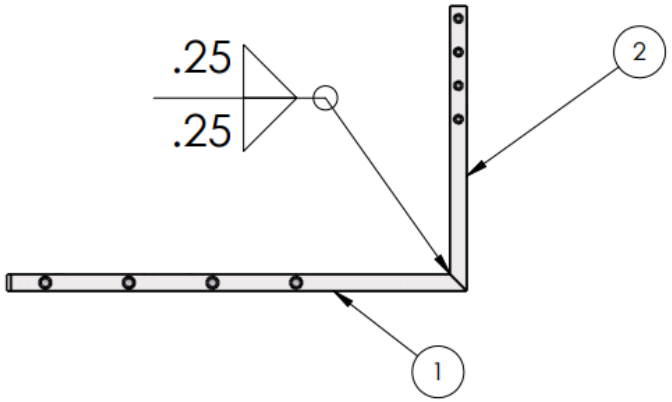
MONTANA STATE UNIVERSITY
MECHANICAL & INDUSTRIAL ENGINEERING
220 ROBERTS HALL
BOZEMAN, MT 59717

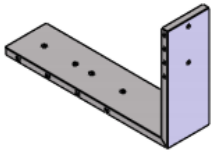
DRAWN BY: AC	DATE: 1/20/19	MATERIAL: -	TITLE: GRIP STIFFENER BOLTED ASM
CHECKED BY: AC	DATE: 1/20/19	MATERIAL SPEC:	DWG NO: 333014002_1 REV: 1
APPROVED BY:	DATE:	FINAL WEIGHT:	SIZE: A SCALE: 1:8 DO NOT SCALE SHEET: 1 OF 1

NOTES:
WELD ALL JOINTS AS NOTED

ITEM NO.	PART NUMBER	DESCRIPTION	QTY.
1	111014002_1	HOUSING BTM PLT	1
2	111009002_1	HOUSING X PLATE	1







NOTICE OF PROPRIETARY RIGHTS
THIS DOCUMENT CONTAINS PROPRIETARY INFORMATION
IT MAY NOT BE REPRODUCED OR USED FOR ANY OTHER
PURPOSE WITHOUT PRIOR WRITTEN PERMISSION.

UNLESS OTHERWISE SPECIFIED
ALL DIMENSIONS ARE IN INCHES
1 PLACE DECIMALS ± 0.100"
2 PLACE DECIMALS ± 0.030"
3 PLACE DECIMALS ± 0.005"
ANGLES ± 1°
INTERPRET GEOMETRIC
TOLERANCING PER
ANSI Y14.5M-1994

DRAWN BY: AC	DATE: 1/29/19	MATERIAL: -	
CHECKED BY: AC	DATE: 1/29/19	MATERIAL SPEC:	
APPROVED BY:	DATE:	FINAL WEIGHT:	

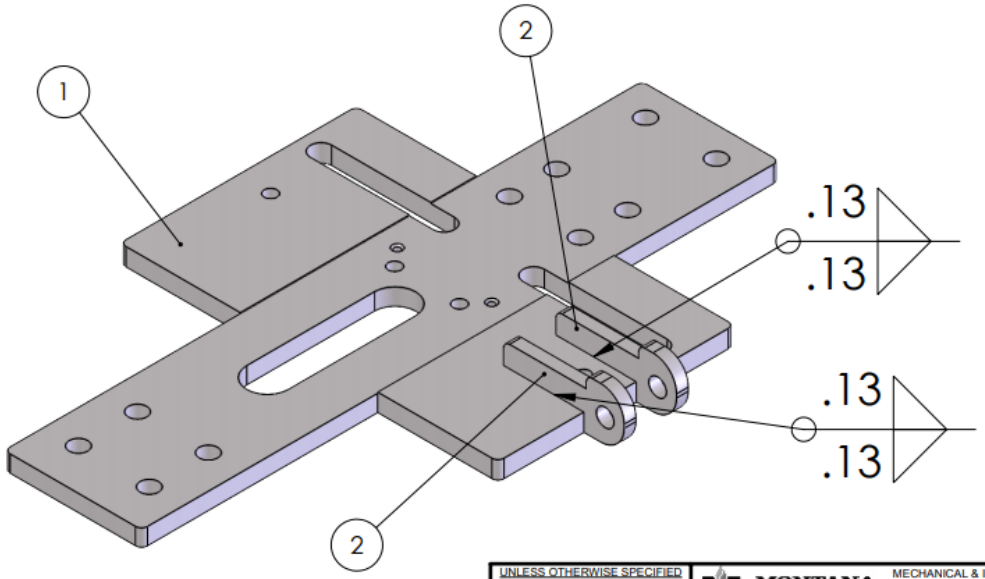
MONTANA STATE UNIVERSITY
MECHANICAL & INDUSTRIAL ENGINEERING
220 ROBERTS HALL
BOZEMAN, MT 59717

TITLE: HOUSING WELDMENT

DWG NO:	REV:	SIZE:	SCALE:		SHEET:
222014001_2	2	A	1:4	DO NOT SCALE	1 OF 1

NOTES:
WELD ALL JOINTS AS NOTED

ITEM NO.	PART NUMBER	DESCRIPTION	QTY.
1	111014003_1	GRIP BASE PLATE	1
2	111003002_1	X CLEVIS SIDE	2



NOTICE OF PROPRIETARY RIGHTS
THIS DOCUMENT CONTAINS PROPRIETARY INFORMATION. IT MAY NOT BE REPRODUCED OR USED FOR ANY OTHER PURPOSE WITHOUT PRIOR WRITTEN PERMISSION.

UNLESS OTHERWISE SPECIFIED
ALL DIMENSIONS ARE IN INCHES
1 PLACE DECIMALS ± 0.100"
2 PLACE DECIMALS ± 0.030"
3 PLACE DECIMALS ± 0.005"
ANGLES ± 1°
INTERPRET GEOMETRIC TOLERANCING PER ANSI Y14.5M-1994

MONTANA STATE UNIVERSITY
MECHANICAL & INDUSTRIAL ENGINEERING
220 ROBERTS HALL
BOZEMAN, MT 59717

DRAWN BY: AC	DATE: 1/29/19	MATERIAL: NA	
CHECKED BY: AC	DATE: 1/29/19	MATERIAL SPEC:	
APPROVED BY:	DATE:	FINAL WEIGHT:	

TITLE: GRIP BASE WELDMENT

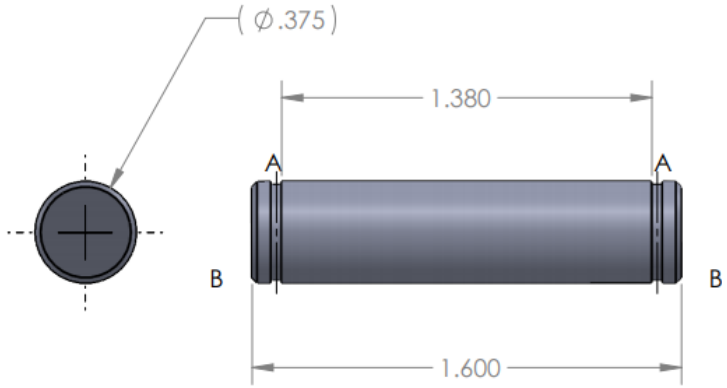
DWG NO: 222014002_2				REV: 2
SIZE: A	SCALE: 1:2	DO NOT SCALE	SHEET: 1 OF 1	

FEATURES:

A: Ø0.352 X .039 GROOVE (2 EA)
B: 0.02 X 45° CHAMFER (2 EA)

NOTES:

THIS PART IS CUT FROM PART 121-012-001



NOTICE OF PROPRIETARY RIGHTS
THIS DOCUMENT CONTAINS PROPRIETARY INFORMATION. IT MAY NOT BE REPRODUCED OR USED FOR ANY OTHER PURPOSE WITHOUT PRIOR WRITTEN PERMISSION.

UNLESS OTHERWISE SPECIFIED
ALL DIMENSIONS ARE IN INCHES
1 PLACE DECIMALS ± 0.100"
2 PLACE DECIMALS ± 0.030"
3 PLACE DECIMALS ± 0.005"
ANGLES ± 1°
INTERPRET GEOMETRIC TOLERANCING PER ANSI Y14.5M-1994

DRAWN BY: AC	DATE: 1/20/19	MATERIAL: 1566 CS	
CHECKED BY: AC	DATE: 1/20/19	MATERIAL SPEC:	
APPROVED BY:	DATE:	FINAL WEIGHT:	

MONTANA STATE UNIVERSITY
MECHANICAL & INDUSTRIAL ENGINEERING
220 ROBERTS HALL
BOZEMAN, MT 59717

TITLE: 0.375 SHAFT

DWG NO: 131002001_1			REV: 1
SIZE: A	SCALE: 2:1	DO NOT SCALE	SHEET: 1 OF 1

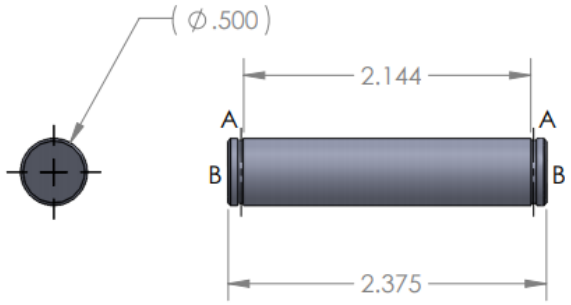
FEATURES:

A: Ø0.468 X 0.039 GROOVE (2 EA)

B: 0.02 X 45° CHAMFER (2 EA)

NOTES:

THIS PART IS CUT FROM PART 121-024-001



NOTICE OF PROPRIETARY RIGHTS
THIS DOCUMENT CONTAINS PROPRIETARY INFORMATION. IT MAY NOT BE REPRODUCED OR USED FOR ANY OTHER PURPOSE WITHOUT PRIOR WRITTEN PERMISSION.

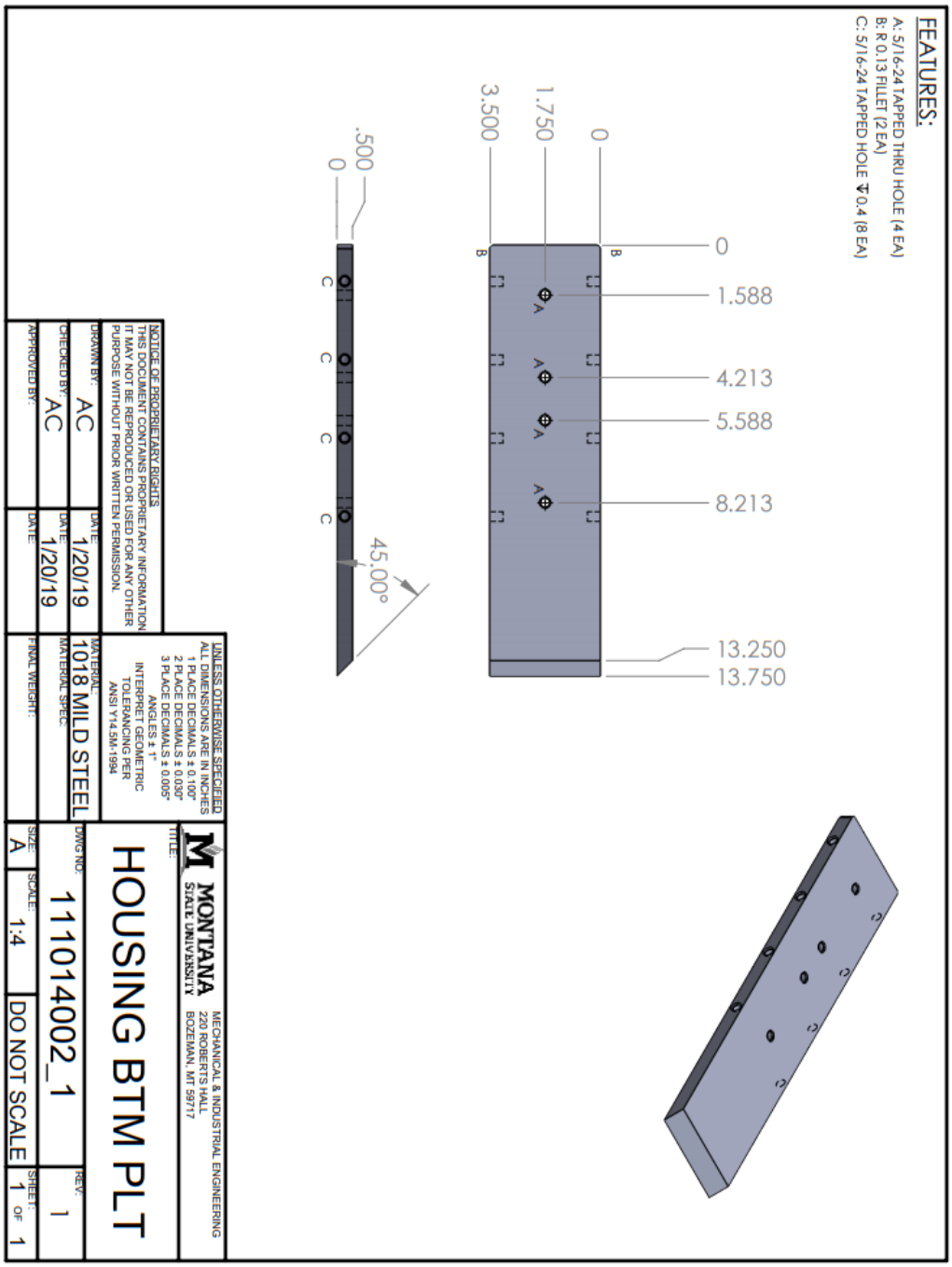
UNLESS OTHERWISE SPECIFIED
ALL DIMENSIONS ARE IN INCHES
1 PLACE DECIMALS ± 0.100"
2 PLACE DECIMALS ± 0.030"
3 PLACE DECIMALS ± 0.005"
ANGLES ± 1°
INTERPRET GEOMETRIC TOLERANCING PER ANSI Y14.5M-1994

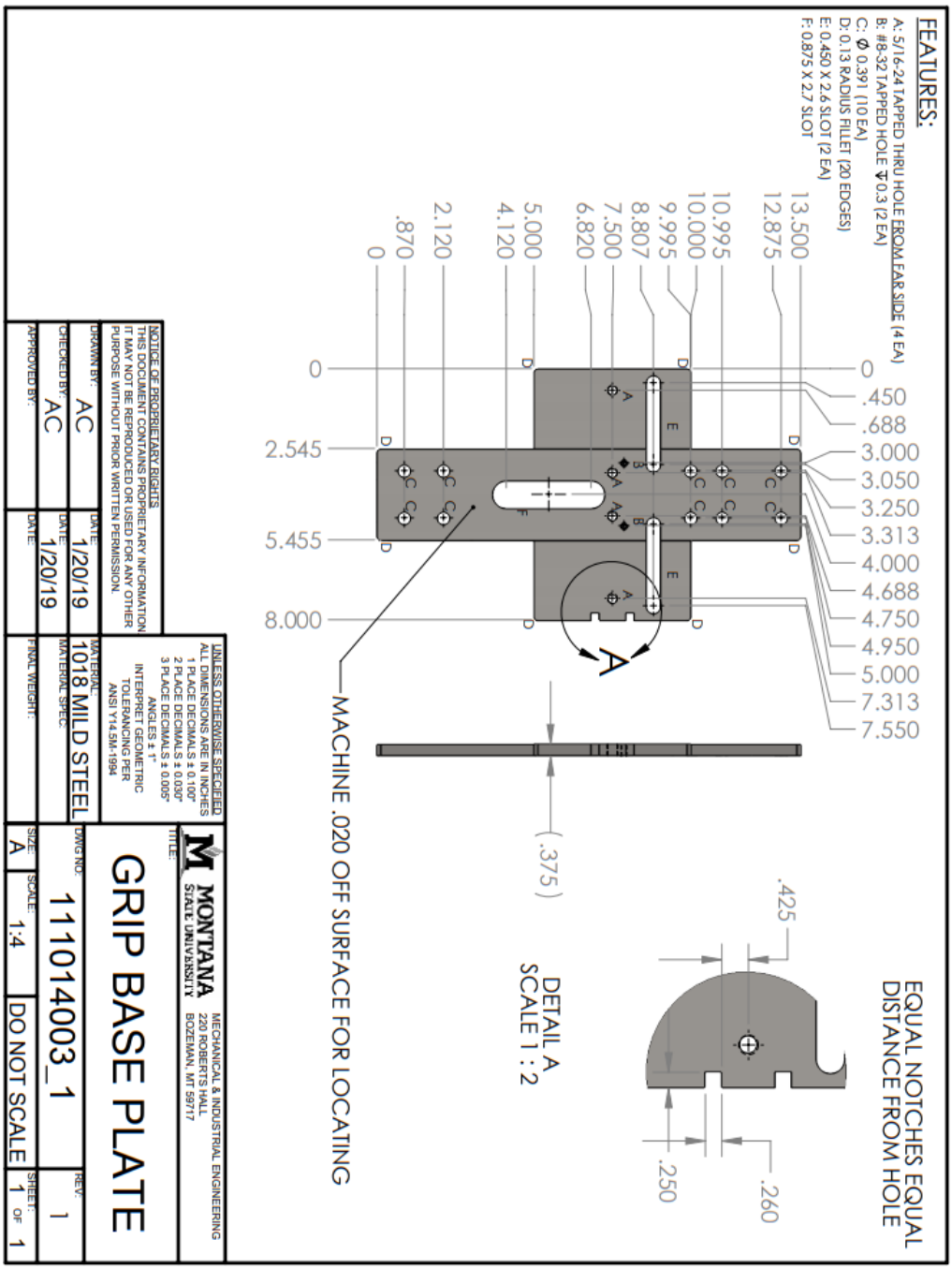
DRAWN BY: AC	DATE: 1/20/19	MATERIAL: 1566 CS	
CHECKED BY: AC	DATE: 1/20/19	MATERIAL SPEC:	
APPROVED BY:	DATE:	FINAL WEIGHT:	

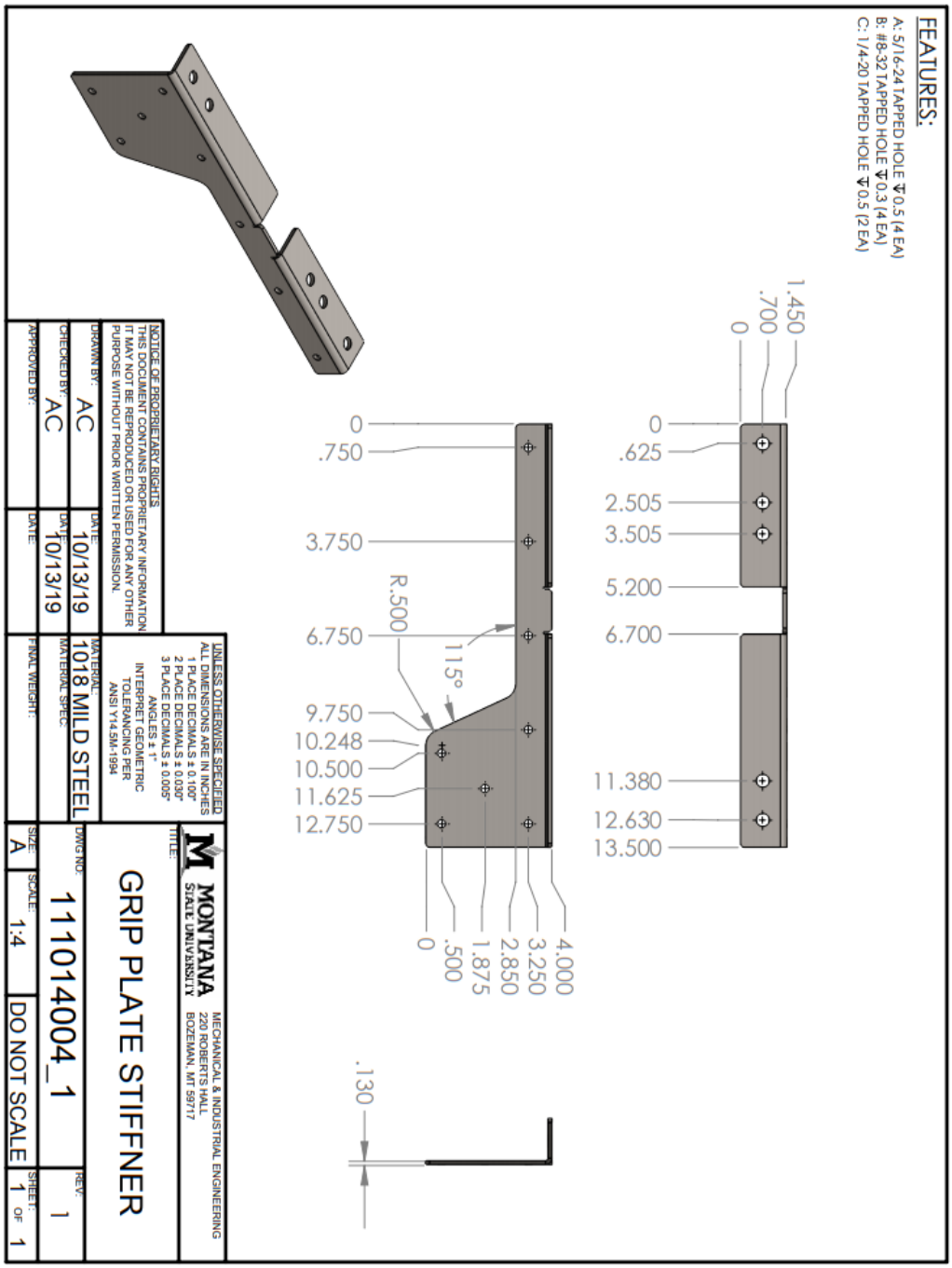
MONTANA STATE UNIVERSITY
MECHANICAL & INDUSTRIAL ENGINEERING
220 ROBERTS HALL
BOZEMAN, MT 59717

TITLE: 0.50 SHAFT

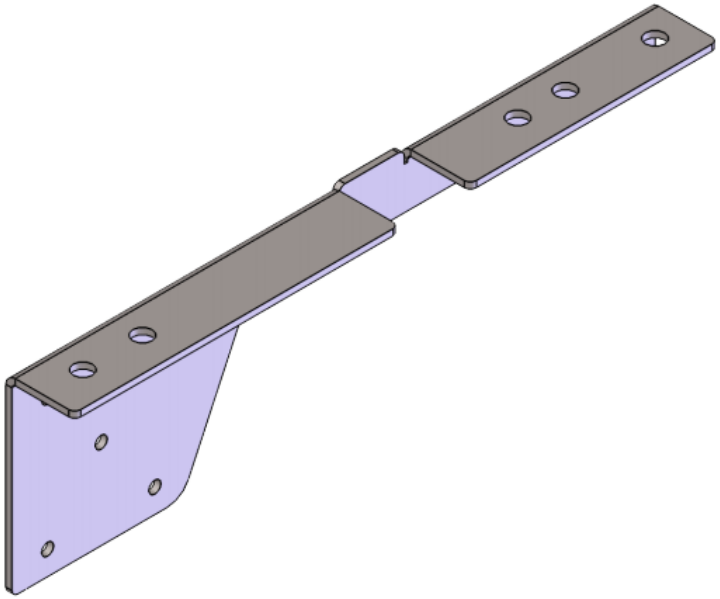
DWG NO: 131003001_1			REV: 1
SIZE: A	SCALE: 1:1	DO NOT SCALE	SHEET: 1 OF 1


FEATURES:
A: 5/16-24 TAPPED THRU HOLE (4 EA)
B: R 0.13 FILLET (2 EA)
C: 5/16-24 TAPPED HOLE ↧0.4 (8 EA)
0
1.750
3.500
0
1.588
4.213
5.588
8.213
13.250
13.750
.500
0
45.00°
NOTICE OF PROPRIETARY RIGHTS
THIS DOCUMENT CONTAINS PROPRIETARY INFORMATION IT MAY NOT BE REPRODUCED OR USED FOR ANY OTHER PURPOSE WITHOUT PRIOR WRITTEN PERMISSION.
UNLESS OTHERWISE SPECIFIED
ALL DIMENSIONS ARE IN INCHES
1 PLACE DECIMALS ± 0.100"
2 PLACE DECIMALS ± 0.030"
3 PLACE DECIMALS ± 0.005"
ANGLES ± 1°
INTERPRET GEOMETRIC TOLERANCING PER ANSI Y14.5M-1994
MONTANA STATE UNIVERSITY
MECHANICAL & INDUSTRIAL ENGINEERING
220 ROBERTS HALL
BOZEMAN, MT 59717
TITLE:
HOUSING BTM PLT
DRAWN BY: AC
DATE: 1/20/19
CHECKED BY: AC
DATE: 1/20/19
APPROVED BY:
DATE:
MATERIAL: 1018 MILD STEEL
MATERIAL SPEC:
FINAL WEIGHT:
DWG NO: 111014002_1
REV: 1
SIZE: A
SCALE: 1:4
DO NOT SCALE
SHEET: 1 OF 1


FEATURES:
A: 5/16-24 TAPPED THRU HOLE FROM FAR SIDE (4 EA)
B: #8-32 TAPPED HOLE ↧0.3 (2 EA)
C: Ø 0.391 (10 EA)
D: 0.13 RADIUS FILLET (20 EDGES)
E: 0.450 X 2.6 SLOT (2 EA)
F: 0.875 X 2.7 SLOT
13.500
12.875
10.995
10.000
9.995
8.807
7.500
6.820
5.000
4.120
2.120
.870
0
0
2.545
5.455
8.000
0
.450
.688
3.000
3.050
3.250
3.313
4.000
4.688
4.750
4.950
5.000
7.313
7.550
EQUAL NOTCHES EQUAL DISTANCE FROM HOLE
.425
.260
.250
DETAIL A
SCALE 1 : 2
(.375)
MACHINE .020 OFF SURFACE FOR LOCATING
NOTICE OF PROPRIETARY RIGHTS
THIS DOCUMENT CONTAINS PROPRIETARY INFORMATION
IT MAY NOT BE REPRODUCED OR USED FOR ANY OTHER PURPOSE WITHOUT PRIOR WRITTEN PERMISSION.
UNLESS OTHERWISE SPECIFIED
ALL DIMENSIONS ARE IN INCHES
1 PLACE DECIMALS ± 0.100"
2 PLACE DECIMALS ± 0.030"
3 PLACE DECIMALS ± 0.005"
ANGLES ± 1°
INTERPRET GEOMETRIC TOLERANCING PER ANSI Y14.5M-1994
MONTANA STATE UNIVERSITY
MECHANICAL & INDUSTRIAL ENGINEERING
220 ROBERTS HALL
BOZEMAN, MT 59717
TITLE:
GRIP BASE PLATE
DRAWN BY: AC
DATE: 1/20/19
CHECKED BY: AC
DATE: 1/20/19
APPROVED BY:
DATE:
MATERIAL: 1018 MILD STEEL
MATERIAL SPEC:
FINAL WEIGHT:
DWG NO: 11014003_1
REV: 1
SIZE: A
SCALE: 1:4
DO NOT SCALE
SHEET: 1 OF 1


FEATURES:
A: 5/16-24 TAPPED HOLE ↧0.5 (4 EA)
B: #8-32 TAPPED HOLE ↧0.3 (4 EA)
C: 1/4-20 TAPPED HOLE ↧0.5 (2 EA)
1.450
.700
0
0
.625
2.505
3.505
5.200
6.700
11.380
12.630
13.500
0
.750
3.750
R.500
6.750
115°
9.750
10.248
10.500
11.625
12.750
4.000
3.250
2.850
1.875
.500
0
.130
NOTICE OF PROPRIETARY RIGHTS
THIS DOCUMENT CONTAINS PROPRIETARY INFORMATION
IT MAY NOT BE REPRODUCED OR USED FOR ANY OTHER
PURPOSE WITHOUT PRIOR WRITTEN PERMISSION.
UNLESS OTHERWISE SPECIFIED
ALL DIMENSIONS ARE IN INCHES
1 PLACE DECIMALS ± 0.100"
2 PLACE DECIMALS ± 0.030"
3 PLACE DECIMALS ± 0.005"
ANGLES ± 1°
INTERPRET GEOMETRIC
TOLERANCING PER
ANSI Y14.5M-1994
MATERIAL:
1018 MILD STEEL
MATERIAL SPEC:
FINAL WEIGHT:
DRAWN BY: AC
DATE: 10/13/19
CHECKED BY: AC
DATE: 10/13/19
APPROVED BY:
DATE:
MONTANA STATE UNIVERSITY
MECHANICAL & INDUSTRIAL ENGINEERING
220 ROBERTS HALL
BOZEMAN, MT 59717
TITLE:
GRIP PLATE STIFFNER
DWG NO: 11101400 4_1
REV: 1
SIZE: A
SCALE: 1:4
DO NOT SCALE
SHEET: 1 OF 1

NOTE:
THIS PART IS AN EXACT MIRROR OF PART 111-014-005
REFER TO THE DRAWING FOR DIMENSIONS AND DETAILS.



NOTICE OF PROPRIETARY RIGHTS
THIS DOCUMENT CONTAINS PROPRIETARY INFORMATION.
IT MAY NOT BE REPRODUCED OR USED FOR ANY OTHER
PURPOSE WITHOUT PRIOR WRITTEN PERMISSION.

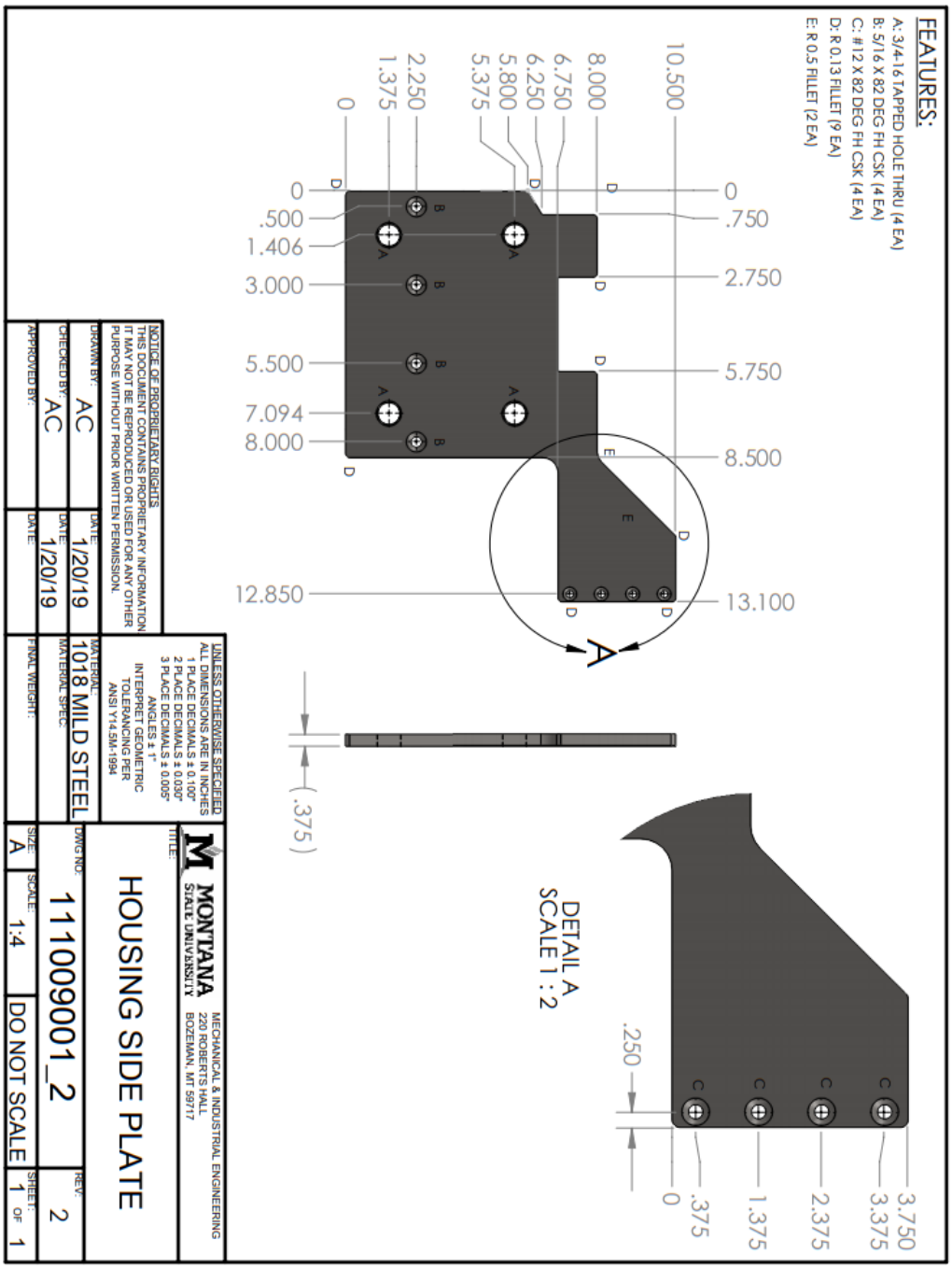
UNLESS OTHERWISE SPECIFIED
ALL DIMENSIONS ARE IN INCHES
1 PLACE DECIMALS ± 0.100"
2 PLACE DECIMALS ± 0.030"
3 PLACE DECIMALS ± 0.005"
ANGLES ± 1°
INTERPRET GEOMETRIC
TOLERANCING PER
ANSI Y14.5M-1994

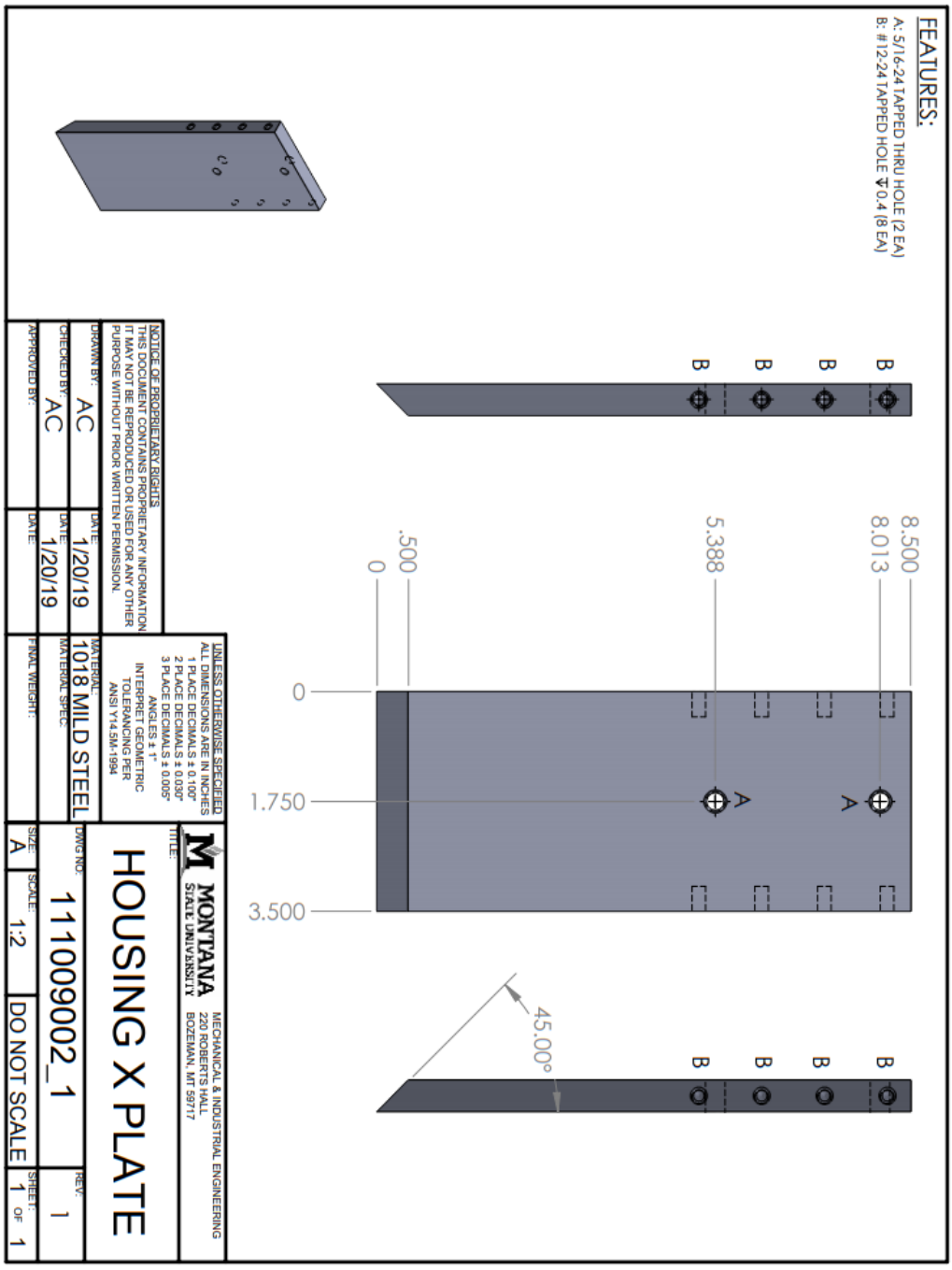
DRAWN BY: AC	DATE: 10/13/19	MATERIAL: -
CHECKED BY: AC	DATE: 10/13/19	MATERIAL SPEC: -
APPROVED BY:	DATE:	FINAL WEIGHT:

MONTANA STATE UNIVERSITY
MECHANICAL & INDUSTRIAL ENGINEERING
220 ROBERTS HALL
BOZEMAN, MT 59717

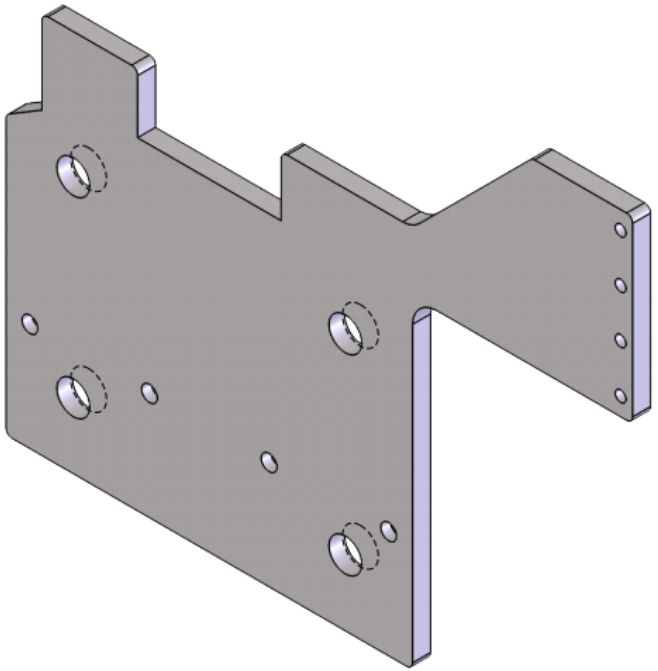
TITLE: GRIP PLATE STIFFNER 2

DWG NO: 111014005_1				REV: 1
SIZE: A	SCALE: 1:4	DO NOT SCALE		SHEET: 1 OF 1


FEATURES:
A: 3/4-16 TAPPED HOLE THRU (4 EA)
B: 5/16 X 82 DEG FH CSK (4 EA)
C: #12 X 82 DEG FH CSK (4 EA)
D: R 0.13 FILLET (9 EA)
E: R 0.5 FILLET (2 EA)
10.500
8.000
6.750
6.250
5.800
5.375
2.250
1.375
0
0
.500
1.406
3.000
5.500
7.094
8.000
0
.750
2.750
5.750
8.500
12.850
13.100
A
(.375)
3.750
3.375
2.375
1.375
.375
0
.250
DETAIL A
SCALE 1 : 2
NOTICE OF PROPRIETARY RIGHTS
THIS DOCUMENT CONTAINS PROPRIETARY INFORMATION
IT MAY NOT BE REPRODUCED OR USED FOR ANY OTHER
PURPOSE WITHOUT PRIOR WRITTEN PERMISSION.
UNLESS OTHERWISE SPECIFIED
ALL DIMENSIONS ARE IN INCHES
1 PLACE DECIMALS ± 0.100"
2 PLACE DECIMALS ± 0.030"
3 PLACE DECIMALS ± 0.005"
ANGLES ± 1°
INTERPRET GEOMETRIC
TOLERANCING PER
ANSI Y14.5M-1994
MONTANA STATE UNIVERSITY
MECHANICAL & INDUSTRIAL ENGINEERING
220 ROBERTS HALL
BOZEMAN, MT 59717
TITLE:
HOUSING SIDE PLATE
DRAWN BY: AC
DATE: 1/20/19
CHECKED BY: AC
DATE: 1/20/19
APPROVED BY:
DATE:
MATERIAL:
1018 MILD STEEL
MATERIAL SPEC:
FINAL WEIGHT:
DWG NO: 11100901_2
REV: 2
SIZE: A
SCALE: 1:4
DO NOT SCALE
SHEET: 1 OF 1


FEATURES:
A: 5/16-24 TAPPED THRU HOLE (2 EA)
B: #12-24 TAPPED HOLE ↧0.4 (8 EA)
8.500
8.013
5.388
.500
0
0
1.750
3.500
45.00°
A
B
NOTICE OF PROPRIETARY RIGHTS
THIS DOCUMENT CONTAINS PROPRIETARY INFORMATION
IT MAY NOT BE REPRODUCED OR USED FOR ANY OTHER
PURPOSE WITHOUT PRIOR WRITTEN PERMISSION.
UNLESS OTHERWISE SPECIFIED
ALL DIMENSIONS ARE IN INCHES
1 PLACE DECIMALS ± 0.100"
2 PLACE DECIMALS ± 0.030"
3 PLACE DECIMALS ± 0.005"
ANGLES ± 1°
INTERPRET GEOMETRIC
TOLERANCING PER
ANSI Y14.5M-1994
MONTANA STATE UNIVERSITY
MECHANICAL & INDUSTRIAL ENGINEERING
220 ROBERTS HALL
BOZEMAN, MT 59717
DRAWN BY: AC
DATE: 1/20/19
CHECKED BY: AC
DATE: 1/20/19
APPROVED BY:
DATE:
MATERIAL: 1018 MILD STEEL
MATERIAL SPEC:
FINAL WEIGHT:
TITLE: HOUSING X PLATE
DWG NO: 11100902_1
REV: 1
SIZE: A
SCALE: 1:2
DO NOT SCALE
SHEET 1 OF 1

NOTES:
THIS IS A MIRROR IMAGE OF PART 111-009-001.
PLEASE SEE REFERENCED DRAWING FOR DIMENSIONS



UNLESS OTHERWISE SPECIFIED
ALL DIMENSIONS ARE IN INCHES
1 PLACE DECIMALS ± 0.100"
2 PLACE DECIMALS ± 0.030"
3 PLACE DECIMALS ± 0.005"
ANGLES ± 1°
INTERPRET GEOMETRIC TOLERANCING PER ANSI Y14.5M-1994

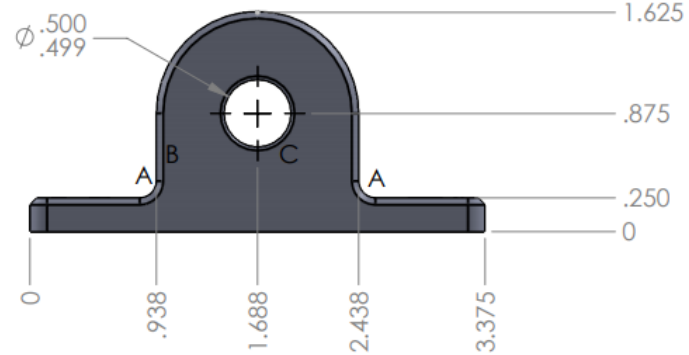
NOTICE OF PROPRIETARY RIGHTS
THIS DOCUMENT CONTAINS PROPRIETARY INFORMATION. IT MAY NOT BE REPRODUCED OR USED FOR ANY OTHER PURPOSE WITHOUT PRIOR WRITTEN PERMISSION.

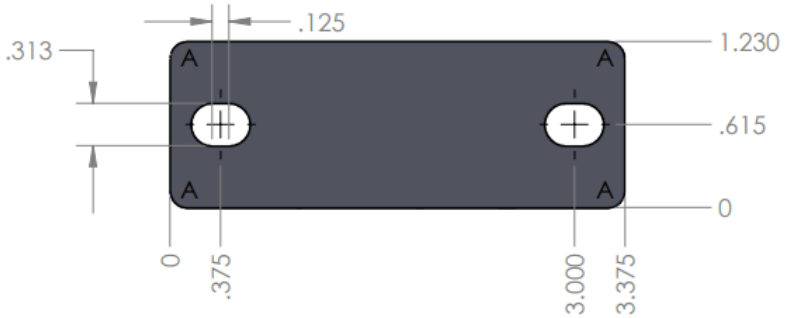
MONTANA STATE UNIVERSITY
MECHANICAL & INDUSTRIAL ENGINEERING
220 ROBERTS HALL
BOZEMAN, MT 59717

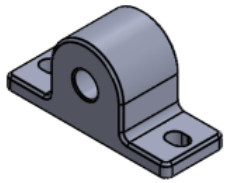
DRAWN BY: AC	DATE: 1/22/19	MATERIAL: 1018 MILD STEEL	TITLE: HOUSING SIDE PLATE MIRROR
CHECKED BY: AC	DATE: 1/22/19	MATERIAL SPEC: -	DWG NO: 111009003_2 / REV: 2
APPROVED BY:	DATE:	FINAL WEIGHT:	SIZE: A / SCALE: 1:2 / DO NOT SCALE / SHEET: 1 OF 1

FEATURES:

A: R 0.13 (6 EA)
B: CHAMFER 45° X .05 AROUND (1 EA)
C: CHAMFER 45° X .03 (2 EA)







NOTICE OF PROPRIETARY RIGHTS
THIS DOCUMENT CONTAINS PROPRIETARY INFORMATION. IT MAY NOT BE REPRODUCED OR USED FOR ANY OTHER PURPOSE WITHOUT PRIOR WRITTEN PERMISSION.

UNLESS OTHERWISE SPECIFIED
ALL DIMENSIONS ARE IN INCHES
1 PLACE DECIMALS ± 0.100"
2 PLACE DECIMALS ± 0.030"
3 PLACE DECIMALS ± 0.005"
ANGLES ± 1°
INTERPRET GEOMETRIC TOLERANCING PER ANSI Y14.5M-1994

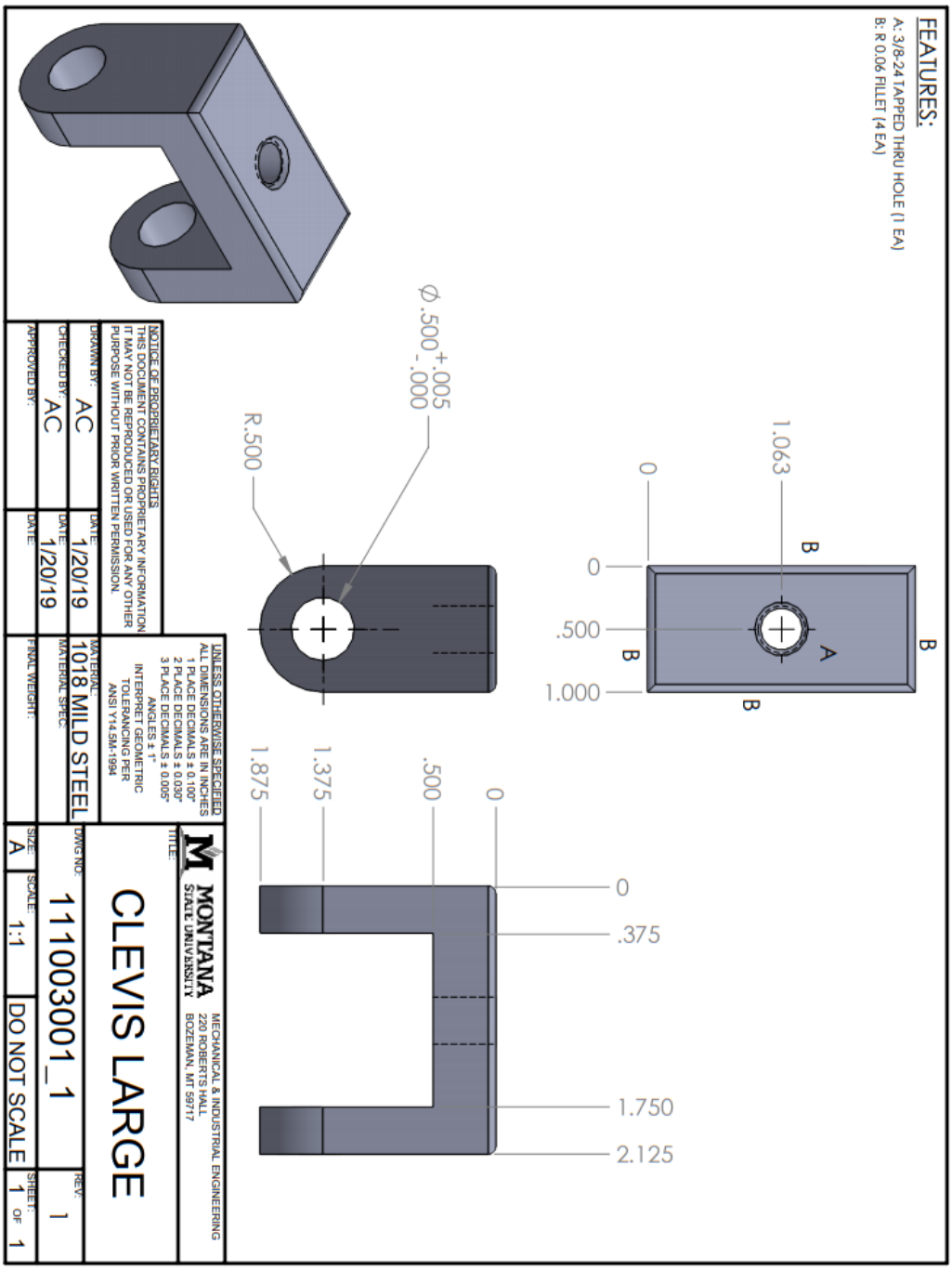
DRAWN BY: AC	DATE: 6/4/19	MATERIAL: 1018 MILD STEEL	
CHECKED BY: AC	DATE: 6/4/19	MATERIAL SPEC:	
APPROVED BY:	DATE:	FINAL WEIGHT:	

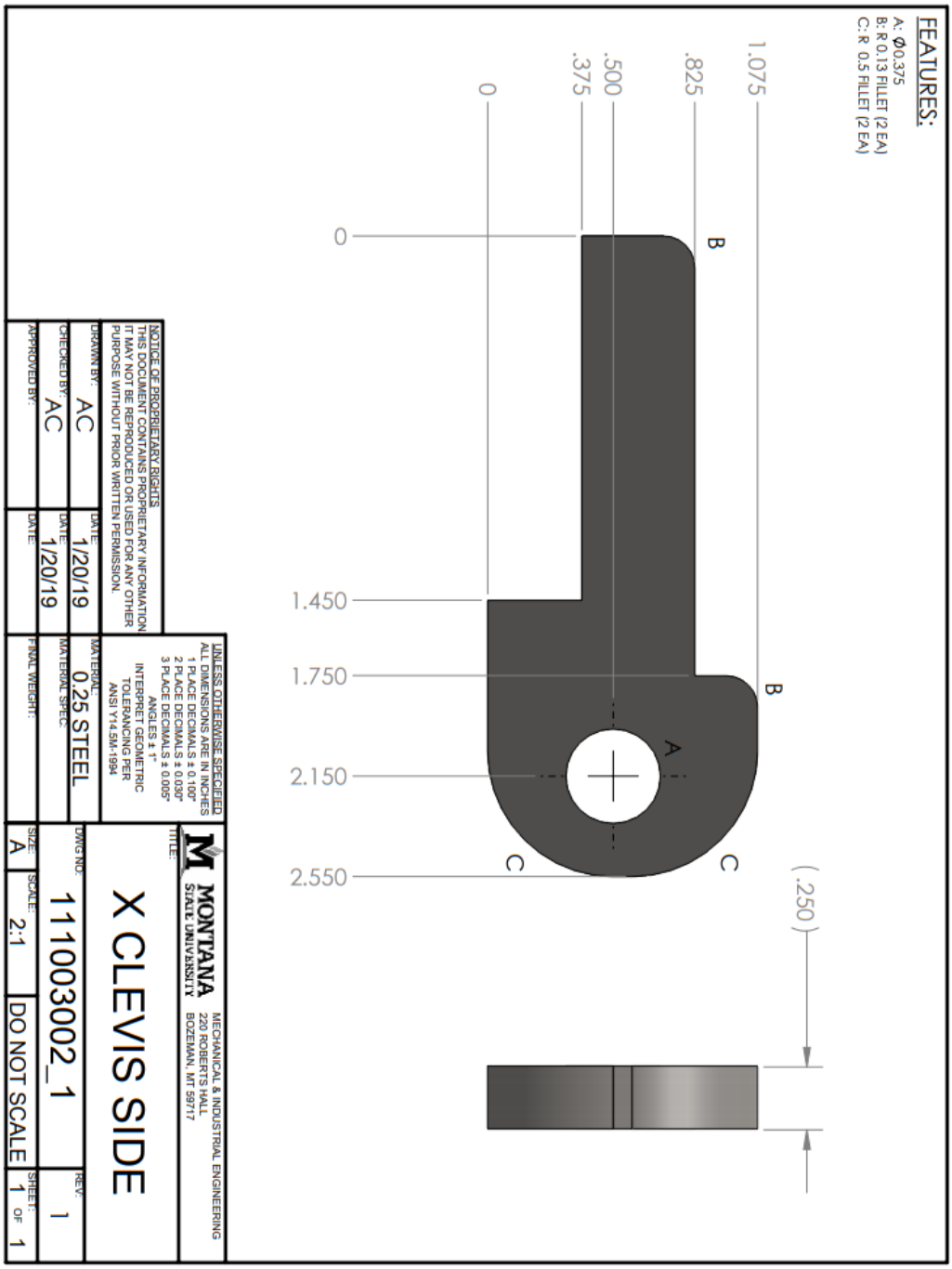
MONTANA STATE UNIVERSITY
MECHANICAL & INDUSTRIAL ENGINEERING
220 ROBERTS HALL
BOZEMAN, MT 59717

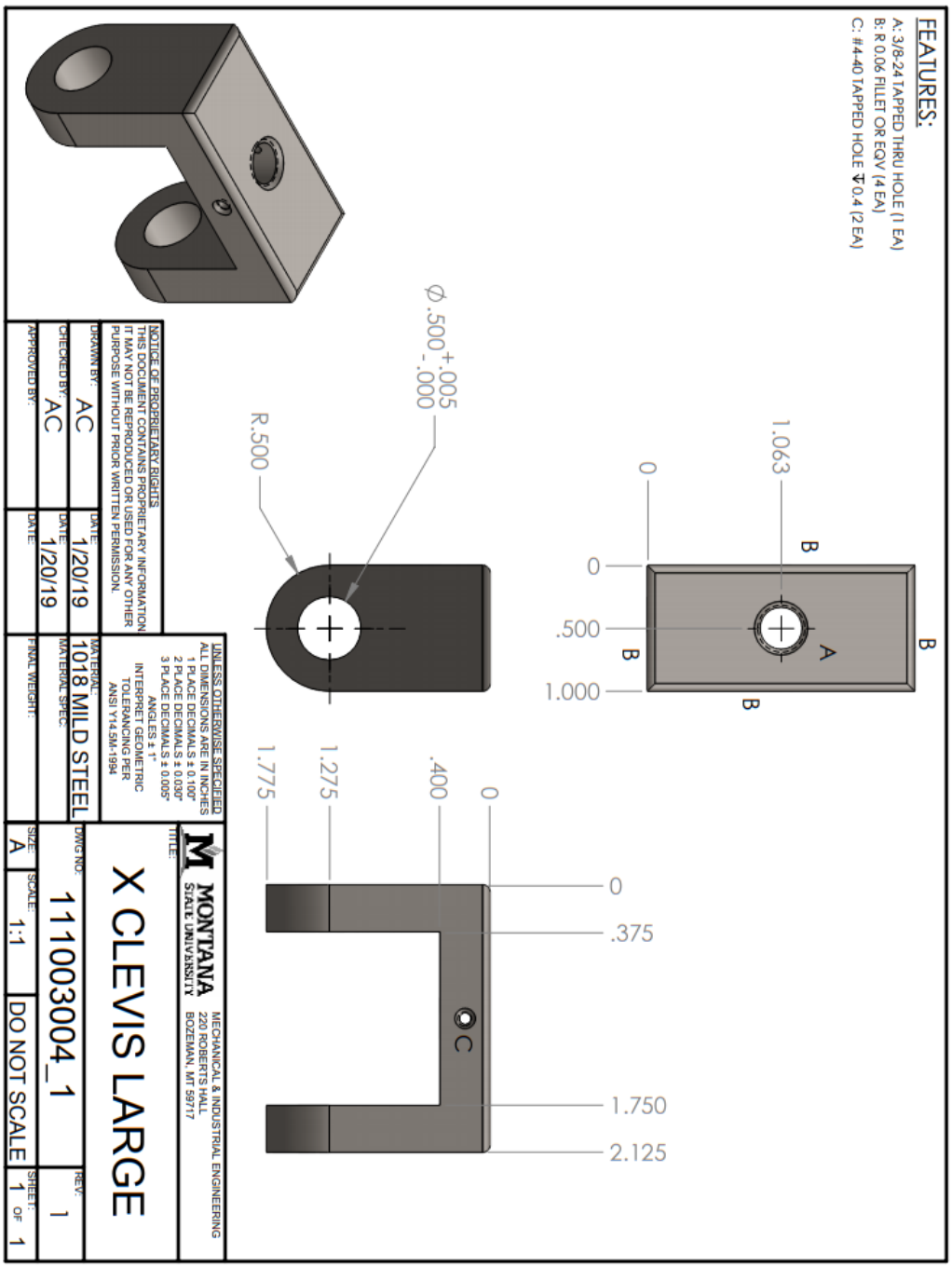
TITLE:

BUSHING HOUSING

DWG NO: 111004001_1				REV: 1
SIZE: A	SCALE: 1:1	DO NOT SCALE	SHEET: 1 OF 1	

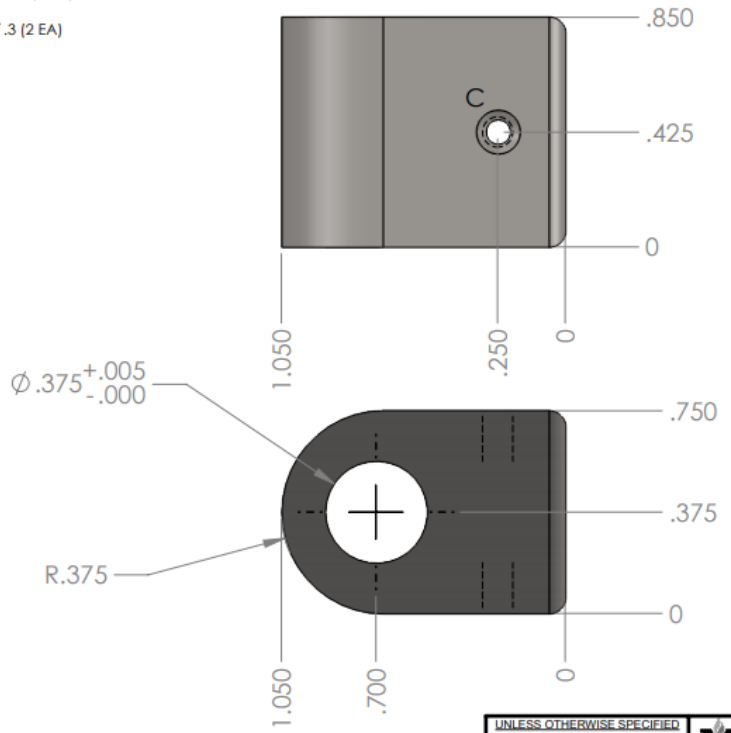

FEATURES:
A: 3/8-24 TAPPED THRU HOLE (1 EA)
B: R 0.06 FILLET (4 EA)
1.063
0
0
.500
1.000
B
A
Ø .500 +.005 -.000
R.500
0
.500
1.375
1.875
0
.375
1.750
2.125
NOTICE OF PROPRIETARY RIGHTS
THIS DOCUMENT CONTAINS PROPRIETARY INFORMATION
IT MAY NOT BE REPRODUCED OR USED FOR ANY OTHER
PURPOSE WITHOUT PRIOR WRITTEN PERMISSION.
DRAWN BY: AC
DATE: 1/20/19
CHECKED BY: AC
DATE: 1/20/19
APPROVED BY:
DATE:
MATERIAL: 1018 MILD STEEL
MATERIAL SPEC:
FINAL WEIGHT:
UNLESS OTHERWISE SPECIFIED
ALL DIMENSIONS ARE IN INCHES
1 PLACE DECIMALS ± 0.100"
2 PLACE DECIMALS ± 0.030"
3 PLACE DECIMALS ± 0.005"
ANGLES ± 1°
INTERPRET GEOMETRIC
TOLERANCING PER
ANSI Y14.5M-1994
MONTANA STATE UNIVERSITY
MECHANICAL & INDUSTRIAL ENGINEERING
220 ROBERTS HALL
BOZEMAN, MT 59717
TITLE:
CLEVIS LARGE
DWG NO: 11100300 1_1
REV: 1
SIZE: A
SCALE: 1:1
DO NOT SCALE
SHEET: 1 OF 1

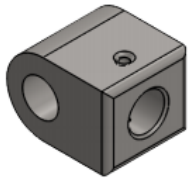

FEATURES:
A: Ø0.375
B: R 0.13 FILLET (2 EA)
C: R 0.5 FILLET (2 EA)
1.075
.825
.500
.375
0
0
1.450
1.750
2.150
2.550
A
B
C
(.250)
NOTICE OF PROPRIETARY RIGHTS
THIS DOCUMENT CONTAINS PROPRIETARY INFORMATION
IT MAY NOT BE REPRODUCED OR USED FOR ANY OTHER
PURPOSE WITHOUT PRIOR WRITTEN PERMISSION.
UNLESS OTHERWISE SPECIFIED
ALL DIMENSIONS ARE IN INCHES
1 PLACE DECIMALS ± 0.100"
2 PLACE DECIMALS ± 0.030"
3 PLACE DECIMALS ± 0.005"
ANGLES ± 1°
INTERPRET GEOMETRIC
TOLERANCING PER
ANSI Y14.5M-1994
MONTANA
STATE UNIVERSITY
MECHANICAL & INDUSTRIAL ENGINEERING
220 ROBERTS HALL
BOZEMAN, MT 59717
DRAWN BY: AC
DATE: 1/20/19
CHECKED BY: AC
DATE: 1/20/19
APPROVED BY:
DATE:
MATERIAL: 0.25 STEEL
MATERIAL SPEC:
FINAL WEIGHT:
TITLE:
X CLEVIS SIDE
DWG NO: 11003002_1
REV: 1
SIZE: A
SCALE: 2:1
DO NOT SCALE
SHEET 1 OF 1


FEATURES:
A: 3/8-24 TAPPED THRU HOLE (1 EA)
B: R 0.06 FILLET OR EQV (4 EA)
C: #4-40 TAPPED HOLE ↧0.4 (2 EA)
1.063
0
0
.500
1.000
B
A
Ø .500 +.005 -.000
R.500
0
.400
1.275
1.775
0
.375
1.750
2.125
C
NOTICE OF PROPRIETARY RIGHTS
THIS DOCUMENT CONTAINS PROPRIETARY INFORMATION IT MAY NOT BE REPRODUCED OR USED FOR ANY OTHER PURPOSE WITHOUT PRIOR WRITTEN PERMISSION.
DRAWN BY: AC DATE: 1/20/19
CHECKED BY: AC DATE: 1/20/19
APPROVED BY: DATE:
UNLESS OTHERWISE SPECIFIED
ALL DIMENSIONS ARE IN INCHES
1 PLACE DECIMALS ± 0.100"
2 PLACE DECIMALS ± 0.030"
3 PLACE DECIMALS ± 0.005"
ANGLES ± 1°
INTERPRET GEOMETRIC TOLERANCING PER ANSI Y14.5M-1994
MATERIAL: 1018 MILD STEEL
MATERIAL SPEC:
FINAL WEIGHT:
MONTANA STATE UNIVERSITY
MECHANICAL & INDUSTRIAL ENGINEERING
220 ROBERTS HALL
BOZEMAN, MT 59717
TITLE:
X CLEVIS LARGE
DWG NO: 11100304_1
REV: 1
SIZE: A
SCALE: 1:1
DO NOT SCALE
SHEET: 1 OF 1

FEATURES:

A: 3/8-24 TAPPED HOLE ↧0.7 (1 EA)
B: R 0.06 FILLET (4 EA)
C: #4-40 TAPPED HOLE ↧.3 (2 EA)





UNLESS OTHERWISE SPECIFIED
ALL DIMENSIONS ARE IN INCHES
1 PLACE DECIMALS ± 0.100"
2 PLACE DECIMALS ± 0.030"
3 PLACE DECIMALS ± 0.005"
ANGLES ± 1°
INTERPRET GEOMETRIC TOLERANCING PER ANSI Y14.5M-1994

NOTICE OF PROPRIETARY RIGHTS
THIS DOCUMENT CONTAINS PROPRIETARY INFORMATION. IT MAY NOT BE REPRODUCED OR USED FOR ANY OTHER PURPOSE WITHOUT PRIOR WRITTEN PERMISSION.

MONTANA STATE UNIVERSITY
MECHANICAL & INDUSTRIAL ENGINEERING
220 ROBERTS HALL
BOZEMAN, MT 59717

DRAWN BY: AC	DATE: 1/20/19	MATERIAL: 1018 MILD STEEL	TITLE: X CLEVIS, FREE
CHECKED BY: AC	DATE: 1/20/19	MATERIAL SPEC:	DWG NO: 111001001_2 REV: 2
APPROVED BY:	DATE:	FINAL WEIGHT:	SIZE: A SCALE: 2:1 DO NOT SCALE SHEET: 1 OF 1

APPENDIX C

APPENDIX C: ADDITIONAL DESIGN INFORMATION

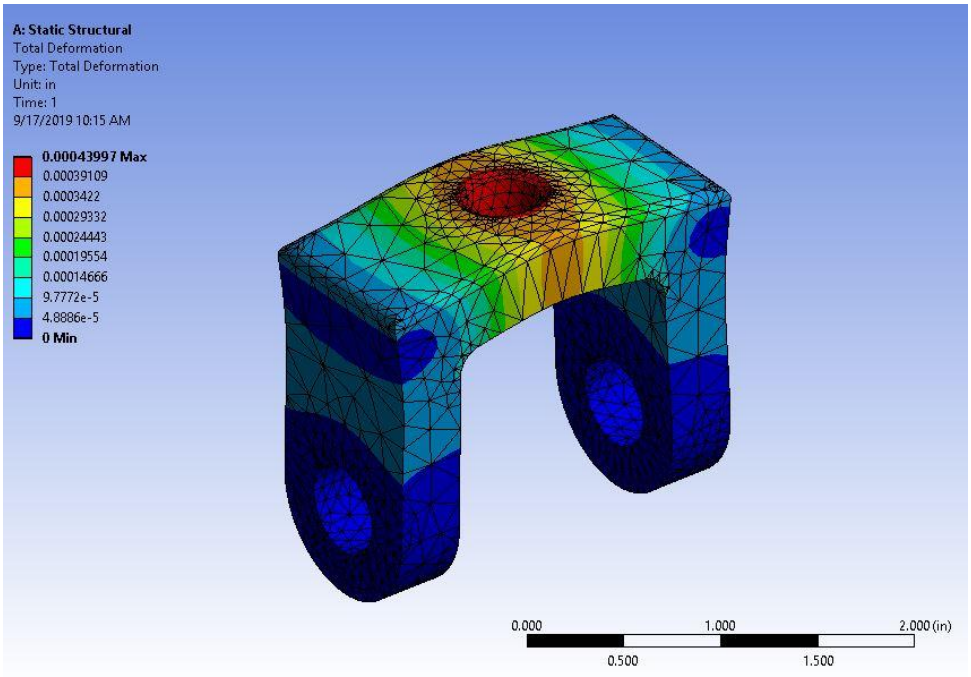


Figure 125: ANSYS FEA screenshot detailing deformation of large clevis (111-003-001) with 1000 lbf applied to the threaded hole.

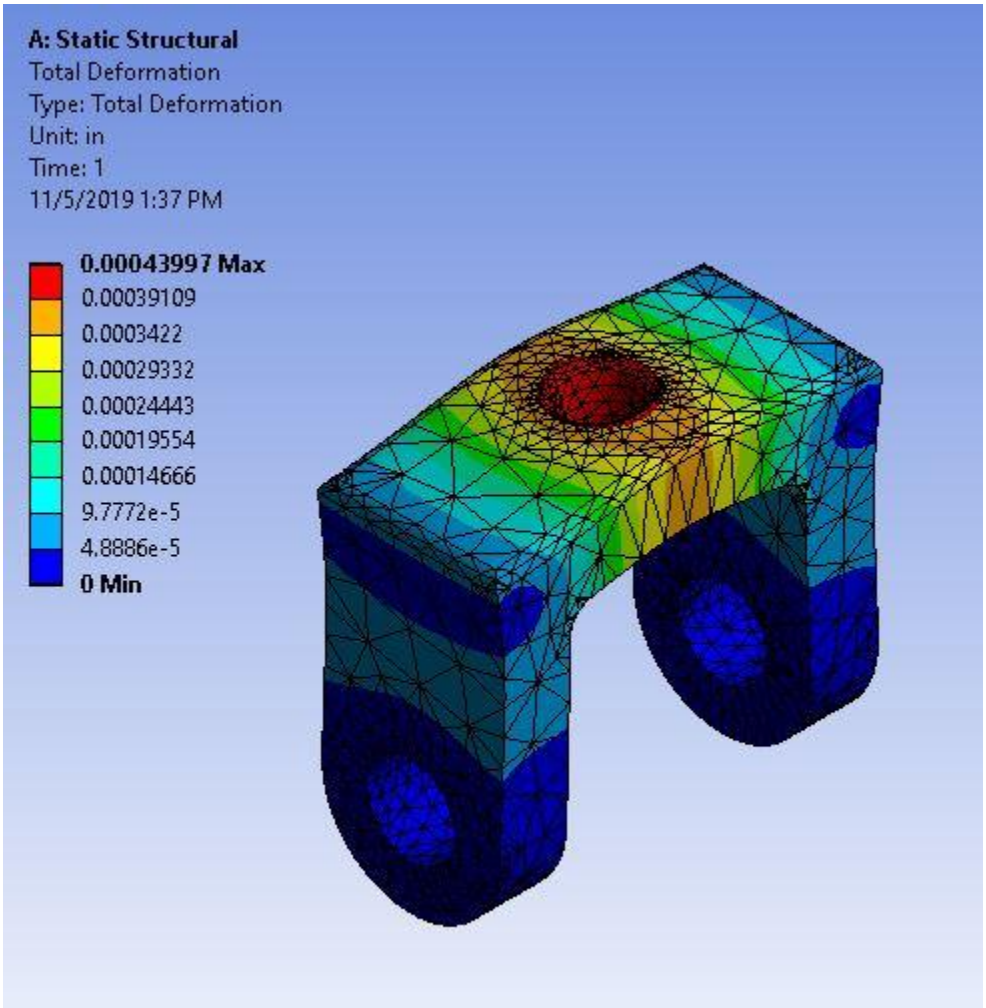


Figure 126: ANSYS FEA screenshot detailing deformation of large X clevis (111-003-004) with 1000 lbf applied to the threaded hole.

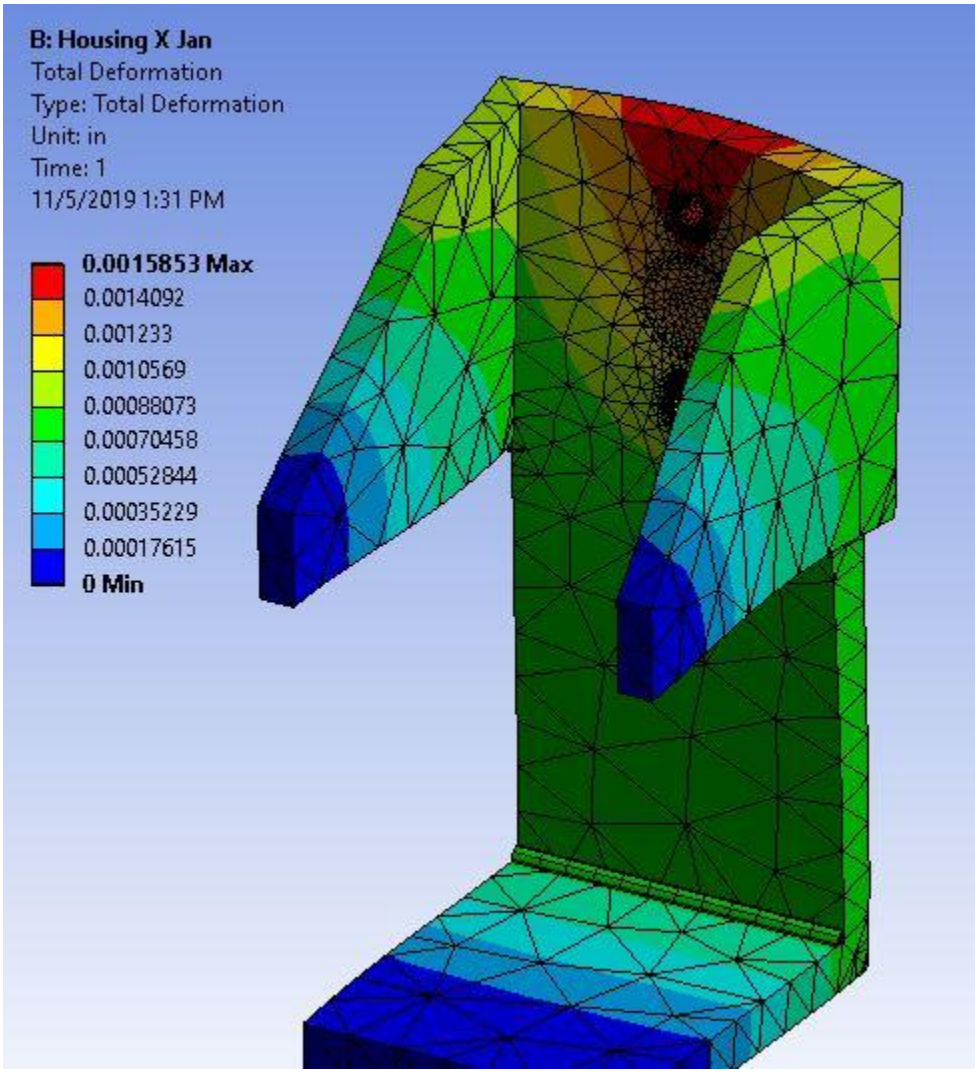


Figure 127: ANSYS FEA screenshot detailing deformation of a portion of the housing assembly (333-014-001) with 1000 lbf applied in the X direction.

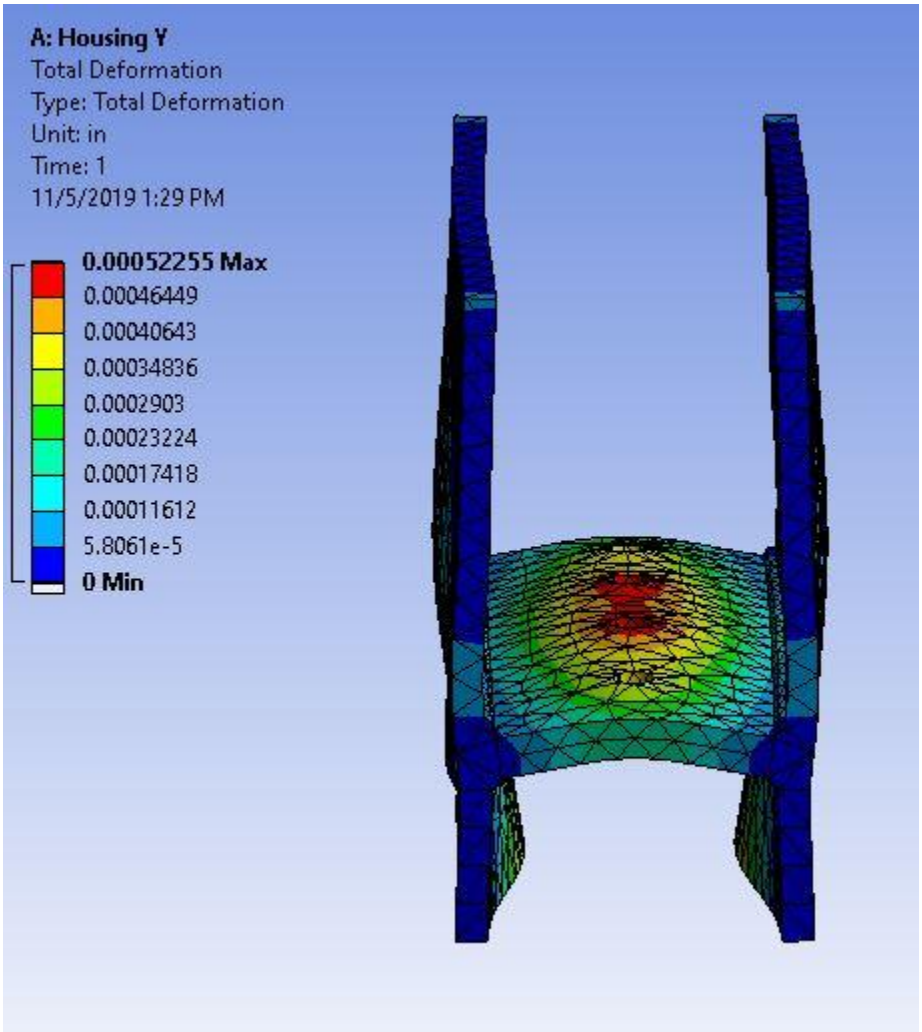


Figure 128: ANSYS FEA screenshot detailing deformation of a portion of the housing assembly with 2000 lbf applied in the Y direction.

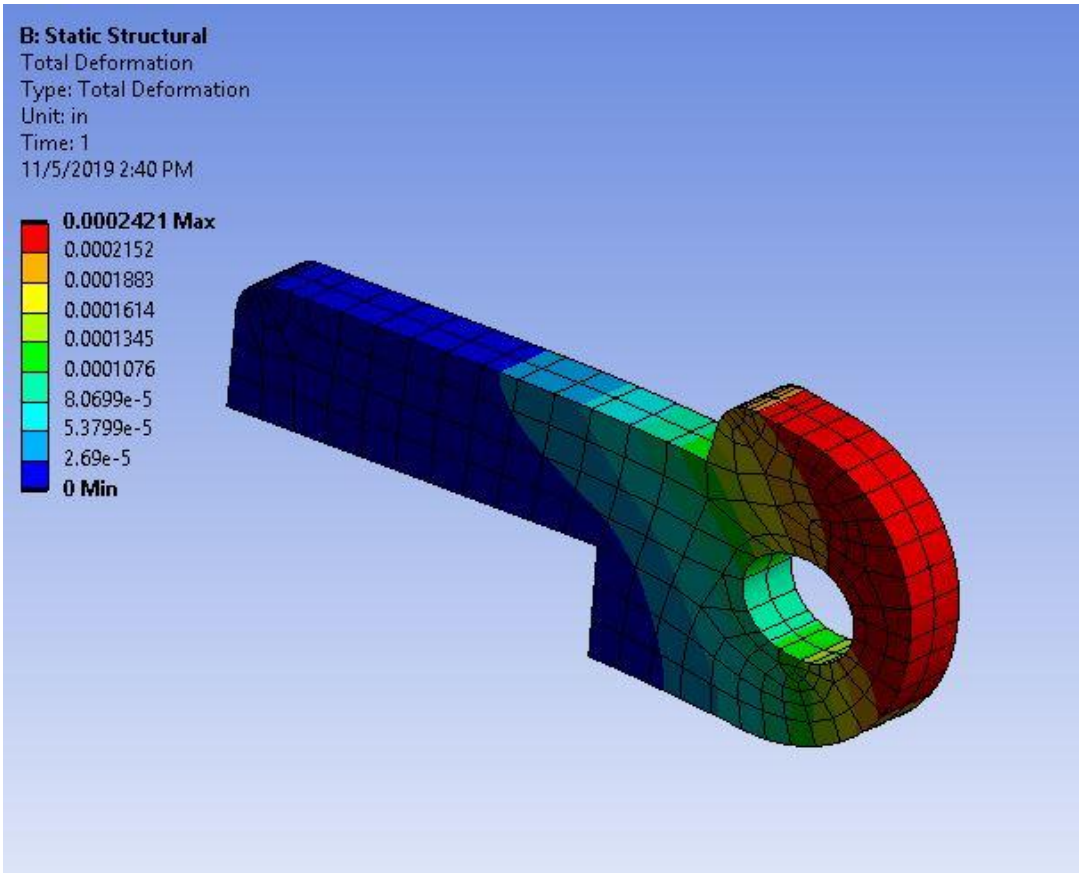


Figure 129: ANSYS FEA screenshot detailing deformation of X side clevis (111-003-002) with 500 lbf applied axially to the hole. (NOTE: There are two of these hence 1000 lbf/2 = 500 lbf)

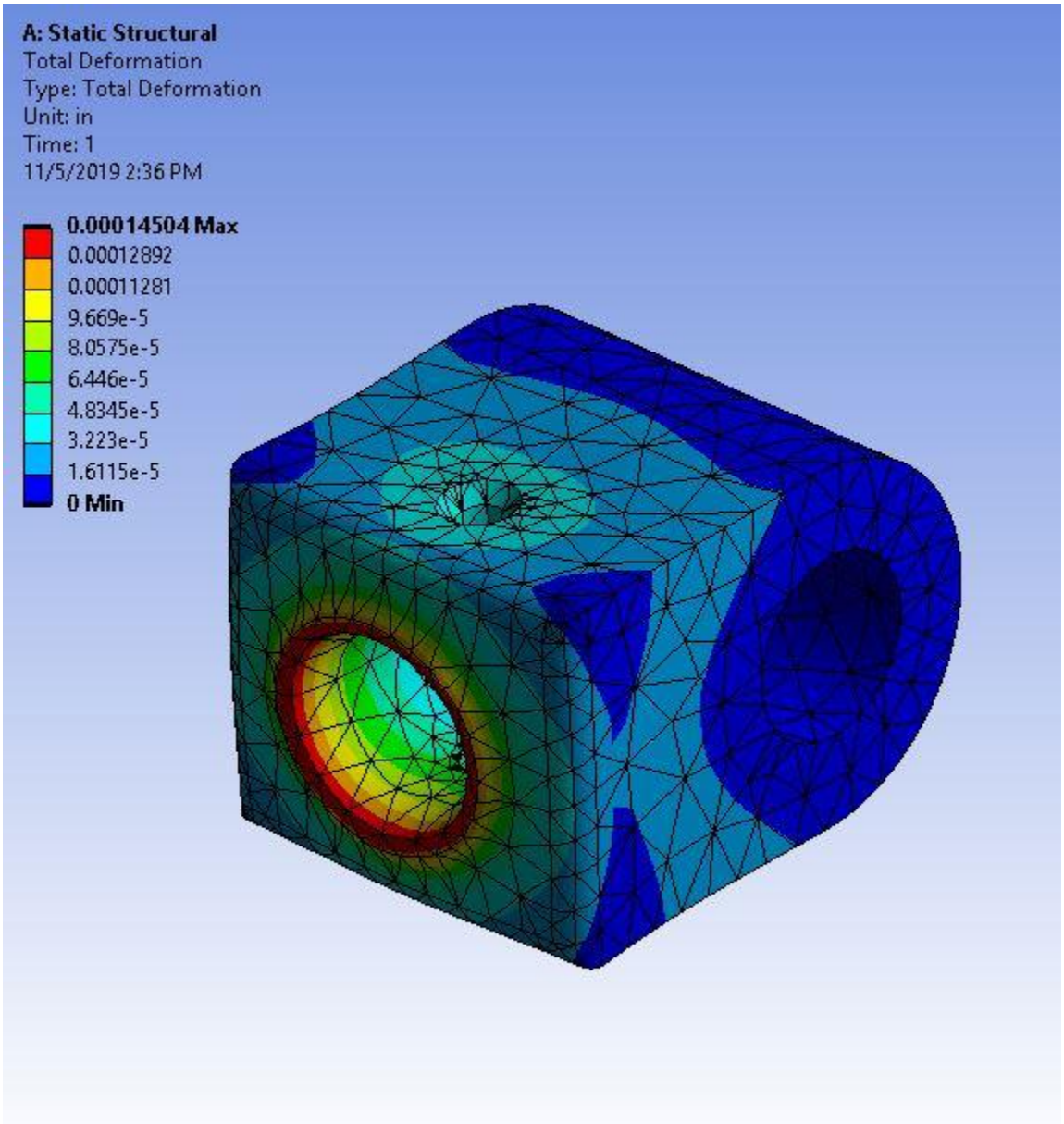


Figure 130: ANSYS FEA screenshot detailing deformation of the free X clevis (111-001-001) with 1000 lbf applied to the threaded hole.

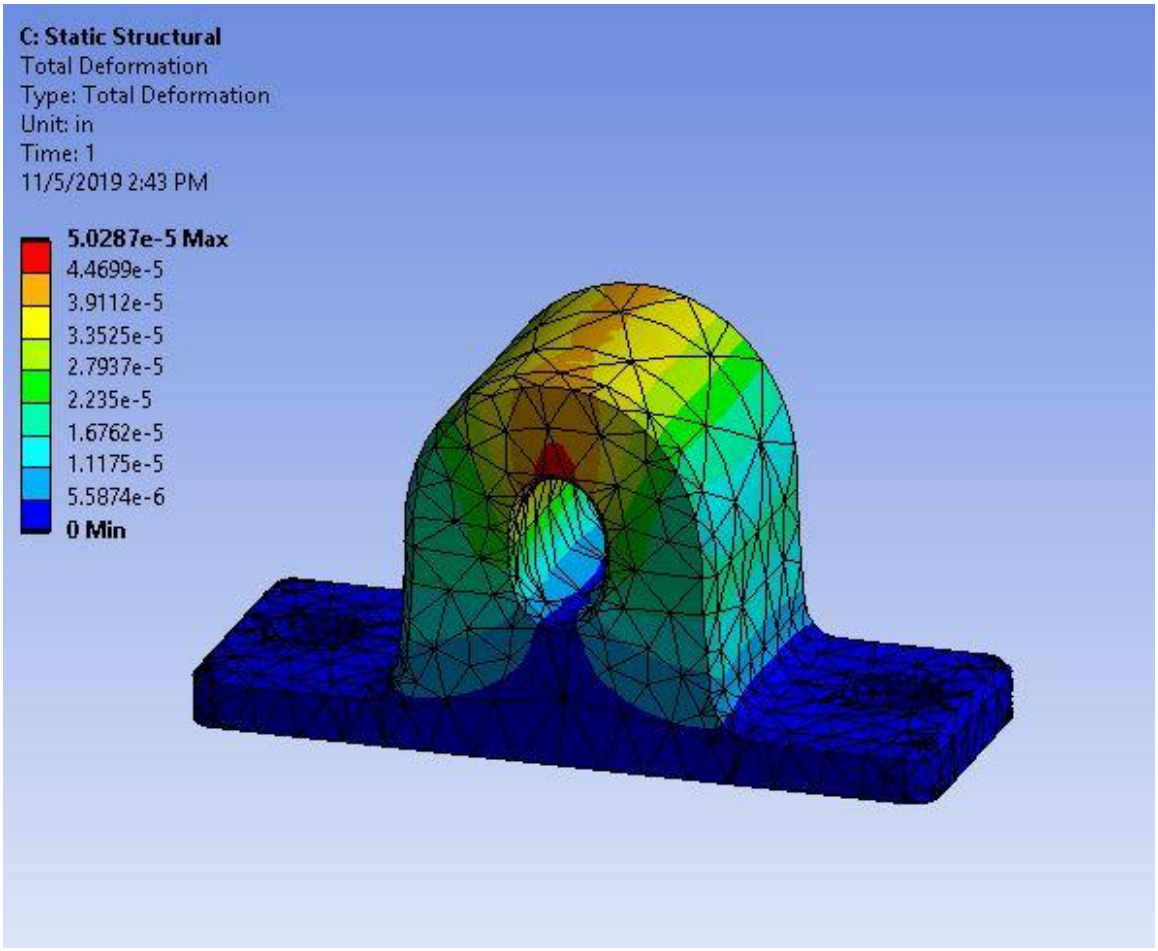


Figure 131: ANSYS FEA screenshot detailing deformation of bushing (111-004-001) with 1000 lbf applied vertically to the pin hole.

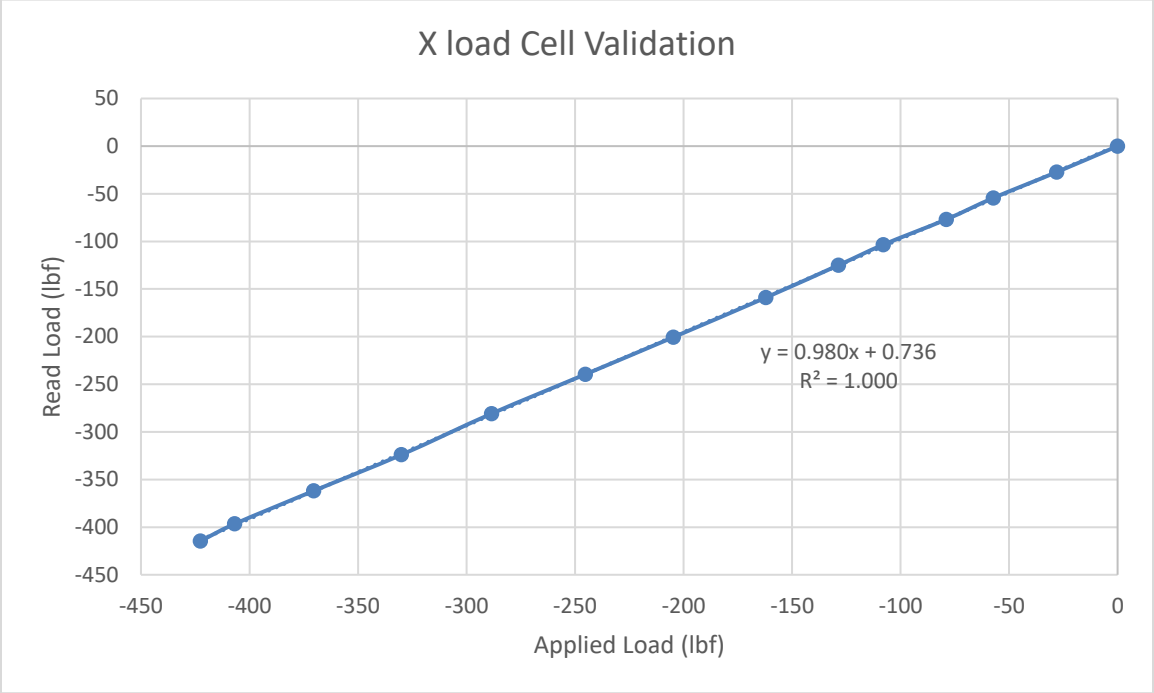


Figure 132: Validation curve for the X direction of the IPL. The process was completed by attaching a calibrated load cell in line with a cable and pulling on a gripped coupon. The small error is considered friction and off-axis loading associated with the procedure.

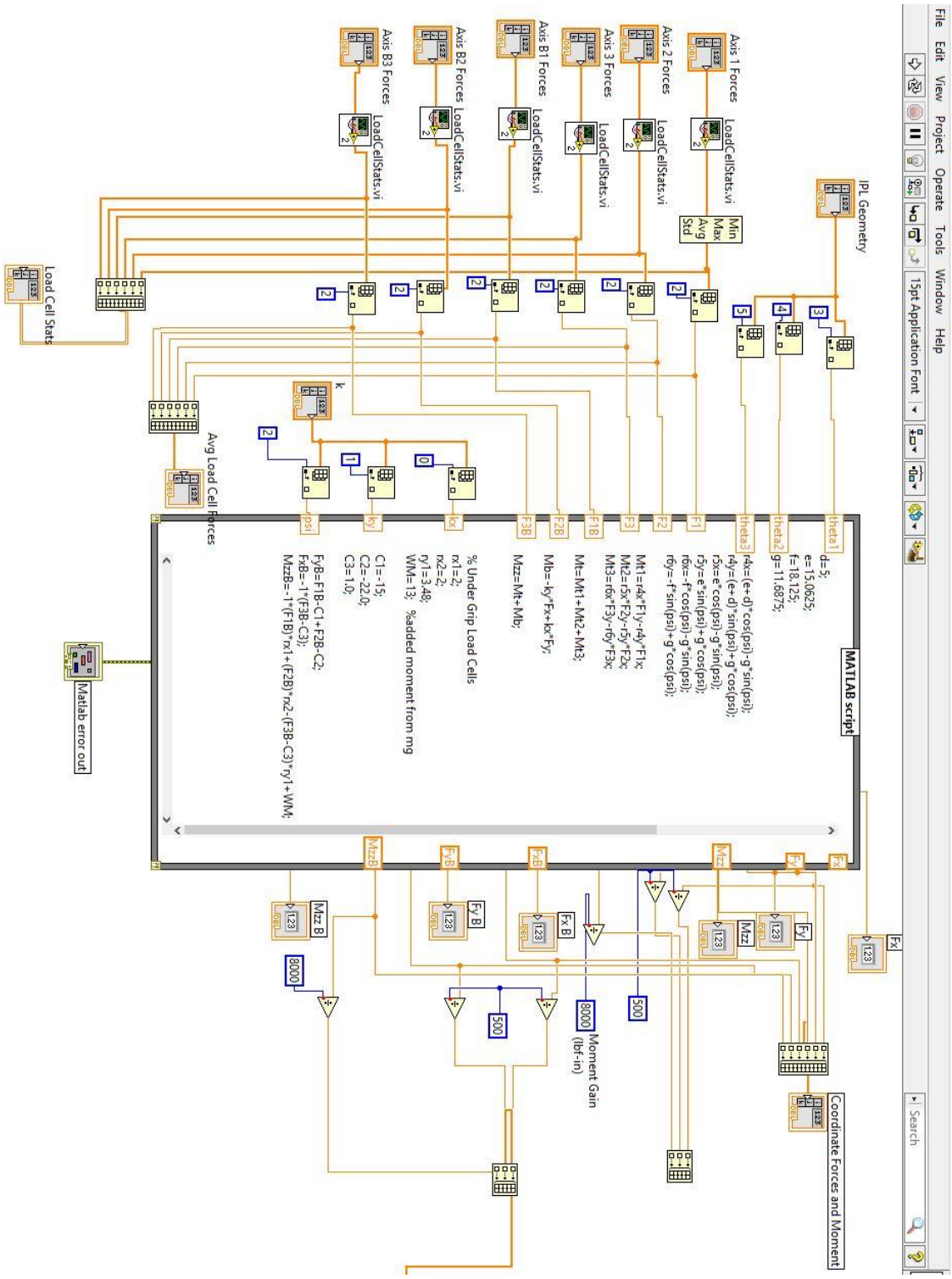


Figure 133: LabVIEW screenshot of sub VI titled "ProcessAxisLoads.vi" which contains the MATLAB script that resolves load components.

APPENDIX D

APPENDIX D: IPL USER GUIDE

IPL User Guide

I was fortunate enough to have another graduate student guide me through the use of the IPL. Unfortunately, the next student to use the IPL will not have that luxury. This instruction manual, along with an instructional video which will also be provided, is intended for anyone who is using the IPL for the first time to get started using it for materials testing.

The IPL is intended for use as a 3 DOF multiaxial test frame. The machine is capable of translation along the X and Y directions, along with rotation about the Z direction. Material specimen should be machined to 5.5” by 1” with some type of notch geometry which optimizes the desired failure. The grips are currently configured to accept a specimen between 0.180” and 0.200” in thickness. The following steps will work through the entire process of running a single test on the IPL. It is noted, this user guide does not include instructions for the use of GOM ARAMIS DIC software, it is mentioned several times in the instructions, but other resources are available for students to become comfortable using DIC for material testing.

First off, there are a few guidelines to follow. The IPL’s load capacity is about 2000 lbf in the Y direction and 1000 lbf in the X direction. The load system was designed to withstand these forces. Test specimen should be designed to fail within these loads to avoid damage to the machine and to avoid excessive flex of the IPL frame. Excessive motion in the negative X direction (crosshead to the left) should be avoided, as actuator 2 can potentially contact the new load system.

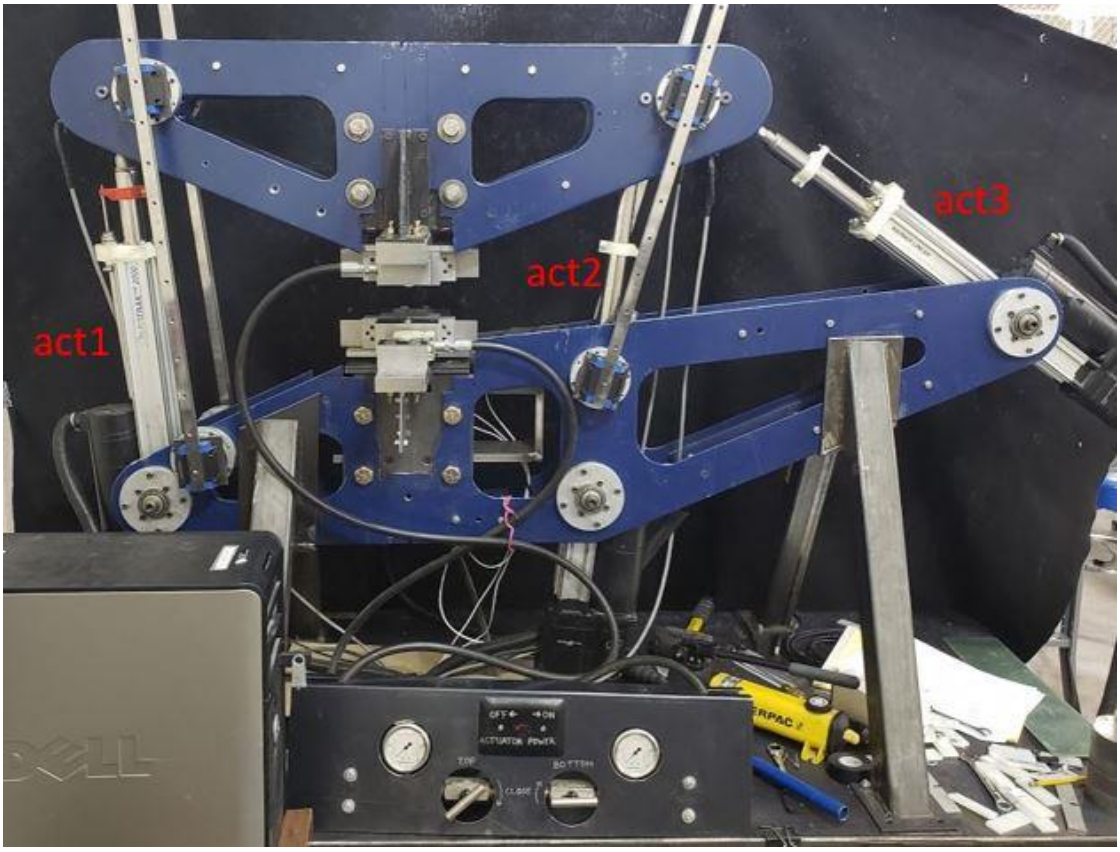


Figure 134: IPL User Guide reference figure.

1. Log in to the IPL computer using your MSU credentials. (NOTE: Sometimes a "disk read error" appears on the screen while it is booting up. To bypass this, remove the IPL flash drive from the computer and allow it to completely boot up before re-inserting it.)
2. On the IPL flash drive, open the LabVIEW VI titled 'IPL_V1' (Removable Disk > IPL). This is the main VI which controls the entire IPL.
3. On the IPL flash drive find and open the LVDT Calibration VI titled 'LVDT_Calib' (Removable Disk > IPL > MATLAB)

4. Turn on the DAQ, LVDTs, and UMI using the three toggle switches on the lower level of the IPL table.
5. Turn on the IPL actuators using the large toggle switch on the IPL Dashboard bracket on the main level of the IPL table.
6. Run the LVDT Calibration VI.
7. Measure the lengths of each actuator (pin to pin) from left to right (actuators 1, 2,3. See Figure 127) from the computer side of the IPL. (NOTE: Actuator 2 is hard to get an exact length for, if you measure over the bearing rail, subtract about 1 cm from your measurement.
8. Enter the actuator lengths into the 'Measured Lengths' window of the LVDT Calibration VI. (NOTE: There are input boxes for both inches, and centimeters, the VI will convert to inches if you have measured the lengths in centimeters) (See Figure 128)

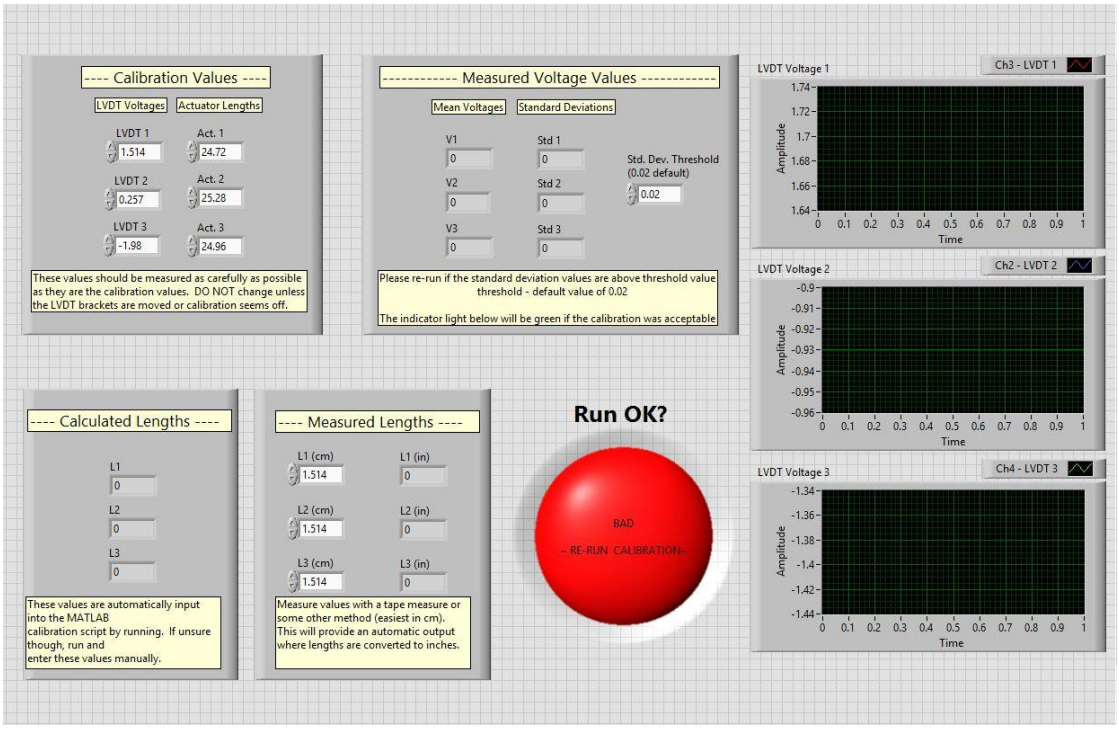


Figure 135: Snapshot of the 'LVDT_Calib' VI.

9. Run the LVDT Calibration VI. This converts the length inputs to inches.
10. Copy and paste the actuator lengths (inches) from the ‘Measured Lengths’ window into their corresponding text boxes in the ‘Calibration Values’ window.
11. Copy and paste the LVDT voltage values from the ‘Measured Voltage Values’ window into the corresponding text boxes ‘Calibration Values’ window.
12. Run the LVDT Calibration VI.
13. If the bubble is green and returns “good”, the LVDTs are calibrated. If it returns a red bubble and “bad”, return to step 7.
14. You are now done using the LVDT Calibration VI.

15. Open the program ‘Notepad’ and save a blank .txt file to your desktop titled ‘Initialize.txt’.

16. Run the IPL_V1 VI, it will run continuously. (See Figure 129)

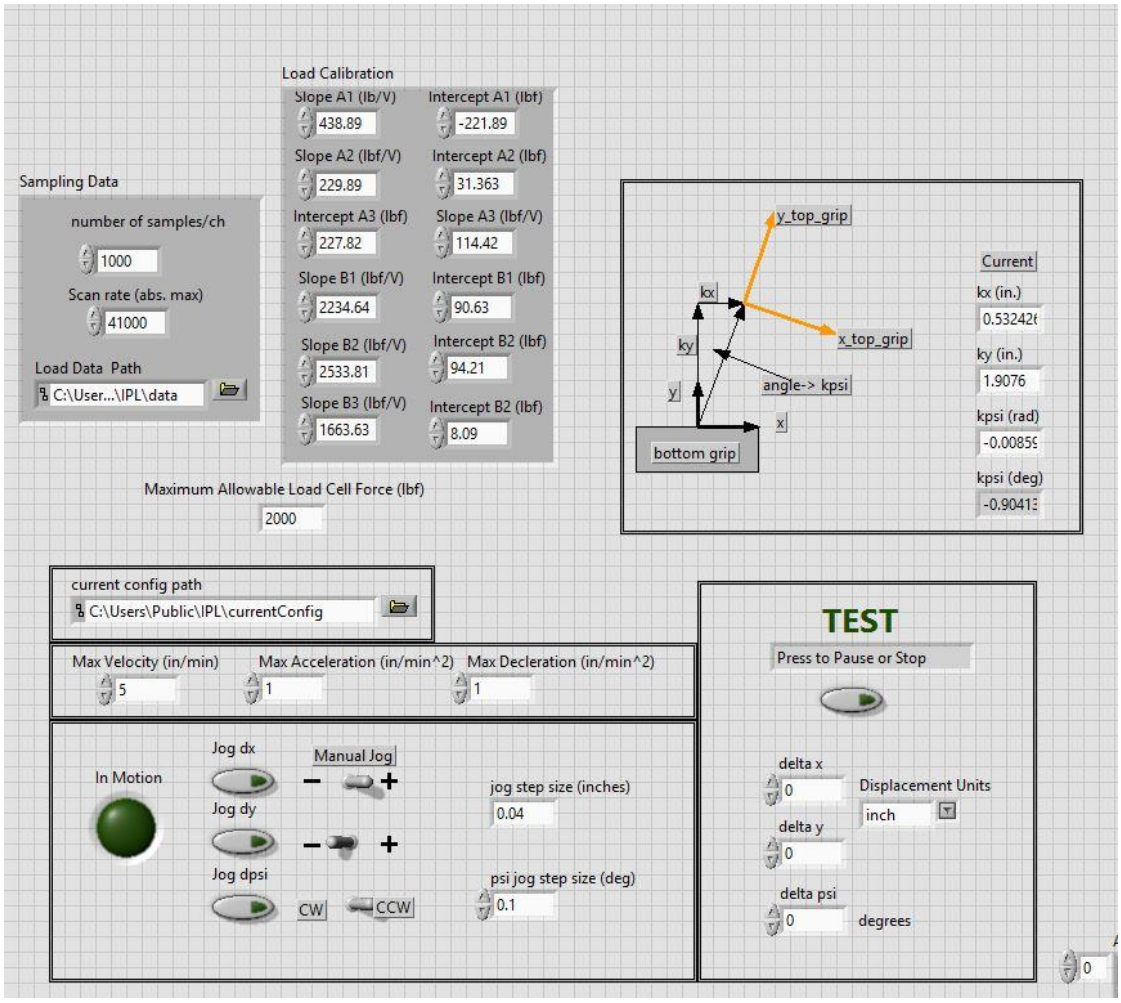


Figure 136: Snapshot of the 'IPL_V1' VI.

17. If you are performing a DIC calibration, use the jog feature (lower left window) to open the IPL wide enough to accept the calibration block. Do this by entering a jog step size and using the toggle switches to choose the direction. Then press the

button corresponding to the direction of translation desired. (NOTE: You can't open the IPL wide enough using only Y translation. You will need some X and rotation to prevent the actuators from reaching their maximum length) If the actuators start making an awful clicking noise shut them off using the main switch on the IPL dashboard bracket, then wait for the jog to stop on LabVIEW before turning them back on.

18. After the DIC calibration has been completed, jog the IPL back into position to hold a coupon. To do this, line up the upper grip parallel to the lower grip, bring the top grip down so a coupon fits with little play, and line up the fixed transverse plates (left) vertically. This process is time consuming and usually takes several jogs to align the grips correctly.
19. Loosen and open the sliding transverse support plates on both the top and bottom grips using two 7/16" wrenches.
20. Insert you test specimen into the grips, be sure to slide the coupon over to the left to contact the fixed transverse support plates.
21. Slide the sliding transverse support plates to contact the other side of the specimen.
22. Use the hydraulic pump to slightly grip the specimen in both grips.
23. Now tap the sliding transverse plates into position using a rubber mallet or hammer and secure the plates into position using two 7/16" wrenches.
24. Use the hydraulic pump to fully grip the specimen to the desired grip pressures. (Usually 4000-6000 psi for plastics and 6000-8000 psi for stronger materials.)
25. Close the grip valves on the IPL dashboard bracket to hold grip pressure.

26. You are now ready to start a test in the ‘IPL_V1’ VI. (the VI should still be running continuously)
27. Start by entering your desired test speed and acceleration.
28. Enter 0 in each of the directional text boxes in the ‘TEST’ window.
29. Press the ‘TEST Start Button’ in the ‘TEST’ window.
30. The file explorer will pop up. Select the blank text file you created earlier in step 15 titled ‘Initialize.txt’ and click save. This initializes all the Sub-VI’s under the main IPL VI. (NOTE: Sometimes the IPL will slightly shift here, my experience is that re-calibrating the LVDTs will fix that.)
31. Plug in your desired displacements into the directional text boxes ‘TEST’ window. Best practice is to keep displacements below 0.5”, but this is material dependent.
32. Press the ‘TEST Start Button’ in the ‘TEST’ window.
33. Enter your desired test name in the file explorer.
34. This is where you would start your DIC test.
35. Click save and the test will start.
36. Wait for the test to complete.
37. The load data will be in the .txt file you just saved. (X load, Y load, and Moment are columns M, N, O, respectively.) The load data is also exported through three analog cables into the DIC software if desired. The cables are on the lower level of the IPL table.
38. Open the grip valves and release the hydraulic pressure from the grips.
39. Remove the failed specimen.

40. To run another test, repeat steps 18 – 39.